IJOCTA
An International Journal of Optimization and Control: Theories & Applications
2010

ISSN:2146-0957
eISSN:2146-5703

Volume:7 Number:2
July 2017

# An International Journal of Optimization and Control:

## Theories & Applications

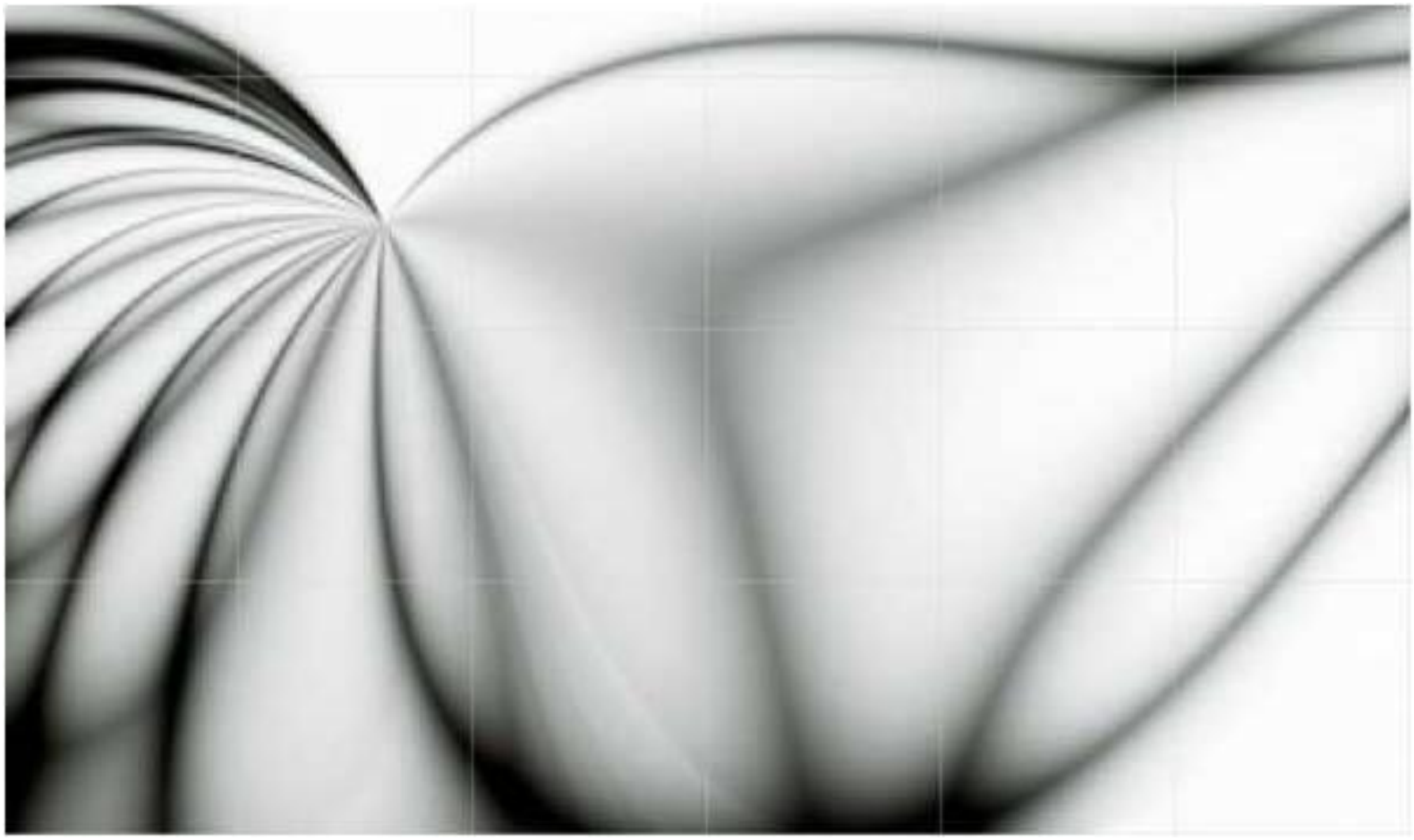

www.ijocta.com

IJOCTA
An International Journal of Optimization and Control: Theories & Applications
2010

www.ijocta.com
info@ijocta.com

# An International Journal of Optimization and Control: Theories & Applications

**Volume: 7, Number: 2**

**July 2017**

Publisher & Owner *(Yayımcı & Sahibi)*:

Prof. Dr. Ramazan YAMAN
Balikesir University, Faculty of Engineering, Department of Industrial Engineering, Cagis Campus, 10145, Balikesir, Turkey
*Balıkesir Üniversitesi, Mühendislik Fakültesi, Endüstri Mühendisliği Bölümü, Çağış Kampüsü, 10145, Balıkesir, Türkiye*

ISSN: 2146-0957
eISSN: 2146-5703

Press *(Basımevi)*:

Bizim Dijital Matbaa (SAGE Publishing), Kazım Karabekir Street, Kültür Market, No:7 / 101-102, İskitler, Ankara, Turkey
*Bizim Dijital Matbaa (SAGE Yayıncılık), Kazım Karabekir Caddesi, Kültür Çarşısı, No:7 / 101-102, İskitler, Ankara, Türkiye*

Date Printed *(Basım Tarihi)*:

July 2017
*Temmuz 2017*

Responsible Director (Sorumlu Müdür):

Prof. Dr. Ramazan YAMAN

IJOCTA is an international, bi-annual, and peer-reviewed journal indexed/ abstracted by *(IJOCTA, yılda iki kez yayımlanan ve aşağıdaki indekslerce taranan/dizinlenen uluslararası hakemli bir dergidir)*:
Cabell's Directories, DOAJ, EBSCO Databases, JournalSeek, Google Scholar, Index Copernicus, International Abstracts in Operations Research, JournalTOCs, Mathematical Reviews (MathSciNet), ProQuest, Ulakbim Engineering and Basic Sciences Database (Tubitak), Ulrich's Periodical Directory, and Zentralblatt Math.

crossref

We Use Plagiarism Detection iThenticate Learn More »

iThenticate and ijocta.balikesir.edu.tr are granted by Balikesir University.

# An International Journal of Optimization and Control:

## Theories & Applications

**Volume: 7 Number: 2**
**July 2017**


## CONTENTS

An International Journal of Optimization and Control: Theories & Applications
ISSN: 2146-0957 eISSN: 2146-5703
Vol.7, No.2, pp.130-141 (2017)
https://doi.org/10.11121/ijocta.01.2017.00309

RESEARCH ARTICLE

# Sizing optimization of skeletal structures using teaching-learning based optimization

Vedat Toğan [a *], Ali Mortazavi [b]

[a] *Department of Civil Engineering, Karadeniz Technical University, Turkey*
[b] *Department of Civil Engineering, Ege University, Turkey*
*togan@ktu.edu.tr, alimortazavi.phd@gmail.com*

ARTICLE INFO

Article history:
*Received: 19 February 2016*
*Accepted: 20 January 2017*
*Available Online: 31 March 2017*

Keywords:
*Optimization*
*Skeletal structures*
*Teaching-learning based optimization*
*Teaching factor*
*Penalty function*

AMS Classification 2010:
*90B50, 90C26, 90C59*

ABSTRACT

Teaching Learning Based Optimization (TLBO) is one of the non-traditional techniques to simulate natural phenomena into a numerical algorithm. TLBO mimics teaching learning process occurring between a teacher and students in a classroom. A parameter named as teaching factor, $T_F$, seems to be the only tuning parameter in TLBO. Although the value of the teaching factor, $T_F$, is determined by an equation, the value of 1 or 2 has been used by the researchers for $T_F$. This study intends to explore the effect of the variation of teaching factor TF on the performances of TLBO. This effect is demonstrated in solving structural optimization problems including truss and frame structures under the stress and displacement constraints. The results indicate that the variation of $T_F$ in the TLBO process does not change the results obtained at the end of the optimization procedure when the computational cost of TLBO is ignored.



## 1. Introduction

Optimization tools emerged as obtaining the optimum solution of optimization problems try to maximize or minimize a real function within a domain which contains the acceptable values of variables while some restrictions are to be satisfied. Among the optimization tools developed and used for the solution of optimization problems, the recent novel and innovative meta-heuristic search techniques emerged use nature as a source of inspiration to establish a numerical search algorithm for solving complex engineering problems and they do not suffer the discrepancies of mathematical programming based optimum design methods [1]. Although genetic algorithms (GAs) based on the principle of survival of the fittest as a computational procedure [2-7] seems to be commonly employed to obtain the optimum solution of structural design problems, many meta-heuristic optimization tools occurred in recent years, which were developed inspiring the different process and phenomena from the nature. The optimization algorithms such as ant colony optimization (ACO) working on the behavior of an ant, particle swarm optimization (PSO) implementing the foraging behavior of a bird for searching food, artificial bee colony (ABC) using the foraging behavior of a honey bee, harmony search (HS) working on the principle of music improvisation in music player, charged system search (CSS) implementing the Coulomb and Gauss's law of electrostatics in physics, and imperialist competitive algorithm (ICA) using a socio-politically motivated strategy might be stated as the new generation meta-heuristic techniques, mine blast algorithm (MBA) simulating the mine bomb explosion, water cycle algorithm (WCA) implementing the main steps of the hydrologic cycle, water wave optimization (WWO) working on the principle of wave motion in recent years, which have been developed mimicking the principles of different natural phenomena and have been effectively employed to attain the optimum solution of structural design problems [1, 8-19]. Moreover, the improved form of these algorithms proposed to enhance performance and ability of those can also be found in the literature [20-22]. On the other hand, the emergence of new computational techniques that are based on the simulation of paradigms found in nature has still continued due to its ability of solving different optimization problems because of their very suitability and effectiveness in finding the solution of

*Corresponding author

structural optimization problems.

One of the meta-heuristic techniques offered from inspiring the natural phenomena is the so-called Teaching-Learning Based Optimization (TLBO). TLBO was developed by [23] as a new optimization method, which mimics teaching-learning process in a class between the teacher and the students (learners). [23] tested the TLBO algorithm on constrained benchmark test functions with different characteristics, benchmark mechanical design problems and mechanical design optimization problems taken from the literature. After that, some optimization problems related with the distinct discipline and features were investigated using the standard TLBO algorithm and the enhancement version of its [24-30]. The numerical results presented in the corresponding researches proved exploration and exploitation capacities of TLBO on different kind of optimization problems in comparison to other metaheuristics algorithms used in these optimization cases.

TLBO algorithm contains two main phases known as Teaching phase and Learning phase and it does not need any control parameters values to start its searching process. The teaching factor $T_F$ placed in the Teaching Phase seems the only tuning parameter although yet $T_F$ was decided with the help of $T_F$ = round[1 + rand (0,1) {2-1}] in [23]. However, the value $T_F$ was taken as 1 or 2 in the studies conducted using TLBO in contrast to the equation given in [26]. For example, [30], [31], and [24] were adopted it as 2 through the TLBO process while [28] taken as [0, 1]. Therefore this study intends to explore the effect of the variation of teaching factor $T_F$ on the performances of TLBO. This effect is demonstrated solving structural optimization problems including truss and frame structures under the stress and displacement constraints.

## 2. Optimization problems

A general mathematical statement for the constrained optimization problem is defined in [32] as follows. In $R^n$ find the design variables $\mathbf{x}=\{x_1, x_2, ..., x_n\}^T$ minimizing an objective function and satisfying the constraints:.

$$\begin{array}{lll} \min & f(\mathbf{x}) & \mathbf{x}\in R^n \\ \text{subject to} & g_i(\mathbf{x}) \le 0 & i=,\ldots,m_1 \\ & h_j(\mathbf{x}) = 0 & j=,\ldots,m_2 \\ & \mathbf{x}_l \le \mathbf{x} \le \mathbf{x}_u & \end{array} \quad (1)$$

In Eq. (1), $g_i(\mathbf{x})$ and $h_j(\mathbf{x})$ represent the inequality and equality constraints, $\mathbf{x}_l$ and $\mathbf{x}_u$ are the vectors showing the lower and upper limit for the design variables, respectively. Since the design variables of the optimization problem are discrete $\mathbf{x}_l$ is equal to 1 whereas $\mathbf{x}_u$ is the maximum section number considered for design variables. Therefore, the optimization problem turns finding a vector of integer values $\mathbf{x}$ corresponding to the sequence numbers of steel sections in a given list to create a vector of cross-sectional areas $\mathbf{A}=\{A_1,A_2,..,A_M\}^T$ for $M$ members of the structure. Such that, the objective function $f$ taken as weight of the structural system is minimized depending on $\mathbf{A}$.

$$f = \sum_{i=1}^{M} \rho L_i A_i \quad (2)$$

In Eq. (2), $M$ is the number of elements in the structural system. $L_i$ and $A_i$ are the length, and the cross-section area of $i$-th element respectively, $\rho$ is the density of the material.

As the meta-heuristic methods are suitable for the unconstrained optimization problems, the constrained optimization problem is converted to the unconstrained one via penalty functions based on the measurement of violation. A penalty functional is added to the objective function to define the fitness value of an infeasible element. The objective function for the design problem incorporating penalty function as well can be expressed as follows;

$$\min \quad W = (1 + f_{penalty})\, f \quad (3)$$

In Eq. (3), $W$ is called the penalized objective function and shows a relative measure of the performance of the solution, $f_{penalty}$ is the penalty function, and $f$ is objective function as in Eq. (2). All penalty functions are based on the violation of the constraints, and usually the degree of penalty for a given solution is adjusted through some coefficients placed in the penalty function. The penalty function taken from [8] as given below is used in the current work.

$$\begin{aligned} & f_{penalty} = (1+C)^{\varepsilon} \\ & \text{where} \quad C = \sum_{i=1}^{m_1} \max[0, g_i(\mathbf{x})], \quad \varepsilon = 2 \end{aligned} \quad (4)$$

In Eq. (4), $C$ is the total value of displacement and stress violations, $\varepsilon$=penalty function exponent, and $m_1$ is number of the total constraints considered as the displacement and/or the stress constraints, $g_i(\mathbf{x})$.

## 3. Teaching-learning based optimization (TLBO)

TLBO simulates the effect of influence of a teacher on learners (students) which is taken as the source of its inspiration. In accordance with this purpose, the method imitates the set of possible solution alternatives of the problem as teacher-student group in a class which struggles to increase the level of the class by attaining the new information on a subject under the existing conditions. It is intended in this simulation that the students in a class increase and move their knowledge level on a subject taught by the teacher towards his or her own level.

A computational procedure by imitating the above teaching-learning process that occurs between the teacher and the students in a class is developed by [23]

and aforementioned process called TLBO consists of two parts; i) "Teaching Phase", and ii) "Learning Phase". In teaching phase, the teacher, who is the most knowledgeable person in a social group and is expected to disseminate information to other learners, is determined whereas in the learning phase, it is provided for the students to acquire new information through the interactions among the learners. As in other meta-heuristic algorithms inspiring from the nature, TLBO is also a population based method.

Each student in a class represents a possible solution, the different subjects offered to learn to students is analogous to different design variables, the students' result obtained through the exam demonstrates the fitness of solution, the teacher is taken as the best solution achieved so far, and finally whole class is considered as the population in TLBO. After this association, the step-wise procedure for the implementation of TLBO is as follows.

### 3.1. Initialize the optimization problems

The parameters required by the optimization algorithm to be used in solving the structural design problems are defined in this step. These are number of population (*np*), maximum number of cycles ($C_{max}$), number of design variables (*nd*), lower and upper limits of design variables ($x_l$ and $x_u$), objective function ($f(x)$) and so on, which are selected depending on the type of problem.

### 3.2. Initialize the population and evaluate the solution

The population is randomly generated according to the parameters described in the previous step as follows.

$$pop=\begin{bmatrix} x_{1,1} & \cdots & x_{1,nd-1} & x_{1,nd} \\ \vdots & \cdots & \cdots & \vdots \\ x_{np,1} & \cdots & x_{np-1,nd-1} & x_{np,nd} \end{bmatrix}\begin{matrix} \rightarrow \\ \rightarrow \\ \rightarrow \end{matrix}\begin{matrix} W(x_1) \\ \vdots \\ W(x_{np}) \end{matrix} \quad (5)$$

In Eq. (5), each row shows a possible solution ($x_i$={$x_{i,1}$ … $x_{i,nd-1}$ $x_{i,nd}$} $i$=1, …, *np*), $W(x_{1,..,np})$ represents the value of the penalized objective function for the evaluation of the potential solutions through Eq. (3), and *pop* demonstrates the population.

### 3.3. Teaching phase

The solution with a minimum value of the penalized objective function in the population is determined at this stage of TLBO ( $\min(W(x_{1,..,np}))$ ). Since this individual is the best of the population it is taken into account as a teacher in the teaching-learning process ($x_{teacher}=x_{=\min(W(x))}$). Then, the other students in the current population are modified in the neighborhood of the teacher by the hope that the level of students will be updated to the level of the teacher. This modification is carried out by using the following equations.

$$x^{*}=x_i+r(x_{teacher}-T_F\,x_{mean}) \quad (6a)$$

In Eq. (6a), $x^*$ shows the renewed form of $x_i$ by Eq. (6a), $r$ is a random number varying [0,1], $T_F$ is a teaching factor being either 1 or 2, which is again a heuristic step and decided randomly with equal probability as $T_F$ = round[1 + rand (0,1) {2-1}] ( in [23]), and $x_{mean}$ symbolizes the mean of the population, which is calculated with column-wise manner as follows.

$$x_{mean}=\lfloor \bar{x}_{i,1} \quad \bar{x}_{i,2} \quad \cdots \quad \bar{x}_{i,nd-1} \quad \bar{x}_{i,nd} \rfloor$$
$$x_{mean}=\bar{x}_{i,j}=\frac{\sum_{i=1}^{np} x_{i,j}}{np} \quad (6b)$$

In Eq. (6b), $i$=1,…,*np*, $j$=1,…,*nd*, *np* and *nd* are the number of solutions and the design variables. As a results of these operations, $x_i$ is taken as $x^*$ if the obtained $x^*$ produces a better value of $W$(.) than $x_i$. Otherwise, $x_i$ is retained.

### 3.4. Learning phase

After the teacher transfers him or her own knowledge to the students by Eq. (6a), the teaching-learning process continues in the form of interaction among students. At this stage of the TLBO algorithm, a student learns new information by interacting with other students who have more knowledge than him or her. The modification formula representing the learning phase can be expressed as:

$$\begin{aligned} &for \quad i=1:np \\ &\text{randomly select } j,\ j\neq i \\ &\text{if } f(x_i)<f(x_j) \\ &difference=x_i-x_j \\ &\text{else} \\ &difference=x_j-x_i \\ &\text{end if} \\ &x^{*}=x_i+r\times difference \\ &\text{end for} \end{aligned} \quad (6c)$$

where, $x^*$ and $x_i$ are the new and existing solution of $i$, $x_j$ is the any solution that is different from $x_i$. If the solution gained new information with help of Eq. (6c), $x^*$, produces better penalized objective function value than $x_i$ change $x_i$ to $x^*$, otherwise preserve $x_i$.

At the end of the learning phase, a cycle (iteration) is completed for the TLBO and the steps in section 3.3 and 3.4 continues until a termination criterion is satisfied, which is adopted as a pre-determined maximum number of cycles ($C_{max}$) in the current work. The vector $x^*$ obtained with application of both Eqs. (6a) and (6c) may contain any design variable being less than $x_l$ or bigger than $x_u$ due to addition and subtraction in the corresponding expressions. In such a case, a controlling procedure should be performed for $x^*$ so as not to encounter any abnormal ending in the algorithm. Therefore, it is ensured that any design variable in $x^*$ must not be bigger than $x_u$ and less than

$x_l$ and if any design variable of $x^*$ is less than $x_l$ or bigger than $x_u$ it is taken into account as $x_l$ or $x_u$, respectively.

The flowchart of TLBO developed in the light of information given above is demonstrated in Figure 1.

## 4. Design examples

The design process, that is explained with the implementation steps given above, of a Teaching Learning Based Optimization (TLBO) technique is properly applied to the example designs such as 52 bar truss, 3-bay 15-story frame, and 582 bar space truss in order to exhibit the effecting of varying the value of $T_F$ on the performance of TLBO algorithm. In the design examples examined, the design variables taken into consideration as the cross-sectional area of the members that make up the structural systems are discrete. In other words, they are represented by the section numbers considered for design variables.

The inequalities shown as follows are kept in mind as constraints in the current work for the examples

$$g_{k_1}(x) = 1.0 - \frac{u_a}{|u|} \le 0 \qquad k_1 = 1,...,c_1 \qquad (7a)$$

$$g_{k_2}(x) = 1.0 - \frac{\sigma_a}{|\sigma|} \le 0 \qquad k_2 = 1,...,c_2 \qquad (7b)$$

where, Eq. (7a) and (7b) demonstrate the displacements and stresses constraints, respectively. $u$ displacement of joint, and $u_a$ is its upper bound. $\sigma$ is stress in a member . $\sigma_a$ is the allowable stresses for the tension and compression members, respectively. $c_1$ and $c_2$ are number of restricted displacements and stresses.

The optimizations process performed using TLBO for the structure systems examined in this study is repeated 20 times by the different populations which are generated independently and randomly at every turn. The best (lightest) one of the 20 runs is propounded as the result of the related examples.

The algorithm and finite element analysis program are coded in Matlab software and implemented on PC with Intel Core i5 2.70 GHz processor and 8 GB RAM memory.

### 4.1. 52 bar truss

A 52 bar plane truss shown in Figure 2 is studied as the first example for demonstrating how to vary the solution process of TLBO depending on the value of $T_F$. It is subjected to single-load case given in Table 1. The truss was optimized by [33] using GA, by [34] using GA with adaptive manner penalty function, and by [35] using rank-based ant system that is a variant of the ACO. Moreover the same example was solved by [36] using MBA and [37] using IMBA.

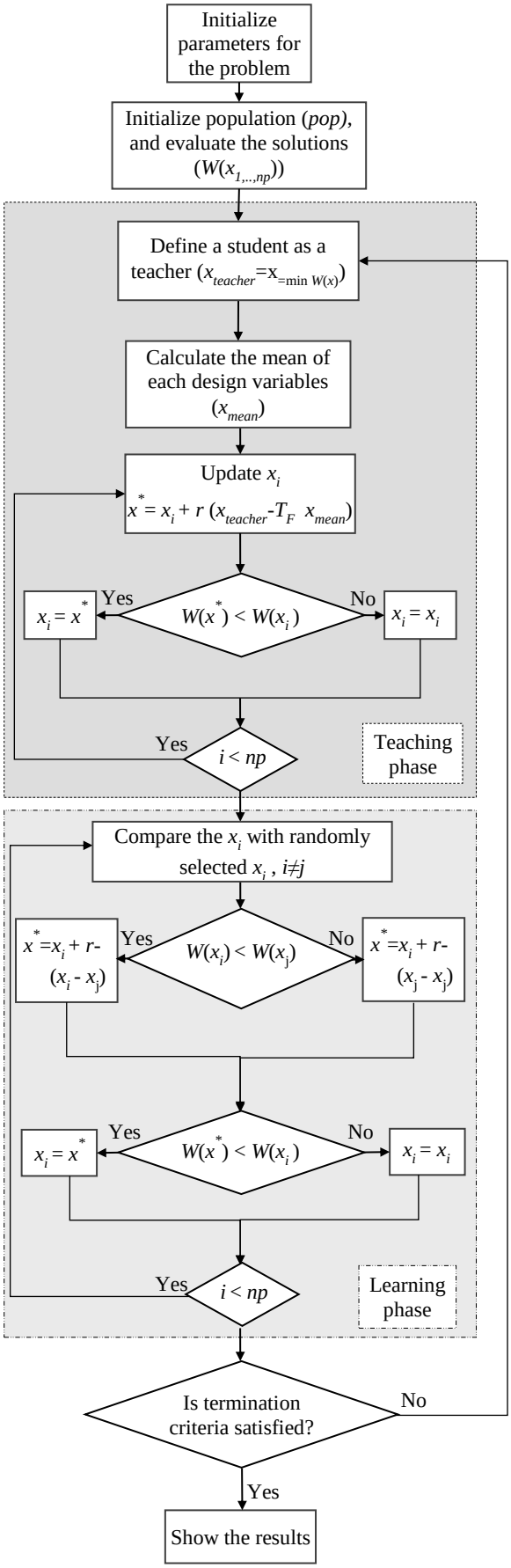


**Figure 1.** Flowchart diagram for TLBO.

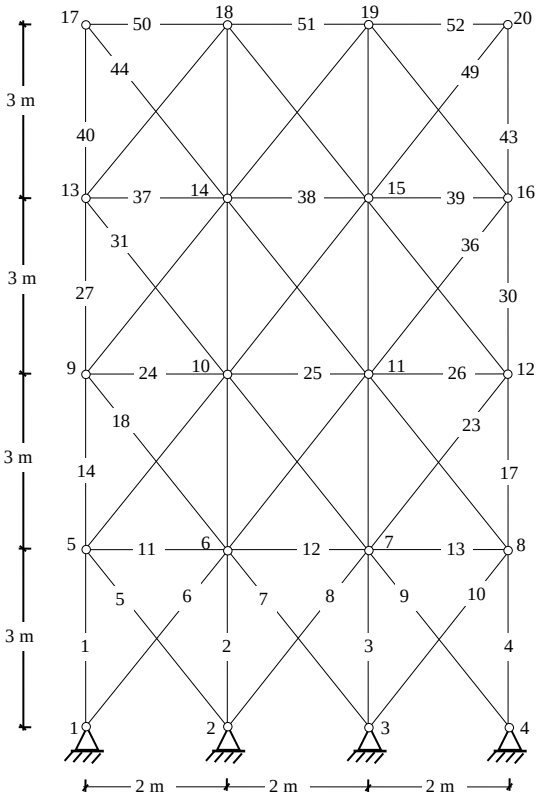


**Figure 2.** 52 bar planar truss.

The young modulus, $E$, is 207 GPa, the density, $\rho$, is 7860 kg/m$^3$, and the allowable stresses are 180 MPa in tension and compression. Constraints are imposed on member stresses. Members of the truss are divided into 12 groups and the cross-sectional areas are to be selected from a list with 64 sections presented in Table 2.

As mentioned previously, in contrast to [30], [31], [24], and [28] in the current work, to show the dependence of the TLBO on the value of $T_F$ each design example examined in this study is optimized taking the value of $T_F$ as 1, 2 and round[1 + rand (0,1) {2-1}], respectively.

The results obtained by the TLBO as well as those from the references cited above are summarized in Table 3. The iteration histories of TLBO process are shown in Figure 3. Figure 3 shows the variations of the penalized objective function during the solution process conducting with TLBO. Figure 3a illustrates this variation for the population size (*pop*) adopted as 50 and a maximum number of cycles($C_{max}$) taken as 150, 100, and 80 respectively.

**Table 1.** Load case for the 52 bar truss.

| Note | $F_x$ (kN) | $F_y$ (kN) |
|---|---|---|
| 17 | 100.0 | 200.0 |
| 18 | 100.0 | 200.0 |
| 19 | 100.0 | 200.0 |
| 20 | 100.0 | 200.0 |

However, Figures 3b and 3c demonstrate the same variation through the solution process for *pop*=40 and *pop*=30, respectively. Each solution process depicted in Figures 3b and 3c is repeated with different $C_{max}$ taken as 150, 100, and 80 respectively while the population size remains the same.

It is noticed that for $T_F$ = round[1 + rand (0,1) {2-1}], the results remain the same for *pop*=30, 40, and 50 when $C_{max}$=150 and 100 as well as for being $T_F$=1. In case of $C_{max}$=80, the results are also same both $T_F$ = round[1 + rand (0,1) {2-1}] and $T_F$=1 when *pop*=40 and *pop*=50. It is observed that TLBO does not produce the same results for $T_F$=2 when $C_{max}$=100 and 80, and *pop*= 30, 40, and 50.

It might be concluded from the observations that TLBO is capable of finding the same results if the parameters of $C_{max}$ and *pop* are rationally selected for the problem under investigation. In addition, it is worthy said that compared with $T_F$=2 the results obtained with $T_F$=1 and $T_F$ = round[1 + rand (0,1) {2-1}] are not more sensitive the changes in the population size and the maximum number of cycles.

**Table 2.** Cross-sectional areas for the 52 bar truss.

| Section no | Area (mm$^2$) | Section no | Area (mm$^2$) |
|---|---|---|---|
| 1 | 71.613 | 33 | 2477.414 |
| 2 | 90.968 | 34 | 2496.769 |
| 3 | 126.450 | 35 | 2503.221 |
| 4 | 161.290 | 36 | 2696.769 |
| 5 | 198.064 | 37 | 2722.575 |
| 6 | 252.258 | 38 | 2896.768 |
| 7 | 285.161 | 39 | 2961.284 |
| 8 | 363.225 | 40 | 3096.768 |
| 9 | 388.386 | 41 | 3206.445 |
| 10 | 494.193 | 42 | 3303.219 |
| 11 | 506.451 | 43 | 3703.218 |
| 12 | 641.289 | 44 | 4658.055 |
| 13 | 645.160 | 45 | 5141.925 |
| 14 | 792.256 | 46 | 5503.215 |
| 15 | 816.773 | 47 | 5999.988 |
| 16 | 940.000 | 48 | 6999.986 |
| 17 | 1008.385 | 49 | 7419.340 |
| 18 | 1045.159 | 50 | 8709.660 |
| 19 | 1161.288 | 51 | 8967.724 |
| 20 | 1283.868 | 52 | 9161.272 |
| 21 | 1374.191 | 53 | 9999.978 |
| 22 | 1535.481 | 54 | 10322.560 |
| 23 | 1690.319 | 55 | 10903.204 |
| 24 | 1696.771 | 56 | 12129.008 |
| 25 | 1858.061 | 57 | 12838.684 |
| 26 | 1890.319 | 58 | 14193.520 |
| 27 | 1993.544 | 59 | 14774.164 |
| 28 | 2019.351 | 60 | 15806.420 |
| 29 | 2180.641 | 61 | 17096.740 |
| 30 | 2238.705 | 62 | 18064.480 |
| 31 | 2290.318 | 63 | 19354.800 |
| 32 | 2341.931 | 64 | 21612.860 |

**Table 3.** Design results for the 52 bar truss.

| Group no | Members | GA [33] | GA [34] | ACO [35] | MBA [36] | IMBA [37] | TLBO This study |
|---|---|---|---|---|---|---|---|
| 1 | 1, 2, 3, 4 | 44 | 44 | 44 | 44 | 44 | 44 |
| 2 | 5, 6,…,10 | 19 | 19 | 19 | 19 | 19 | 19 |
| 3 | 11, 12, 13 | 13 | 10 | 11 | 10 | 10 | 11 |
| 4 | 14,…,17 | 42 | 42 | 42 | 42 | 42 | 42 |
| 5 | 18,…,23 | 18 | 16 | 16 | 16 | 16 | 16 |
| 6 | 24, 25, 26 | 10 | 12 | 11 | 10 | 10 | 11 |
| 7 | 27,…,30 | 33 | 30 | 30 | 30 | 30 | 30 |
| 8 | 31,…,36 | 18 | 17 | 17 | 17 | 17 | 17 |
| 9 | 37, 38, 39 | 7 | 8 | 9 | 10 | 10 | 9 |
| 10 | 40,…,43 | 24 | 20 | 20 | 20 | 20 | 20 |
| 11 | 44,…,49 | 18 | 19 | 19 | 19 | 19 | 19 |
| 12 | 50, 51, 52 | 12 | 10 | 11 | 10 | 10 | 11 |
| Best (kg) | | 1970.142 | 1903.366 | 1899.350 | 1902.605 | 1902.605 | 1899.350 |
| Evaluations+ | | 60000 | 17500 | 17500 | 5450 | 4750 | 6440 |

+ shows the maximum numbers of structural analysis to obtain the optimal design presented in Table

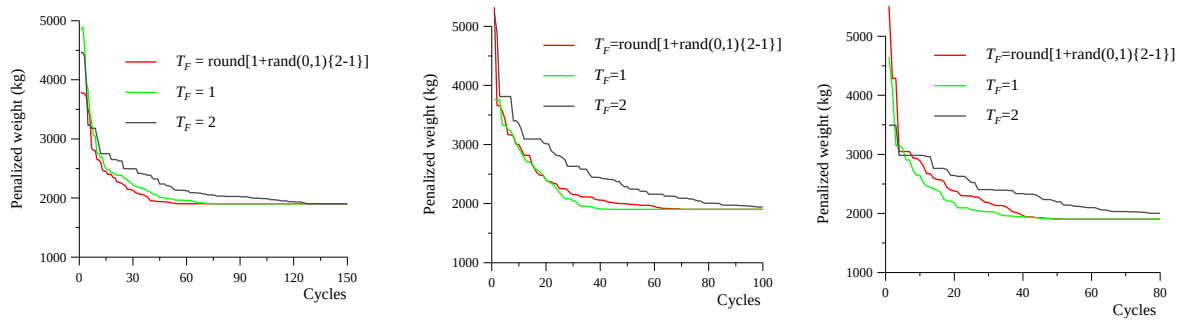


**(a)** Variation of objective function for *pop* = 50.

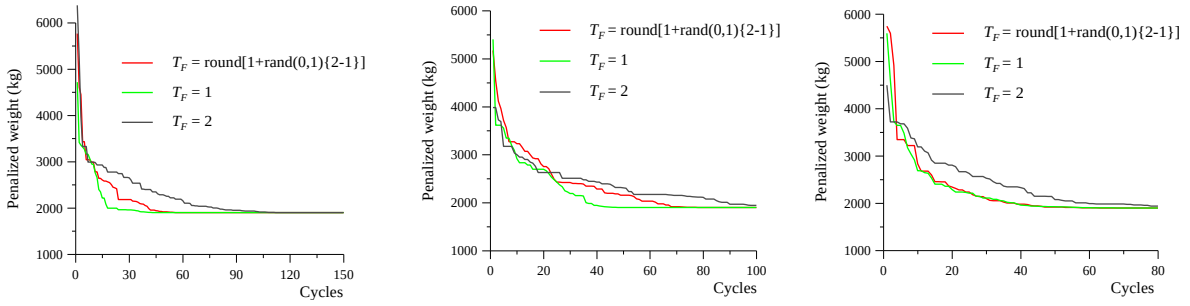


**(b)** Variation of objective function for *pop* = 40.

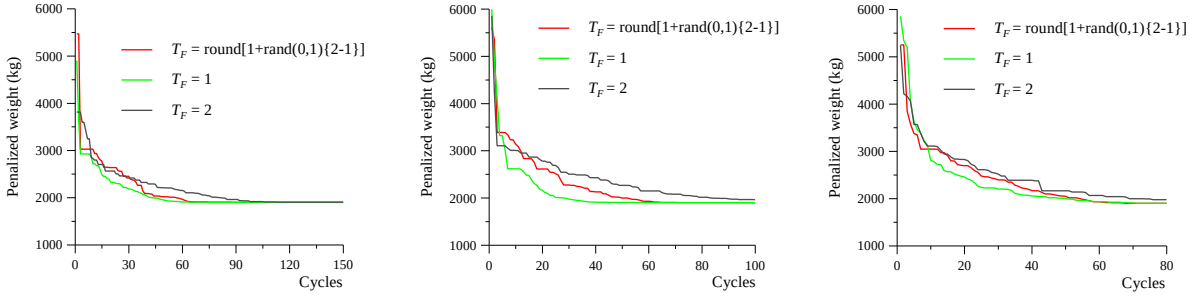


**(c)** Variation of objective function for *pop* = 30.

**Figure 3.** Histories of TLBO process of 52-bar truss example.

The TLBO algorithm produces identical design to the design reported by [35]. However, TLBO algorithm uses 80 generations with a population size 40 resulting in 6440 truss analyses to converge to a solution and the required truss analyses to converge to a solution for the TLBO algorithm is more less than 60000, 17500, and 17500 analyses required by GA [33, 34] and ACO [35], respectively. However, [36] and [37] reported the required truss analyses number as 5450 and 4750 to acquire the optimal solutions using MBA and IMBA respectively. Studying the figures given by [36] and [37], it can be stated that maximum number of iteration was set as 500 in their algorithms. Since the results did not change around 100 iterations, it seems that the reported analyses numbers were calculated considering this iteration number in contrast to maximum number of iteration adopted as 500. Keeping this in mind, TLBO find the results presented in Table 3 at 55$^{th}$ iteration(see last graphic illustrated in Figure 3b). In this case, TLBO requires 4440 truss analyses to produce the optimal results.

Although both ACO and TLBO reach the same solution the design slightly violates stress constraints (0.012%). In the optimization application taken from the literature, certain results that violate the constraints less than the level of 0.1% might sometimes be encountered. The rationale of this might be meaningful due to the results from the point of view of engineering.

Statistical optimization result of TLBO algorithm is presented in Table 4.

**Table 4.** Load case for the 52 bar truss.

| Exp. | Best optimized weight / volume | Average optimized weight / volume | Worst optimized weight / volume | Standard deviation on weight / volume |
|---|---|---|---|---|
| Exp[1] | 1899.350 (kg) | 1904.430 (kg) | 1920.396 (kg) | 6.705 (kg) |
| Exp[2] | 402.94 (kN) | 408.44 (kN) | 412.13 (kN) | 3.99 (kN) |
| Exp[3] | 20.304 ($m^3$) | 21.073 ($m^3$) | 24.104 ($m^3$) | 1.143 ($m^3$) |

Note: Exp[1]= 52 bar truss; Exp[1]= 3 bay-15 story frame; Exp[3]= 582 bar truss tower

### 4.2. Three-bay 15 story frame

Figure 4 shows configuration of three-bay 15-story frame consisting of 105 members and its node, element numbering patterns and the loading. The material properties are a modulus of elasticity of $E$=200 GPa and a yield stress of $f_y$=248.2 MPa. The frame is designed following the AISC-LRFD specification [38] and uses a displacement constraint (the sway of the top story < 23.5 cm). The effective length factors, $K_x$, of the members are calculated as $K_x \geq 0$ for a sway-permitted frame and the out-of-plane effective length factor $K_y$ is considered as 1.0. All columns are considered as non-braced along their lengths and the non-braced length for each beam member is specified as one-fifth of the span length.

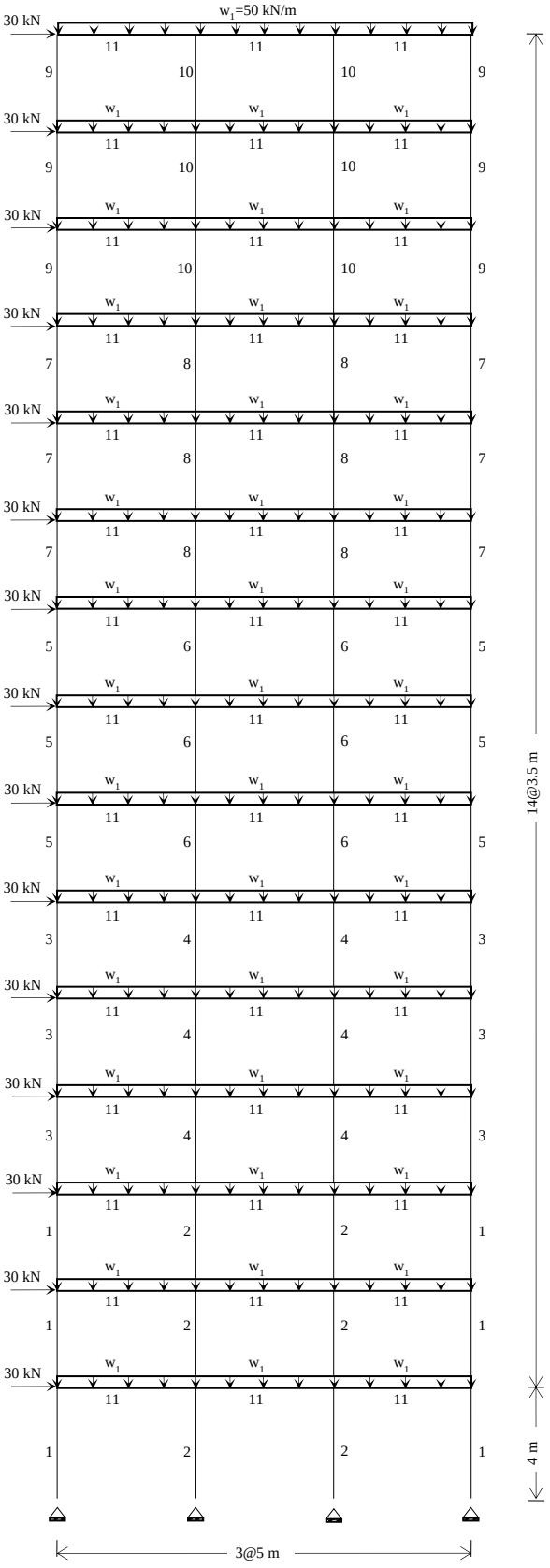


**Figure 4.** Topology of the 3-bay 15-story frame.

The optimum design of the frame is obtained after 9030 analyses by using the TLBO, having the minimum weight of 402.94 kN. The optimum design for ICA [14] has the weight of 417.466 kN. Table 5 summarizes the optimal designs for ICA and TLBO. The ICA could find the result after 6000 analyses. The results obtained by TLBO is nearly 3.5% lighter than the that of the ICA [14].

As aforementioned, to investigate the effect of $T_F$ on the results to be obtained, the total number of cycles required for TLBO process is varied by taking the different the population size (*pop*) and by considering distinct $T_F$ value, i.e. $T_F$=1, $T_F$=2, and $T_F$= round[1 + rand (0,1) {2-1}].

The results reported here correspond to the best having the least weight and they are obtained when the following parameter values are taken into consideration in TLBO process; *pop*=30, $C_{max}$ = 150, $T_F$=1 and $T_F$= round[1 + rand (0,1) {2-1}]. However when $T_F$=2, to reach the results presented in the last column of Table 5 TLBO requires more cycles. Figure 5 shows the histories of the best solutions obtained for all cases, which are performed using different values of *pop*, $T_F$ and $C_{max}$ in order to shorten the computational cost of TLBO process and to demonstrate the effect of $T_F$.

**Table 5.** Design results for the three-bay 15-story frame.

| Grp. No | Members | ICA [14] | TLBO This study | TLBO This study |
|---|---|---|---|---|
| 1 | column 1-3S, E | W24×117 | W24×117 | W12×106 |
| 2 | column 1-3S, I | W21×147 | W36×160 | W27×161 |
| 3 | column 4-6S, E | W27×84 | W14×82 | W24×87 |
| 4 | column 4-6S, I | W27×114 | W30×116 | W21×111 |
| 5 | column 7-9S, E | W14×74 | W21×68 | W12×65 |
| 6 | column 7-9S, I | W18×86 | W30×90 | W16×89 |
| 7 | column 10-12S, E | W12×96 | W12×50 | W10×49 |
| 8 | column 10-12S, I | W24×68 | W12×65 | W12×65 |
| 9 | column 13-15S, E | W10×39 | W12×30 | W8×31 |
| 10 | column 13-15S, I | W12×40 | W12×40 | W16×40 |
| 11 | beams | W21×44 | W21×44 | W21×44 |
| Best (kN) | | 417.466 | 408.03 | 402.94 |
| Evaluations+ | | 6000 | 6030 | 9030 |

+ shows the maximum numbers of structural analysis to obtain the optimal design presented in Table
Note: Grp = Group; S = Story; E = Exterior column; I = Interior column.

It might be realized from Figure 5 that although the design achieved by TLBO for all cases has the same weight of frame, to achieve the results obtained when

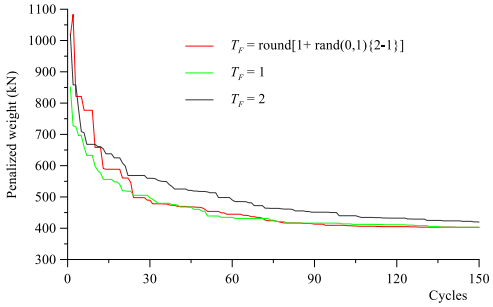


**(a)** Variation of objective function for *pop*=40.

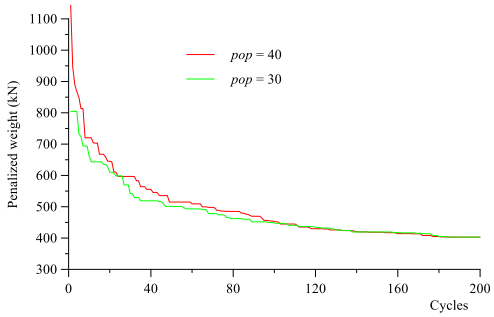


**(b)** Variation of objective function for $T_F$ =2.

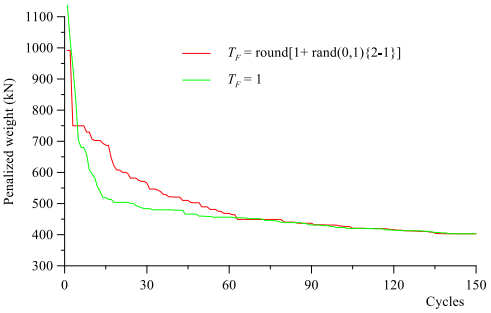


**(c)** Variation of objective function for *pop*=30.

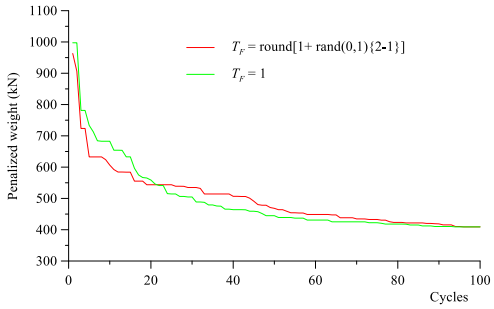


**(d)** Variation of objective function for *pop*=30.

**Figure 5.** Histories of TLBO process of three-bay 15-story frame example.

*pop*=30, $C_{max}$=150, $T_F$=1, and $T_F$= round[1 + rand (0,1) {2-1}] the maximum number of cycles should be increased from 150 to 200 when the teaching factor is considered as 2 (see Figure 5b).

Moreover, if the required frame analyses to reach the best design was adopted 6,000 as well as in the ICA

[14] TLBO would produce a frame having a weight of 408.03 kN, which is 2.26% lighter than that of the ICA (see Figure 5d). This indicates that even though varying the $T_F$ in TLBO process results in different computational cost, the results remain the same or closely the same with small differences.

The global sway at the top story is 13.61 cm, which is less than the maximum sway. The maximum value for the stress ratio is equal to 99.60%. Also, the maximum drift story is equal to 1.11 cm. Statistical optimization result of TLBO algorithm for this example is presented in Table 4.

### 4.3. 582 bar space truss

The geometry and group numbering of a 582 bar space tower, previously studied by [39] using Particle Swarm Optimization (PSO), is given in Figure 6. The structural members of the space tower are linked together into 32 groups. The modulus of elasticity, the material density of all members and yield stress are 29000 ksi, 0.2836 lb/in.$^3$ and 36 ksi, respectively. The maximum displacement of all the nodes is not allowed to exceed 8 cm (3.15 in.) for all directions. A single loading condition is considered to be applied such that the lateral loads of 5 kN (1.12 kips) are applied to all nodes in both $x$ and $y$-directions, and vertical loads of -30 kN (−6.74 kips) are applied, respectively, to all nodes in the upper and lower parts of the tower in $z$ direction. A discrete set of 140 W-shape steel profiles given in Table 6 is used to size the design variables. In association with [39], cross-sectional areas of 140 W-shape steel profiles vary between 6.16 in.$^2$ (39.74 cm$^2$) and 215.0 in.$^2$ (1387.09 cm$^2$).

According to ASD-AISC the maximum slenderness ratio of $i$-th member is limited to 300 and 200 for tension and compression, respectively ( $\lambda_i = K_i L_i / r_i \le \lambda_{allowed}$ , in here $K_i$ is the effective length factor which was taken to be 1, $L_i$ is the length and $r_i$ is minimum radii of gyration). The stress and stability limitations of the members also are imposed according to the provisions of ASD-AISC.

Table 7 lists the designs developed by the PSO [39], the DHPSACO [40] and the IMBA [37]. The TLBO algorithm needs 30050 truss analyses to converge to a solution, while the 50000 analyses are required by PSO [39]. However, studying [39], it can be observed that the results are obtained within 17500 structural analyses although optimization process that ends up 50000 analyses. This case is also the same for the structural analyses number reported by other researchers. For instance, for this example, even though [37] finished the optimization process at the end of the 350 iterations they presented the structural analyses as 15100. This analyses number indicates the obtaining the reported volume firstly. Therefore, the structural analyses number reported as 15550 (155 iteraton) in the current work although TLBO process runs until 300 iterations. Figure 7 shows the convergence histories for the optimum designs obtained by the TLBO algorithm, which is utilized with $pop$=50, $T_F$ =1, $T_F$ =2 and $T_F$ = round[1 + rand (0,1) {2-1}] in order to demonstrate the effect of $T_F$.

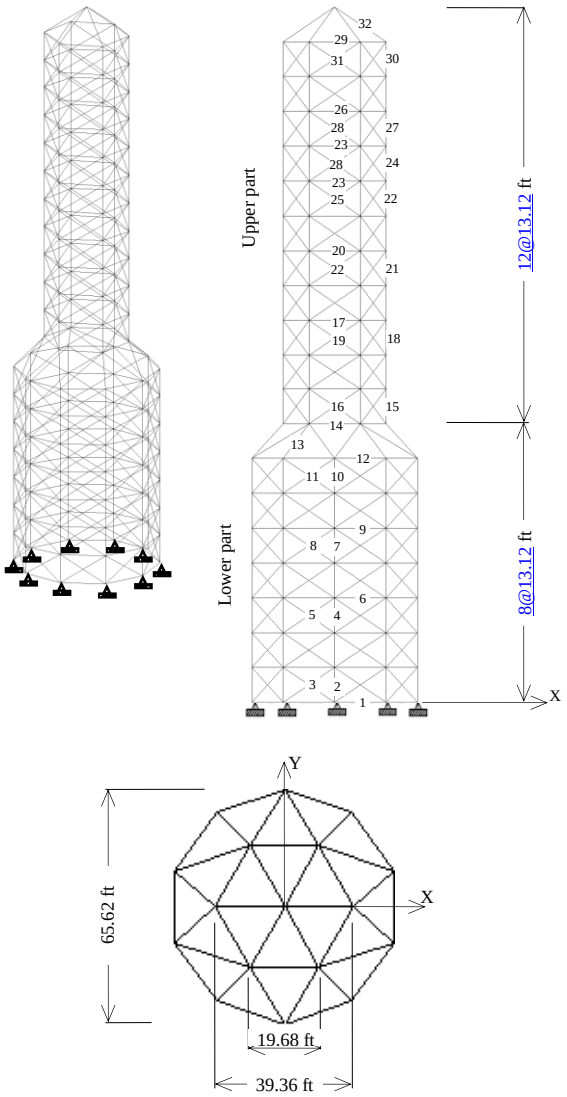


**Figure 6.** The 582-bar space tower truss.

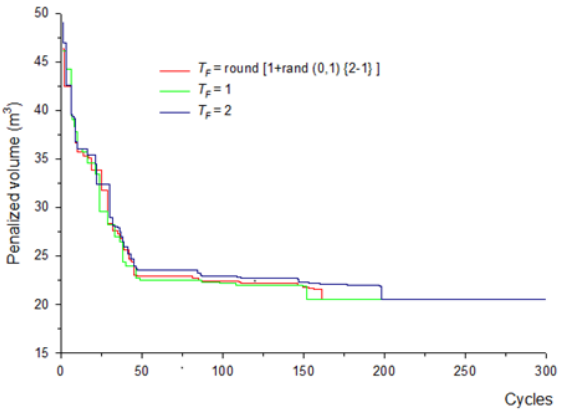


**Figure 7.** Histories of TLBO process of 582 bar space truss example ($pop$=50).

**Table 6.** Profile list for the 582 bar space tower.

| W-shape profile list * | | | |
|---|---|---|---|
| W27 x 178 | W21 x 122 | W18 x 50 | W14 x 455 |
| W27 x 161 | W21 x 111 | W18 x 46 | W14 x 426 |
| W27 x 146 | W21 x 101 | W18 x 40 | W14 x 398 |
| W27 x 114 | W21 x 93 | W18 x 35 | W14 x 370 |
| W27 x 102 | W21 x 83 | W16 x 100 | W14 x 342 |
| W27 x 94 | W21 x 73 | W16 x 89 | W14 x 311 |
| W27 x 84 | W21 x 68 | W16 x 77 | W14 x 283 |
| W24 x 162 | W21 x 62 | W16 x 67 | W14 x 257 |
| W24 x 146 | W21 x 57 | W16 x 57 | W14 x 233 |
| W24 x 131 | W21 x 50 | W16 x 50 | W14 x 211 |
| W24 x 117 | W21 x 44 | W16 x 45 | W14 x 193 |
| W24 x 104 | W18 x 119 | W16 x 40 | W14 x 176 |
| W24 x 94 | W18 x 106 | W16 x 36 | W14 x 159 |
| W24 x 84 | W18 x 97 | W16 x 31 | W14 x 145 |
| W24 x 76 | W18 x 86 | W16 x 26 | W14 x 132 |
| W24 x 68 | W18 x 76 | W14 x 730 | W14 x 120 |
| W24 x 62 | W18 x 71 | W14 x 665 | W14 x 109 |
| W24 x 55 | W18 x 65 | W14 x 605 | W14 x 99 |
| W21 x 147 | W18 x 60 | W14 x 550 | W14 x 90 |
| W21 x 132 | W18 x 55 | W14 x 500 | W14 x 82 |
| W14 x 74 | W12 x 230 | W12 x 50 | W10 x 45 |
| W14 x 68 | W12 x 210 | W12 x 45 | W10 x 39 |
| W14 x 61 | W12 x 190 | W12 x 40 | W10 x 33 |
| W14 x 53 | W12 x 170 | W12 x 35 | W10 x 30 |
| W14 x 48 | W12 x 152 | W12 x 30 | W10 x 26 |
| W14 x 43 | W12 x 136 | W12 x 26 | W10 x 22 |
| W14 x 38 | W12 x 120 | W12 x 22 | W8 x 67 |
| W14 x 34 | W12 x 106 | W10 x 112 | W8 x 58 |
| W14 x 30 | W12 x 96 | W10 x 100 | W8 x 48 |
| W14 x 26 | W12 x 87 | W10 x 88 | W8 x 40 |
| W14 x 22 | W12 x 79 | W10 x 77 | W8 x 35 |
| W12 x 336 | W12 x 72 | W10 x 68 | W8 x 31 |
| W12 x 305 | W12 x 65 | W10 x 60 | W8 x 28 |
| W12 x 279 | W12 x 58 | W10 x 54 | W8 x 24 |
| W12 x 252 | W12 x 53 | W10 x 49 | W8 x 21 |

* the corresponding profile list was taken from Sadollah et al. [37]

Studying on Figure 7 and ignoring the computational cost of TLBO process, it is worthy to state that varying the value of teaching factor, i.e. $T_F$=1, $T_F$=2, and $T_F$= round[1 + rand (0,1) {2-1}], does not affect the results obtained by the TLBO. Statistical optimization result of TLBO algorithm is presented in Table 4.

## 5. Conclusion

Three design examples consisting of two trusses and one frame are considered to illustrate the effect of teaching factor $T_F$ on the optimal design for all examples. The comparisons of the numerical results obtained by the TLBO with $T_F$=1, $T_F$=2, and $T_F$= round[1 + rand (0,1) {2-1}] and those obtained by other optimization methods based on the meta-heuristic concepts are presented to show the capability of the TLBO algorithm in finding good results. Simulations show that reaching the optimum designs by TLBO is insensitive to the parameter of $T_F$ and TLBO produces the same results for all case of $T_F$ when the computational cost of TLBO and the number

**Table 7.** Design results for the 582 bar sapce tower truss.

| Elm. grp. | PSO [39] | DHPSACO [40] | IMBA [37] | TLBO This study |
|---|---|---|---|---|
| 1 | W8×21 | W8×24 | W8×21 | W8×21 |
| 2 | W12×79 | W12×72 | W24×76 | W24×84 |
| 3 | W8×24 | W8 × 28 | W8 × 21 | W8 × 21 |
| 4 | W10×60 | W12×58 | W12×65 | W24×62 |
| 5 | W8×24 | W8×24 | W8×21 | W8×21 |
| 6 | W8×21 | W8×24 | W8×21 | W8×21 |
| 7 | W8×48 | W10×49 | W10×54 | W16×57 |
| 8 | W8×24 | W8×24 | W8×21 | W8×21 |
| 9 | W8×21 | W8×24 | W8×21 | W8×21 |
| 10 | W10×45 | W12×40 | W12×50 | W12×53 |
| 11 | W8×24 | W12×30 | W8×21 | W8×21 |
| 12 | W10×68 | W12×72 | W10×68 | W10×77 |
| 13 | W14×74 | W18×76 | W24×76 | W21×83 |
| 14 | W8×48 | W10×49 | W14×53 | W21×57 |
| 15 | W18×76 | W14×82 | W12×79 | W18×76 |
| 16 | W8×31 | W8×31 | W8 × 21 | W8 × 21 |
| 17 | W8×21 | W14×61 | W12×65 | W10×22 |
| 18 | W16×67 | W8×24 | W8×21 | W18×55 |
| 19 | W8×24 | W8×21 | W8×21 | W8×21 |
| 20 | W8×21 | W12×40 | W12×45 | W8×21 |
| 21 | W8×40 | W8×24 | W8×21 | W14×30 |
| 22 | W8×24 | W14 × 22 | W8 × 21 | W8 × 21 |
| 23 | W8×21 | W8×31 | W16×26 | W8 × 21 |
| 24 | W10×22 | W8×28 | W8×21 | W8×21 |
| 25 | W8×24 | W8×21 | W8×21 | W8×21 |
| 26 | W8×21 | W8×21 | W8×21 | W8 × 21 |
| 27 | W8×21 | W8 × 24 | W8 × 21 | W10×22 |
| 28 | W8×24 | W8 × 28 | W8 × 21 | W8×21 |
| 29 | W8×21 | W16×36 | W8×21 | W8×21 |
| 30 | W8×21 | W8×24 | W8×21 | W8×31 |
| 31 | W8×24 | W8×21 | W8×21 | W8×21 |
| 32 | W8×24 | W8×24 | W8×21 | W12×22 |
| Vol. | 22.3958 | 22.0607 | 20.0688 | 20.304 |
| Eval+. | 17500 | 17500 | 15300 | 15550 |

Note: Vol.= Volume ($m^3$); Eval.= Evaluations

+ shows the maximum numbers of structural analysis to

obtain the optimal design presented in Table

analyses required to obtain the best design are ignored. Comparisons of the numerical results obtained by TLBO with those by other optimization methods are performed to demonstrate the efficiency of the TLBO algorithm in terms of reaching the best designs. Consequently, it is useful to express that $T_F$=1 and $T_F$= round[1 + rand (0,1) {2-1}] would be more suitable when it is intended to find good results in a less number of iterations.

## References


[1] Saka, M.P., Optimum Design of Steel Frames Using Stochastic Search Techniques Based on Natural Phenomena: A Review. In: Topping B.H.V., editor, Civil Engineering Computation Tools and Techniques, Chapter 6, Saxe-Coburg Publication, Stirlingshire (2007).

[2] Dede, T., Bekiroğlu, S. and Ayvaz, Y., Weight minimization of trusses with genetic algorithm. Applied Soft Computing, 11, 2565-2575 (2011).

[3] Jenkins, W.M., A decimal-coded evolutionary algorithm for constrained optimization. Computers & Structures, 80, 471-480 (2002).

[4] Rajeev, S. and Krishnamoorthy, C.S., Discrete optimization of structures using genetic algorithms. Journal of Structural Engineering, 118, 1233–1250 (1992).

[5] Reynolds, B.J. and Azarm, S., A Multi-objective heuristic-based hybrid genetic algorithm. Mechanics Based Design of Structures and Machines, 30, 463-491 (2002).

[6] Toğan, V. and Daloğlu, A., Shape and size optimization of 3d trusses with genetic algorithms. Technical Journal of Turkish Chamber of Civil Engineering, 17, 3809-3825 (2006).

[7] Zhang, J., Wang, B., Niu, F. and Cheng, G., Design optimization of connection section for concentrated force diffusion. Mechanics Based Design of Structures and Machines, 43, 209-231 (2015).

[8] Camp, C.V., Bichon, B.J. and Stovall, S.P., Design of steel frames using ant colony optimization. Journal of Structural Engineering, 131, 369–379 (2005).

[9] Değertekin, S.O., Optimum design of frames using harmony search. Structural Multidisciplinary Optimization, 36, 393-401 (2008).

[10] Eskandar, H., Sadollah, A. and Bahreininejad, A., Water cycle algorithm – A novel metaheuristic optimization method for solving constrained engineering optimization problems. Computers & Structures, 110, 151–166 (2012).

[11] Geem, Z.W., Kim, J.H. and Loganathan, G.V., A new heuristic optimization algorithm: Harmony search. Simulation, 76, 60-68 (2001).

[12] Karaboğa, D., An idea based on honey bee swarm for numerical optimization. Technical Report, TR06, Erciyes University (2005).

[13] Kaveh, A. and Talatahari, S., An improved ant colony optimization for the design of planar steel frames. Engineering Structures, 32, 864-873 (2010).

[14] Kaveh, A. and Talatahari, S., Optimum design of skeletal structures using imperialist competitive algorithm. Computers & Structures, 88, 1220–1229 (2010).

[15] Kennedy, J. and Eberhart, R., Particle swarm optimization. Proc. IEEE international conference on neural networks, pp 1942–1948 (2005).

[16] Sadollah, A., Bahreininejad, A., Eskandar, H. and Hamdi, M., Mine blast algorithm: A new population based algorithm for solving constrained engineering optimization problems. Applied Soft Computing, 13, 2592–2612 (2013).

[17] Seyedpoor, S.M. and Salajegheh, J., Adaptive neuro-fuzzy inference system for high-speed computing in optimal shape design of arch dams subjected to earthquake loading. Mechanics Based Design of Structures and Machines, 37, 31-59 (2009).

[18] Sönmez, M., Discrete optimum design of truss structures using artificial bee colony algorithm. Structural Multidisciplinary Optimization, 43, 85-97 (2011).

[19] Zheng, Y.J., Water wave optimization: A new nature-inspired metaheuristic. Computers and Operations Research, 55, 1–11 (2015).

[20] Hasançebi, O., Erdal, F. and Saka, M.P., Adaptive harmony search method for structural optimization. Journal of Structural Engineering, 136, 419-431 (2010).

[21] Toğan, V. and Daloğlu, A., Optimization of 3d trusses with adaptive approach in genetic algorithms. Engineering Structures, 28, 1019–1027 (2006).

[22] Toğan, V. and Daloğlu, A., An improved genetic algorithm with initial population strategy and self-adaptive member grouping. Computers & Structures, 86, 1204–1218 (2008).

[23] Rao, R.V., Savsani, V.J. and Vakharia, D.P., Teaching–learning-based optimization: A novel method for constrained mechanical design optimization problems. Computer-Aided Design, 43, 303-315 (2011).

[24] Camp, C.V. and Farshchin, M., Design of space trusses using modified teaching-learning based optimization. Engineering Structures, 62, 87-97 (2014).

[25] Cheng, W., Liu, F. and Li, L.J., Size and Geometry Optimization of Trusses Using Teaching-Learning-Based Optimization. International Journal Optimization Civil Engineering, 3, 431-444 (2013).

[26] Dede, T. and Ayvaz, Y., Combined size and shape optimization of structures with a new meta-heuristic algorithm. Applied Soft Computing, 28, 250-258 (2015).

[27] Dede, T. and Toğan, V., A teaching learning based optimization for truss structures with frequency constraints. Structural Engineering and Mechanics, 53(4), 833-845 (2015).

[28] Değertekin, S.O. and Hayalioğlu M.S., Sizing truss structures using teaching-learning-based optimization. Computers & Structures, 119, 177-188 (2013).

[29] Rao, R.V. and Patel, V., An improved teaching-learning-based optimization algorithm for solving unconstrained optimization problems. Scientia Iranica, 20, 710-720 (2013).

[30] Toğan, V., Design of planar steel frames using teaching–learning based optimization. Engineering Structures, 34, 225-232 (2012).

[31] Dede, T., Optimum Design of Grillage structures to LRFD-AISC with teaching-learning based optimization. Structural Multidisciplinary Optimization, 48, 955–964 (2013).

[32] Arora, J.S., Introduction to optimum design. Elsevier Academic Press, California (2011).

[33] Wu, S.J. and Chow, P.T., Steady-state genetic algorithms for discrete optimization of trusses. Computers & Structures, 56, 979-991 (1995).

[34] Lemonge, A.C.C. and Barbosa, H.J.C., An adaptive penalty scheme for genetic algorithms in structural optimization. International Journal for Numerical Methods in Engineering, 59, 703–736 (2004).

[35] Capriles, P.V.S.Z., Fonseca, L.G., Barbosa, H.J.C. and Lemonge, A.C.C., Rank-based ant colony algorithms for truss weight minimization with discrete variables. Communications in Numerical Methods in Engineering, 23, 553–575 (2007).

[36] Sadollah, A., Bahreininejad, A., Eskandar, H. and Hamdi, M., Mine blast algorithm for optimization of truss structures with discrete variables. Computers & Structures, 102, 49–63 (2012).

[37] Sadollah, A., Eskandar, H., Bahreininejad, A. and Kim, J.H., Water cycle, mine blast and improved mine blast algorithms for discrete sizing optimization of truss structures. Computers and Structures, 149, 1–16 (2015).

[38] American Institute of Steel Construction Manual of Steel Construction: Load and Resistance Factor Design. 3rd ed. Chicago (2001).

[39] Hasançebi, O., Çarbaş, S., Doğan, E., Erdal, F. and Saka, M.P., Performance evaluation of metaheuristic search techniques in the optimum design of real size pin jointed structures. Computers and Structures, 87, 284–302 (2009).

[40] Kaveh, A. and Talatahari, S., A particle swarm ant colony optimization for truss structures with discrete variables. Journal of Constructional Steel Research, 65, 1558–68 (2009).

***Vedat Toğan*** *received the B.Sc. and M.Sc. degrees in 2000 and 2004 from the Department of Civil Engineering from Karadeniz Technical University, Turkey respectively. He received his Ph.D. degree from the same university in 2009. He is working as an Associate Professor at Civil Engineering Department of Karadeniz Technical University. His research interest includes meta-heuristic algorithms, optimization, reliability analysis, and construction managements.*

***Ali Mortazavi*** *received the B.Sc. and M.Sc. degrees in 2007 and 2010 from the Department of Civil Engineering from Azad University, Iran respectively. He has continued his doctoral studies at Civil Engineering Department of Ege University since 2011. His research interest includes finite element method, optimization, computer programming, and structural behaviors.*



An International Journal of Optimization and Control: Theories & Applications
ISSN: 2146-0957eISSN: 2146-5703
Vol.7, No.2, pp.142-148 (2017)
https://doi.org/10.11121/ijocta.01.2017.00458

RESEARCH ARTICLE

# The road disturbance attenuation for quarter car active suspension system via a new static two-degree-of-freedom design

Yusuf Altun*

*Department of Computer Engineering, Faculty of Engineerig, Duzce University, Turkey*
*yusufaltun@duzce.edu.tr*

ARTICLE INFO

Article history:
*Received: 15 February 2017*
*Accepted: 13 April 2017*
*Available Online: 13 June 2017*

Keywords:
*Active suspension*
*Quarter car*
*The road disturbance rejection*
*feedforward compensation*

AMS Classification 2010:
*37N35, 49N05, 70Q05*

ABSTRACT

The main aim of this paper is to attenuate the effects of the road disturbance on the quarter-car active suspension system (ASS) for the passenger comfort by using design. Therefore, a new static disturbance compensator is proposed by using linear matrix inequality method such that the disturbance compensator and feedback controller are simultaneously designed for the disturbances in the linear time-invariant systems, which are measurable or predictable. They have static structure, and the disturbance compensator is designed on the feedforward path. The design is applied against the road disturbance affecting the quarter car ASS. The effectiveness of the design is demonstrated with the simulations.



## 1. Introduction

Feedforward compensator designs are used for the disturbance rejection or the reference-tracking problem where the external disturbances are measurable or predictable since the designed feedforward element produces an additional control signal according to the measured disturbance values. The disturbance compensator or controller designs to attenuate disturbances are applied to the many chemical and process systems [1-5]. For instance, in [5], a general structure is presented for single-input-single output (SISO) process system. The disturbance compensator/controller designs are used together with a feedback controller [2,3,6-8]. This is why, the feedback controller provides the stability of the system and the disturbance compensator/controller does not affect the stability. In these designs, there are two approaches. The first one: both of these are simultaneously designed as in [1]. The second one: previously the feedback controller is obtained, and then the disturbance compensator/controller is obtained as in [9,10]. In the literature, feedforward designs are proposed by using different approaches for the linear time invariant systems. In view of literature, there are a few studies based on $H_\infty$ approach. The forefront ones among the studies are as in [3,9-12]. In [3], $H_\infty$ dynamic feedforward design is tackled with obtaining the system inverse. In [9], a dynamic controller is obtained for linear parameter varying (LPV) systems. In [10], a static feedforward controller is proposed for LPV systems while there is a feedback controller. In [11], a reduced order $H_\infty$ controller is designed against the disturbances for active vibration system. In [12], the feedforward designs are obtained with mixed-sensitivity based on inverse of system.

A vehicle suspension system comprises of the springs, damper and linkages that link its wheels to a vehicle. Its essential role is to reduce the vertical acceleration conveyed to the vehicle body. Because, this affects the passenger comfort. The vehicle suspension is generally designed to satisfy three requirements, which are road handling, passenger comfort and load carrying. The suspension system must provide the road handling, load carrying and the passenger comfort, which is provided by an efficient isolation of passengers from the road disturbances. The parameters of a passive suspension consisting of springs and dampers are mostly constant, which are chosen to achieve a specific performance level by considering the road handling, ride comfort and load carrying. Therefore, especially the performances are unchangeable during driving. As for an ASS, it can affect the performances of the road handling and ride comfort by introducing energy by adding an actuator to the system. In view of many road

*Corresponding author

inputs or the unevenness of road, the performance of passive suspension is not adequate in contrast to ASS. Thus, the control of ASS is a challenging research topic for the automotive applications in the literature such as [13-15]. In [13], a robust control is made for a quarter-car ASS against the variations on the vehicle body by designing a sliding mode controller with the algebraic estimator for the vehicle body mass. In [14], a fuzzy logic controller is designed to get the desired ride performance under different road profiles corresponding with the quarter-car ASS model. In [15], the control of an electromagnetic ASS with high bandwidth is tackled for a quarter car model. In [16], an adaptive control for vibration rejection is presented in the case of unknown narrow band disturbances in ASS. In [17], the finite-time tracking control with a disturbance compensator is tackled against the external disturbance for ASS. In [18], $H_\infty$ gain-scheduled controller is proposed via convex optimization by using only frequency-domain data. In [19], an output-feedback $H_\infty$ control is proposed for half-vehicle ASS under time-varying input delay. In [20], $H_\infty$ and H2 optimal control are designed to minimize vehicle vibrations and to improve the comfort of passenger exposed to road disturbances for an ASS model. In [21], a static output-feedback controller is designed for a half car ASS with limited information structure to simultaneously improve the ride comfort and stability. In [22], the $H_\infty$ control is designed via dynamic-output feedback approach for active seat suspension systems. In [23], a mathematical model and $H_\infty$ control are proposed to improve the ride comfort with road handling for an ASS which is subjected to different road profiles. In [24], a feedback controller with feedforward controller is proposed to attenuate vibration for discrete-time ASS.

In this paper, a new simultaneous design of static optimal disturbance compensator and static feedback controller is proposed to minimize the road disturbances on the quarter-car ASS. The proposed design is based on $H_\infty$ control technique via linear matrix inequality. The road handling and passenger comfort are improved by adding extra signal to feedback control input thanks to the disturbance compensator.

## 2. Problem formulation and disturbance compensator design

In this section, the control problem is formulated. Eq. (1) defines linear time-invariant generalized system *G* which is generally used $H_\infty$ controller design, where $u(t) \in \mathcal{R}^{n_u}$ is the controller signal, $x(t) \in \mathcal{R}^{n_x}$ are state variables, $z(t) \in \mathcal{R}^{n_z}$ are controlled outputs, $y(t) \in \mathcal{R}^{n_y}$ are the measured outputs, $\omega(t) \in \mathcal{R}^{n_\omega}$ are the disturbance signals.

$$\begin{aligned} \dot{x}(t) &= Ax(t) + B_1\omega(t) + B_2u(t) \\ z(t) &= Cx(t) + D_1\omega(t) + D_2u(t) \\ y(t) &= x(t) \end{aligned} \tag{1}$$

The closed-loop state space model from $\omega(t)$to $z(t)$ becomes as in Eq. (2) when the controller is realized with $u(t)$ for Eq. (1).

$$\begin{aligned} \dot{x}(t) &= A_{cl}x(t) + B_{cl}\omega(t) \\ z(t) &= C_{cl}x(t) + D_{cl}\omega(t) \end{aligned} \tag{2}$$

Figure 1 shows the block diagram of the ASS coupled with the proposed design, where $K_{ff}$ shows disturbance compensator matrix, $K_{fb}$ shows feedback controller, $u_{ff}$ shows the produced control signal of feedforward path, $u_{fb}$ shows the produced control signal of feedback path, $u$ shows the total applied control signals to the system and $\omega$ shows the road disturbance signal to the system. In Section 3, the suspension system is modelled as in Eq. (1).

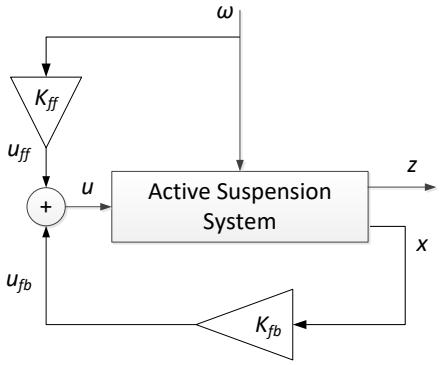


**Figure 1.** The disturbance compensator and feedback control system

As in Figure 1, the control system contains active suspension model, disturbance compensator and feedback components. The proposed disturbance compensator generates a feedforward signal in addition to feedback signal. Thus, ASS provides better performance during online operation against the road disturbance predictable or measurable.

The proposed feedforward matrix $K_{ff}$ and feedback matrix $K_{fb}$, which have static structure, are simultaneously designed by using $H_\infty$ control technique based on linear matrix inequality. Accordingly, Lemma 1 is known as bounded real lemma in the literature, and it is commonly used for $H_\infty$ control design.

**Lemma 1**. *Let* $G(s) = C_{cl}\left(sI - A_{cl}\right)^{-1}B_{cl} + D_{cl}$ *be transfer matrix of the closed loop system Eq. (2). If and only if* $\gamma^2 I - D_{cl}^T D_{cl} \succ 0$ . $\left\|G(s)\right\|_\infty \prec \gamma$ *and the following states are equivalent.*

*a. If there exists a positive symmetric matrix* $P \in \Re^{n\times n}$, *the following inequality holds.*

$$\begin{aligned} &A^TP + PA \\ &+\left(B^TP + D^TC\right)^T\left(\gamma^2 I - D^TD\right)^{-1}\left(B^TP + D^TC\right) \\ &+C^TC \prec 0 \end{aligned}$$

b. *If there exists a positive symmetric matrix* $P \in \Re^{n\times n}$, *the linear matrix inequality (3) holds.*

$$\begin{bmatrix} A_{cl}^T P + P A_{cl} & P B_{cl} & C_{cl}^T \\ B_{cl}^T P & -\gamma I & D_{cl}^T \\ C_{cl} & D_{cl} & -\gamma I \end{bmatrix} \prec 0 \tag{3}$$

***Proof.*** See [25].

In the literature, the matrix inequality in the Theorem 1 based on Lemma 1 is commonly used for the static state feedback $H_\infty$ controller.

**Theorem 1.** *If there exist a symmetric positive Q in (4) and a matrix R, there exists a static feedback controller* $u(t) = Kx(t)$, *which stabilizes the system in Eq. (1).Thus, the optimal* $H_\infty$ *controller is obtained from* $K = RQ^{-1}$.

$$\begin{bmatrix} AQ + QA^T + B_2 R + R^T B_2^T & B_1 & QC^T + R^T D_2^T \\ B_1^T & -\gamma I & D_1^T \\ CQ + D_2 R & D_1 & -\gamma I \end{bmatrix} \prec 0 \tag{4}$$

***Proof.*** See [25].

**Remark 1.** As in the theorem, the present form is already appropriate in order to optimize the effects of the disturbances $\omega(t)$ to the outputs $z(t)$ for the system in (1). However, it is known that the feedback controller is here designed by considering potential disturbances. However, in the design of this paper, the proposed disturbance compensator works at minimizing their effects on the outputs according to the online measured or estimated disturbances by including an additional control signal on the feedback controller. In addition, disturbance compensator together is simultaneously designed with feedback controller for the disturbance rejection. Theorem 2 presents the proposed disturbance compensator and feedback controller design of the problem in Figure 1.

**Theorem 2**: *If there exist a symmetric positive Y in (5) and a matrix F, there exists a static feedback controller* $u_{fb}(t) = K_{fb}x(t)$, *which stabilizes the system in Eq. (1), and a static disturbance compensator* $u_{ff}(t) = K_{ff}\omega(t)$, *which attenuates the disturbances. In this case, the optimal* $H_\infty$ *controller and disturbance compensator are computed by (6).*

$$\begin{bmatrix} AY + B_2 F + (*)^T & B_1 + B_2 K_F & YC^T + F^T D_2^T \\ B_1^T + K_F^T B_2^T & -\gamma I & D_1^T + K_F^T D_2^T \\ CY + D_2 F & D_1 + D_2 K_F & -\gamma I \end{bmatrix} \prec 0 \tag{5}$$

$$\begin{aligned} K_{fb} &= FY^{-1} \\ K_{ff} &= K_F \end{aligned} \tag{6}$$

***Proof.*** Considering the control system in Figure 1, the controller signal is as in Eq. (7).

$$u(t) = \begin{bmatrix} K_{ff} & K_{fb} \end{bmatrix} \begin{bmatrix} \omega(t) \\ x(t) \end{bmatrix} \tag{7}$$

If Eq. (7)is substituted into (1), the closed loop system from $\omega(t)$ to $z(t)$in Eq. (2) becomes as in Eq. (8).

$$\begin{bmatrix} \dot{x}(t) \\ z(t) \end{bmatrix} = \begin{bmatrix} A + B_2 K_{fb} & B_1 + B_2 K_{ff} \\ C + D_2 K_{fb} & D_1 + D_2 K_{ff} \end{bmatrix} \begin{bmatrix} x(t) \\ \omega(t) \end{bmatrix} \tag{8}$$

The state space matrices are as in (9) according to Eq. (8).

$$\begin{aligned} A_{cl} &= A + B_2 K_{fb},\ B_{cl} = B_1 + B_2 K_{ff} \\ C_{cl} &= C + D_2 K_{fb},\ D_{cl} = D_1 + D_2 K_{ff} \end{aligned} \tag{9}$$

When the obtained closed loop matrices are substituted into (3) in Lemma 1, the matrix inequality (10) is obtained.

$$\begin{bmatrix} PA + PB_2 K_{fb} + (*)^T & * & * \\ B_1^T P + K_{ff}^T B_2^T P & -\gamma I & * \\ C + D_2 K_{fb} & D_1 + D_2 K_{ff} & -\gamma I \end{bmatrix} \prec 0 \tag{10}$$

Nevertheless, the inequality is not linear due to the products of unknown matrices. In order to linearize, it is pre- and post-multiplied with the matrix in (11) and its transpose respectively, and so the linear matrix inequality (5)is acquired.

$$\begin{bmatrix} P^{-1} & 0 & 0 \\ 0 & I & 0 \\ 0 & 0 & I \end{bmatrix} \tag{11}$$

The definitions of variables are as in Eq. (12) with regard to the linear matrix inequality (5).

$$Y = P^{-1},\ F = K_{fb}Y^{-1},\ K_F = K_{ff} \tag{12}$$

## 3. Quarter car active suspension system model

Figure 2 shows a quarter car ASS model which is one fourth of full vehicle model (one wheel system), where $m_1$ is one fourth of vehicle body mass (sprung mass), $m_2$ is suspension mass (usprung mass - tire and axles), $k_1$ is suspension spring constant, $k_2$ is spring constant of wheel and tire, $b_1$ is suspension damping constant, $b_2$ is damping constant of wheel and tire, $u$ is generating external force. The tire is modelled as a linear spring having a stiffness constant $k_2$. The suspension system consists of a passive spring $k_1$ and a damper $b_1$ in parallel with an active control element actuator generating a force $u$. These passive elements assure a minimum standard of safety and performance, whereas the active one is designed to improve the safety and performance. Hence, the model is a quarter car ASS model where an actuator generating the control force $u$ is included to the passive one in order to improve the

safety and comfort performance for different road disturbances.

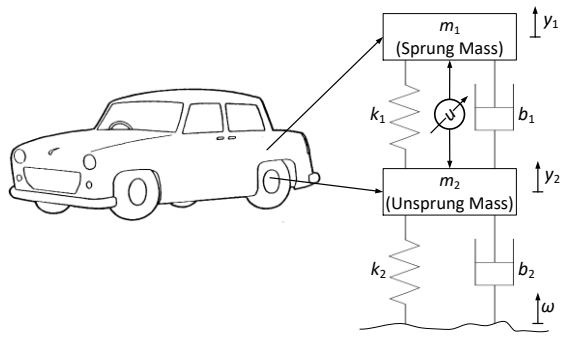


**Figure 2.** The quarter car ASS

The differential equations are obtained as in (13) by using Newton's law according to Figure 2.

$$\begin{aligned} m_1\ddot{y}_1 &= u - k_1(y_1 - y_2) - b_1(\dot{y}_1 - \dot{y}_2) \\ m_2\ddot{y}_2 &= -u + k_1(y_1 - y_2) + b_1(\dot{y}_1 - \dot{y}_2) \\ &+ k_2(\omega - y_2) + b_2(\dot{\omega} - \dot{y}_2) \end{aligned} \tag{13}$$

The state space model is needed for the controller design. Accordingly, if the states $x$ are defined as $x_1 = y_1,\ x_2 = \dot{y}_1,\ x_3 = y_1 - y_2,\ x_4 = \dot{y}_1 - \dot{y}_2$ and we define integral action state $x_5 = \int y_1 - y_2$, the state space model is obtained as in (14) where the state space matrices are as in (15) and (16).

$$\begin{aligned} \dot{x}(t) &= Ax(t) + B_1\omega(t) + B_2u(t) \\ z(t) &= Cx(t) + D_1\omega(t) + D_2u(t) \end{aligned} \tag{14}$$

$$A = \begin{bmatrix} 0 & 1 & 0 & 0 & 0 \\ \dfrac{-(b_1b_2)}{(m_1m_2)} & 0 & \left(\dfrac{b_1}{m_1}\right)\left[\left(\dfrac{b_1}{m_1}\right)+\left(\dfrac{b_1}{m_2}\right)+\left(\dfrac{b_2}{m_2}\right)\right]-\left(\dfrac{k_1}{m_1}\right) & -\left(\dfrac{b_1}{m_1}\right) & 0 \\ \dfrac{b_2}{m_2} & 0 & -\left(\dfrac{b_1}{m_1}+\dfrac{b_1}{m_2}+\dfrac{b_2}{m_2}\right) & 1 & 0 \\ \dfrac{k_2}{m_2} & 0 & -\left(\dfrac{k_1}{m_1}+\dfrac{k_1}{m_2}+\dfrac{k_2}{m_2}\right) & 0 & 0 \\ 0 & 0 & 1 & 0 & 0 \end{bmatrix} \tag{15}$$

$$B_1 = \begin{bmatrix} 0 \\ \dfrac{b_1b_2}{m_1m_2} \\ -\dfrac{b_2}{m_2} \\ -\dfrac{k_2}{m_2} \\ 0 \end{bmatrix}, B_2 = \begin{bmatrix} 0 \\ \dfrac{1}{m_1} \\ 0 \\ \dfrac{1}{m_1}+\dfrac{1}{m_2} \\ 0 \end{bmatrix},$$

$$C = \begin{bmatrix} \dfrac{-(b_1b_2)}{(m_1m_2)} & 0 & \left(\dfrac{b_1}{m_1}\right)\left[\left(\dfrac{b_1}{m_1}\right)+\left(\dfrac{b_1}{m_2}\right)+\left(\dfrac{b_2}{m_2}\right)\right]-\left(\dfrac{k_1}{m_1}\right) & -\left(\dfrac{b_1}{m_1}\right) & 0 \\ 1 & 0 & -1 & 0 & 0 \end{bmatrix} \tag{16}$$

$$D_1 = \begin{bmatrix} \dfrac{b_1b_2}{m_1m_2} \\ -1 \end{bmatrix},\ D_2 = \begin{bmatrix} \dfrac{1}{m_1} \\ 0 \end{bmatrix}$$

## 4. Simulation results

The simulation results are acquired via Matlab with Yalmip parser [26] and Sedumi solver [27]. Figure 3 shows the simulation block diagram for the system. In addition, the ASS parameters are as in Table 1for the simulation.

**Table 1.** ASS parameters.

| parameter | value | unit |
|---|---|---|
| $m_1$ | 320 | kg |
| $m_2$ | 45 | kg |
| $k_1$ | 27000 | N/m |
| $k_2$ | 211180 | N/m |
| $b_1$ | 935 | N.s/m |
| $b_2$ | 20 | N.s/m |

In this case, the obtained state space matrices are as in (17).

$$A=\begin{bmatrix} 0 & 1 & 0 & 0 & 0 \\ -1.2986 & 0 & -13.829 & -2.9219 & 0 \\ 0.44444 & 0 & -24.144 & 1 & 0 \\ 4692.9 & 0 & -5377.3 & 0 & 0 \\ 0 & 0 & 1 & 0 & 0 \end{bmatrix},$$

$$B_1=\begin{bmatrix} 0 \\ 1.2986 \\ -0.44444 \\ -4692.9 \\ 0 \end{bmatrix},\quad B_2=\begin{bmatrix} 0 \\ 0.003125 \\ 0 \\ 0.025347 \\ 0 \end{bmatrix}, \qquad (17)$$

$$C=\begin{bmatrix} 1.2986 & 0 & -13.829 & -2.9219 & 0 \\ 1 & 0 & -1 & 0 & 0 \end{bmatrix},$$

$$D_1=\begin{bmatrix} 1.2986 \\ -1 \end{bmatrix},\quad D_2=\begin{bmatrix} 0.003125 \\ 0 \end{bmatrix}$$

In addition, the obtained classic $H_\infty$ controller matrix is $K$=[207.34 -514.74 4448.6 933.5 -0.0081947] whereas the proposed controller matrix with compensator is $K$=[212.26 -508.11 4450 933.9 -0.0078739 -574.68].

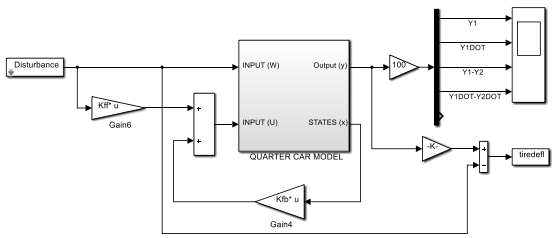


**Figure 3.** The simulation block diagram for the control of quarter-car ASS

The road disturbance is given in Figure 4. According to the simulation, the results are as in Figure 5-8. Figure 5 shows the vehicle body displacements, Figure 6 shows the wheel deflections, Figure 7 shows the car body accelerations, Figure 8 shows the applied control forces.

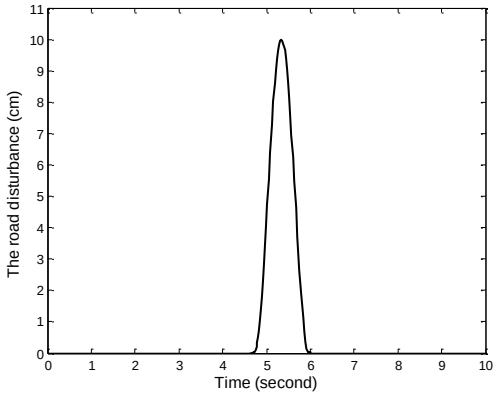


**Figure 4.** The road disturbance

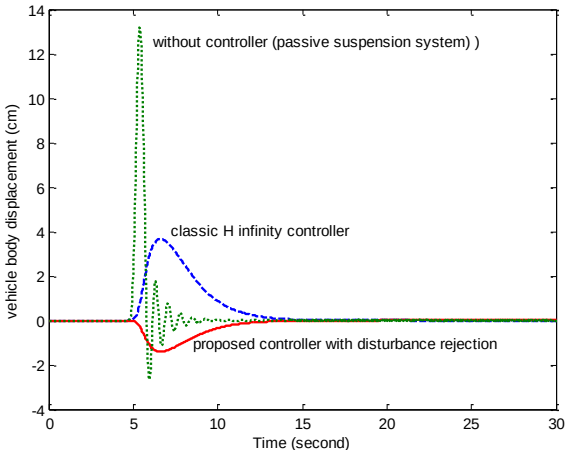


**Figure 5.** The vehicle body displacement

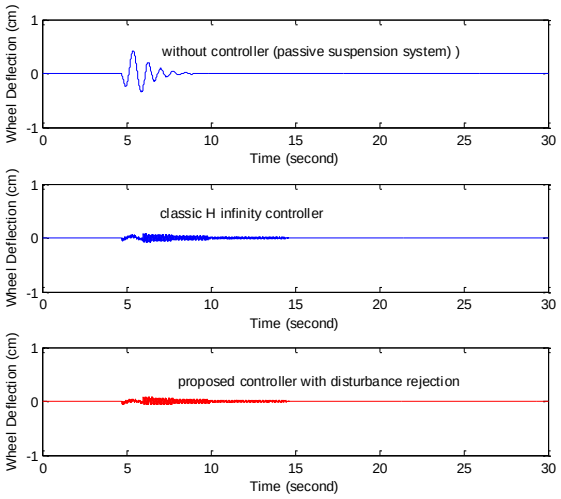


**Figure 6.** The wheel deflection

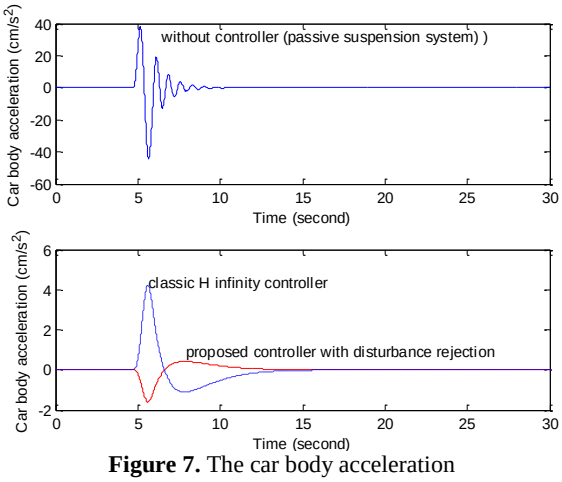


**Figure 7.** The car body acceleration

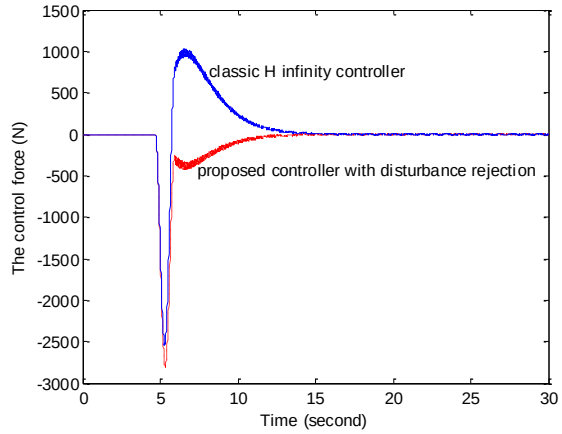


**Figure 8.** The control force

As shown in Figure 5, the peak vehicle displacement is nearly 3.8 cm when the classic $H_\infty$ controller is applied to the system. However, the value is nearly -1.5 cm for the proposed design and so the proposed design has a better response.In addition, the vehicle displacement negatively changes since the control force generating by adding the feedforward one to the feedback control force is negative as shown in Figure 8. The wheel deflections, which directly affect the road safety, are almost same for both control designs as shown in Figure 6. In view of the vehicle body accelerations, which directly affect the passenger comfort, the proposed design is quite successful as shown in Figure 7. The peak value for classic one is nearly 4.1 whereas the value for the proposed one is nearly -1.5, and so the system becomes more comfortable by the proposed design. The applied total control force of the proposed disturbance compensator controller is as shown in Figure 8 in order to acquire the successes. Hence, the proposed approach has better results than the classic one for the ASS control system in point of the road comfort.

## 5. Conclusion

This paper shows that a new static disturbance rejection design for the ASS of quarter vehicle model. The disturbance compensator and state feedback controller are simultaneously designed for the disturbance rejection with respect to passenger comfort. The proposed design is based on optimal $H_\infty$ control method via linear matrix inequality. The simulations have shown that the proposed design has better performance according to classic state feedback $H_\infty$ control against the road disturbance with regard to the passenger comfort. In addition, the design can be used for other dynamic systems, which are multi-input-multi output.

## References

[1] Adam, E. J. and Marchetti, J. L., Designing and tuning robust feedforward controllers, *Computers and Chemical Engineering*, 28(9) 1899–1911 (2004).

[2] Méndez-Acosta, H. O., Campos-Delgado, D. U., Femat, R. and González-Alvarez, V., A robust feedforward/feedback control for an anaerobic digester, *Computers & Chemical Engineering*, 29 (7), 1613–1623 (2005).

[3] Peng, C., Zhang, Z., Zou, J., Li, K. and Zhang, J., Internal model based robust inversion feedforward and feedback 2DOF control for LPV system with disturbance, *Journal of Process Control*, 23, (10), 1415–1425 (2013).

[4] Guzmán, J. L., Hägglund, T., Veronesi, M. and Visioli, A., Performance indices for feedforward control, *Journal of Process Control*, 26, 26–34, (2015).

[5] Rodríguez, C., Normey-Rico, J. E., Guzmán, J. L. and Berenguel, M., On the filtered Smith predictor with feedforward compensation, *Journal of Process Control*, 41, 35–46, (2016).

[6] Graichen, K., Treuer, M. and Zeitz, M., Swing-up of the double pendulum on a cart by feedforward and feedback control with experimental validation, *Automatica*, 43(1), 63–71 (2007).

[7] Jin, N., Wang, X., Gao, H. and Liu, J., Sliding mode based speed regulating of PMSM MTPA control system for electrical vehicles, in *Electronic and Mechanical Engineering and Information Technology (EMEIT), 2011 International Conference on*, 2, 987–992 (2011).

[8] Babazadeh, M. and Karimi, H., A robust two-degree-of-freedom control strategy for an islanded microgrid, *IEEE Transactions on Power Delivery*, 28(3), 1339–1347 (2013).

[9] Altun, Y. and Gulez, K., Linear parameter varying feedforward control synthesis using parameter-dependent Lyapunov function, *Nonlinear Dynamics*, 78(4), 2293–2307 (2014).

[10] Altun, Y., Gulez, K. and Mumcu, T. V., Static LPV feedforward controller synthesis for Linear Parameter Varying systems, *Control Conference (ASCC), 9th Asian*. 1–4 (2013).

[11] Alma, M., Martinez, J. J., Landau, I. D. and Buche, G., Design and Tuning of Reduced Order H-Infinity Feedforward Compensators for Active Vibration Control, *IEEE Transactions on Control Systems Technology*, 20(2), 554–561 (2012).

[12] Zhang, J., Xu, H., Zou, Q. and Peng, C., Inversion-based robust feedforward–feedback two-degree-of-freedom control approach for multi-input multi-output systems with uncertainty, *IET Control Theory*

*& Applications*, 6(14), 2279–2291 (2012).
[13] Alvarez-Sánchez, E., A Quarter-Car Suspension System: Car Body Mass Estimator and Sliding Mode Control, *Procedia Technology*, 7, 208–214 (2013).
[14] Foda, S. G., Fuzzy control of a quarter-car suspension system, in *Proceedings of the International Conference on Microelectronics, ICM*, vol. 2000–October, 231–234 (2000).
[15] Van Der Sande, T. P. J., Gysen, B. L. J., Besselink, I. J. M., Paulides, J. J. H., Lomonova, E. A. and Nijmeijer, H., Robust control of an electromagnetic active suspension system: Simulations and measurements, *Mechatronics*, 23(2), 204–212 (2013).
[16] Chen, X. and Tomizuka, M., Selective model inversion and adaptive disturbance observer for time-varying vibration rejection on an active-suspension benchmark, *European Journal of Control*, 19(4), 300–312 (2013).
[17] Pan, H., Jing, X. and Sun, W., Robust finite-time tracking control for nonlinear suspension systems via disturbance compensation, *Mechanical Systems and Signal Processing*, 88, 49–61 (2017).
[18] Karimi, A. and Emedi, Z., $H_\infty$ gain-scheduled controller design for rejection of time-varying narrow-band disturbances applied to a benchmark problem, *European Journal of Control*, 19(4), 279–288 (2013).
[19] Choi, H. D., Ahn, C. K., Lim, M. T. and Song, M. K., Dynamic output-feedback $H_\infty$ control for active half-vehicle suspension systems with time-varying input delay, *International Journal of Control, Automation and Systems*, 14(1), 59–68 (2016).
[20] Shukla, P., Ghodki, D., Manjarekar, N. S., and Singru, P. M., A Study of H infinity and H2 synthesis for Active Vibration Control, *IFAC-PapersOnLine*, 49(1), 623–628 (2016).
[21] Wang, G., Chen, C. and Yu, S., Optimization and static output-feedback control for half-car active suspensions with constrained information, *Journal of Sound and Vibration*, 378, 1–13 (2016).
[22] Sun, W., Li, J., Zhao, Y. and Gao, H., Vibration control for active seat suspension systems via dynamic output feedback with limited frequency characteristic, *Mechatronics*, 21(1), 250–260 (2011).
[23] Ghazaly, N. M., Ahmed, A. E. N. S., Ali, A. S. and El-Jaber, G. T. A., $H_\infty$ control of active suspension system for a quarter car model, *International Journal of Vehicle Structures and Systems*, 8(1), 35–40 (2016).
[24] Han, S. Y., Chen, Y. H., Ma, K., Wang, D., Abraham, A. and Liu, Z. G., Feedforward and feedback optimal vibration rejection for active suspension discrete-time systems under in-vehicle networks, in *2014 6th World Congress on Nature and Biologically Inspired Computing, NaBIC 2014*, 139–144 (2014).
[25] Boyd, S. P., El Ghaoui, L., Feron, E. and Balakrishnan, V., *Linear matrix inequalities in system and control theory*, 15th SIAM (1994).
[26] Löfberg, J., Automatic robust convex programming, *Optimization Methods and Software*, 27(1), 115–129 (2012).
[27] Labit, Y., Peaucelle, D. and Henrion, D., SEDUMI INTERFACE 1.02: A tool for solving LMI problems with SEDUMI, in *2002 IEEE International Symposium on Computer Aided Control System Design, CACSD 2002 - Proceedings*, 272–277 (2002).

***Dr. Yusuf Altun*** *received the Doctoral degree in Electrical Engineering from Yildiz Technical University, Istanbul, Turkey in 2012. He has worked as Assistant Professor at the Duzce University, in Department of Computer Engineering, Duzce, in Turkey since 2013. His main research interests are in areas of the control of mechatronic systems such as vehicle, humanoid robot, and electromechanical systems.*



An International Journal of Optimization and Control: Theories & Applications
ISSN: 2146-0957 eISSN: 2146-5703
Vol.7, No.2, pp.149-157 (2017)
https://doi.org/10.11121/ijocta.01.2017.00462

RESEARCH ARTICLE

# Determination of optimum insulation thicknesses using economical analyse for exterior walls of buildings with different masses

Okan KON*

*Department of Mechanical Engineering, Balikesir University, Turkey*
*okan@balikesir.edu.tr*

ARTICLE INFO

Article history:
*Received: 15 March 2017*
*Accepted: 12 June 2017*
*Available Online: 05 July 2017*

Keywords:
*Building mass*
*Optimization*
*Thermal insulation*
*Lifecycle cost analysis*
*Degree-day method*

AMS Classification 2010:
*80A05, 80A20*

ABSTRACT

In this study, five different cities were selected from the five climatic zones according to Turkish standard TS 825, and insulation thicknesses of exterior walls of sample buildings were calculated by using optimization. Vertical perforated bricks with density of 550 kg/m$^3$ and 1000 kg/m$^3$werechosen within the study content. Glass wool, expanded polystyrene (XPS), extruded polystyrene (EPS) were considered as insulation materials. Additionally, natural gas, coal, fuel oil and LPG were utilized as fuel for heating process while electricity was used for cooling. Life cycle cost (LCC) analysis and degree-day method were the approaches for optimum insulation thickness calculations. As a result, in case of usage vertical perforated bricks with density of 550 kg/m$^3$ and 1000 kg/m$^3$ resulted different values in between 0.005-0.007 m (5-7 mm) in the optimum insulation thickness calculations under different insulation materials. Minimum optimum insulation thickness was calculated in case XPS was preferred as insulation material, and the maximum one was calculated in case of using glass wool.



## 1. Introduction

Heat insulation is the most important pillar of the developed policies about the concept of energy efficiency all over the world. The fact that the housing and building sector in Turkey consumes about 30-35% of the total energy and has a great saving potency increased the interest in the sectoral manner [1].

In heat insulation applications, energy loss and air pollution can be reduced by increasing the thickness of insulation material. However, it may be neither economical nor practical to use increasingly large amounts of insulation so as to achieve energy savings. A balance should be established between the insulation investment and the savings to be provided from the insulated building. The best insulation thickness is considered as mentioned balance. The insulation thickness, which provides the minimum insulation and operating costs for a given economic lifetime is called the optimal insulation thickness [2].

When the studies existed in the literature were examined, the optimum insulation thickness was calculated for the exterior walls of the building. To realize it, fuels such as natural gas, coal, fuel-oil, LPG, electricity and a wide range of insulating materials are used. Optimization calculations are made using the degree-day method and lifecycle cost analysis (LCC) for heating, cooling and both heating and cooling of buildings [1,3-8]. On the other hand, in some studies, the degree-day method and the economic model of P1-P2 were used as the optimization method [9-14]. In the study of Ucar [15], the optimum insulation thickness was found using exergoeconomic analysis considering the condensation of the insulation in the outer walls. In four climate characteristics dominated in four cities of Turkey, optimum insulation thicknesses were performed. Polystyrene is considered as insulation and coal as fuel. Nyers et al. [16] analyzed the optimum energy-economical thickness of the thermal insulation layers for the exterior walls of the building. The economic model is composed of energy and economic sections. The economic part of the model includes algebraic equations, investment, savings and usage periods. In the study of Kaynakli [17], heating and cooling degree-days, building life, inflation and interest rate, insulation material price, fuel price, external wall resistance, thermal conductivity value of insulating

*Corresponding author

material, heating and cooling system efficiencies and solar radiation parameters were examined for optimum insulation thickness.

The purpose of this study is to calculate the insulation thicknessesby using optimization in the outer walls of sample buildings with different mass for five different cities in five climatic zones according to Turkish Standard TS 825. For different mass, vertical perforated brick with a thermal conductivity value of 0.32 W/m.K with a density of 550 kg/m$^3$, and a thermal conductivity value of 0.45 W/m.K with a density of 1000 kg/m$^3$ are considered. Optimum insulation thickness is the value that makes the total costs minimum for heating, cooling and heating+cooling. Glass wool, expanded polystyrene (XPS), extruded polystyrene (EPS) are considered as insulation materials. Also natural gas, coal, fuel oil, LPG are used as fuel for heating process while electricity is used for cooling. Lifecycle cost (LCC) analysis and degree-day method are used for optimum insulation thickness calculations. For optimum insulation thickness calculations, only heating case, only cooling case and both heatingplus cooling cases are considered.

## 2. Material and method

### 2.1. Total cost for heating, cooling and heating + cooling

Heat loss per unit area of the exterior wall of a building is computed as follows:

$$q = U(T_i - T_d) \tag{1}$$

Annual heat loss per unit area based upon degree-day concept is computed by the following equation.

$$q = 86400.DD.U \tag{2}$$

The total heat transfer coefficient for the wall is given by Equation 3, while the total thermal resistance for the uninsulated wall is determined according to Rt, w and the total heat transfer coefficient of the wall is obtained through Equation 4.

$$U = \frac{1}{\left(R_i + R_w + (x/k) + R_d\right)} \tag{3}$$

$$U = \frac{1}{\left(R_{t,w} + (x/k)\right)} \tag{4}$$

Here, Ri and Ro are internal and external thermal resistances. x is the insulation thickness. k is the thermal conductivity coefficient of the insulation material.

Heating fuel cost is computed as follows:

$$C_{A,H} = \left(\frac{86400.PWF.C_f.HDD}{(R_{t,w} + x/k).H_u.\eta}\right) \tag{5}$$

Total heating cost; the addition of insulation cost and the cost of fuel is:

$$C_{t,H} = \left(\frac{86400.PWF.C_f.HDD}{(R_{t,w} + x/k).H_u.\eta}\right) + \left(C_{ins}.x\right) \tag{6}$$

If the derivation of the total heating cost equations (insulation thickness) x is equal to zero, the optimum insulation thickness equation is obtained for the heating given below.

$$x_{opt,,H} = 293.94.\left(\frac{HDD.C_f.k.PWF}{H_u.C_{ins}.\eta}\right)^{1/2} - k.R_{t,w} \tag{7}$$

Cooling fuel cost is:

$$C_{A,C} = \left(\frac{86400.PWF.C_e.CDD}{(R_{t,w} + x/k).COP}\right) \tag{8}$$

Total cooling cost; the addition of insulation cost and the fuel cost is:

$$C_{t,C} = \left(\frac{86400.PWF.C_e.CDD}{(R_{t,w} + x/k).COP}\right) + \left(C_{ins}.x\right) \tag{9}$$

If the derivative of total cooling cost equations (insulation thickness) x is equal to zero, the optimum insulation thickness equation for cooling given below is obtained.

$$x_{opt,C} = 293.94.\left(\frac{CDD.C_e.k.PWF}{C_{ins}.COP}\right)^{1/2} - k.R_{t,w} \tag{10}$$

The total fuel cost for heating + cooling is the sum of heating and cooling fuel costs:

$$C_{A,H,C} = \left(\frac{86400.PWF.C_f.HDD}{(R_{t,w} + x/k).H_u.\eta} + \frac{86400.PWF.C_e.CDD}{(R_{t,w} + x/k).COP}\right) \tag{11}$$

Total cost is the sum of heating and cooling costs and insulation cost.

$$C_{t,H,C} = \left( \frac{86400.PWF.C_f.HDD}{(R_{t,w} + x/k).H_u.\eta} + \frac{86400.PWF.C_e.CDD}{(R_{t,w} + x/k).COP} \right) + (C_{ins}.x) \quad (12)$$

$$x_{opt,H,C} = 293.94.\left( \frac{HDD.C_f.k.PWF}{H_u.C_{ins}.\eta} + \frac{CDD.C_e.k.PWF}{C_{ins}.COP} \right)^{1/2} - k.R_{t,w} \quad (13)$$

If the derivative of the total cost equation (insulation thickness) x is equal to zero, the optimum insulation thickness equation is obtained for heating pluscooling that is given below [1,3,7,10,12,13,17,18].

Here, $H_u$ is the lower temperature value, η is heating system efficiency, COP is cooling performance value, k is insulation material heat conductivity coefficient, $C_f$ is fuel price, $C_e$ is electricity price, $C_{ins}$ is insulation material price, HDD and CDD are heating and cooling degree-day values, respectively.

LCC analysis is performed for optimum insulation thickness calculation.The total heating cost is evaluated by the present worth factor (PWF) for the N year lifetime [8]. The present worth factor is calculated as follows [8,19];

$$PWF = \frac{(1+r)^N - 1}{r.(1+r)^N} \quad (14)$$

If i> g; then the actual interest rate is,

$$r = \frac{i-g}{1+g} \quad (15)$$

If i<g then;

$$r = \frac{g-i}{1+i} \quad (16)$$

If i=g then;

$$PWF = \frac{N}{1+i} \quad (17)$$

**2.2. Values used in calculations**

The outer wall structures and heat transfer coefficients are given in Table 1. Table 2 shows heating and cooling degree-day values for cities in five different climatic regions. The basic temperature was selected to be 19.5 $^0$C for heating and 22 $^0$C for cooling.Table 3 shows fuels used for heating. The electricity price and cooling performance value (COP) value used for cooling are shown in Table 4. The insulation materials and properties used on the outer walls were given in Table 5. In addition, financial values including inflation and interest rates were given in Table 6.

**Table 1.** External wall building components andheat conduction coefficients [18].

| Thickness | Component | Value |
|---|---|---|
| | $R_i$ (Internal film thermal resistance) | 0.130 $m^2$.K/W |
| 0.030 m | Lime mortar-cement mortar internal plaster | 1.000 W/m.K |
| 0.190 m | Vertical Perforated Brick | 0.32 ve 0.45 W/m.K |
| x m | Insulation | $k_{ins}$ W/m.K |
| 0.030 m | Cement mortar outer plaster | 1.600 W/m.K |
| | $R_d$ (External film thermal resistance) | 0.040 $m^2$.K/W |

In the study, the effect of using bricks of different density on the insulation thickness was investigated. In addition, it is suggested that heating and cooling periods should be considered together while insulating buildings are prevealing for hot climate zones.

**Table 2.** Heating and Cooling Degree-days for different climate zones in cities [20].

| Climate Zones | City | Heating Degree-days | Cooling Degree-days | Latitude | Longitude | Elevation (m) |
|---|---|---|---|---|---|---|
| 1 | İzmir | 1480 | 617 | 38.43 | 27.17 | 28.55 |
| 2 | Balıkesir | 2312 | 369 | 39.65 | 27.87 | 147.00 |
| 3 | Konya | 3162 | 275 | 37.87 | 32.48 | 1028.59 |
| 4 | Sivas | 3643 | 171 | 39.75 | 37.02 | 1285.00 |
| 5 | Kars | 4770 | 96 | 40.62 | 43.10 | 1775.00 |

**Table 3.** Fuels and properties[21].

| Fuel | Price | Lower thermal value ($H_u$) | Heating system efficiency($\eta_s$) |
|---|---|---|---|
| Natural Gas | 0.3601 \$/m$^3$ | 34.526 $10^6$J/m$^3$ | 0.93 |
| Coal | 0.2216 \$/kg | 29.295 $10^6$J/kg | 0.65 |
| Fuel-oil | 0.7340 \$/kg | 40.594 $10^6$J/kg | 0.80 |
| LPG | 1.6411 \$/kg | 46.453 $10^6$J/kg | 0.90 |

**Table 4.**Electricity price and cooling COP [9,22].

| Parameter | Value |
|---|---|
| Price | 0.174 \$/kWh |
| Cooling COP | 2.5 |

**Table 5.** Insulation materials and properties [3].

| Insulation Materials | k (W/m.K) | $C_{ins}$ (\$/m$^3$) |
|---|---|---|
| Glass wool | 0.040 | 75 |
| Expanded polystyrene (EPS) | 0.039 | 120 |
| Ekstrüde polystyrene (XPS) | 0.031 | 180 |

**Table 6.** Financial values [3].

| Financial Values | Value |
|---|---|
| **Interest rate, (i)** | % 8.25 |
| **Inflation rate, (g)** | % 7.91 |
| **Lifecycle time, N** | 10 yıl |
| **PWF** | 9.83 |

## 3. Results

In Figure 1, cost curves of optimum insulation thickness for a) heating period b) cooling period c) heating plus cooling period for Izmir city in case of vertical perforated brick with density of 550 kg/m$^3$ and thermal conductivity of 0.32 W/m.K, glass wool as insulation material and natural gas as fuel usage. Figure 2 shows the results of cost curves for optimum insulation thickness a) heating period b) cooling period c) heating plus cooling period for Kars city in case of vertical perforated brick with density of 1000 kg/m$^3$ and thermal conductivity of 0.45 W/m.K, XPS as insulation material, and coal as fuel usage. Table 7 shows the optimum insulation thickness because of various fuel and insulation materials usage for vertical perforated brick with 550 kg/m$^3$ density and 0.32 W/m.K heat conduction in the heating period. Table 8 represents the optimum insulation thickness due to various fuel and insulation materials usage for vertical perforated brick with 1000 kg/m$^3$ density and 0.45 W/m.K heat conduction in the heating period. In Table 9, the optimum insulation thickness due to various fuel and insulation materials usage for vertical perforated brick with 550 kg/m$^3$ density and 0.32 W/m.K heat conduction in the cooling period. In Table 10, the optimum insulation thickness due to various fuel and insulation materials usage for vertical perforated brick with 1000 kg/m$^3$ density and 0.45 W/m.K heat conduction in the cooling period. Table 11 shows the optimum insulation thickness due to various fuel and insulation materials usage for vertical perforated brick with 550 kg/m$^3$ density and 0.32 W/m.K heat conduction in the heating+cooling period. Table 12 represents the optimum insulation thickness due to various fuel and insulation materials usage for vertical perforated brick with 1000 kg/m$^3$ density and 0.45 W/m.K heat conduction in the heating+cooling period.

## 4. Discussion

During the heating period, in case of vertical perforated brick with a density of 550 kg/m$^3$ usage, the optimum insulation thickness range in different fuel and insulation materials are as follows; 0.024-0.130 m in Izmir, 0.036-0.170 m in Balıkesir, 0.047-0.221 m in Konya, 0.052-0.222 m in Sivas, and 0.063-0.259 m in Kars. On the other hand, these results during the cooling period are; 0.017-0.041 m in Izmir, 0.000-0.024 m in Balıkesir, 0.000-0.017 m Konya, while it was found that the optimum economic choice for Sivas and Kars was not to use insulation Besides, in the heating plus cooling period; results are found to be 0.039-0.146 m in Izmir, 0.044-0.178 m observed in Balıkesir, 0.052-0.226 m observed in Konya, 0.055-0.225 m in Sivas and 0.065-0.260 m observed in Kars.

During the cooling period, in case of vertical perforated brick with a density of 1000 kg/m$^3$ usage, the optimum insulation thickness range in different fuel and insulation materials are as follows; 0.029-0.136 m in Izmir , 0.042-0.177 m in Balıkesir, 0.052-0.228 m in Konya, 0.057-0.229 m in Sivas , 0.069 -0.266 m in Kars. In the cooling period, 0.022-0.048 m in Izmir, 0.012-0.031 m in Balıkesir, 0.000-0.023 m in Konya and 0.000-0.013 m in Sivas and It was found that the optimum economic choice for Kars was not to use insulation. And finally, in the heating + cooling period, 0.044-0.152 m in Izmir, 0.050-0.185 m in Balıkesir, 0.057-0.233 m in Konya, 0.061-0.232 m in Sivas and 0.070-0.267 m in Kars.

When vertical hole bricks are used in the external walls of the example building at 550 kg/m$^3$ and 1000 kg/m$^3$ density, the lower optimum thickness of insulation is calculated at the low density brick refering 550 kg/m$^3$ for all provinces.

In the literature studies, bricks of different density are used. In general, high-density bricks are used. This affects the insulation thickness. As shown in this study, when using low density bricks, the insulation thickness is lower. This is also very important factor in terms of cost and additional workmanship.

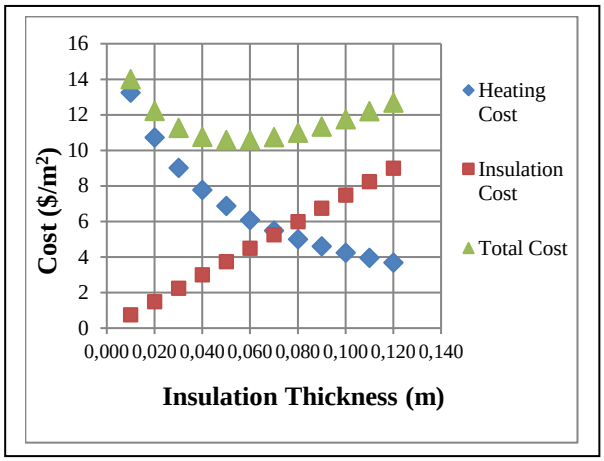


(a)

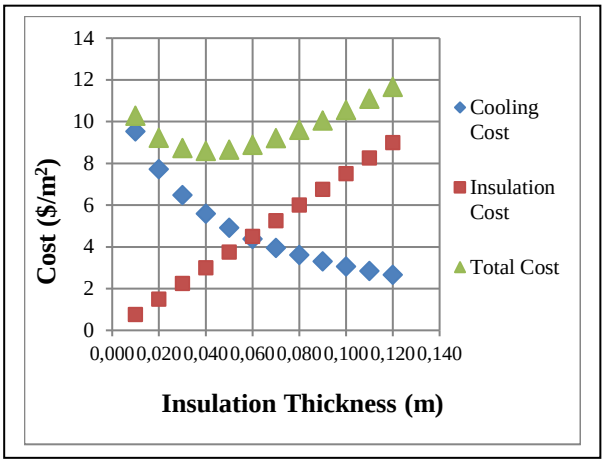


(b)

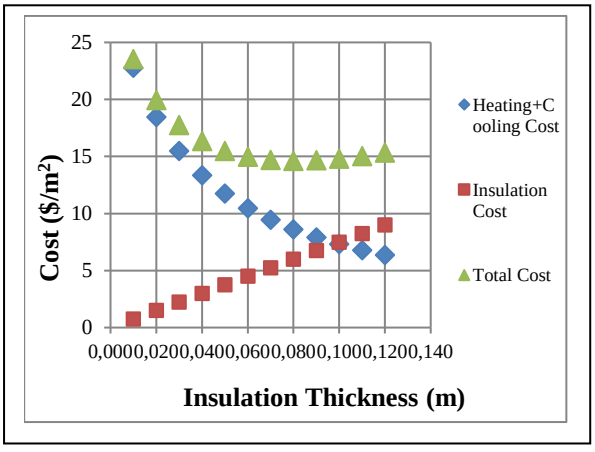


(c)

**Figure 1.**Cost curves of optimum insulation thickness for (a) heating period (b) cooling period (c) heating + cooling period for Izmir city in case of vertical perforated brick with density of 550 kg/m$^3$ and thermal conductivity of 0.32 W/m.K, glass wool as insulation material and natural gas as fuel usage.

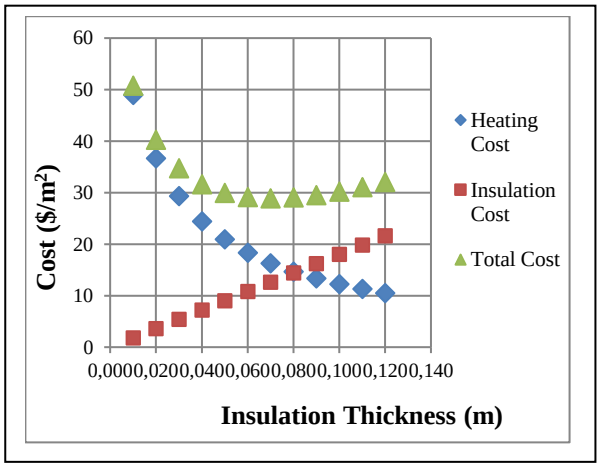


(a)

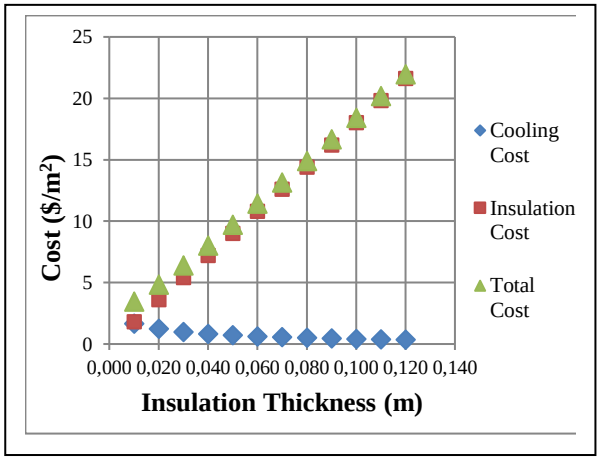


(b)

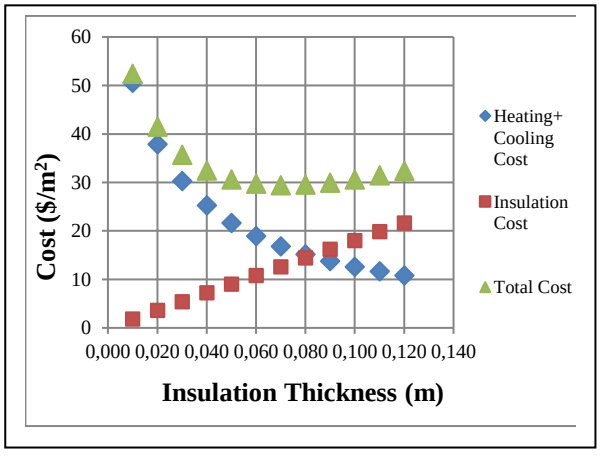


(c)

**Figure 2.** shows the results of cost curves for optimum insulation thickness (a) heating period (b) cooling period (c) heating + cooling period for Kars city in case of vertical perforated brick with density of 1000 kg/m$^3$ and thermal conductivity of 0.45 W/m.K, XPS as insulation material, and coal as fuel usage.

**Table 7.** Optimum insulation thickness due to various fuel and insulation materials usage for vertical perforated brick with 550 kg/m$^3$ density and 0.32 W/m.K heat conduction in the heating period(m)

| City | Fuel | | | | | | | | | | | |
|---|---|---|---|---|---|---|---|---|---|---|---|---|
| | Natural Gas | | | Coal | | | Fuel-oil | | | LPG | | |
| | Glass wool | EPS | XPS | Glass wool | EPS | XPS | Glass wool | EPS | XPS | Glass wool | EPS | XPS |
| **İzmir** | 0.054 | 0.036 | 0.024 | 0.056 | 0.037 | 0.025 | 0.091 | 0.064 | 0.045 | 0.130 | 0.095 | 0.067 |
| **Balıkesir** | 0.076 | 0.053 | 0.036 | 0.078 | 0.054 | 0.038 | 0.121 | 0.088 | 0.062 | 0.170 | 0.127 | 0.090 |
| **Konya** | 0.094 | 0.067 | 0.047 | 0.097 | 0.069 | 0.048 | 0.147 | 0.109 | 0.077 | 0.221 | 0.166 | 0.119 |
| **Sivas** | 0.104 | 0.075 | 0.052 | 0.106 | 0.076 | 0.053 | 0.161 | 0.119 | 0.085 | 0.222 | 0.167 | 0.119 |
| **Kars** | 0.123 | 0.090 | 0.063 | 0.126 | 0.092 | 0.065 | 0.188 | 0.141 | 0.100 | 0.259 | 0.196 | 0.140 |

**Table 8.** Optimum insulation thickness due to various fuel and insulation materials usage for vertical perforated brick with 1000 kg/m$^3$ density and 0.45 W/m.K heat conduction in the heating period (m)

| City | Fuel | | | | | | | | | | | |
|---|---|---|---|---|---|---|---|---|---|---|---|---|
| | Natural Gas | | | Coal | | | Fuel-oil | | | LPG | | |
| | Glass wool | EPS | XPS | Glass wool | EPS | XPS | Glass wool | EPS | XPS | Glass wool | EPS | XPS |
| **İzmir** | 0.061 | 0.043 | 0.029 | 0.063 | 0.044 | 0.030 | 0.097 | 0.071 | 0.050 | 0.136 | 0.102 | 0.072 |
| **Balıkesir** | 0.083 | 0.060 | 0.042 | 0.085 | 0.062 | 0.043 | 0.128 | 0.095 | 0.067 | 0.177 | 0.133 | 0.095 |
| **Konya** | 0.101 | 0.074 | 0.052 | 0.103 | 0.076 | 0.053 | 0.154 | 0.115 | 0.082 | 0.228 | 0.173 | 0.124 |
| **Sivas** | 0.110 | 0.081 | 0.057 | 0.113 | 0.083 | 0.059 | 0.168 | 0.126 | 0.090 | 0.229 | 0.174 | 0.125 |
| **Kars** | 0.130 | 0.097 | 0.069 | 0.133 | 0.099 | 0.070 | 0.195 | 0.148 | 0.106 | 0.266 | 0.202 | 0.146 |

**Table 9.** Optimum insulation thickness due to electric and insulation materials usage for vertical perforated brick with 550 kg/m$^3$ density and 0.32 W/m.K heat conduction in the cooling period (m)

| City | Glass wool | EPS | XPS |
|---|---|---|---|
| **İzmir** | 0.041 | 0.026 | 0.017 |
| **Balıkesir** | 0.024 | 0.013 | --- |
| **Konya** | 0.017 | --- | --- |
| **Sivas** | --- | --- | --- |
| **Kars** | --- | --- | --- |

**Table 10.** optimum insulation thickness due to electric and insulation materials usage for vertical perforated brick with 1000 kg/m$^3$ density and 0.45 W/m.K heat conduction in the cooling period (m)

| City | Glass wool | EPS | XPS |
|---|---|---|---|
| **İzmir** | 0.048 | 0.032 | 0.022 |
| **Balıkesir** | 0.031 | 0.019 | 0.012 |
| **Konya** | 0.023 | 0.013 | --- |
| **Sivas** | 0.013 | --- | --- |
| **Kars** | --- | --- | --- |

**Table 11.** Optimum ınsulation thickness due to various fuel and insulation materials usage for vertical perforated brick with 550 kg/m$^3$ density and 0.32 W/m.K heat conduction in the heating+cooling period (m)

| City | Fuel | | | | | | | | | | | |
|---|---|---|---|---|---|---|---|---|---|---|---|---|
| | Natural Gas+Electricity | | | Coal+Electricity | | | Fuel-oil+Electricity | | | LPG+Electricity | | |
| | Glass wool | EPS | XPS | Glass wool | EPS | XPS | Glass wool | EPS | XPS | Glass wool | EPS | XPS |
| **İzmir** | 0.081 | 0.057 | 0.039 | 0.082 | 0.058 | 0.040 | 0.111 | 0.080 | 0.056 | 0.146 | 0.107 | 0.076 |
| **Balıkesir** | 0.090 | 0.064 | 0.044 | 0.092 | 0.065 | 0.045 | 0.131 | 0.096 | 0.068 | 0.178 | 0.133 | 0.094 |
| **Konya** | 0.103 | 0.074 | 0.052 | 0.106 | 0.076 | 0.053 | 0.153 | 0.114 | 0.081 | 0.226 | 0.170 | 0.122 |
| **Sivas** | 0.109 | 0.078 | 0.055 | 0.111 | 0.081 | 0.057 | 0.164 | 0.122 | 0.087 | 0.225 | 0.169 | 0.121 |
| **Kars** | 0.126 | 0.092 | 0.065 | 0.129 | 0.094 | 0.066 | 0.190 | 0.142 | 0.101 | 0.260 | 0.197 | 0.141 |

**Table 12.** Optimum insulation thickness due to various fuel and insulation materials usage for vertical perforated brick with 1000 kg/m$^3$ density and 0.45 W/m.K heat conduction in the heating+cooling period (m)

| City | Fuel | | | | | | | | | | | |
|---|---|---|---|---|---|---|---|---|---|---|---|---|
| | Natural Gas+Electricity | | | Coal+Electricity | | | Fuel-oil+Electricity | | | LPG+Electricity | | |
| | Glass wool | EPS | XPS | Glass wool | EPS | XPS | Glass wool | EPS | XPS | Glass wool | EPS | XPS |
| **İzmir** | 0.084 | 0.064 | 0.044 | 0.089 | 0.065 | 0.045 | 0.118 | 0.086 | 0.062 | 0.152 | 0.114 | 0.081 |
| **Balıkesir** | 0.097 | 0.071 | 0.050 | 0.099 | 0.072 | 0.051 | 0.138 | 0.103 | 0.073 | 0.185 | 0.139 | 0.100 |
| **Konya** | 0.110 | 0.081 | 0.057 | 0.112 | 0.083 | 0.059 | 0.161 | 0.121 | 0.086 | 0.233 | 0.177 | 0.127 |
| **Sivas** | 0.116 | 0.085 | 0.061 | 0.118 | 0.087 | 0.062 | 0.171 | 0.129 | 0.092 | 0.232 | 0.176 | 0.126 |
| **Kars** | 0.133 | 0.099 | 0.070 | 0.136 | 0.101 | 0.072 | 0.197 | 0.149 | 0.107 | 0.267 | 0.203 | 0.147 |

In addition, the heating and cooling period must be considered together for some provinces when insulation is applied. In particular, the cooling period should be taken into account as well as heating for hot climates such as the first and second region. In cold climates such as the fourth and fifth region, only the heating period can be considered. For some provinces, faults can only be made in the insulation application by considering the heating period.

## 5. Conclusion

Vertical perforated bricks with a density of 550 kg/m$^3$, a thermal conductivity of 0.32 W/m.K and vertical perforated bricks with a density of 1000 kg/m$^3$ with thermal conductivity of 0.45 W/m.K are used for optimum insulation thickness calculations for different insulation materials, and a difference ranging from 0.005 to 0.007 m (5-7 mm) is found. The optimum insulation thickness will be much larger in construction materials where the difference between the density and the thermal conductivity value is higher.

The minimum optimum insulation thickness is calculated when natural gas and XPS are used, while the maximum optimum insulation thickness is found when LPG and glass wool are used in the period of heating+cooling and heating. In the cooling period, the optimum insulation thickness was found in case of 550 kg/m$^3$ density vertical perforated brick usage Izmir, Balikesir and Konya. In the case of using 1000 kg/m$^3$ density vertical perforated brick, the optimum insulation thickness was found for the cities of Izmir, Balıkesir, Konya and Sivas. The highest optimum insulation thickness was obtained from glass wool and the lowest from XPS**.**

When utilizing low density bricks, the optimum insulation thickness is reduced. The labour cost increases when the density is increased. This also yields an increase in the cost of the building due to the use of additional materials and component. In addition, production of $CO_2$ and $SO_2$ emissions due to building components will increase. As a result, it is recommended to use low density bricks in terms of both cost and production carbon emission release.

## References

[1] Kaynaklı, Ö., Kılıç, M., Yamankaradeniz, R.,Isıtma ve soğutma süreci için dış duvar optimum yalıtım kalınlığı hesabı, TTMD Isıtma, Soğutma, Havalandırma, Klima, Yangın ve Sıhhi Tesisat Dergisi, 65, 39-45 (2010).

[2] Şişman N., Determination of optimum insulation thickness of building exterial walls in different degree day regions by using economical analyse method when different insulation and wall structure materials are used, Osmangazi University, Master Thesis (2005).

[3] Kurekçi N. A., Determination of optimum insulation thickness for building walls by using heating and cooling degree-day values of all Turkey's provincial centers, Energy and Buildings, 118, 197-213(2016).

[4]Kaynakli, Ö. A., study on residental heating energy requirement and optimum insulation thickness. Renewable Energy, 33,6,1164-1172 (2008).

[5] Yuan J., Farnham C., Emura K., Alam M. A.,Proposal for optimum combination of reflectivity and insulation thickness of building exterior walls for annual thermal load in Japan, Building and Environment, 103, 228-237 (2016).

[6] Barrau J., Ibanez M., Badia F.,Impact of the optimization criteria on the determination of the insulation thickness. Energy and Buildings, 76 459–469 (2014).

[7] Kaynaklı, Ö., Mutlu, M., Kılıç, M., Bina duvarlarına uygulanan ısıl yalıtım kalınlığının enerji maliyeti odaklı optimizasyonu, Tesisat Mühendisliği, 126, 48-54(2011).

[8] Dombaycı, Ö. A., Gölcü, M., Pancar, Y., Optimization of insulation for external walls using different energy-sources, Applied Energy, 83, 9, 921-928 (2006).

[9] Bolattürk, A., Optimum insulation thicknesses for building walls with respect to cooling and heating degree-hours in the warmest zone of Turkey. Building and Environment, 43,6,1055-1064 (2008).

[10] Uçar, A. and Balo, F., Effect of fuel type on the optimum thickness of selected insulation materials for the four different climatic of Turkey. Applied Energy, 86,5,730-736 (2009).

[11] Yu, J, Yang, C., Tian, L. and Liao, D., A study on optimum insulation thicknesses of external walls in hot summer and cold winter zone of China. Applied Energy, 86,11,2520-2529 (2009).

[12] Uçar, A. and Balo, F., Determination of the energy savings and the optimum insulation thickness in the four different insulated exterior walls. Renewable Energy, 35,1,88-94 (2010).

[13] Kaynakli O., A review of the economical and optimum thermal insulation thickness for building applications, Renewable and Sustainable Energy Reviews, 16, 415–425 (2012).

[14] Vincelas F. F. C., Ghislain T., The determination of the most economical combination between external wall and the optimum insulation material in Cameroonian's buildings, Journal of Building Engineering, 9,155–163 (2017).

[15] Uçar, A., Thermoeconomic analysis method for optimization of insulation thickness for the four different climatic regions of Turkey. Energy, 35,4,1854-1864 (2010).

[16] Nyers J., Kajtar L., Tomi´c S., Nyers A., Investment-savings method for energy-economic optimization ofexternal wall thermal insulation thickness, Energy and Buildings, 86,268–274 (2015).

[17] Kaynakli, Ö., Parametric investigation of optimum thermal insulation thickness for external walls. Energies, 4,6,913-927 (2011).

[18] TS 825, Thermal Insulation Regulations in Buildings, Turkish Standard, December 2013.

[19] Okka, O., Mühendislik Ekonomisi, Nobel Press, 3rd Edition, Ankara, 2000.

[20] Dombaycı Ö. A., Degree-days maps of Turkey for various base temperatures, Energy, 34, 1807–1812 (2009).

[21] Yildiz A. and Ersöz M. A., The effect of wind speed on the economical optimum insulation thickness for HVAC duct applications, Renewable and Sustainable Energy Reviews,55,1289-1300 (2016).

[22] Uludag Electricity Distribution Inc. Datas

**NOMENCLATURE**

| | | | |
|---|---|---|---|
| HDD | Heating degree-day | **Index** | |
| CDD | Cooling degree-day | ins | insulation |
| x | Insulation thickness (m) | H | heating |
| k | Insulation material heat conduction coefficient (W/m.K) | C | cooling |
| η | Heating system efficiency | f | fuel |
| $H_u$ | Lower thermal value (J/m$^3$) | e | electricity |
| COP | Cooling performance coefficient | t,w | Uninsulated wall |
| C | Price ($) | f | fuel |
| XPS | Extruded polystyrene | t | total |
| EPS | Expanded polystyrene | t,H | Heating, total |
| PWF | Present Worth Factor | t,C | Cooling, total |
| i | Interest rate | w | Wall |
| g | Inflation rate | i | internal |
| R | Thermal resistance (m$^2$.K/W) | d | external |
| U | Heat transfer coefficient (W/m$^2$.K) | | |
| T | Temperature ($^0$C) | | |

*Asst. Prof. Dr. Okan Kon graduated from Balikesir University, Engineering Faculty Department of Mechanical Engineering in 2000. He completed his master's degree in 2004 and PhD in 2014. Since 2001, he has been working in the Department of Thermodynamics at the Department of Mechanical Engineering. His study fields are energy systems and renewable energy sources.*



An International Journal of Optimization and Control: Theories & Applications
ISSN: 2146-0957 eISSN: 2146-5703
Vol.7, No.2, pp.158-166 (2017)
https://doi.org/10.11121/ijocta.01.2017.00440

RESEARCH ARTICLE

# Design and optimization of a power supply unit for low profile LCD/LED TVs

Revna Acar Vural [a*], İbrahim Demirel [b], Burcu Erkmen [a],

[a] *Department of Electronics and Communication Engineering, Yildiz Technical University, Turkey*
[b] *Arcelik A.Ş., Turkey*
*racar@yildiz.edu.tr, ibrahim.demirel@arcelik.com, bkapan@yildiz.edu.tr*

ARTICLE INFO

Article history:
*Received: 18 January 2017*
*Accepted: 5 June 2017*
*Available Online: 5 July 2017*

Keywords:
*DC-DC converters*
*Power density*
*Power supply unit*
*TV power card*

AMS Classification 2010:
*94C99, 93C95*

ABSTRACT

The ongoing demand for smaller and lighter power supplies is driving the motivation to increase power density while maintaining a robust design compatible with international harmonic standards. Transformer design is a major challenge for low profile and high power density TV power cards. In addition to these, for electromagnetic interference standard and for providing efficient thermal management for heat emission, it is required to minimize EMI noise. In this study, by taking these stated criteria into consideration, a TV power card has been designed, which has 220W output power and can be used in low profile televisions. Proposed power card will meet desired critical parameters such as surface area and output power of the referenced card which has 13.5mm height, the heat, and power consumption at standby mode. Moreover, it is designed with 10mm height limit without any engraving on PCB in a way that it will meet International Electrotechnical Commission (IEC) current harmonic standard to which TVs are subjected. Experimental results demonstrate that the proposed power supply with 10mm height has 34% higher power density with respect to its counterpart having 13.5 mm height.



## NOMENCLATURE

| | |
|---|---|
| $V_g$ | Switching component trigger voltage |
| $V_{DS}$ | Voltage stress on switching component |
| $V_o$ | Voltage on output capacitor |
| $V_{SN}$ | Snubber circuit voltage |
| $I_{PRI}$ | Primary current |
| $I_{SEC}$ | Secondary current |
| $I_{ripple}$ | Ripple current |
| *PDP* | Plasma Display Panel |
| *LCD* | Liquid Crystal Display |
| *LED* | Light Emitting Diode |
| *ZVT* | Zero Voltage Transmission |
| *ZVS* | Zero Voltage Switching |
| *SMPS* | Switch Mode Power Supply |
| *PFC* | Power Factor Correction |
| *PCCM* | Pseudo Continuous Conduction Mode |
| *CrM* | Critical Conduction Mode |
| *ESR* | Equivalent Series Resistance |
| *CSD* | Current Source Driver |
| *PSU* | Power Supply Unit |
| *EMI* | Electromagnetic Interference |
| *PCM* | Printed Circuit Board |
| *DCM* | Discontinuous Conduction Mode |
| *IC* | Integrated Circuit |
| *FHA* | Fundamental Harmonic Approximation |
| *DC* | Direct Current |
| *AC* | Alternative Current |

*Corresponding author

## 1. Introduction

Emergence of plasma display panel (PDP), liquid crystal display (LCD) and light emitting diode (LED) technologies created important decrease in the dimension and weight of TVs. Orientation of customers to thinner and lighter TVs has led to the height limitation of power card design, which is one of the main constituents of low profile TVs. Different voltage levels are obtained as outputs in the power card of this kind of TVs. Power consumption standards which the developing technology reveals have made the usage of topologies having maximum efficiency obligatory in TV power cards [1-5].

For middle level power applications, among various DC-DC converters developed so far, LLC resonant converters, has the advantages as the simplicity of circuit configurations and the acquisition of big voltage gains in narrow frequency interval when compared to the serial/parallel resonant converters. Due to the limitations of high current effects, output regulation and power density of traditional resonant converters, novel topologies and switching modes for the design of LLC resonant converters have been proposed in the literature [6-9].

The most challenging part of thin power card design with high power density is the transformer design. Design of converter using flat magnetic component is difficult because of the increase in the temperature of flat transformer at high switching frequencies. In [10], for decreasing the temperature of this transformer, a power module composed of two flat transformers is designed. In [11], to give high output power, a new LLC resonant converter with two transformers is presented. In this structure, to decrease imbalance in primary current, two transformers are applied to LLC converter with their primaries serially connected and secondaries parallelly connected to each other. In [12], a new frequency controlled soft-switching resonant converter is proposed which has high power density, high efficiency, low switching losses and circuit components whose profile depth is decreased. In [13] a flyback converter with partial resonance was developed. In this type of converter, semi conductive power component's transmission with zero voltage transmission (ZVT) and cut-off with zero voltage switching (ZVS) is provided. Two output LLC converter circuit [14] having 10mm profile depth consists of two transformers, which are serially connected in the primary side and parallelly connected in the secondary side. Serial primary-parallel secondary connection type provides high power density; moreover, secondary leakage inductance reduction is achievable.

Since a switch mode power supply (SMPS) behaves as a nonlinear load, power factor has to be corrected. Power factor's being close to ideal provides the increase of system efficiency, the prevention of overloading of the line and the production transmission devices and the decrease in harmonics and losses [15, 16]. In TV power card design, power factor correction (PFC) circuits are used to provide the adjustment of low harmonic impairments and the necessary harmonic standards. A Boost type PFC converter turns standard network voltage into regulated DC output voltage, thus feeds power converter layer. In addition, it enhances power factor and current harmonics. In [17], a pseudo continuous conduction mode (PCCM) boost type PFC converter and control methods related to this structure were presented. In low and middle power class TV applications, boost type converters which are activated in critical conduction mode (CrM) are used. High efficiency can be achieved with this CrM, however it brings disadvantages such as increase in the component amount and ripples in output current. In order to overcome these ripples, integrated circuits (IC) having interleaved topology are designed in [18]. These ICs employ ZVS and have features such as wide input voltage gap and wide output load gap. Suggested CrM PFC controller is suitable for flat devices, where wide bulky components such as inductor and capacitor are divided and scattered thus decreasing profile thinness. In [19], frequency clenched CrM controlled PFC converter design associated with interleaved topology enabled the usage of small size passive components. In [20], a digital adaptive current source driver (CSD) is proposed for the interleaved Boost PFC converter under CrM to reduce the high turn-off loss and gate drive loss.

Topology and selection of material are important criteria to provide high efficiency and high power density in the design of power modules. In [21], a method is proposed for the improvement of high-current density PCB design while maintaining power supply unit (PSU) load balance. For medium power solid state lighting applications, a new topology along with the use of film technology capacitors which has a longer lifetime than standard electrolytics is presented for effective power factor correction to comply with the harmonic injection and energy saving standards [22]. Methods proposed in [7-12, 18-19] are used to optimize the efficiency of power sources used in LCD TVs. By using LLC resonance converters, 89.43% efficiency for 40 inch LCD TV in [7], high efficiency (full loading 96.5%) and low cost for power sources used in 42 inch PDP TVs in [8] are achieved. In [10, 11] LLC resonant converters designed for PDP TV are presented, in [10] design of 14 mm transformer is done and total efficiency is calculated as 96.6 %. Serial converter with two transformers proposed in [11] is used in 50 inch PDP TV system. In [12] half bridge resonant converter, with its LCD TV power source having 46/47 inch active PFC circuit and standby converter, is designed. Permanent conduction mode PFC controller proposed in [18] is suitable for flat devices, where profile depth is decreased by dividing and scattering bulky inductors and capacitors. Flyback converter design, having 12.5mm height high efficiency which enables the design of decreased depth LCD TV, is given in detail in [19]. Moreover, electromagnetic interference (EMI)

noise has to be minimized to provide efficient thermal management for heat emission.

Considering the abovementioned criteria, the aim of this study, is to design a PSU with high efficiency and optimized power density which can be used in low profile TVs. For this purpose, a PSU having 13,5mm height and 220W output power has been redesigned as having 10mm height and the same output power with the referenced card. In the second part of the study, flyback converter, LLC resonant converter and PFC converter typologies used in PSU design are explained. When power levels of TV power source of today's technology is analyzed, a power need for 75-240W that can change according to screen dimension is determined. Outputs of designed power supply in this study are 5.2V/4.2A, 24V/6A and 12V/4.5A. Flyback topology is preferred for 100W and less power levels because of its features such as simple structure, low cost and its enabling input and output isolation. 24V/6A and 12V/4.5A output LLC converter topology, with its serial primary and parallel secondary connection type, provides high power density. In this topology [14], secondary windings have asymmetrical connection and leakage inductances resulting from current imbalances are decreased. For power levels below 300W, because of high power factor correction, low cost and simple control structure; Boost type PFC converter, which operates in CrM, is used. Third section includes circuit based studies related to the optimization of power density, operating in high switching frequencies, design of magnetic components, soft-switching technique and component selection. In the fourth section, experimental results related to the physical realization of power card are presented. Final section presents the concluding remarks and a discussion of optimization results.

## 2. Design of low profile PSU

In this study a power card, which meets the specifications of a regular TV power card and whose height is reduced in order to be suitable for low profile televisions, having 10 mm height and 220W output, is designed without any engraving process on printed circuit board (PCB). Proposed design meets the critical parameters such as referenced card's surface area, heat, power consumption in standby mode and the international security standards. Sub blocks used in the design of TV power card are given in Fig.1.

For power levels in 100W and below it, flyback converter topology is preferred for low cost, simple structure and its enabling input and output isolation. Above 100W level, LLC resonant converters are preferred in the design of power card due to its functions such as density of power and power efficiency they provide, control ease of output regulation over a wide load range and usage of soft-switching techniques that reduce high frequency switching losses [14]. Below 300W level power value, due to its high power factor correction, low cost, simple control structure, boost type PFC converter that operates on CrM is used. In Figure 1, proposed PSU design is given as a block diagram and optimization techniques are explained in sub-chapters.

### 2.1. Design of flyback converter

Circuit components are selected as flyback converter's output voltage being 5.2V and output current being 4.2A. Because of the limitations in the dimensions of magnetic component, inductance value is determined having switching in discontinuous conduction mode (DCM). DCM operating allows smaller size transformer to be used in circuit design. Since the average power dissipation is less, it is possible to decrease the loss of power consumption with less coiling. Figure 2 shows the flyback converter topology. Controller IC of MOSFET switch is not shown in the figure but it is used in the exact design of Flyback Converter.

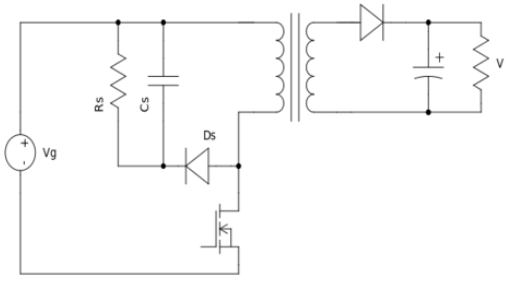


**Figure 2.** Flyback converter topology

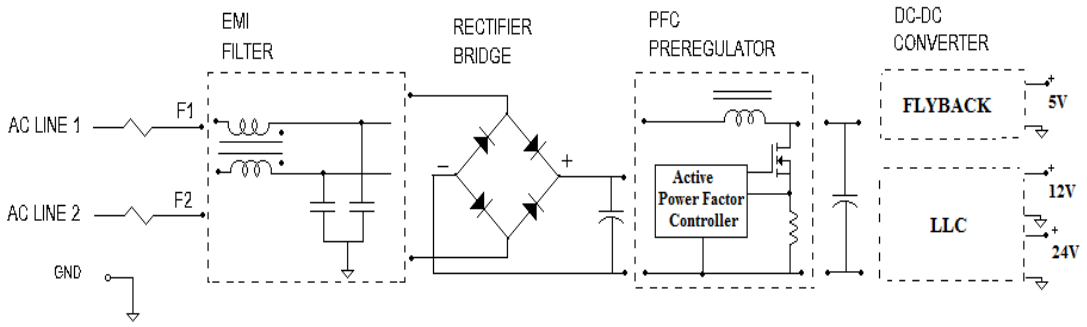


**Figure 1.** Sub-blocks of the PSU design

### 2.2. Design of LLC resonance converter

Output values (12V/4.5A, 24V/6A) of two output LLC converter circuits of which topology is presented in [14] is determined in accordance with the needs of optimized 40-42" TVs. Switching losses are decreased using soft-switching technique in high frequencies. Acquisition and input-output function are obtained using Fundamental Harmonic Approximation (FHA) analysis. With the aim of decreasing the current imbalance caused by leakage inductances, asymmetrical connection design is analyzed in [14]. LLC Converter topology is provided in Figure 3.

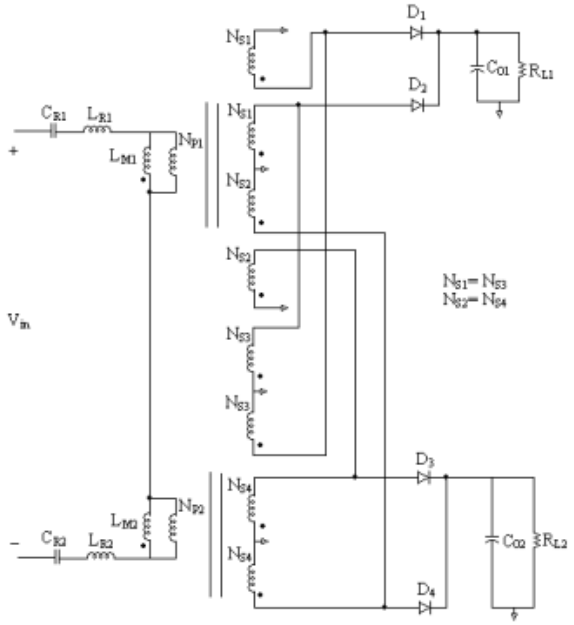


**Figure 3.** LLC resonant converter topology [14]

### 2.3. Design of boost type PFC converter

Common reasons for the usage of Boost PFC converter topology [23,24] are mainly input current shaping, isolation, and fast output voltage regulation that are performed in one single stage [23]. In control unit, a filtered DC output voltage is compared with reference voltage by using an error amplifier output of which is applied to the multiplier circuit. Output waveform of multiplier circuit follows the shape of AC input voltage and the shape of AC line voltage, the bobbin current of which was corrected. Gate drive pin controls the amplitude of bobbin current and thus output voltage is fixed. Boost type PFC converter topology is given in Figure 4.

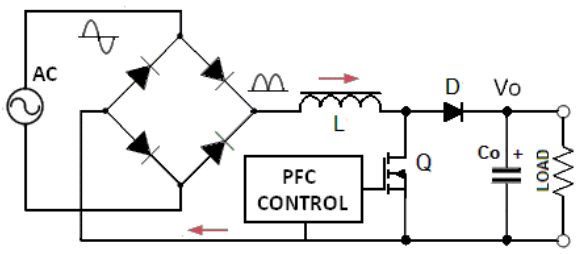


**Figure 4.** Boost type PFC converter topology

## 3. Power density optimization for LCD/LED TVs

The concept of power density in TVs defines the relationship between the power gained from the power card and dimensions of the power card. Circuit based studies related to the optimization of power density include operating in high switching frequencies, design of magnetic components, soft-switching techniques and component selection.

### 3.1. Selection of passive components and cooler

In case height limit of a TV power source is reduced, the most important limiting component is the dimension of passive components. Capacitor, bobbin and transformer are the group of passive components which compel the height limit. The bulk capacitor used in PFC converter output is a primary component which compels the height limit. This capacitor decreases the ripple of input voltage of other converters.

In addition to this, regulated source continues to provide regulated output voltage while ensuring hold up time in the absence of alternative input voltage which occurs in a sudden power failure. Equivalent series resistance (ESR) of output filter capacitor used in converters has to be as low as possible. ESR in high switching frequency applications has a great effect on the peak and active values of ripples in output voltages. Changes in the peak value of output voltage by a change in the load in the shape of a digit depend on ESR value of the capacitor [15]. Active current values of lower capacitors decreases in direct proportion with the dimensions. In case of increasing load in low profile structures, solution to increased stress on output capacitor is gathered by adding more than one capacitor to it.

When thin design is aimed, the necessity of providing input-output isolation is inevitable and the design of transformer compatible with reliability standards becomes more challenging. Decreasing the size of magnetic core reduces plastic cover options suitable for this material. Switching frequency can be increased to decrease magnetic core size, but this leads to the increase of losses on magnetic component and thus heating problems. Interleaving the windings of transformer can be a solution to the height limit of passive component. In order to gather the necessary power, two transformers are designed, having primaries serially connected and secondaries parallelly connected [14].

Selection of cooler is as important as the selection of passive components, since keeping the temperature values during power density optimization in the limits provided by the manufacturers is essential. Switching components used in primary side and corrective diodes used in secondary side are main components that require cooler. The surface area of coolers is determined by aiming a temperature value that does not exceed maximum junction temperature. In behalf of providing the heat flux of power source, materials that are predicted to warm are placed separately in a

position that it doesn't block air flow and there is no gap between it and PCB surface. Cooling surface areas are calculated to meet the temperature standards of the company with which this study is carried out.

### 3.2. Selection of topology and conduction modes

When traditional power supply needs are taken into consideration, the most important factor that determines topology is the power level. When the power levels of today's technology's TV power sources are examined, a power need between 75-240W that changes according to TV screen dimensions is determined. Flyback converter topology is preferred for 100W and power levels below it due to some features such as simple structure, low cost and its enabling of input and output isolation. In this topology, dynamic fast-answering DCM is used for the magnetic induction of transformer [25].

PFC converter structures, which operate in CrM because of the low cost of power factor correction and its simple control structure, are used in power values below 300W.By using high voltage obtained by PFC converter in resonant topology, high efficiency and high output power can be obtained.

Switching losses can be majorly decreased by the soft switching method used in LLC resonant topology. Decreasing this loss also provides an increase in the efficiency and the usage of smaller cooling material. Moreover, when the height limit is decreased, the power that magnetic component can provide is also limited and thermal problems arise. As a solution, more than one magnetic components need to be connected serial-parallely to reach a high power level.

## 4. Low profile PSU implementation and experimental results

In this study, a TV power card is designed which has 10 mm height and multi-output, 220W in total that can be used in televisions which have a panel size changing between 40- 47". Optimization progress related to the reduction of height by protecting the surface area of 13.5mm power cards is done compatible with international TV standards. For PFC converter and DC-DC converters used in power card, three transformer designs that doesn't exceed height limit are carried out. Switching components are placed in a way to prevent temperature problems that can occur because of the reduction in height limit and special coolers for output capacitors are designed.

Surface view of the designed card is given in Fig. 5. To provide height limit of power card designed for low profile television, components which vertically exceed height limit on PCB are placed by tilting. Detailed view related to the height of the card is given in Fig 6.

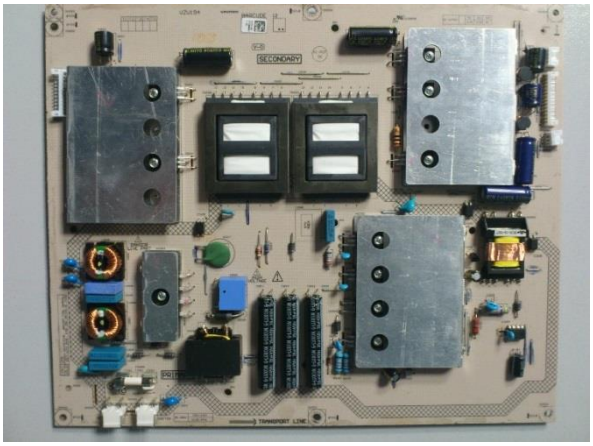

**Figure 5**. Surface view of the designed card

A TV power card having 13,5mm height and 220W output power is redesigned as having 10mm height and 220W output power by selecting optimal topology and material. In this study which focuses on the reduction of card height, the power density is enhanced at the rate of 34%. The card designed with 291mmx240mmx10mm dimensions operates at nominal load condition with 84% efficiency. The most calescent module on the card is transformer and thermal analysis result is given in Fig. 7.

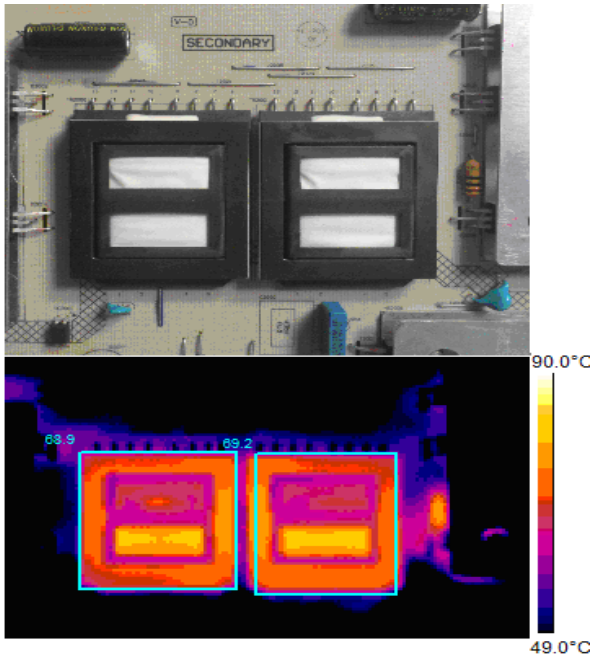


**Figure 7.** Thermal analysis under 25°C ambient temperature [14]

**Figure 6.** Detailed view of the height of the designed card

### 4.1. LLC resonant converter design converter

LLC resonance converter topology is used to gain 200W output power in the range of 330V-400V. Voltage acquired from PFC converter output is provided as an input to LLC topology and topology gives 12V/4.5A and 24V/6A outputs. Components used in LLC resonant converter is given in Table 1. Detailed simulation results of the LLC resonant converter are provided in [14].

**Table 1.** Components of LLC resonant converter [14]

| Circuit Component | Definition | Value |
|---|---|---|
| LLC MOSFET | Magnachip | MDF5N50 (x2) |
| Resonant capacitor | $C_R$ | 22nF |
| Magnetic inductance | $L_M$ | 693uH |
| Resonant inductance | $L_R$ | 171.2uH |
| LLC IC | Fairchild | Fan7621 |
| Output Diodes | D | SBR30A100 |

### 4.2. Flyback converter design results

A flyback converter, which operates for 5V output layer and standby mode in DCM is designed with its components are tabulated in Table 2. Voltage and current measurements are given in Fig. 8-10. Fig. 8 and Fig. 9 shows the switching behavior of flyback converter. From these figures, one can observe that energy is stored with the current flowing through primary winding when switch is on. When switch is off, this energy is transferred to secondary winding dependent on ratio of turns. High voltage and switching losses arise when switch is off. In order to protect the switch, a snubber circuit is used. In Fig. 10, voltage stress on switching component and snubber circuit voltage is given.

**Table 2.** Components of flyback converter

| Circuit Component | Definition | Value |
|---|---|---|
| Snubber Resistor | $R_S$ | 47kΩ |
| Snubber Capacitor | $C_S$ | 1nF |
| Integrated Circuit (IC) | U2 | FSB147H |
| Transformer Inductance | $L_M$ | 600uH |
| Output Diode | D | 30A 60V |
| Output Capacitors | $C_O$ | 2,2mF(x2) |

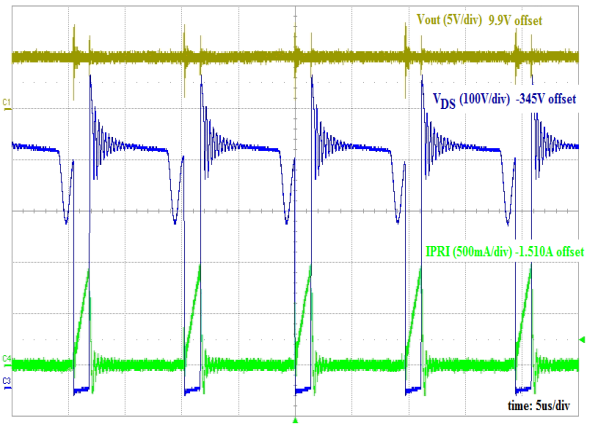


**Figure 8.** Flyback converter output voltage ($V_{OUT}$), voltage stress on switching component ($V_{DS}$) and primary current ($I_{PRI}$)

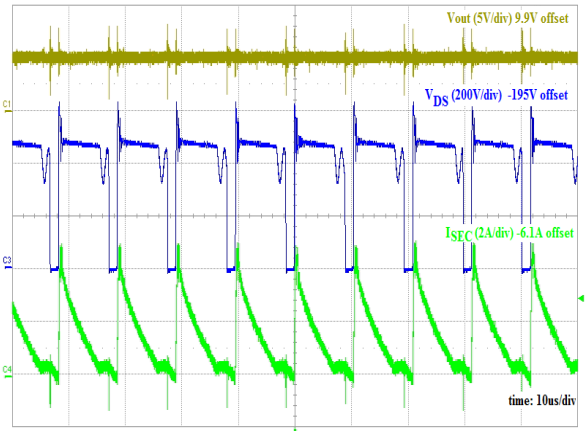


**Figure 9.** Flyback converter output voltage ($V_{OUT}$), voltage stress on switching component ($V_{DS}$) and secondary current ($I_{SEC}$)

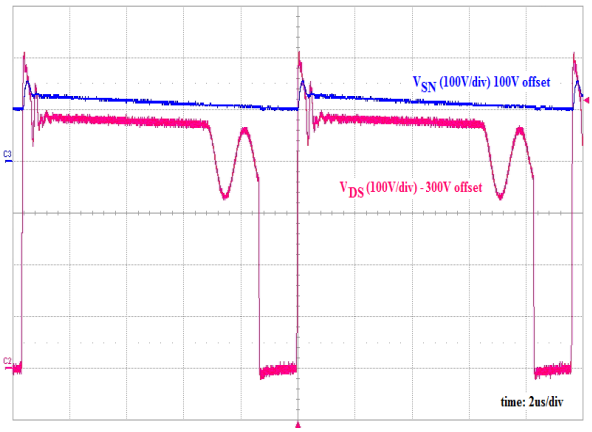


**Figure 10.** Voltage stress on switching component ($V_{DS}$) and snubber circuit voltage ($V_{SN}$).

### 4.3. Boost type PFC converter design results

Output voltage of PFC converter layer is selected as 400V to feed other layers. In Fig. 11, CrM PFC converter bobbin current ($I_L$), voltage on current measurement node ($V_{CS}$) and switching component

trigger voltage (Vg) are shown. When $V_{CS}$ reaches to the stated threshold point, trigger voltage Vg is cut, in addition to corrected network voltage, inducted current creates a voltage on bobbin and then it is transferred on output capacitor via output diodes. Thus, a higher voltage than the network voltage which is corrected with boost type PFC converter is acquired. In Fig. 12, voltage stress on switching component, switching component trigger voltage and current on PFC converter diode waveforms are given. Voltage on output capacitor and ripple current for over two periods are given in Fig. 13. Components used in PFC converter are tabulated in Table 3.

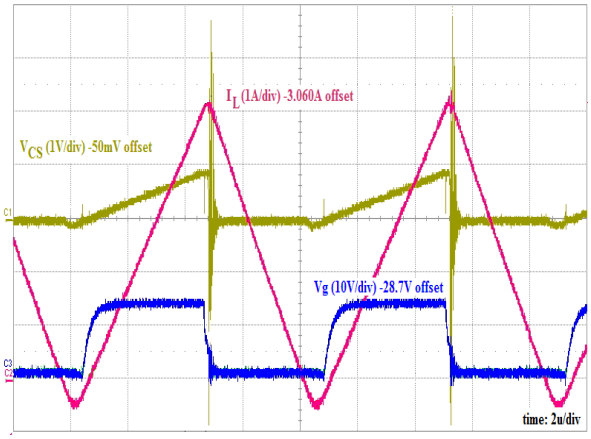


**Figure 11.** CrM PFC converter bobbin current ($I_L$), voltage on current measurement node ($V_{CS}$) and switching component trigger voltage ($V_g$)

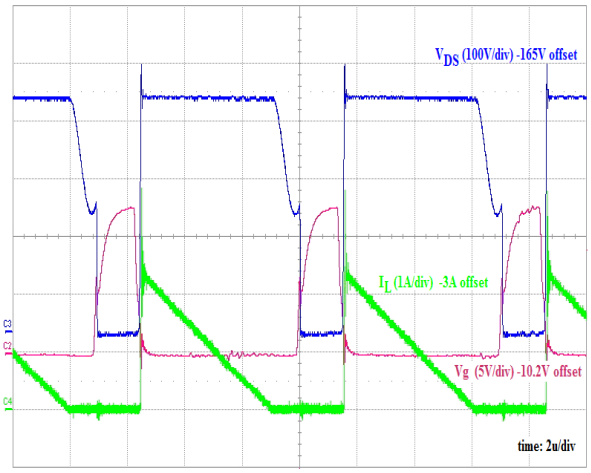


**Figure 12.** Voltage stress on switching component ($V_{DS}$), switching component trigger voltage ($V_g$) and current on PFC converter diode ($I_g$)

## 5. Conclusion

Considering the slim TV trend that today's TV technology reveals, orientation of customers to thinner and lighter TVs has led to the limitation of the design of the power card, which is one of the main constituents of low profile TVs. In this study, a TV power card having 13,5mm height and 220W output power has been redesigned as having 10mm height and the same output power with the referenced card. Topology and conduction modes of the converters are selected in order to provide 10 mm criterion for low profile TVs. Optimization of the power density of the card is targeted during the design procedure. Smaller cooling materials are used in order to reduce switching losses and thermal problems related height limit are minimized. TV power card with optimized power density is constructed with 200W LLC converter, 20W Flyback DC/DC converter, Boost PFC and EMI filter. In this study, power density of low profile TVs, which have various panel dimensions in a range of 40-47", is enhanced at the rate of 34%. The results are compatible with the International Electrotechnical Commission (IEC) 61000-3-2 current harmonic standard.

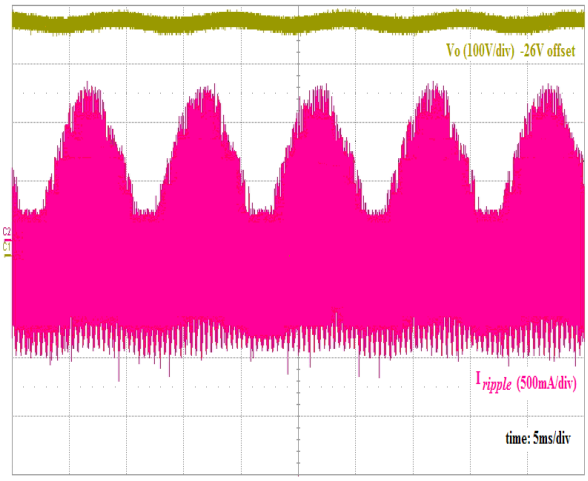


**Figure 13.** Voltage on output capacitor ($V_O$) and ripple current ($I_{ripple}$)

**Table 3.** Components of PFC converter

| Circuit Component | Definition | Value |
|---|---|---|
| PFC bobbin | $L_M$ | 200uH |
| PFC IC | Fairchild | Fan7930c |
| PFC MOSFET | Magnachip | MDF11N60 |
| PFC Diode | NXP | BYV29X |
| Output Capacitors | $C_O$ | 39uF (x3) |

## Acknowledgements

This work was supported by the electronic division of Arcelik A.Ş under Grant AR20D11T04.

## References

[1] Choi, H.C. and Shin, H.B., A New Soft-Switched PWM Boost Converter with a Lossless Auxiliary Circuit, International Journal of Electronics, 93, 805-817 (2006).

[2] Saha, S.S., Majumdar, B., Haldar, T. and Biswas, S.K., Optimized Design of a Fully Soft-Switched

Boost-Converter Suitable for Power Factor Correction, International Journal of Electronics, 93, 755-768 (2006).

[3] Arulselvi, S. and Uma, G., Design and Implementation of CF-ZVS-QRC Using Analog Resonant Controller UC3861, International Journal of Electronics, 94, 55-73 (2007).

[4] Lin, B.R., Huang, Y.S. and Chen, J.J., Analysis of ZVS PWM Active Clamp Isolated Converter with Secondary Voltage Step up, International Journal of Electronics, 96, 977-988 (2009).

[5] Knott, A., Andersen, T.M., Kamby, P., Pedersen, J.A., Madsen, M.P. and Andersen, M.A.E., Evolution of Very High Frequency Power Supplies, IEEE Journal of Emerging and Selected Topics in Power Electronics, 2, 386-394 (2014).

[6] Lin, B. R., Yang, W.R., Chen, J.J., Huang, C.L. and Yu, M.H., Interleaved LLC Series Converter with Output Voltage Doubler, Proceedings of IEEE International Power Electronics Conference, 92-98 (2010).

[7] Choi, Y., Cho, S.H., Hong, S.S., Cho, K.S., Oh, D.S. and Han, S.K., A New Tightly- Regulated Dual-Output LLC Resonant Converter, Proceeding of 8th International Conference on Power Electronics, 839-845 (2011).

[8] Cho, S.H., Roh, C.W., Hong, S.S. and Han, S.K., High-Efficiency and Low-Cost Tightly-Regulated Dual-Output LLC Resonant Converter, Proceeding of International Symposium on Industrial Electronics, Italy, 862-869 (2010).

[9] Fang, X., Hu, H., Chen, F., Somani, U., Auadisian, E., Shen, J. and Batarseh, I., Efficiency-Oriented Optimal Design of the LLC Resonant Converter Based on Peak Gain Placement, IEEE Transactions on Power Electronics, 28, 2285 – 2296 (2013).

[10] Yang, S., Abe S. and Shoyama, M., Design Consideration of a Flat Transformer in LLC Resonant Converter for Low Core Loss, Proceeding of IEEE International Power Electronics Conference, 343-348 (2010).

[11] Kim, E.S., Kim, J.H., Kang, S.I., Park, H.J., Lee, J.S., Huh, D.Y. and Jung, Y.C., Low Profile LLC Series Resonant Converter with Two Transformers, Proceedings of 25th Annual IEEE Applied Power Electronics Conference and Exposition, Palm Springs, CA, 1885-1889 (2010).

[12] Liang, S.A., Design Optimization for LCD TV Power Supply with Resonant Technique, Proceedings of IEEE Power Electronics Specialists Conference, Orlando, Florida, 702-707 (2007).

[13] Aksoy, I., Bodur, H. and Bakan, A.F., Kısmi Rezonanslı ve Geri Dönüşlü Bir DC Güç Kaynağının Geliştirilmesi, İncelenmesi ve Gerçekleştirilmesi, Elektrik-Elektronik-Bilgisayar Mühendisligi 11. Ulusal Kongresi, Istanbul, 187-190 (2005).

[14] Demirel, I. and Erkmen, B., A Very Low-Profile Dual Output LLC Resonant Converter for LCD/LED TV Applications, IEEE Transactions on Power Electronics, 29, 3514-3524 (2014).

[15] Mohan, N., Undeland, M.T. and Robbins, W.P., Power Electronics: Converters, Applications and Design, 3rd Ed., John Wiley&Sons, Chichester (2003).

[16] Rashid, M.H., Resonant and Soft Switching Converters, Power Electronics Handbook, Academic Press, Canada, 271-287 (2001).

[17] Zhang, F. and Xu, J., A Novel PCCM Boost PFC Converter with Fast Dynamic Response, IEEE Transactions on Industrial Electronics, 58, 4207-4216 (2011).

[18] Wu T.F., Tsai J.R., Chen Y.M., and Tsai Z.H., Integrated Circuits of a PFC Controller for Interleaved Critical-Mode Boost Converters, in Proc. IEEE 22th Annual Applied Power Electronics Conference, Anaheim, CA, 1347-1350 (2007).

[19] Louvel J. P., 300 W High Performance Slim LCD Tv Solution, ON Semiconductor, Phoenix, AZ, USA, Tech. Report, TND401/D Rev.2 (2010).

[20] Zhang Z., Xu C. and Liu Y.F., A Digital Adaptive Discontinuous Current Source Driver for High-Frequency Interleaved Boost PFC Converters, IEEE Transactions on Power Electronics, 29, 1298-1310 (2014).

[21] Chen, H.C. and Bai, Y.W., Improvement of High-Current Density PCB Design With PSU Load Balance and Redundancy on a High End Server System, Proceedings of Canadian Journal of Electrical and Computer Engineering, 37, 203-211 (2014).

[22] Sichirollo, F., Alonso, J. M., and Spiazzi, G., A Novel Double Integrated Buck Offline Power Supply for Solid-State Lighting Applications, IEEE Transactions on Industry Applications, 51, 1268-1276 (2015)

[23] Qiao, C. and Smedley, K.M., A topology survey of single-stage power factor corrector with a boost type input-current-shaper, IEEE Transactions on Power Electronics, 16, 360-368 (2001).

[24] Critical Conduction Mode PFC Controller, Fairchild Semiconductor Corporation Tech. Report FAN7930C, Rev. 1.0.2, (2010).

[25] Salimi, M. and Hajbani, V., Sliding mode control of the DC-Dcflyback Converter in Discontinius Conduction Mode, Proceedings of 6th Power Electronics, Drives Systems & Technologies Conference, Tehran, Iran, 13 – 18 (2015).

***Revna Acar Vural*** *received the B.S., M.S. and Ph.D degrees in electronics and communication engineering from Yildiz Technical University, Istanbul, Turkey, in 2002, 2004 and 2011 respectively. She is currently working as assistant professor in the Department of Electronics and Communications Engineering, Yildiz Technical University. Her current research interests include circuit design optimization, automated synthesis, analog integrated circuit design, and evolutionary algorithms.*

***İbrahim Demirel*** *received the B.S. degree in electronics engineering from Uludag University, Bursa, Turkey, in 2010. He is currently working toward the M.S. degree in electronics and communications engineering from Yıldız Technical University from Istanbul, Turkey. He is currently with Arcelik Electronics, Istanbul, Turkey as an R&D Engineer. His research interests include design of switching power supplies, resonant converters, high-efficiency and high-power density dc–dc converters, optoelectronics, and audio and acoustics signal analysis.*

***Burcu Erkmen*** *received the B.S., M.S., and Ph.D. degrees in electronics and communication engineering from Yildiz Technical University, Istanbul, Turkey, in 1999, 2001, and 2007, respectively. From 2009 to 2015, she was an assistant professor in the Department of Electronics and Communications Engineering, Yildiz Technical University, where she has been an associate professor since 2015. She was also engaged in industrial projects involving power electronics. Her current research interests include switching power supplies, resonant converters, high-efficiency and high-power-density DC-DC converters, and optimization techniques in electronic circuits.*



An International Journal of Optimization and Control: Theories & Applications
ISSN:2146-0957 eISSN:2146-5703
Vol.7, No.2, pp.167-176 (2017)
http://doi.org/10.11121/ijocta.01.2017.00328

RESEARCH ARTICLE

# Identical parallel machine scheduling with nonlinear deterioration and multiple rate modifying activities

Ömer Öztürkoğlu

*Department of Business Administration, Yasar University,Turkey*
*omer.ozturkoglu@yasar.edu.tr*

ARTICLE INFO

Article History:
*Received 05 January 2017*
*Accepted 23 February 2017*
*Available 15 July 2017*

Keywords:
*Parallel machine*
*Scheduling*
*Deterioration*
*Rate-modifying activity*

AMS Classification 2010:
*90B35, 68M20, 90C10*

ABSTRACT

This study focuses on identical parallel machine scheduling of jobs with deteriorating processing times and rate-modifying activities. We consider nonlinearly increasing processing times of jobs based on their position assignment. Rate modifying activities (RMAs) are also considered to recover the increase in processing times of jobs due to deterioration. We also propose heuristics algorithms that rely on ant colony optimization and simulated annealing algorithms to solve the problem with multiple RMAs in a reasonable amount of time. Finally, we show that ant colony optimization algorithm generates close optimal solutions and superior results than simulated annealing algorithm.



## 1. Introduction

In the last two decades, time-dependent processing times of jobs in scheduling literature have received increasing attention. The awareness of human perspective on scheduling jobs or Total productive maintenance (TPM) on productivity lead researchers think out of the box. Although many studies have to included some type of uncertainties in scheduling or sequencing problems (see [1–3] for details) in literature, some of the issues have been restricted by assumptions so as to simplify the problems. Boudreau et al. [4] discussed some of these issues from the human perspective that labor and task times are assumed to be deterministic and predictable as if they are always available.

In scheduling problems, Gupta and Gupta [5] introduced a variable processing time of a job described by a polynomial function of its starting time to include some dynamic parameters of systems discussed by Gupta et al. [6] and some Russian papers (see [7] for details). Browne and Yechiali [8] also introduced the concept of deteriorating jobs of which their processing time increases as they await to be processed. For example, awaiting steel material in the inventory to be processed might corrode, a drop in the temperature of an ingot needs to be reheated, a delay in medical treatment. Several papers can be given as appropriate examples to deteriorating jobs as a linear function of processing time of a job [5,8,9]. Kunnathur and Gupta [10] proposed a model with piecewise increasing processing times. Mosheiov [11] presented non-linear deterioration according to a job-dependent step function. Ozturkoglu and Bulfin [12] proposed a position-based, nonlinear increasing function of processing time of a job. We also implement a non-linear deterioration in our models. Up to now, all studies have studied on single machine scheduling problem. Additional literatures about time-dependent processing times in a single machine scheduling can be seen in [13] and [14]. Lodree et al. [15] also presented a detailed survey study about sequence-dependent studies from the perspective of human factors.

Mosheiov [11] formulated parallel, multiple machine scheduling problem with a job-dependent step deterioration as an integer program and proposed a heuristic algorithm for the problem. Chen [16] also studied on parallel machine scheduling problem that minimizes total completion time with a consideration of a simple linear deterioration. The author showed that this problem is NP-complete in the ordinary sense, not in the strong sense even with a fixed number of machines. Mosheiov [17] studied parallel, identical machines for makespan minimization of deteriorating jobs with simple linear function of their starting times. Mosheiov [17] showed that the multi-machine scheduling problem is NP-complete by reduction to the single-machine problem and presented an asymptotically optimal heuristic for minimization of makespan. For studies published by 2004, some additional discussions about multi-machine scheduling problems and their NP-completeness can be seen in [14]. Kang and Ng [18] presented a fully-polynomial time approximation scheme (FPTAS) for scheduling linearly deteriorating jobs on $m$ identical parallel machines with the objective of makespan. Ji and Cheng [19] also proposed another FPTAS for parallel-machine total completion time problem with linearly deteriorating jobs. Ji and Cheng [20] developed FPTAS for parallel-machine scheduling of simple linear deteriorating jobs with the objective of minimizing makespan, total completion time and total machine load. Ji and Cheng [20] also showed the makespan problem is strongly NP-hard for the fixed number of machines. All of the above studies considered deteriorating jobs in which the processing time of a job increases due to delay of processing of jobs, depreciation of machines or workers fatigue.

Lee and Leon [21] introduced the concept of rate-modifying activities to the scheduling literature. A rate-modifying activity (RMA) is an activity that affects and changes the speed or rate of the resource. Maintenance activities for machines and rest periods for workers can be given as examples to this concept. Lee and Lin [22] considered single-machine scheduling with the objectives of minimizing makespan, total completion time, total weighted completion time and maximum lateness. In their model, they evaluate the placement of fixed length RMA as well as sequencing of tasks. They proposed polynomial time algorithm for makespan and total completion time problems, and pseudo-polynomial time algorithms for several different objectives. Lee and Lin [22] also studied single machine scheduling problems with rate-modifying activities considering stochastic machine breakdown. In their model, if the RMA is scheduled before a breakdown, then processing times of jobs are reduced. If a breakdown occurs, then repair activity is applied then the resource works with its normal rates. They considered makespan, total completion time and maximum lateness as an objective function. Mosheiov and Sidney [23] developed an efficient polynomial algorithm that minimizes makespan for sequencing tasks with both learning and a RMA. All these studies have considered rate modifying activities on a single machine scheduling without consideration of the deteriorating jobs.

Lodree et al. [15] integrated two distinct concepts, deteriorating jobs and RMAs in scheduling models whose processing times are represented by linear increasing function of their starting times. In several studies, the single machine scheduling problem with deteriorating jobs and multiple RMAs is modeled under different objectives, such as minimizing makespan and total completion time [12, 24–26]. In these studies, researchers applied position dependent, non-linear function of processing times for jobs. Additionally, Lee and Wu [27] consider deteriorating jobs with maintenance activities of scheduling jobs on parallel machines. They applied simple, linear deterioration of jobs. In their model, maintenance period is known in advance for each machine. They evaluated makespan for this problem considering both resumable and non-resumable cases. Recently, Dalfard and Mohammadi [28] developed a model for a multi-objective parallel machine scheduling problem with maintenance activity excluding deterioration in processing times. Authors also solved the problem by using simulated annealing and hybrid genetic algorithms. Cheng et al. [29] proposed an improved ant colony optimization algorithm for a parallel machine scheduling problem in which jobs are processed in batches. Wang and Wei [30] showed that an identical parallel machine scheduling problem with linear deterioration and rate-modifying activities can be solvable in polynomial time even the objectives are minimization of total absolute differences in both completion and waiting times. Wang et al. [31] also studied an identical parallel scheduling problem in which machines are deteriorated due to delaying maintenance activities that cause an increment in maintenance time. After a maintenance activity, processing times of jobs decrease. Authors proposed a polynomial time algorithm to solve total completion time for this scheduling problem. Yang and Yang [32] proposed two polynomial time algorithms for unrelated parallel machine scheduling problems with multiple-rate modifying activities.

They considered that processing times of jobs are constant until a rate-modifying activity is performed, afterwards it decreases with a constant rate. Yang et al. [33] developed a polynomial time algorithm to solve unrelated parallel machine scheduling problem with controllable processing times and rate-modifying activities. The cost function in their model comprises total completion time and total job compressions.

To the best of our knowledge, our model is the first to attempt to evaluate the optimal sequence of non-linearly deteriorating jobs and sequences of multiple rate-modifying activities at identical parallel machines. We use fixed length RMA time and position-based, nonlinear deterioration similar to the [12]. The remainder of the paper is organized as follows. In the next section, we present a mathematical model for this problem. In the later sections, we implement ant colony optimization (ACO) and simulated annealing (SA) algorithms to solve this problem. Last, we solve the models and compared their performances.

## 2. Mathematical model

In our model, we schedule a set of $n$ jobs as $J = \{J_1, J_2, ..., J_n\}$ and at most $b$ number of RMAs on identical $R$ set of parallel machines, $R = \{R_1, R_2, ..., R_m\}$. Jobs are non-preemptive and each job is assigned to only one machine. We assume that jobs and machines are available at the beginning of the scheduling, and jobs are available when a machine is available for processing. A RMA can be given only after a job is completely processed at a machine (jobs are non-resumable). The rest of the model parameters are given in Table 1.

Initial processing time of jobs ($p_j$) are the same at any machines. Deteriorating processing times of jobs are nonlinear, increasing functions of $p_j$ based on the positions of assigned jobs. If a job is assigned to the $i^{th}$ position after the beginning of the schedule or a given RMA, $p_{ji}$ is formulated in the equation (1) defined by [12]. Additionally, we assume that jobs revert to their base processing time as soon as a RMA is performed.

$$p_{ji} = (1+\alpha)^{i-1} \cdot p_j \tag{1}$$

**Table 1.** The mathematical model parameters..

| | |
|---|---|
| $i$ | the position number of scheduled jobs at machines |
| $j$ | the index number of jobs |
| $k$ | the position number where an RMA is given before processing a job at the $k^{th}$ position |
| $m$ | the index number of machines |
| $\alpha$ | constant deterioration rate of processing time of jobs, $0 < \alpha \leq 1$ |
| $q$ | fixed period of time to perform an RMA |
| $p_j$ | the initial (base) processing time of job $j$ at identical machines |
| $p_{ji}$ | is the processing time of deteriorated job $j$ at position $i$ |
| $x_{ijkm}$ | 1, if job $j$ is assigned to the $i^{th}$ position after an RMA at the $k^{th}$ position on machine $m$, otherwise 0 |
| $y_{km}$ | 1 if an RMA is assigned at position $k$ on machine $m$ |
| $C_{im}$ | completion time of the job in position $i$ on machine $m$ |

Hence, the developed integer programming (IP) model can ben described as followings.

$$\min \quad Z = C_{max} \tag{2}$$

subject to

$$C_{max} \geq C_{nm} \quad \forall m \in R \tag{3}$$

$$C_{1,m} = \sum_{j=1}^{n} p_{j1} \cdot x_{1j0m} \tag{4}$$

$$C_{im} = C_{(i-1)m} + \sum_{k=1}^{i} \sum_{j=1}^{n} p_{jk} \cdot x_{ij(i-k)m} + q_i \cdot y_{im}, \quad \forall i = 2, ..., n \quad \text{and} \quad \forall m \in R \tag{5}$$

$$\sum_{j=1}^{n} \sum_{k=0}^{i-1} x_{ijkm} = 1, \quad \forall i = 1, ..., n, \forall m \in R \tag{6}$$

$$\sum_{i=1}^{n} \sum_{k=0}^{i-1} \sum_{m \in R} x_{ijkm} = 1, \quad \forall j = 1, ..., n \tag{7}$$

$$x_{kjim} \leq y_{(i+1)m}, \quad \forall m \in R, \forall i = 1, ..., k-1, \forall j \in J, \forall k = 2, ..., n \tag{8}$$

$$\sum_{i+1}^{n} y_{im} \leq b, \quad \forall m \in R \tag{9}$$

$$x_{ijkm} \in \{0,1\}, y_{im} \in \{0,1\} \tag{10}$$

The equation (2) is the objective of minimizing makespan where $C_{max} = \max\{C_{z1}, C_{z2}, ..., C_{zm}\}$, maximum of the completion time of the last job $z$

in each machine $m$. This is formulated by Equation (3). Equations (4) shows the completion time of the jobs at the first position based on base processing times of jobs. Equation (5) calculates the completion time of jobs at the later positions considering nonlinear deterioration of processing times and RMA time if given. Equation (6) restricts that each positions on each machine can only take one job. Equation (7) shows that each job should be assigned only to one position on each machine. Equation (8) arranges the order of RMAs based on the scheduled jobs. To make this constraint clear, if a job is assigned to position 2 after given a RMA at the end of the first position at machine 1 ($x_{2j11} = 1$), then $y_{21}$, which represents that a RMA is given at the beginning of position 2 at machine 1, should be one. Equation (9) controls the maximum number of allowable RMAs in the sequence. Additionally, equations (10) are the binary constraints.

Mosheiov [11] showed that multi-machine scheduling with linear deterioration is NP-hard even for two machines, our problem is also NP-hard because this is an extended model with the decision of optimal sequence of RMAs in a optimal sequence of jobs of which their processing time is nonlinearly deteriorated. Lee and Wu [27] also claimed that the scheduling problems with linearly deteriorating jobs and maintenance period are also NP-hard.

## 3. Ant colony optimization algorithm

Because our problem is also in NP-hard class, in this section we propose a unique ant colonoy optimization (ACO) algorithm which is originally developed by [34]. Sankar et al. [35] studied decentralized distributed scheduling problem in a parallel machine shop environment applying an ACO algorithm to the problem. Tkindt et al. [36] proposed an ACO algorithm and a heuristic based on simulated annealing (SA) algorithm for two serial machine scheduling problem for minimizing both makespan and total completion time together. Alaykiran et al. [37] proposed an ACO algorithm to solve hybrid flow shop problems considering makespan as an objective. Arnaout et al. [38] and Arnaout [39] proposed an ACO algorithm to non-preemptive, unrelated parallel machine scheduling problem with machine- and job sequence-dependent setup times. They compared the algorithm with tabu search algorithm and one of the existing heuristics in literature. They showed that ACO algorithm outperformed the other algorithms. Rossi and Boschi [40] developed a heuristic basis on a genetic algorithm (GA) and ACO for the flexible manufacturing systems. In their heuristic, GA and ACO co-evolve in parallel so as to improve the performance of the algorithm. Behnamian et al. [41] integrated three heuristics, ACO, SA and variable neighborhood search (VNS) to solve the parallel machine scheduling problem with sequence-dependent setup times for minimizing the makespan.

In our algorithms, we use a permutation based encoding which represents the sequence of job positions, split parameters and RMA parameters. There are $(m-1)$ number of split parameters ($s_i$) in the encoding shows the position where jobs are distributed to machines. $r_{im}$ represents the position of given maximum of $b$ number of RMAs at machine $m$. Hence, the encoding can be shown as $\{J_1, J_2, ...J_n|\ s_1, s_2, ..., s_{m-1}|r_{11}, ..., r_{x1}|...|r_{1m}, ..., r_{xm}|\}$. Additionally, $0 \leq r_{11} \leq ... \leq r_{k1} \leq s_1 < ... < s_{m-1} \leq r_{1m} \leq ... \leq r_{xm}$. For example, let encoding scheme $\{3\,5\,8\,1\,4\,2\,9\,6\,7\,10\,|\,4\,|\,2\,|\,7\}$ represent a solution for a scheduling 10 jobs at parallel two machines with at most one RMA. Hence, jobs 3, 5, 8 and 1 are scheduled at machine 1 because $s_1$ is 1, other jobs are at machine 2. An RMA is scheduled after job 5 at machine 1 ($r_{11} = 2$ meaning that RMA is given after the second position at machine 1) and one RMA is given after job 9 at machine 2. If any one of the RMA factors is equal to 0 (start position) or the same as split factor, it means that RMA is not actually needed at that machine. The rest of the parameters for our ACO algorithm is given in Table 2.

We solve our problem with ACO in two stages: sequencing and assigning. In the sequencing stage, we allocate $n$ jobs to the positions like assigning them to a single machine. In the assigning stage, we firstly split jobs into machines and allocate RMAs in each machine. The sequencing and assignment are based on the pheromone amounts on trails or positions and computed by probabilistically as in equation (11). After calculating probability of assigning next job, we select the job based on simple tournament selection applying under $q_0$ strategy. $q_0$ strategy is used in classical ACO to balance the exploration and exploitation. If a random number is greater than $q_0$, we use tournament selection, otherwise we select the job which has the maximum value of $(\tau_{ij})^{\alpha} \cdot (\eta_{ij})^{\beta}$. After constructing a full schedule, we select the split factors and then positions of RMAs.

**Table 2.** The model parameters for the ACO algorithm.

| | |
|---|---|
| $a$ | number of ants in population |
| $T$ | number of iterations |
| $\tau_{ij}(t)$ | the intensity of the pheromone trail on the path between jobs $i$ and $j$ at time $t$ |
| $\eta_{ij}(t)$ | the heuristic value (visibility) $1/p_j$ where $p_j$ is the processing time of job $j$ at time $t$ |
| $\lambda_k^{s_i}(t)$ | the intensity of the pheromone on positions $k$ for split factors at time $t$ |
| $\mu_k^{r_{im}}(t)$ | the intensity of the pheromone on positions $k$ for RMA factors at time $t$ |
| $\alpha$ | the relative importance of the pheromone trail |
| $\beta$ | the relative importance of the visibility |
| $\Delta$ | addition of pheromone on trail $ij$ or between positions $kn$ at time $t$ |
| $\rho$ | evaporation factor, $0 < \rho < 1$ |
| $\xi$ | factor of the online pheromone update, usually $= 0.1$ |
| $\tau_0$ | initial pheromone amount on all paths and positions |
| $\tau_{min}$ | minimum allowance of the pheromone amount on paths or positions |
| $\tau_{max}$ | maximum allowance of the pheromone amount on paths or positions |

$$P_{ij}^{y}(t) = \frac{(\tau_{ij})^{\alpha} \cdot (\eta_{ij})^{\beta}}{\sum_{l \in N_i^y} (\tau_{ij})^{\alpha} \cdot (\eta_{ij})^{\beta}}, \quad \forall y = 1, .., a \tag{11}$$

$$P_{sk}^{y}(t) = \frac{(\lambda_k)^{\alpha}}{\sum_{i \in N_s} (\lambda_k)^{\alpha}}, \quad \forall y = 1, .., a \tag{12}$$

$$P_{xk}^{y}(t) = \frac{(\mu_k)^{\alpha}}{\sum_{l \in N_x} (\mu_k)^{\alpha}}, \quad \forall y = 1, .., a \tag{13}$$

where, $P_{ij}^{y}(t)$ is the probability of selecting job $j$ if job $i$ is scheduled for ant $y$ at time $t$. $N_i^y$ is the neighborhood of ant $y$ that comprises unscheduled jobs up to that time. $N_s$ is the whole available positions for splitting, and $N_x$ is the appropriate positions for placing an RMA. $P_{sk}^{y}$ and $P_{xk}^{y}$ are the probability of selecting positions for splitting and RMAs, respectively, and these only account for the pheromone amounts at the positions.

We also use two pheromone updating processes, local and global updates, in our ACO algorithm. In the local update, as soon as an ant constructs a full schedule including splits and RMAs they change the pheromone amount based on the equations (14), (15) and (16).

$$\tau_{ij}(t+1) = (1-\xi) \cdot \tau_{ij}(t) + \xi \cdot \tau \tag{14}$$

$$\lambda_k(t+1) = (1-\xi) \cdot \lambda_k(t) + \xi \cdot \lambda \tag{15}$$

$$\mu_k(t+1) = (1-\xi) \cdot \mu_k(t) + \xi \cdot \mu \tag{16}$$

In the global update, after all ants construct a solution, firstly some pheromone is evaporated, then ants contribute to the appropriate paths and positions based on the equations (17), (18) and (19).

The pheromone amount is added to $ij$ path if jobs $i$ and $j$ are scheduled consecutively in the sequence of a machine. After global updates, if the pheromone amount on trail or at positions exceeds maximum level or goes below the minimum level, we set the pheromone amounts to the closest limit.

$$\tau_{ij}(t+1) = \rho \cdot \tau_{ij}(t) + \sum_{y=1}^{a} \Delta_y \tag{17}$$

$$\lambda_k(t+1) = \rho \cdot \lambda_{ij}(t) + \sum_{y=1}^{a} \Delta_y \tag{18}$$

$$\mu_k(t+1) = \rho \cdot \mu_{ij}(t) + \sum_{y=1}^{a} \Delta_y, \tag{19}$$

where, $\Delta_y = \max\{C_{yz1}, C_{yz2}, ..., C_{yzm}\}$, the maximum of completion time of the last job in each machine based on the given solutions by ant $y$.

The pseudo-code for our ACO algorithm is explained as in the followings. In this algorithm, we implement a local search procedure (LS1) to improve the solution of an ant at every $g$ number of iterations.

In this local search, if base processing time of a randomly chosen job is larger than the the scheduled job at its previous position, we simply remove that job in the sequence of the machine and insert this job either to the first position or any position after a given RMA. Hence, we aim to decrease the amount of deterioration by performing the local search.

Initialize parameters, pheromone amounts, and ants
Do{ until termination criterion is met.
Do { for all ants
Construct a full schedule, including splits and RMAs using tournament selection
Evaluate the makespan of an ant
If an ant is better than the best ant, update best ant
Otherwise, at each $g$ iterations do a local search (LS1) on the ant, then compare it with the best ant again
Do online pheromone update after each ant
Do global pheromone update after all ants controlled by ($\tau_{min}$, $\tau_{max}$)
}
}

## 4. Simulated annealing algorithm

Kirkpatrick et al. [42] proposed an iterative, stochastic, neighbor-based search method based on the analogy of heating and cooling of materials. Koulamas [43] developed a polynomial decomposition heuristic to minimize total tardiness on parallel machines. They embedded SA algorithm into their heuristic to do local search by swapping jobs. Park and Kim [44] suggested SA and TS algorithms that minimize order holding costs for scheduling these orders on identical parallel machines with ready times and due date. TS, SA and GA techniques are implemented to the scheduling problems with non-preemptable jobs on identical parallel machines [45]. Hindi and Mhlanga [46] developed SA and steepest descent algorithms to solve the makespan minimization problem of jobs having simple, linear and general linear deterioration on identical parallel machines. Kim et al. [47] proposed a SA algorithm to minimize total tardiness for scheduling jobs on unrelated parallel machines with sequence-dependent setup times. As discussed before, SA is also implemented to the parallel machine scheduling problem in studies [36, 41].

We use the same encoding that we discussed in the previous section in our SA algorithm. In this study, we modified the canonical SA algorithm by embedding two local searches so as to improve the solutions. The first one is the LS1, which is explained in the previous section. The second local heuristic (LS2) considers whole neighborhood of the scheduled jobs in the machine. It utilizes simple swap operator. Hence, LS2 swaps all jobs in a machine and if it finds a better solution than the current one, it updates the current solution. Additionally, the split factors and RMA factors are randomly chosen at the beginning of each iteration. The pseudo-code for this algorithm is as in the following.

Initialize parameters and randomly generate an initial solution
Do{ until termination criterion is met.
Do { for all stages
Move the split and RMA factors randomly for the schedule
Implement a local search (LS2) for the given split and RMA factors
If the temporary solution is better than the current, update the current solution
Otherwise accept the non-improving solution probabilistically
If the current solution is better than the best, update best
If there is no improvement on the best solution for $g$ number of iterations, implement a local search (LS1) on the best solution.
}
}

The probability of accepting non-improving solutions is calculated using Equation (20) defined by [42]. Based on this equation, probability of accepting non-improving solutions is higher at the higher temperatures, and it decreases as the temperature decreases.

$$P = \exp\left(-\frac{\Delta E}{c \cdot T'}\right), \tag{20}$$

where, $\Delta E$ is the difference of the makespan between the temporary solution and the current solution. $c$ is a Boltzmann constant, and $T$ is the current temperature level. The other model parameters used in the SA algorithm are: $T_0$ is initial temperature, $\pi$ is the cooling parameter ($0 < \pi < 1$) and $\nu$ is the number of moves at each stage where the local search is applied.

## 5. Simulation results

In this study, we only work on identical two parallel machines ($m = 2$). However, our models are capable of considering multiple machines. We solve our parallel machine scheduling problem for 10, 20, 30 and 50 jobs to investigate the effects of heuristics. We randomly generate processing times of jobs based on a uniform distribution that resides between 1 and 160. We use 10 different data set for each job set separately. We assume that RMA time is 5 unit time, and deterioration

rate is selected 0.08. After a simple tuning operation by trial-and-error, we decide to have 15 ants in the population in ACO algorithm. The evaporation rate is 0.70 so as to enhance more diversity. The other ACO parameters are $\alpha = 1$, $\beta = 2$, $\xi = 0.1$, $q_0 = 0.1$, $\tau_{min} = 0.1$ and $\tau_{max} = 0.49$. Last, the algorithm is terminated after 1000 iterations. The SA algorithm is simulated for 500 iterations and 5 stages at each iteration. Initial temperature is selected 100, the cooling parameter is 0.99, and the Boltzmann constant is 0.4. Finally, the mathematical model (MM) is coded and solved in IBM ILOG OPL CPLEX Optimization Studio 12.6. Because of the NP-Hardness of the problem, solution time is restricted to 3 hours. If a global optimum integer solution is not obtained by 3 hours, we used the best integer objective value found for the comparisons. The ACO and SA algorithms are coded with JAVA. They all are run on Intel(R) Core(TM) i5 3.5 GHz PC with 2GB ram. Additionally, we also conduct 10 replications on the ACO and SA algorithms for each data set. We use the simple average of the ten replications for the comparisons.

Tables 3, 4 and 5 show the detailed solutions of the algorithms. In Table 3, "Gap(%)" represents absolute tolerance on the gap between the best integer objective and the objective of the best node remaining when the model is terminated. As seen in this table, the gap increases as the number of jobs increases, especially for 50 jobs due to NP-hardness of the problem. "Best found solution" column in Tables 4 and 5 show the best solution obtained by ACO and SA, respectively at the end of iterations. "CPU time" in these tables is the computational time that algorithms spend to obtain the solution over iterations. The average computational times of ACO algorithm for 10-, 20-, 30- and 50 job-problems are 0.6, 2, 4.8 and 15 seconds. For SA, these are 0.2, 3, 7.8 and 95.8 seconds. As seen, SA algorithm takes more time than ACO as the number of jobs increases due to intensive local search.

In order to compare solution quality of ACO and SA algorithms, we calculate their percentage error that represents the difference of their solutions with MM as a basis on mathematical model solutions. These errors are given in Table 6. As seen in the table, for small number of jobs ACO provides close solutions to the mathematical model. The average error of ACO is about 4% for 30 jobs and it takes only 4.8 seconds. However, the SA algorithm does not provide as good solutions as the ACO algorithm. The average error of SA is about 7.7% for 30 jobs. In terms of computational time, even though SA is faster than ACO for 10 jobs, SA requires more time than ACO as the number of jobs increases. The reason of this observation is due to the intensive local search algorithm in SA.

## 6. Conclusion

In this study, we developed an integer programming model for parallel machine scheduling with deteriorating jobs and rate modifying activities. We consider non-linearly increasing function of processing times based on the sequence of the job. We also consider rate-modifying activities to recover the loss in processing times of the jobs. Because this problem is NP-hard, we proposed two meta-heuristic algorithms that rely on Ant colony optimization and Simulated annealing algorithms. In the ACO algorithm, we proposed different pheromone update schemes for the problem. We run our mathematical model and heuristics with two identical parallel machines for four different sets of jobs; 10, 20, 30 and 50. Results show that the ACO algorithm performs better than SA and generates close optimal solutions for with an average error of 0.7%, 1.6%, 4% and 8.8% for 10, 20, 30 and 50 jobs, respectively. In terms of computational time, ACO is also superior than SA as numbers of job increases. For future studies, the proposed ACO algorithm might be powered by an efficient local search algorithm to obtain closer solutions to the best found solutions.

## References

[1] Mohring, R. and Rademacher, F., *An Introduction to Stochastic Scheduling Problems* . In: Neumann, K. and Pallaschke, D. (Eds.), Contributions to Operations Research, Springer, Berlin, (1985).

[2] Righter, R., *Stochastic Scheduling* . In: Skaked, M. and Shanthikumar, G. (Eds.), Academic Press, San Diego, CA, (1994).

[3] Pinedo, M., *Scheduling, Theory, Algorithms and Systems* . Prentice-Hall, Englewood Cliffs, NJ, (1995).

[4] Boudreau, J., Hopp, W., McClain, J., and Thomas, L., On the Interface Between Operations and Human Resources Management . *Manufacturing and Service Operations Management*, 5(3), 179–202, (2003).

[5] Gupta, J. and Gupta, S., Single Facility Scheduling with Nonlinear Processing Times . *Computers and Industrial Engineering*, 14, 387–393, (1988).

[6] Gupta, S., Kunnathur, A., and Dandapani, K., Optimal Repayment Policies for Multiple Loans . *OMEGA*, 15(4), 323–330, (1987).

[7] Tanaev, V., Gordon, V., and Shafransky, Y., *Scheduling Theory, Single-stage Systems* . Kluwer, Dordrecht, (1994).

[8] Browne, S. and Yechiali, U., Scheduling Deteriorating Jobs on a Single Processor . *Operations Research*, 38, 495–498, (1990).

[9] Gawiejnowicz, S. and Pankowska, L., Scheduling Jobs with Varying Processing Times . *Information Processing Letters*, 54(3), 175–178, (1995).

**Table 3.** Mathematical model solutions.

| | Best Found Integer Solution | | | | Gap (%) | | | |
|---|---|---|---|---|---|---|---|---|
| $n$ | 10 | 20 | 30 | 50 | 10 | 20 | 30 | 50 |
| Data 1 | 536.85 | 459.62 | 1250.6 | 2526.53 | 0.00 | 0.01 | 0.01 | 1.13 |
| Data 2 | 340.9 | 473.94 | 1545.4 | 2646.81 | 0.02 | 0.00 | 0.08 | 2.01 |
| Data 3 | 306.92 | 466.66 | 1539.9 | 2648.31 | 0.00 | 0.10 | 0.01 | 5.08 |
| Data 4 | 394.83 | 943.87 | 1153.8 | 2848.57 | 0.00 | 0.01 | 0.00 | 1.70 |
| Data 5 | 437.03 | 248.17 | 1434.8 | 3010.16 | 0.01 | 0.00 | 0.00 | 4.43 |
| Data 6 | 475.68 | 232.98 | 1991.3 | 2530.86 | 0.01 | 1.6 | 0.01 | 3.11 |
| Data 7 | 495.38 | 1156.5 | 1646.00 | 2758.91 | 0.0 | 0.00 | 0.02 | 1.16 |
| Data 8 | 360.28 | 857.80 | 1158.70 | 2271.40 | 0.03 | 0.01 | 0.01 | 6.85 |
| Data 9 | 315.61 | 665.27 | 1768.8 | 2320.72 | 0.01 | 0.06 | 0.05 | 3.60 |
| Data 10 | 453.61 | 885.32 | 1364.8 | 2581.11 | 0.00 | 0.00 | 0.01 | 1.20 |

**Table 4.** Ant colony optimization algorithm solutions.

| | Best Found Solution | | | | CPU Time (sec.) | | | |
|---|---|---|---|---|---|---|---|---|
| $n$ | 10 | 20 | 30 | 50 | 10 | 20 | 30 | 50 |
| Data 1 | 541.32 | 469.06 | 1314.68 | 2758.19 | 0.6 | 2.0 | 4.8 | 15.0 |
| Data 2 | 344.10 | 475.57 | 1605.71 | 2899.70 | 0.6 | 2.0 | 5.0 | 14.8 |
| Data 3 | 310.13 | 469.94 | 1593.11 | 2682.29 | 0.6 | 1.8 | 4.8 | 14.4 |
| Data 4 | 399.25 | 964.71 | 1208.12 | 3042.29 | 0.6 | 2.0 | 5.0 | 15.2 |
| Data 5 | 443.52 | 253.84 | 1492.18 | 3212.44 | 0.6 | 2.0 | 4.8 | 14.8 |
| Data 6 | 478.37 | 233.61 | 2041.39 | 2741.60 | 0.6 | 2.0 | 4.8 | 15.4 |
| Data 7 | 497.35 | 1178.58 | 1718.31 | 2963.06 | 0.6 | 2.0 | 4.8 | 15.0 |
| Data 8 | 365.52 | 878.28 | 1210.17 | 2503.02 | 0.6 | 2.0 | 4.8 | 14.8 |
| Data 9 | 319.61 | 677.15 | 1841.23 | 2535.55 | 0.6 | 2.0 | 4.8 | 14.8 |
| Data 10 | 455.71 | 906.78 | 1422.92 | 2808.14 | 0.6 | 2.0 | 4.8 | 15.4 |

**Table 5.** Simulated annealing algorithm solutions.

| | Best Found Solution | | | | CPU Time (sec.) | | | |
|---|---|---|---|---|---|---|---|---|
| $n$ | 10 | 20 | 30 | 50 | 10 | 20 | 30 | 50 |
| Data 1 | 546.70 | 470.72 | 1309.87 | 2885.99 | 0.2 | 3.0 | 13.6 | 95.0 |
| Data 2 | 345.06 | 480.00 | 1669.84 | 3186.85 | 0.2 | 3.0 | 14.0 | 96.0 |
| Data 3 | 313.08 | 470.48 | 1673.91 | 2867.50 | 0.2 | 3.2 | 14.0 | 94.8 |
| Data 4 | 408.04 | 991.29 | 1263.99 | 3216.51 | 0.2 | 3.0 | 13.8 | 95.8 |
| Data 5 | 447.87 | 265.17 | 1534.22 | 3464.48 | 0.2 | 3.0 | 14.0 | 95.0 |
| Data 6 | 496.52 | 236.13 | 2086.18 | 2940.05 | 0.2 | 3.0 | 13.8 | 95.6 |
| Data 7 | 510.22 | 1202.72 | 1758.61 | 3189.91 | 0.2 | 3.0 | 13.8 | 95.6 |
| Data 8 | 369.02 | 918.02 | 1282.63 | 2583.84 | 0.2 | 3.0 | 14.0 | 95.6 |
| Data 9 | 336.81 | 705.75 | 1930.59 | 2723.22 | 0.2 | 3.0 | 13.8 | 95.6 |
| Data 10 | 466.09 | 945.45 | 1461.22 | 2893.22 | 0.2 | 3.0 | 13.8 | 95.6 |

[10] Kunnathur, A. and Gupta, S., Minimizing the Makespan with Late Start Penalties Added to Processing Times in a Single Facility Scheduling Problem . *European Journal of Operational Research*, 47(1), 56–64, (1990).

[11] Mosheiov, G., Scheduling Jobs With Step-Deterioration ; Minimizing Makespan on a Single and Multi-Machine . *Computers and Industrial Engineering*, 28(4), 869–879, (1995)

[12] Ozturkoglu, Y. and Bulfin, R. L., A Unique Integer Mathematical Model for Scheduling Deteriorating Jobs with Rate-Modifying Activities on a Single Machine. *The International Journal of Advanced Manufacturing Technology*, 57(5-8), 753–762, (2011).

[13] Alidaee, B. and Womer, N., Scheduling with Time Dependent Processing Times: Review and Extensions. *Journal of the Operational Research Society*, 50(7), 711–721, (1999).

[14] Cheng, T., Ding, Q., and Lin, B., A Concise Survey of Scheduling with Time-Dependent Processing Times . *European Journal of Operational Research*, 152, 1–13, (2004).

[15] Lodree, E., Geiger, C., and Jiang, X., Taxonomy for Integrating Scheduling Theory and Human Factors:

**Table 6.** The percentage gap among MM, ACO and SA algorithms.

| | ACO vs. MM | | | | SA vs. MM | | | |
|---|---|---|---|---|---|---|---|---|
| $n$ | 10 | 20 | 30 | 50 | 10 | 20 | 30 | 50 |
| Data 1 | 0.83 | 2.05 | 5.21 | 9.17 | 1.83 | 2.42 | 4.74 | 14.23 |
| Data 2 | 0.94 | 0.34 | 3.90 | 9.55 | 1.22 | 1.28 | 8.05 | 20.4 |
| Data 3 | 0.91 | 0.69 | 3.46 | 8.67 | 2.01 | 0.82 | 8.70 | 16.17 |
| Data 4 | 0.83 | 2.21 | 4.71 | 6.80 | 3.35 | 5.02 | 9.55 | 12.92 |
| Data 5 | 0.75 | 2.28 | 4.00 | 6.72 | 2.48 | 6.85 | 6.93 | 15.09 |
| Data 6 | 0.57 | 0.27 | 2.52 | 8.33 | 4.38 | 1.35 | 4.76 | 16.17 |
| Data 7 | 0.40 | 1.91 | 4.39 | 7.40 | 3.00 | 4.00 | 6.84 | 15.62 |
| Data 8 | 0.81 | 2.39 | 4.44 | 10.20 | 2.43 | 7.03 | 10.70 | 13.76 |
| Data 9 | 0.80 | 1.79 | 4.09 | 9.26 | 6.72 | 6.08 | 9.15 | 17.34 |
| Data 10 | 0.46 | 2.42 | 4.26 | 8.80 | 2.75 | 6.79 | 7.06 | 12.09 |
| Average | 0.73 | 1.64 | 4.09 | 8.49 | 3.02 | 4.16 | 7.65 | 15.38 |

Review and Research Opportunities . *International Journal of Industrial Ergonomics*, 39, 39–51, (2009).

[16] Chen, Z., Parallel Machine Scheduling with Time Dependent Processing Times . *Discrete Applied Mathematics*, 70, 81–93, (1996).

[17] Mosheiov, G., Multi-machine Scheduling with Linear Deterioration. *Infor*, 36, 205–214, (1998).

[18] Kang, L. and Ng, C., A Note on a Fully Polynomial-Time Approximation Scheme for Parallel-Machine Scheduling with Deteriorating Jobs . *International Journal of Production Economics*, 109, 180–184, (2007).

[19] Ji, M. and Cheng, T., Parallel-Machine Scheduling with Simple Linear Deterioration to Minimize Total Completion Time . *European Journal of Operational Research*, 188, 341–347, (2008).

[20] Ji, M. and Cheng, T., Parallel-Machine Scheduling of Simple Linear Deteriorating Jobs . *Theoretical Computer Science*, 410, 3761–3768, (2009).

[21] Lee, C.-Y. and Leon, V., Machine Scheduling with Rate-Modifying Activity . *European Journal of Operational Research*, 128, 493–513, (2001).

[22] Lee, C.-Y. and Lin, C.-S., Single Machine Scheduling with Maintenance and Repair Rate-Modifying Activities . *European Journal of Operational Research*, 135, 495–513, (2001).

[23] Mosheiov, G. and Sidney, J., New Results on Sequencing with Rate Modification . *Information Systems and Operational Research*, 41(2), 155–163, (2003).

[24] Ozturkoglu, Y., A Bi-Criteria Single Machine Scheduling with Rate-Modifying-Activity. *Gazi University Journal of Science*, 26(1), 97–106, (2013).

[25] Kim, B. S. and Ozturkoglu, Y., Scheduling a Single Machine With Multiple Preventive Maintenance Activities And Position-Based Deteriorations Using Genetic Algorithms. *The International Journal of Advanced Manufacturing Technology*, 67(5-8), 1127–1137, (2013).

[26] Ozturkoglu, Y., An Efficient Time Algorithm for Makespan Objectives. *An International Journal of Optimization and Control: Theories & Applications (IJOCTA)*, 5(2), 75-80, (2015).

[27] Lee, W.-C. and Wu, C.-C., Multi-Machine Scheduling with Deteriorating Jobs and Scheduled Maintenance . *Applied Mathematical Modeling*, 32, 362–373, (2008).

[28] Dalfard, V. M. and Mohammadi, G., Two Meta-Heuristic Algorithms for Solving Multi-Objective Flexible Job-Shop Scheduling with Parallel Machine and Maintenance Constraints. *Computers & Mathematics with Applications*, 64(6), 2111–2117, (2012).

[29] Cheng, B., Wang, Q., Yang, S., and Hu, X., An Improved Ant Colony Optimization for Scheduling Identical Parallel Batching Machines With Arbitrary Job Sizes. *Applied Soft Computing*, 13(2):765–772, (2013).

[30] Wang, J.-B. and Wei, C.-M., Parallel Machine Scheduling With a Deteriorating Maintenance Activity And Total Absolute Differences Penalties. *Applied Mathematics and Computation*, 217(20), 8093–8099, (2011).

[31] Wang, J.-J., Wang, J.-B., and Liu, F., Parallel Machines Scheduling With a Deteriorating Maintenance Activity. *Journal of the Operational Research Society*, 62(10), 1898–1902, (2011).

[32] Yang, D.-L. and Yang, S.-J., Unrelated Parallel-Machine Scheduling Problems with Multiple Rate-Modifying Activities. *Information Sciences*, 235, 280–286, (2013).

[33] Yang, D.-L., Cheng, T., and Yang, S.-J., Parallel-Machine Scheduling With Controllable Processing Times and Rate-Modifying Activities to Minimise Total Cost Involving Total Completion Time and Job Compressions. *International Journal of Production Research*, 52(4), 1133–1141, (2014).

[34] Dorigo, M., Maniezzo, V., and Colorni, A., Positive Feedback as a Search Strategy . *Technical Report 91-016, Dip. Elettronica,Politecnico di Milano, Italy*, (1991).

[35] Sankar, S., Ponnambalam, S., Rathinavel, V., and Visveshvaren, M., Scheduling in Parallel Machine Shop: An Ant Colony Optimization Approach . *Industrial Technology, ICIT, IEEE Industrial Conference*, pages 276–280, (2005).

[36] Tkindt, V., Monmarche, N. Tercinet, F., and Laugt, D., An Ant Colony Optimization Algorithm to Solve a 2-Machine Bicriteria Flowshop Scheduling Problem . *European Journal of Operational Research*, 142, 250–257, (2002).

[37] Alaykiran, K., Engin, O., and Doyen, A., Using Ant Colony Optimization to Solve Hybrid Flowshop Scheduling Problems . *International Journal of Advanced Manufacturing Technology*, 35, 541–550, (2007).

[38] Arnaout, J.-P., Musa, R., and Rabadi, G., Ant Colony Optimization Algorithm to Parallel Machine Scheduling Problem with Setups . *4th IEEE Conference on Automation Science Engineering, Washington DC, USA*, pages 578–582, (2008).

[39] Arnaout, J.P. and Rabadi, G. and Musa, R. A Two-Stage Ant Colony Optimization Algorithm to Minimize the Makespan on Unrelated Parallel Machines with Sequence-Dependent Setup Times . *Journal of Intelligent Manufacturing*, 21(6), 693-701, (2010).

[40] Rossi, A. and Boschi, E., A Hybrid Heuristic to Solve the Parallel Machines Job-shop Scheuling Problem . *Advances in Engineering Software*, 40, 118–127, (2009).

[41] Behnamian, J., Zandieh, M., and Ghomi, S., Parallel-Machine Scheduling Problems with Sequence-Dependent Setup Times using an ACO, SA and VNS Hybrid Algorithm . *Experts Systems with Applications*, 36, 9637–9644, (2009).

[42] Kirkpatrick, S., Gelatt, C., and Vecchi, M., Optimization by Simulated Annealing . *Science*, 220, 671–680, (1983).

[43] Koulamas, C., Decomposition and Hybrid Simulated Annealing Heuristics for the Parallel-Machine Total Tardiness Problem . *Naval Research Logistics*, 44, 105–125, (1997).

[44] Park, M.-W. and Kim, Y.-D., Search Heuristics for a Parallel Machine Scheduling Problem with Ready Times and Due Dates . *Computers and Industrial Engineering*, 33(3-4), 793–796, (1997).

[45] Józefowska, J., Mika, M., Różycki, R., and Waligóra, G., Local Search Metaheuristics for Discrete-Continuous Scheduling Problems . *European Journal of Operational Research*, 107, 354–370, (1998).

[46] Hindi, K. and Mhlanga, S., Scheduling Linearly Deteriorating Jobs on Parallel Machines: A Simulated Annealing Approach . *Production Planning and Control*, 12(1), 76–80, (2001).

[47] Kim, D.-W., Kim, K.-H., Jang, W., and Chen, F., Unrelated Parallel Machine Scheduling with Setup Times Using Simulated Annealing . *Robotics and Computer Integrated Manufacturing*, 18(3-4), 223–231, (2002).

***Ömer Öztürkoğlu*** *is an Assistant Professor in Business Administration at Yasar University, Izmir, Turkey. He teaches related courses to Logistics Facilities, Warehousing, and Production and Operations Analysis. In general, his research interests are production and operations systems analysis and design.*



An International Journal of Optimization and Control: Theories & Applications
ISSN:2146-0957 eISSN:2146-5703
Vol.7, No.2, pp.177-185 (2017)
http://doi.org/10.11121/ijocta.01.2017.00339

RESEARCH ARTICLE

# A modified quadratic hybridization of Polak-Ribière-Polyak and Fletcher-Reeves conjugate gradient method for unconstrained optimization problems

Sindhu Narayanan, P. Kaelo* and M.V. Thuto

*Department of Mathematics, University of Botswana, Private Bag UB00704, Gaborone, Botswana*
*sindhu.op@gmail.com, kaelop@mopipi.ub.bw, thutomv@mopipi.ub.bw*

ARTICLE INFO

Article History:
*Received 15 December 2016*
*Accepted 23 February 2017*
*Available 15 July 2017*

Keywords:
*Hybridization*
*Conjugate gradient*
*Wolfe line search conditions*
*Global convergence*

AMS Classification 2010:
*90C06, 90C30, 65K05*

ABSTRACT

This article presents a modified quadratic hybridization of the Polak–Ribière–Polyak and Fletcher–Reeves conjugate gradient method for solving unconstrained optimization problems. Global convergence, with the strong Wolfe line search conditions, of the proposed quadratic hybrid conjugate gradient method is established. The new method is tested on a number of benchmark problems that have been extensively used in the literature and numerical results show the competitiveness of the new hybrid method.



## 1. Introduction

Nonlinear conjugate gradient method is a very powerful technique for solving large scale unconstrained optimization problems

$$\min\{f(x) : x \in \mathbb{R}^n\}, \tag{1}$$

where $f : \mathbb{R}^n \to \mathbb{R}$ is a continuously differentiable function. It has advantages over Newton and quasi-Newton methods in that it only needs the first order derivative and hence less storage capacity is needed. It is also relatively simple to program.

Given an initial guess $x_0 \in \mathbb{R}^n$, the nonlinear conjugate gradient method generates a sequence $\{x_k\}$ for problem (1) as

$$x_{k+1} = x_k + \alpha_k d_k, \qquad k = 0, 1, 2, \ldots, \tag{2}$$

where $\alpha_k$ is a step length which is determined by a line search and $d_k$ is a descent direction of $f$ at $x_k$ generated as

$$d_k = \begin{cases} -g_k, & \text{if} \quad k = 0, \\ -g_k + \beta_k d_{k-1}, & \text{if} \quad k \geq 1, \end{cases} \tag{3}$$

where $g_k = \nabla f(x_k)$ is the gradient of $f$ at $x_k$ and $\beta_k$ is a parameter.

Conjugate gradient methods differ in their way of defining the parameter $\beta_k$. Over the years, several choices of $\beta_k$, which give rise to different conjugate gradient methods, have been proposed. The most famous formulas for $\beta_k$ are Fletcher-Reeves (FR) method [20]

$$\beta_k^{FR} = \frac{||g_k||^2}{||g_{k-1}||^2},$$

Polak-Ribiére-Polyak (PRP) method [32, 33]

$$\beta_k^{PRP} = \frac{g_k^T y_{k-1}}{||g_{k-1}||^2},$$

Dai-Yuan (DY) method [12]

$$\beta_k^{DY} = \frac{||g_k||^2}{d_{k-1}^T y_{k-1}},$$

and the Hestenes-Stiefel (HS) method [18, 23]

*Corresponding Author

$$\beta_k^{HS} = \frac{g_k^T y_{k-1}}{d_{k-1}^T y_{k-1}},$$

where $y_{k-1} = g_k - g_{k-1}$ and $||\cdot||$ denotes the Euclidean norm of vectors. These were the first scalars $\beta_k$ for nonlinear conjugate gradient methods to be proposed. Since then, other parameters $\beta_k$ have been proposed in the literature (see for example [1,2,4–6,14,15,17,19,22,28,35,39,40] and references therein).

From the literature, it is well known that FR and DY methods have strong convergence properties. However, they may not perform well in practice. On the other side, PRP and HS methods are known to perform better numerically but may not converge in general. Given this, researchers try to devise some new methods, which have the advantages of these two kinds of methods. This has been done mostly by combining two or more $\beta_k$ parameters in the same conjugate gradient method to come up with hybrid methods. Thus, hybrids try to combine attractive features of different algorithms. For example, Touati-Ahmed and Storey [36] proposed this hybrid method

$$\beta_k^{TS} = \max\left\{0, \min(\beta_k^{FR}, \beta_k^{PRP})\right\}$$

to take advantage of the attractive convergence properties of $\beta_k^{FR}$ and numerical performance of $\beta_k^{PRP}$.

Many other hybrids have been proposed by parametrically combining different parameters $\beta_k$. In Dai and Yuan [11], for instance, a one-parameter family of conjugate gradient methods is proposed as

$$\beta_k = \frac{||g_k||^2}{\lambda_k||g_{k-1}||^2 + (1-\lambda_k)d_{k-1}^T y_{k-1}},$$

where the parameter $\lambda_k$ is such that $\lambda_k \in [0,1]$. Liu and Li [28] proposes a convex combination of $\beta_k^{LS}$ and $\beta_k^{DY}$ to get

$$\beta_k = (1-\gamma_k)\beta_k^{LS} + \gamma_k\beta_k^{DY},$$

where $\beta_k^{LS} = -\frac{g_k^T y_{k-1}}{d_{k-1}^T g_{k-1}}$ is the Liu-Storey (LS) [26] parameter and $\gamma_k \in [0,1]$. Other hybrid conjugate gradient methods can be found in [2, 4–8, 13, 21, 22, 24, 25, 27, 29, 35, 38, 41].

The step length $\alpha_k$ is often chosen to satisfy certain line search conditions. It is very important in the convergence analysis and implementation of conjugate gradient methods. The line search in the conjugate gradient methods is often based on the weak Wolfe conditions

$$f(x_k + \alpha_k d_k) \leq f(x_k) + \mu\alpha_k g_k^T d_k \tag{4}$$

and

$$g(x_k + \alpha_k d_k)^T d_k \geq \sigma g_k^T d_k, \tag{5}$$

or the stronger version of the Wolfe line search conditions

$$f(x_k + \alpha_k d_k) \leq f(x_k) + \mu\alpha_k g_k^T d_k \tag{6}$$

and

$$|g(x_k + \alpha_k d_k)^T d_k| \leq -\sigma g_k^T d_k, \tag{7}$$

where $0 < \mu < \sigma < 1$. More information on these line search methods and other line search methods can be found in the literature [9, 14, 25, 31, 34, 37, 39, 41]. In this paper, we suggest another approach to get a new hybrid nonlinear conjugate gradient method.

The rest of the paper is organised as follows. In section 2, we present the proposed method. In Section 3 we prove that the proposed algorithm (method) globally converges. Section 4 presents some numerical experiments and conclusion is given in Section 5.

## 2. A new hybrid conjugate gradient method

We now present our proposed hybrid conjugate gradient method. The hybrid method we propose is motivated by the work of Babaie-Kafaki [4, 5] and Mo, Gu and Wei [29]. Babaie-Kafaki [4, 5] suggested a quadratic hybridization of $\beta_k^{FR}$ and $\beta_k^{PRP}$ method of the form

$$\beta_k^{HQ\pm} = \begin{cases} \beta_k^{+}(\theta_k^{\pm}), & \theta_k^{\pm} \in [-1,1], \\ \beta_k^{PRP+}, & \theta_k^{\pm} \in \mathbb{C}, \\ -\beta_k^{FR}, & \theta_k^{\pm} < -1, \\ \beta_k^{FR}, & \theta_k^{\pm} > 1, \end{cases} \tag{8}$$

where

$$\beta_k^{+}(\theta_k) = (1-\theta_k^2)\beta_k^{PRP} + \theta_k\beta_k^{FR}, \qquad \theta_k \in [-1,1],$$

and

$$\theta_k^{\pm} = \frac{\beta_k^{FR} \pm \sqrt{(\beta_k^{FR})^2 - 4\beta_k^{PRP}(\beta_k^{HS} - \beta_k^{PRP})}}{2\beta_k^{PRP}}$$

is the solution of the quadratic equation

$$\theta_k^2 \beta_k^{PRP} - \theta_k \beta_k^{FR} + \beta_k^{HS} - \beta_k^{PRP} = 0.$$

Thus, the author suggested two methods $\beta_k^{HQ+}$ and $\beta_k^{HQ-}$. The parameter

$$\beta_k^{PRP+} = \max\{0, \beta_k^{PRP}\}$$

is a hybrid parameter that was suggested by Gilbert and Nocedal [21] to improve on the convergence properties of $\beta_k^{PRP}$.

In Mo, Gu and Wei [29], the authors suggest a $\beta_k^*$ defined by

$$\beta_k^* = \beta_k^{PRP} + \frac{2g_k^T g_{k-1}}{\|g_{k-1}\|^2}, \tag{9}$$

which then modifies the Touati-Ahmed and Storey method [36] to give

$$\beta_k = \max\left\{0, \min(\beta_k^{FR}, \beta_k^{PRP}, \beta_k^*)\right\}.$$

This method by Mo et al. [29] was shown to be very competitive with the other hybrids in the literature and it was shown to perform much better than the original $\beta_k^{PRP}$.

Now, motivated by this suggestion (9) from [29] and the work of Babaie-Kafaki [4,5], in this work we modify Babaie-Kafaki's method by introducing $\beta_k^S$ as

$$\beta_k^S = \begin{cases} \beta_k^+(\theta_k), & \theta_k \in [-1,1], \\ \max\{0, \beta_k^*\}, & \theta_k \in \mathbb{C}, \\ -\beta_k^{FR}, & \theta_k < -1, \\ \beta_k^{FR}, & \theta_k > 1, \end{cases} \tag{10}$$

where

$$\theta_k = \frac{\beta_k^{FR} - \sqrt{(\beta_k^{FR})^2 - 4\beta_k^*(\beta_k^{HS} - \beta_k^*)}}{2\beta_k^*}$$

and

$$\beta_k^+(\theta_k) = (1-\theta_k^2)(\max\{0, \beta_k^*\}) + \theta_k \beta_k^{FR}, \quad \theta_k \in [-1,1], \tag{11}$$

where $\beta_k^*$ is as defined in (9), and then define

$$d_k = \begin{cases} -g_k, & k = 0, \\ -g_k + \beta_{k-1}^S d_{k-1}, & k \geq 1. \end{cases} \tag{12}$$

This leads to our hybrid conjugate gradient method presented below.

**Algorithm 1.** *New Hybrid $\beta_k^S$ Conjugate Gradient Method*

Step 1 *Give initial guess $x_0 \in \mathbb{R}^n$, and the parameters $0 < \mu < \sigma < 1$ and $\epsilon > 0$.*
Step 2 *Set $d_0 = -g_0$ and $k = 0$. If $||g_0|| < \epsilon$, stop.*
Step 3 *Compute $\alpha_k$ using the strong Wolfe conditions (6) and (7).*
Step 4 *Set $x_{k+1} = x_k + \alpha_k d_k$, $k = k + 1$.*
Step 5 *If $||g_k|| < \epsilon$, stop.*
Step 6 *Compute $\beta_k$ using (10–11).*
Step 7 *Compute $d_k = -g_k + \beta_k^S d_{k-1}$, go to Step 3.*

## 3. Global convergence of the proposed method

The global convergence analysis in this section follows that of Babaie-Kafaki [4, 5]. To analyze the global convergence property of our hybrid method, the following assumptions are required. These assumptions have been used extensively in the literature for the global convergence analysis of conjugate gradient methods.

**Assumption 1.** *Let the level set*

$$\Omega = \{x \in \mathbb{R}^n : f(x) \leq f(x_0)\},$$

*where $x_0$ is the initial guess, be bounded. That is, there exists a positive constant $B$ such that*

$$\|x\| \leq B, \quad \forall x \in \Omega. \tag{13}$$

**Assumption 2.** *In some neighbourhood $N$ of $\Omega$, the function $f$ is continuously differentiable and its gradient, $g(x) = \nabla f(x)$, is Lipschitz continuous, that is, there exists a constant $L > 0$ such that*

$$\|g(x) - g(y)\| \leq L\|x - y\|$$

*for all $x, y \in N$.*

These assumptions imply that there exists a positive constant $\hat{\gamma}$ such that

$$\|g(x)\| \leq \hat{\gamma}. \tag{14}$$

Also, under **Assumptions** 1 and 2, the following lemma can be established.

**Lemma 1** (Zoutendijk lemma)**.** *Consider any iteration of the form $x_{k+1} = x_k + \alpha_k d_k$, where $d_k$ is a descent direction and $\alpha_k$ satisfies the weak Wolfe conditions (4) and (5). Suppose **Assumptions** 1 and 2 hold, then*

$$\sum_{k=0}^{\infty} \cos^2\theta_k \|g_k\|^2 < \infty.$$

It follows from **Lemma 1** and the sufficient descent condition with the Wolfe line search that

$$\sum_{k=0}^{\infty} \frac{\|g_k\|^4}{\|d_k\|^2} < \infty. \tag{15}$$

**Lemma 2.** *Suppose that **Assumptions** 1 and 2 hold. Consider any conjugate gradient method in the form of*

$$x_{k+1} = x_k + \alpha_k d_k, \quad k = 0, 1, 2, \cdots,$$

*and (12) in which, for all $k \geq 0$, the search direction $d_k$ is a descent direction and the step length $\alpha_k$ is determined to satisfy the Wolfe conditions. If*

$$\sum_{k=0}^{\infty} \frac{1}{\|d_k\|^2} = \infty, \tag{16}$$

*then the method converges in the sense that*

$$\liminf_{k \longrightarrow \infty} \|g_k\| = 0. \tag{17}$$

**Lemma 3.** *Suppose that **Assumptions** 1 and 2 hold. Consider any conjugate gradient method in the form of*

$$x_{k+1} = x_k + \alpha_k d_k, \quad k = 0, 1, 2, \cdots,$$

*and (12), with the conjugate gradient parameter $\beta_k^+(\theta_k)$ defined by (11), in which the step length $\alpha_k$ is determined to satisfy the strong Wolfe conditions (6) and (7).*

*Also assume that the descent condition*

$$d_k^T g_k < 0, \quad \forall k \geq 0 \tag{18}$$

*holds and there exists a positive constant $\xi$ such that*

$$|\theta_k| \leq \xi \alpha_k, \quad \forall k \geq 0. \tag{19}$$

*If, for a positive constant $\gamma$, we have*

$$\|g_k\| \geq \gamma, \quad \forall k \geq 0, \tag{20}$$

*then $d_k \neq 0$ and*

$$\sum_{k=0}^{\infty} \|u_{k+1} - u_k\|^2 < \infty, \tag{21}$$

*where $u_k = \frac{d_k}{\|d_k\|}$.*

***Proof.*** Firstly, note that the descent condition (18) guarantees that $d_k \neq 0$. So, $u_k$ is well-defined. Moreover, from (20) and **Lemma 2**, we have

$$\sum_{k=0}^{\infty} \frac{1}{\|d_k\|^2} < \infty, \tag{22}$$

since otherwise (17) holds contradicting (20). Now, we divide $\beta_k^+(\theta_k)$ into two parts as

$$\beta_k^{(1)} = (1 - \theta_k^2)\max(0, \beta_k^*), \quad \beta_k^{(2)} = \theta_k \beta_k^{FR},$$

and, for all $k \geq 0$, we define

$$r_{k+1} = \frac{v_{k+1}}{\|d_{k+1}\|}, \quad \delta_{k+1} = \beta_k^{(1)} \frac{\|d_k\|}{\|d_{k+1}\|},$$

where

$$v_{k+1} = -g_{k+1} + \beta_k^{(2)} d_k.$$

Therefore, from (12) we obtain that

$$u_{k+1} = r_{k+1} + \delta_{k+1} u_k. \tag{23}$$

Since $\|u_k\| = \|u_{k+1}\| = 1$, from (23) we can write

$$\|r_{k+1}\| = \|u_{k+1} - \delta_{k+1} u_k\| = \|\delta_{k+1} u_{k+1} - u_k\|. \tag{24}$$

Because $\theta_k \in [-1, 1]$, we have $\delta_{k+1} \geq 0$. Using the condition $\delta_{k+1} \geq 0$, the triangle inequality and (24), we get

$$\begin{aligned} \|u_{k+1} - u_k\| &\leq \|(1 + \delta_{k+1})u_{k+1} - (1 + \delta_{k+1})u_k\| \\ &\leq \|u_{k+1} - \delta_{k+1} u_k\| + \|\delta_{k+1} u_{k+1} - u_k\| \\ &= 2\|r_{k+1}\|. \end{aligned} \tag{25}$$

Also, from (13), (14), (19) and (20) we have

$$\begin{aligned}
\|v_{k+1}\| &= \| - g_{k+1} + \beta_k^{(2)} d_k\| \\
&= \| - g_{k+1} + \theta_k \tfrac{\|g_{k+1}\|^2}{\|g_k\|^2} d_k\| \\
&\leq \|g_{k+1}\| + |\theta_k| \tfrac{\|g_{k+1}\|^2}{\|g_k\|^2} \|d_k\| \\
&\leq \hat{\gamma} + \tfrac{\xi \alpha_k \hat{\gamma}^2}{\gamma^2} \|d_k\| \qquad (26) \\
&= \hat{\gamma} + \tfrac{\xi \hat{\gamma}^2 \|x_{k+1} - x_k\|}{\gamma^2} \\
&\leq \hat{\gamma} + \tfrac{\xi \hat{\gamma}^2 (\|x_{k+1}\| + \|x_k\|)}{\gamma^2} \\
&\leq \hat{\gamma} + \tfrac{2B\xi\hat{\gamma}^2}{\gamma^2}.
\end{aligned}$$

Now, from (22), (25), and (26) we have

$$\begin{aligned}
\sum_{k=0}^{\infty} \|u_{k+1} - u_k\|^2 &\leq 4 \sum_{k=0}^{\infty} \|r_{k+1}\|^2 \\
&= 4 \sum_{k=0}^{\infty} \frac{\|v_{k+1}\|^2}{\|d_{k+1}\|^2} \\
&\leq 4 \left(\hat{\gamma} + \tfrac{2B\hat{\gamma}^2\xi}{\gamma^2}\right)^2 \sum_{k=0}^{\infty} \frac{1}{\|d_{k+1}\|^2} \\
&\leq 4 \left(\hat{\gamma} + \tfrac{2B\hat{\gamma}^2\xi}{\gamma^2}\right)^2 \tfrac{1}{\gamma^4} \sum_{k=0}^{\infty} \frac{\|g_k\|^4}{\|d_{k+1}\|^2} \\
&< \infty
\end{aligned} \qquad (27)$$

□

We now define the following property, called property (*).

**Definition 1.** *[10] Consider any conjugate gradient method in the form of*

$$x_{k+1} = x_k + \alpha_k d_k, \quad k = 0, 1, 2, \cdots,$$

*and (12). Suppose that for a positive constant $\gamma$ the inequality (20) holds. Under this assumption, we say that the method has property (*) if and only if there exist constants $b > 1$ and $\lambda > 0$ such that for all $k \geq 0$,*

$$|\beta_k| \leq b, \qquad (28)$$

*and*

$$\|\alpha_k d_k\| \leq \lambda \Rightarrow |\beta_k| \leq \frac{1}{b}. \qquad (29)$$

**Theorem 1.** *Suppose that **Assumptions** 1 and 2 hold. Consider any conjugate gradient method in the form of*

$$x_{k+1} = x_k + \alpha_k d_k, \quad k = 0, 1, 2, \cdots,$$

*and (12), with the conjugate gradient parameter $\beta_k^+(\theta_k)$ defined by (11), in which the step length $\alpha_k$ is determined to satisfy the strong Wolfe conditions (6) and (7). If the search directions satisfy the descent condition (18) and there exists a positive constant $\eta$ such that*

$$|\theta_k| \leq \eta \|\alpha_k d_k\|, \quad \forall k \geq 0, \qquad (30)$$

*then the method converges in the sense that*

$$\liminf_{k \to \infty} \|g_k\| = 0.$$

***Proof.*** Because of the descent condition and strong Wolfe conditions, we have proven that the sequence $\{x_k\}_{k \geq 0}$ is a subset of the level set $\Omega$. Also, since all the assumptions of **Lemma 2** hold, the inequality (21) holds. Now, to prove the convergence, it is enough to show that the method has property (*).
Since $\theta_k \in [-1, 1]$, from (11), (14), and (20) we have

$$\begin{aligned}
|\beta_k^+(\theta_k)| &= |(1 - \theta_k)^2 (\max\{0, \beta_k^*\}) + \theta_k \beta_k^{FR}| \\
&\leq |(1 - \theta_k)^2| \left|\beta_k^{PRP} + \tfrac{2 g_{k+1}^T g_k}{\|g_k\|^2}\right| + |\theta_k| |\beta_k^{FR}| \\
&\leq |\beta_k^{PRP}| + \tfrac{|2 g_{k+1}^T g_k|}{\|g_k\|^2} + \beta_k^{FR} \\
&\leq \tfrac{\|g_{k+1}\|(\|g_{k+1}\| + \|g_k\|)}{\|g_k\|^2} + \tfrac{2\|g_{k+1}\|\|g_k\|}{\|g_k\|^2} + \tfrac{\|g_{k+1}\|^2}{\|g_k\|^2} \\
&\leq \tfrac{2\hat{\gamma}^2}{\gamma^2} + \tfrac{2\hat{\gamma}^2}{\gamma^2} + \tfrac{\hat{\gamma}^2}{\gamma^2} \\
&= \tfrac{5\hat{\gamma}^2}{\gamma^2}.
\end{aligned} \qquad (31)$$

Moreover, from **Assumption** 2 and equations (11), (14), (20), and (30) we get

$$\begin{aligned}
|\beta_k^+(\theta_k)| &= |(1 - \theta_k)^2 (\max\{0, \beta_k^*\}) + \theta_k \beta_k^{FR}| \\
&\leq |(1 - \theta_k)^2| \left|\beta_k^{PRP} + \tfrac{2 g_{k+1}^T g_k}{\|g_k\|^2}\right| + |\theta_k| |\beta_k^{FR}| \\
&\leq |\beta_k^{PRP}| + \tfrac{|2 g_{k+1}^T g_k|}{\|g_k\|^2} + |\theta_k| \beta_k^{FR} \\
&\leq \tfrac{\|g_{k+1}\|\|g_{k+1} - g_k\|}{\|g_k\|^2} + \tfrac{2\|g_{k+1}\|\|g_k\|}{\|g_k\|^2} + |\theta_k| \tfrac{\|g_{k+1}\|^2}{\|g_k\|^2}
\end{aligned}$$

$$\begin{aligned} &\leq \frac{L\hat{\gamma}\|x_{k+1}-x_k\|}{\gamma^2} + \frac{2\hat{\gamma}^2}{\gamma^2} + \frac{\eta\hat{\gamma}^2}{\gamma^2}\|\alpha_k d_k\| \\ &\leq \frac{L\hat{\gamma}}{\gamma^2}\|\alpha_k d_k\| + \frac{2\eta\hat{\gamma}^2}{\gamma^2}\|\alpha_k d_k\| + \frac{\eta\hat{\gamma}^2}{\gamma^2}\|\alpha_k d_k\| \qquad (32) \\ &= \frac{L\hat{\gamma}+3\eta\hat{\gamma}^2}{\gamma^2}\|\alpha_k d_k\|. \end{aligned}$$

So, from (31) and (32), if we let

$$b = \frac{5\hat{\gamma}^2}{\gamma^2} \quad \text{and} \quad \lambda = \frac{\gamma^2}{b(L\hat{\gamma}+3\eta\hat{\gamma}^2)},$$

then (28) and (29) hold and consequently, the method has property (*). □

## 4. Numerical Experiments

We now present numerical experiments obtained by our method on some test problems chosen from Morè, et al. [30] and Andrei [3] to analyse its efficiency and effectiveness. A number of these test problems are widely used in the literature for testing unconstrained optimization methods. We present these test problems in Table 1, where the columns 'Prob' and 'Dim', respectively, represent the name and dimension of the test problem, and the dimensions of the problems range from 2 to 20000.

We compare our proposed new hybrid conjugate gradient method ($\beta_k^S$) with the quadratic hybridization $\beta_k^{HQ-}$ of Babaie-Kafaki [4, 5] and the method $\beta_k^*$ by Mo, Gu and Wei [29]. In [4], $\beta_k^{HQ-}$ was shown to be the better hybridization as compared to $\beta_k^{HQ+}$, hence our comparison will only focus on $\beta_k^{HQ-}$. For all the methods, we considered the stopping condition to be $\epsilon = 10^{-5}$, that is, the algorithms (methods) were stopped once the condition $||g_k|| < 10^{-5}$ was satisfied, or the maximum number of iterations of 5000 was reached. For the line search, the strong Wolfe conditions (6) and (7) were used to find the step length $\alpha_k$, with $\mu = 0.0001$ and $\sigma = 0.16$. All the methods were coded in MATLAB R2015b and numerical results are compared based on number of gradient evaluations, function evaluations and CPU time.

In Table 1, we present the number of functions evaluations ($NFE$) and gradient evaluations ($NGE$) obtained for the methods $\beta_k^{HQ-}$, $\beta_k^S$ and $\beta_k^*$, where the best results for each problem are indicated in bold. We observe from the table that, overall, the incorporation of $\beta_k^*$ in the quadratic hybridization has a positive effect on $\beta_k^{HQ-}$, even though for some problems it is worse off.

We also compare the methods using the performance profiles tool suggested by Dolan and Moré [16] which, over the years, has been used extensively to judge the performance of different methods on a given set of test problems. The tool evaluates and then compares the performance of the set of methods $S$ on a set $P$ of test problems. That is, using the ratio

$$r_{p,s} = \frac{t_{p,s}}{\min\{t_{p,s} : s \in S\}},$$

where $t_{p,s}$ is (function, gradient, CPU time) evaluations required to solve $p$ by method $s$, the overall performance profile function is

$$\rho_s(\tau) = \frac{1}{n_p}\text{size}\{p : 1 \leq p \leq n_p, \log(r_{p,s}) \leq \tau\},$$

where $n_p$ is the total number of problems in $P$ and $\tau \geq 0$.

In case the method $s$ fails to solve problem $p$, the ratio $r_{p,s}$ is set to some sufficiently large number. The function $\rho_s(\tau)$ is then plotted against $\tau$ to give the performance profile. Notice that the function $\rho_s(\tau)$ takes the values $\rho_s(\tau) \in [0, 1]$ and so the inequality $\rho_s(\tau_1) < \rho_t(\tau_1)$ shows that the method $t$ outperforms the method $s$ at $\tau_1$.

We now present the plots of these performance profiles on function evaluations, gradient evaluations and CPU time as figures. The function evaluations performance profile is presented in Figure 1, gradient evaluations in Figure 2 and CPU time in Figure 3. It is clear from the figures that replacing $\beta_k^{PRP}$ by $\beta_k^*$ in the quadratic hybridization $\beta_k^{HQ-}$ has a positive effect. From the figures, we observe that $\beta_k^*$ is the best method overall. As for $\beta_k^S$ and $\beta_k^{HQ-}$, we see that in Figures 1 and 2, for $\tau \leq 0.5$, $\beta_k^{HQ-}$ is slightly better than $\beta_k^S$. However, in Figure 3, the plot shows that in terms of CPU time, there is not much difference between $\beta_k^S$ and $\beta_k^{HQ-}$ with the methods being much competitive. Overall the figures show the influence of $\beta_k^*$ on the quadratic hybridization over the use of $\beta_k^{PRP}$.

**Table 1.** Results of test problems.

| Prob | Dim | $\beta_k^{HQ-}$ | | $\beta_k^{S}$ | | $\beta_k^{*}$ | |
|---|---|---|---|---|---|---|---|
| | | NFE | NGE | NFE | NGE | NFE | NGE |
| Rosenbrock | 2 | 133 | 63 | **95** | 43 | **95** | **38** |
| Freud and Roth | 2 | 40 | **14** | 45 | 16 | **39** | **14** |
| Beale | 2 | **40** | **24** | 74 | 38 | 48 | 28 |
| Helical valley | 3 | **130** | **50** | 264 | 103 | 152 | 61 |
| Bard | 3 | 91 | 53 | **66** | **44** | 75 | 50 |
| Gaussian | 3 | **7** | **6** | 9 | 7 | 9 | 7 |
| Box | 3 | **41** | **30** | 44 | 32 | 47 | 37 |
| Powell Singular | 4 | 508 | 236 | 351 | 168 | **208** | **110** |
| Wood | 4 | 592 | 160 | 414 | 134 | **211** | **70** |
| Biggs EXP6 | 6 | **201** | **139** | 502 | 374 | 338 | 284 |
| Osborne 2 | 11 | **660** | **344** | 684 | 352 | 1557 | 762 |
| Broyden tridiagonal | 30 | **90** | **33** | **90** | **33** | 94 | 35 |
| Ext. TET | 100 | **17** | **10** | 28 | 15 | 20 | 11 |
| Gen. White & Holst | 100 | 11088 | 2614 | **9477** | **2329** | 14012 | 3451 |
| Ext. Penalty | 500 | 63 | 20 | **51** | **15** | 52 | **15** |
| Ext. Maratos | 500 | **234** | 109 | 630 | 259 | 257 | **105** |
| Gen. Rosenbrock | 1000 | **21985** | **4574** | 22010 | 4581 | 25069 | 6558 |
| Fletcher | 1000 | **15881** | **4664** | **15881** | **4664** | 27857 | 7616 |
| Ext. Rosenbrock | 5000 | 133 | 63 | **100** | 45 | 103 | **42** |
| | 10000 | 133 | 63 | **100** | 45 | 103 | **42** |
| Ext. Powell singular | 10000 | **257** | **136** | 623 | 294 | 273 | 154 |
| | 20000 | 475 | 236 | 1370 | 656 | **217** | **121** |
| Raydan 2 | 5000 | 52 | 52 | 7 | 7 | **6** | **6** |
| | 10000 | 101 | 101 | 8 | 8 | **6** | **6** |
| Ext. Beale | 10000 | 77 | 45 | 70 | 42 | **69** | **41** |
| | 20000 | 77 | 45 | 70 | 42 | **69** | **41** |
| Ext. Himmelblau | 10000 | **32** | **13** | 38 | 15 | 35 | 14 |
| | 20000 | **32** | **13** | 38 | 15 | 35 | 14 |
| Ext. DENSCHNB | 10000 | **15** | **9** | 19 | 13 | 17 | 10 |
| Ext. DENSCHNF | 10000 | 75 | 33 | 90 | 36 | **64** | **29** |
| Ext. Freud & Roth | 10000 | 40 | 14 | 45 | 16 | **39** | **14** |
| Ext. White & Holst | 10000 | 300 | 124 | 247 | 92 | **137** | **62** |
| Ext. Wood | 10000 | 757 | 200 | 450 | 145 | **224** | **74** |
| NONSCOMP | 10000 | **147** | **59** | 151 | 61 | 173 | 72 |
| Quartic | 10000 | 81 | 80 | **28** | **27** | 44 | 43 |

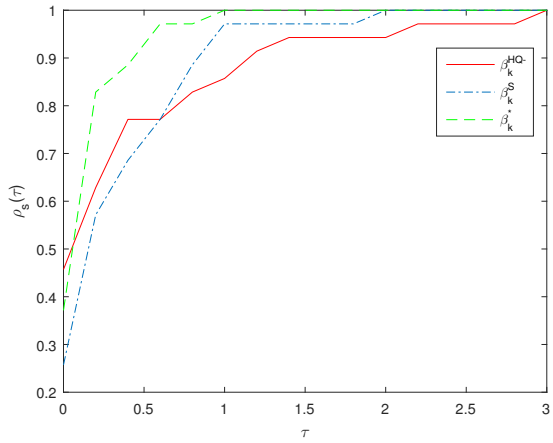


**Figure 1.** Function evaluations profile.

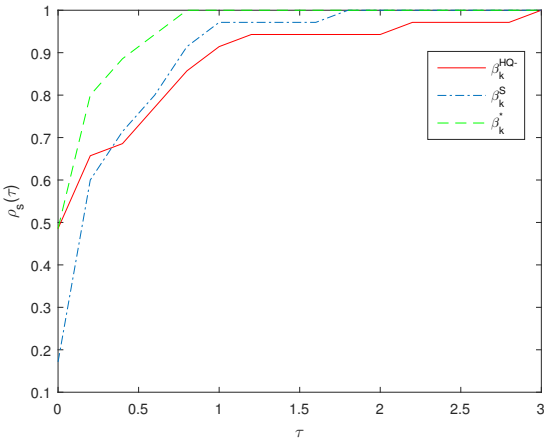


**Figure 2.** Gradient evaluations profile.

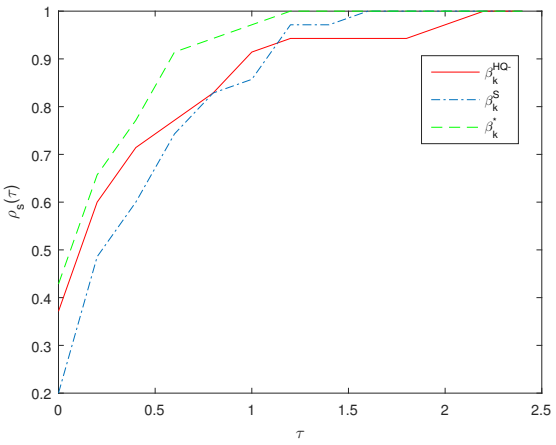


**Figure 3.** CPU time profile.

## 5. Conclusion

In this article, a modified quadratic hybridization of Polak–Ribière–Polyak and Fletcher–Reeves conjugate gradient method ($\beta_k^S$) was presented. Its global convergence under the strong Wolfe line search conditions was also established. The $\beta_k^S$ method presented was tested on a number of unconstrained problems that have been extensively used in the literature and compared to the original quadratic hybridization of Polak–Ribière–Polyak and Fletcher–Reeves conjugate gradient method $\beta_k^{HQ-}$. The numerical results show that this proposed modification has a positive effect on the performance of $\beta_k^{HQ-}$. However, the numerical results from this study show that further research to improve the efficiency and effectiveness of $\beta_k^{HQ-}$ and other conjugate gradient hybrids is still needed. A number of hybrid conjugate gradient methods have been proposed in the literature but there are many problems that are currently not properly handled by these methods, hence the need for more research in this field.

## Acknowledgments

The authors thank the anonymous Referees and the Editors whose comments and suggestions largely improved this work.

## References

[1] Al-Baali, M., Narushima, Y. and Yabe, H., A family of three term conjugate gradient methods with sufficient descent property for unconstrained optimization, Comput. Optim. Appl., 60, 89–110 (2015).

[2] Andrei, N., A new three-term conjugate gradient algorithm for unconstrained optimization, Numer. Algorithms, 68, 305–321 (2015).

[3] Andrei, N., An unconstrained optimization test functions collection, Adv. Model. Optim., 10(1), 147–161 (2008).

[4] Babaie-Kafaki, S., A quadratic hybridization of Polak-Ribiere-Polyak and Fletcher-Reeves conjugate gradient methods, J Optim. Theory Appl., 154(3), 916-932 (2012).

[5] Babaie-Kafaki, S., A Note on the global convergence of the quadratic hybridization of Polak-Ribiere-Polyak and Fletcher-Reeves conjugate gradient methods, J Optim. Theory Appl., 157(1), 297-298 (2013).

[6] Babaie-Kafaki, S., Two modified scaled nonlinear conjugate gradient methods, J Comput. Appl. Math., 261, 172–182 (2014).

[7] Babaie-Kafaki, S., Fatemi, M., and Mahdavi-Amiri, N., Two effective hybrid conjugate gradient algorithms based on modified BFGS updates, Numer. Algorithms, 58, 315–331 (2011).

[8] Babaie-Kafaki, S. and Ghanbari, R., A descent extension of the Polak-Ribière-Polyak conjugate gradient method, Comp. Math. Appl., 68, 2005–2011 (2014).

[9] Dai, Y.-H., Conjugate gradient methods with Armijo-type line searches, Acta Math. Appl. Sin. Engl. Ser., 18(1), 123–130 (2002).

[10] Dai, Y.-H. and Liao, L.Z., New conjugacy conditions and related nonlinear conjugate gradient methods, Appl. Math. Optim., 43, 87–101 (2001).

[11] Dai, Y.-H. and Yuan, Y., A class of globally convergent conjugate gradient methods, Sci. China Ser. A., 46(2), 251–261 (2003).

[12] Dai, Y.-H. and Yuan, Y., A nonlinear conjugate gradient method with strong global convergence property, SIAM J. Optim., 10(1), 177-182 (1999).

[13] Dai, Y.-H., and Yuan, Y., An efficient hybrid conjugate gradient method for unconstrained optimization, Ann. Oper. Res., 103, 33–47 (2001).

[14] Dai, Z. and Wen, F., Another improved Wei-Yao-Liu nonlinear conjugate gradient method with sufficient descent property, Appl. Math. Comput., 218:7421–7430 (2012).

[15] Dai, Z.-F. and Tian, B.-S., Global convergence of some modified PRP nonlinear conjugate gradient methods, Optim. Lett., 5, 615–630 (2011).

[16] Dolan, E.D. and Moré, J.J., Benchmarking optimization software with profile performance profiles, Math. Program., 91(2), 201–213 (2002).

[17] Dong, X.L., Liu, H. and He, Y., A self-adjusting conjugate gradient method with sufficient descent condition and conjugacy condition, J Optim. Theory Appl., 165, 225–241 (2015).

[18] Dong, X.L., Liu, H.W., He, Y.B. and Yang, X.M., A modified Hestenes-Stiefel conjugate gradient method with sufficient descent condition and conjugacy condition, J Comput. Appl. Math., 281, 239–249 (2015).

[19] Dong, Y., A practical PR+ conjugate gradient method only using gradient, Appl. Math. Comput., 219(4), 2041-2052 (2012).

[20] Fletcher, R. and Reeves, C., Function minimization by conjugate gradients, Comp. J., 7, 149–154 (1964).

[21] Gilbert, J.C., and Nocedal, J., Global convergence properties of conjugate gradient methods for optimization, SIAM J. Optim., 2(1), 21–42 (1992).

[22] Hager, W.W., and Zhang, H., A survey of nonlinear conjugate gradient methods, Pac. J. Optim., 2(1), 35–58 (2006).

[23] Hestenes, M.R., and Stiefel, E., Methods for conjugate gradients for solving linear systems, J Res. Natl. Bur. Stand., 49, 409–436 (1952).

[24] Jia, W., Zong, J. and Wang, X., An improved mixed conjugate gradient method, Systems Engineering Procedia 2, 219–225 (2012).
[25] Liu, H., A mixture conjugate gradient method for unconstrained optimization, Third International Symposium on Intelligent Information Technology and Security Informatics, IEEE, 26–29 (2010).
[26] Liu, Y. and Storey, C., Efficient generalized conjugate gradient algorithms, Part 1: theory, J Optim. Theory Appl., 69, 129-137 (1992).
[27] Liu, J., A hybrid nonlinear conjugate gradient method, Lobachevskii J. Math., 33(3), 195–199 (2012).
[28] Liu, J.K. and Li, S.J., New hybrid conjugate gradient method for unconstrained optimization, Appl. Math. Comput., 245, 36–43 (2014).
[29] Mo, J., Gu, N. and Wei, Z., Hybrid conjugate gradient methods for unconstrained optimization, Optim. Methods Softw., 22(2), 297–307 (2007).
[30] Moré, J.J., Garbow, B.S. and Hillstrom, K.E., Testing unconstrained optimization software, ACM Trans. Math. Software, 7, 17–41 (1981).
[31] Nocedal, J. and Wright, S.J., Numerical Optimization, 2nd Edition, Springer Science+ Business Media, LLC. Printed in the United States of Ameraica (2006).
[32] Polak, E., and Ribière, G., Note sur la convergence de mèthodes de directions conjuguèes, Rev. Française d'Infom. Recherche Opèrationnelle, 3(16), 35–43 (1969).
[33] Polyak, B.T., The conjugate gradient method in Extreme problems, USSR Comput. Math. Math. Phys., 9(4), 94–112 (1969).
[34] Shi, Z.-J., Convergence of line search methods for unconstrained optimization, Appl. Math. Comput., 157, 393–405 (2004).
[35] Sun, M. and Liu, J., Three modified Polak-Ribière-Polyak conjugate gradient methods with sufficient descent property, Journal of Inequalities and Applications, 2015–2125 (2015).
[36] Touati-Ahmed, D. and Storey, C., Efficient hybrid conjugate gradient techniques, J Optim. Theory Appl., 64(2), 379–397 (1990).
[37] Yabe, H. and Sakaiwa, N., A new nonlinear conjugate gradient method for unconstrained optimization, J Oper. Res., 48(4), 284–296 (2005).
[38] Yan, H., Chen, L. and Jiao, B., HS-LS-CD hybrid conjugate gradient algorithm for unconstrained optimization, Second International Workshop on Computer Science and Engineering, IEEE, 264–268 (2009).
[39] Yuan, G. and Lu, X., A modified PRP conjugate gradient method, Ann. Oper. Res., 166, 73–90 (2009).
[40] Zhang, L., Zhou, W. and Li, D.-H., A descent modified Polak-Ribière-Polyak conjugate gradient method and its global convergence, IMA J. Numer. Anal., 26, 629–640 (2006).
[41] Zhou, A., Zhu, Z., Fan, H. and Qing, Q., Three new hybrid conjugate gradient methods for optimization, Appl. Math., 2(3), 303–308 (2011).

***S. Narayanan*** *graduated with an MSc in Mathematics from the Department of Mathematics, University of Botswana, in 2015. She is currently pursuing her PhD in Mathematics from the Department of Mathematics, University of Botswana. Her research interests are in Optimization and Analysis.*

***P. Kaelo*** *is a lecturer in the Department of Mathematics, University of Botswana. He obtained his PhD in Mathematics from the University of the Witwatersrand, Johannesburg, South Africa, in 2005. His research interests include Optimization, Optimal Control Theory, Numerical Analysis and Functional Analysis.*

***M. V. Thuto*** *is a lecturer in the Department of Mathematics, University of Botswana. He obtained his PhD in Mathematics from the University of Exeter, England, United Kingdom, in 2000. His research interests are in Control Theory, Optimization and Functional Analysis.*



An International Journal of Optimization and Control: Theories & Applications
ISSN:2146-0957 eISSN:2146-5703
Vol.7, No.2, pp.186-194 (2017)
http://doi.org/10.11121/ijocta.01.2017.00360

RESEARCH ARTICLE

# Numerical solution of neutral functional-differential equations with proportional delays

Mehmet Giyas Sakar

*Department of Mathematics, Yuzuncu Yil University, Van, Turkey*
*giyassakar@hotmail.com*

ARTICLE INFO

Article History:
*Received 22 June 2016*
*Accepted 22 March 2017*
*Available 15 July 2017*

Keywords:
*Homotopy analysis method*
*Residual error function*
*Convergence*
*Neutral functional-differential equation*
*Proportional delay*

AMS Classification 2010:
*58B05, 34K06*

ABSTRACT

In this paper, homotopy analysis method is improved with optimal determination of auxiliary parameter by use of residual error function for solving neutral functional-differential equations (NFDEs) with proportional delays. Convergence analysis and error estimate of method are given. Some numerical examples are solved and comparisons are made with the existing results. The numerical results show that the homotopy analysis method with residual error function is very effective and simple.



## 1. Introduction

Neutral functional-differential equations with proportional delays represent a specific form of delay differential equations. Such equations arise in various fields of science and engineering and play a significant role in the mathematical modeling of real-world phenomena [1]. Clearly, most of these equations cannot be solved with well-known exact methods. For this reason, it is necessary to design efficient numerical treatment to approximate solutions. Ishiwata et al. used the rational approximation method and the collocation method to obtain numerical solutions of NFDEs with proportional delays [2,3]. Hu et al. applied linear multi step methods to obtain numerical solutions for NFDEs [4]. Wang et al. obtained approximate solutions for NFDEs by continuous Runge-Kutta methods and one-leg-$\theta$ method [5-7]. Chen and Wang applied the variational iteration method for solving NFDEs with proportional delays [8]. Biazar and Ghanbari applied the homotopy perturbation method to obtain numerical solution of NFDEs with proportional delays [9] and so on [10,11].

Homotopy analysis method (HAM) is proposed by Liao [12,13]. This method has been successfully employed to handle a wide variety of scientific and engineering applications. Alomari et al. used modified HAM for solution of delay differential equation in [14]. Kumar and Rashidi applied fractional homotopy analysis transform method to obtain approximate analytical solution of nonlinear homogeneous and nonhomogeneous time-fractional gas dynamics equations in [15]. Abbasbandy employed HAM to find a family of travelling-wave solutions of the Kawahara equation in [16]. Jafari and Seifi used HAM for solution of linear and nonlinear fractional diffusion-wave equation in [17]. Sakar and Erdogan applied the HAM and Adomian's decomposition method for solving the time-fractional Fornberg-Whitham equation in [18]. HAM is different from the perturbation methods it provides the convenient way to control and adjust the convergence region and convergence rate of the series solution. However, for some type of auxiliary operator, in other words some type of base functions, it is generally time-consuming to get high order approximation, and

very large terms appearing in high order approximation [19]. The homotopy-series solution is not only dependent upon $t$ but also the convergence-control parameter $\hbar$. Convergence-control parameter $\hbar$ which supplies us a convenient way to guarantee the convergence of homotopy-series solution. When the approximations contain unknown convergence-control parameters and other physical parameters, it is time-consuming to compute the square residual error at high-order of approximations. To avoid the time-consuming calculation, we will employ averaged square residual error function [19,20].

The aim of this paper is to extend the homotopy analysis method with residual error function to obtain the numerical solution of the following neutral functional-differential equations with proportional delays [8,9],

$$(u(t)+a(t)u(p_nt))^{(n)}=\sum_{k=0}^{n-1}b_k(t)u^{(k)}(p_kt)+\beta u(t)+f(t),\ \ t\geq 0 \quad (1)$$

with the initial conditions

$$\sum_{k=0}^{n-1}c_{ik}u^{(k)}(0)=\lambda_i,\quad i=0,1,...,n-1. \quad (2)$$

Here, $a(t)$ and $b_k(t),(k=0,1,...,n-1)$ are given analytical functions, and $\beta$, $p_k$, $c_{ik}$, $\lambda_i$ denote given constant with $0<p_k<1,(k=0,1,...,n)$.

This paper is organized as follows: In Section 2, homotopy analysis method with residual error function is presented. Section 3 is devoted to the convergence analysis of the method. Section 4 contains numerical comparisons between the results obtained by the homotopy analysis method in this work and some existing methods. Finally, concluding remarks are given in the last section.

## 2. Homotopy analysis method with residual error function

We consider the following nonlinear differential equation

$$N[u(t)]=(u(t)+a(t)u(p_nt))^{(n)}-\beta u(t)-\sum_{k=0}^{n-1}b_k(t)u^{(k)}(p_kt)-f(t)=0 \quad (3)$$

where, $N$ is a nonlinear differential operator, $t$ denotes independent variable, $u(t)$ is an unknown function. By means of generalizing the traditional homotopy method, Liao [12] constructs the so-called *zero-order deformation equation*

$$(1-p)L[\phi(t;p)-u_0(t)]=p\hbar H(t)N[\phi(t;p)] \quad (4)$$

here, $p\in[0,1]$ is the embedding parameter, $\hbar\neq 0$ is a non-zero auxiliary parameter, $H(t)\neq 0$ is non-zero auxiliary function, $L$ is an auxiliary linear operator. $u_0(t)$ is the initial guess of $u(t)$ and $\phi(t;p)$ is unknown function, respectively. It is important that one has great freedom to choose auxiliary things such as $\hbar$ and $L$ in homotopy analysis method. Obviously, when $p=0$ and $p=1$ , it holds

$$\phi(t;0)=u_0(t),\quad \phi(t;1)=u(t), \quad (5)$$

respectively. Thus, as $p$ increases from 0 to 1, the solution $\phi(t;p)$ varies from the initial guesses $u_0(t)$ to the solution $u(x,t)$. Expanding $\phi(t;p)$ in Taylor series with respect to $p$, we have

$$\phi(t;p)=u_0(t)+\sum_{m=1}^{\infty}u_m(t)\,p^m, \quad (6)$$

where

$$u_m(t)=\frac{1}{m!}\frac{\partial^m\phi(t;p)}{\partial p^m}\ |_{p=0}. \quad (7)$$

If the auxiliary linear operator, the initial guess, the auxiliary operator $\hbar$, and the auxiliary functions are so properly chosen, then the series Eq.(6) converges at $p=1$ and

$$\phi(t;1)=u_0(t)+\sum_{m=1}^{\infty}u_m(t), \quad (8)$$

which must be one of the solutions of the original nonlinear equations, as proved by Liao [12]. According to Eq.(7), the governing equations can be deduced from *zeroth-order deformation equation* Eq.(4).

Define the vector

$$\overrightarrow{u_n}=\{u_0(t),\,u_1(t),...,u_n(t)\}. \quad (9)$$

Differentiating Eq.(4) $m$-times with respect to the embedding parameter $p$ and then setting $p=0$ and finally dividing them by $m!$, we obtain the $m$th-*order deformation equation*, with the assumption $H(t)=1$,

$$L\left[u_m\left(t\right)-\chi_m u_{m-1}\left(t\right)\right]=\hbar R_m(\overrightarrow{u}_{m-1}), \quad (10)$$

where,

$$R_m(\overrightarrow{u}_{m-1})=\sum_{m=1}^{\infty}\frac{1}{(m-1)!}\frac{\partial^{m-1}N[\phi(t;p)]}{\partial p^{m-1}}\mid_{p=0}$$

and

$$\chi_m=\begin{cases}0, & m\leq 1,\\ 1, & m>1.\end{cases}$$

The $m$th-order approximation series solution is given as

$$u\left(t\right)=\sum_{k=0}^{m}u_k\left(t\right). \quad (11)$$

It is clear from Eq.(11) that $u\left(t\right)$ contains unknown convergence-control parameter $\hbar$ which determine the convergence region and rate of the homotopy-series solution.

### 2.1. Selection of optimal value of $\hbar$ with residual error function

As given by Liao [19], at the $m$th-order of approximation, one can define the exact square residual error as,

$$\Delta_m=\int_{\Omega}\left(N\left(\sum_{i=0}^{m}u_i\left(t\right)\right)\right)^2 dt. \quad (12)$$

Here, $\Delta_m$ contains $\hbar$ unknown convergence-control parameter. For $m$th-order approximation, optimal values of the convergence-control parameter $\hbar$ is given by the minimum of $\Delta_m$, namely

$$\frac{d\Delta_m}{d\hbar}=0. \quad (13)$$

However, it is proven by Liao [19] that the exact residual error $\Delta_m$ defined by Eq.(13) needs too much CPU time to calculate even if the order of approximation is not very high. Thus, to greatly decrease the CPU time, we use here the so-called averaged square residual error $\sqrt{E_m}$ defined by

$$E_m=\frac{1}{n+1}\sum_{j=0}^{n}\left(N\left(\sum_{i=0}^{m}u_i\left(\frac{j}{n},\hbar\right)\right)\right)^2. \quad (14)$$

## 3. Convergence analysis and error estimate

In this section we present convergence analysis and error estimate for our method.

**Theorem 1.** *If the homotopy series Eq.(8) converges, then* $\sum_{m=1}^{\infty}R_m(\overrightarrow{u}_{m-1}(t))=0$.

**Theorem 2.** *If the homotopy series Eq.(8) converges, it must be the solution of original nonlinear Eq.(3).*

The proofs of Theorem 1. and Theorem 2. can be found in [12].

**Theorem 3.** *Let the solution components* $u_n\left(t\right)$ *be defined in Banach space* $(C[0,1],\|.\|)$. *Then the series solution* $\sum_{n=0}^{\infty}u_n(t)$ *defined in Eq.(11) converges to the solution of Eq.(3), if* $\exists\ 0<\gamma<1$ *such that* $\|u_{n+1}\|\leq\gamma\|u_n\|$, $\forall n\geq n_0$, *for some* $n_0\in N$.

***Proof.*** Assume that $\left(C\left[0,1\right],\|.\|\right)$ is the Banach space, the space of all continuous functions on $[0,1]$. Define that $\{S_n\}$ is the sequence of partial sums of the series Eq.(11) as,

$$\begin{cases}S_0=u_0(t),\\ S_1=u_0(t)+u_1(t),\\ S_2=u_0(t)+u_1(t)+u_2(t),\\ \vdots\\ S_n=u_0(t)+u_1(t)+u_2(t)+...+u_n(t).\end{cases}$$

We need to show that $\{S_n\}_{n=0}^{\infty}$ is a Cauchy sequence in Banach space $(C[0,1],\|.\|)$. For this purpose, we consider,

$$\begin{aligned}\|S_{n+1}-S_n\| &= \|u_{n+1}(t)\|\\ &\leq \gamma\left\|u_n\left(t\right)\right\|\\ &\leq \gamma^2\left\|u_{n-1}(t)\right\|\\ &\leq ...\leq\gamma^{n+1}\left\|u_0\left(t\right)\right\|. \quad (15)\end{aligned}$$

For every, $n,m\in N$, $n\geq m$, by using Eq.(15) and triangle inequality successively, we have,

$$\begin{aligned}\|S_n-S_m\| &= \|(S_n-S_{n-1})+\ldots+(S_{m+1}-S_m)\|\\ &\leq \|(S_n-S_{n-1})\|+\|(S_{n-1}-S_{n-2})\|\\ &\quad +...+\|(S_{m+1}-S_m)\|\\ &\leq \gamma^n\|u_0(t)\|+\gamma^{n-1}\|u_0(t)\|\\ &\quad +...+\gamma^{m+1}\|u_0(t)\|\\ &= \frac{1-\gamma^{n-m}}{1-\gamma}\gamma^{m+1}\|u_0(t)\|. \quad (16)\end{aligned}$$

Since $0 < \gamma < 1$, we have $1 - \gamma^{n-m} < 1$; then,

$$\|S_n - S_m\| \leq \frac{\gamma^{m+1}}{1-\gamma} \max_{\forall t \in [0,1]} \|u_0(t)\|.$$

Since $u_0(t)$ is bounded,

$$\lim_{n,m\to\infty} \|S_n - S_m\| = 0.$$

Therefore, $\{S_n\}_{n=0}^{\infty}$ is a Cauchy sequence in the Banach space $(C[0,1], \|.\|)$, so the series solution defined in Eq.(11), converges. This completes the proof. □

**Theorem 4.** *Assume that the series solution* $\sum_{n=0}^{\infty} u_n(t)$ *defined in Eq.(11), is convergent to the solution* $u(t)$. *If the truncated series* $\sum_{n=0}^{m} u_n(t)$ *is used as an approximation to the solution* $u(t)$ *of Eq.(3), then the maximum absolute truncated error is estimated as,*

$$\left\| u(t) - \sum_{n=0}^{m} u_n(t) \right\| \leq \frac{\gamma^{m+1}}{(1-\gamma)} \|u_0(t)\|. \quad (17)$$

***Proof.*** From Theorem 3. and Eq.(16), we have

$$\|S_n - S_m\| = \frac{1-\gamma^{n-m}}{1-\gamma} \gamma^{m+1} \|u_0(t)\|,$$

for $n \geq m$. Now, as $n \to \infty$ then $S_n \to u(t)$. So,

$$\|u(t) - S_m\| \leq \frac{\gamma^{m+1}}{(1-\gamma)} \|u_0(t)\|.$$

Since $0 < \gamma < 1$, we have $1 - \gamma^{n-m} < 1$. Herewith the above inequality becomes,

$$\left\| u(t) - \sum_{n=0}^{m} u_n(t) \right\| \leq \frac{\gamma^{m+1}}{(1-\gamma)} \|u_0(t)\|. \quad (18)$$

This completes the proof. □

**Remark 1.** *If we define for every* $j \in \mathrm{N} \cup \{0\}$, *the parameters,*

$$\gamma_j = \begin{cases} \frac{\|u_{j+1}\|}{\|u_j\|}, \|u_j\| \neq 0 \\ 0, \quad \|u_j\| = 0 \end{cases}$$

*then the solution* $\sum_{n=0}^{\infty} u_n(t)$ *of Eq.(3) converges to an exact solution* $u(t)$, *when* $0 \leq \gamma_j < 1, \forall j \in \mathrm{N} \cup \{0\}$. *Moreover, as stated in Theorem 4., the maximum absolute truncation error is estimated to be,*

$$\left\| u(t) - \sum_{n=0}^{\infty} u_n(t) \right\| \leq \frac{1}{1-\gamma} \gamma^{i+1} \|u_0(t)\|,$$

*where*
$\gamma = \max\{\gamma_j,\ j = 0, 1, ..., i\}$.

## 4. Numerical examples

Now, we apply the homotopy analysis method with residual error function which presented in Section 2-3 to some NFDEs with proportional delay.

**Example 1.** *We consider the following first-order NFDE with proportional delay [8,9]:*

$$u'(t) = -u(t) + \frac{1}{2}u(\frac{t}{2}) + \frac{1}{2}u'(\frac{t}{2}),\ \ 0 \leq t \leq 1, \quad (19)$$

*with initial condition,*

$$u(0) = 1. \quad (20)$$

*The exact solution is* $u(t) = \exp(-t)$ *[8].*

We select auxiliary linear operator,

$$L(\phi(t;p)) = \frac{d\phi(t;p)}{dt}, \quad (21)$$

with property

$$L(c_1) = 0, \quad (22)$$

in which $c_1$ is an integral constant to be determined by initial condition Eq.(20).

Furthermore, Eq.(19) suggest that we define a nonlinear operator as

$$\begin{aligned} N[\phi(t;p)] &= \frac{d\phi(t;p)}{dt} + \phi(t;p) \\ &- \frac{1}{2}\phi(\frac{t}{2};p) - \frac{1}{2}\frac{d\phi(\frac{t}{2};p)}{dt}. \end{aligned} \quad (23)$$

From $m$th-order deformation equation we can obtain following components,

$$\begin{aligned} u_1(t) &= \frac{1}{2}\hbar t, \\ u_2(t) &= \frac{1}{2}\hbar t + \frac{3}{16}\hbar^2 t^2 + \frac{1}{4}\hbar^2 t, \\ &\vdots \end{aligned}$$

Then the solution is,

$$u(t) = u_0(t) + \sum_{m=1}^{n} u_m(t), \quad (24)$$

where $n$ is the number of terms.

We define the following residual error function,

$$r_7(t,\hbar) = \sum_{m=1}^{7} u'_m(t,\hbar) + \sum_{m=1}^{7} u_m(t,\hbar) - \frac{1}{2}\sum_{m=1}^{7} u_m(\frac{t}{2},\hbar) - \frac{1}{2}\sum_{m=1}^{7} u'_m(t,\hbar), \quad (25)$$

for obtaining optimal value of $\hbar$. Figure 1(b) shows averaged square residual error function for the 7th-order approximation, i.e.,

$$\sqrt{E_m} = \left( \frac{1}{201} \sum_{j=0}^{200} r_7 \left( \frac{j}{200}, \hbar \right)^2 \right)^{1/2} \quad (26)$$

with respect to $\hbar$ for $t \in [0,1]$.

To determine the region of validity of the convergence-control parameter $\hbar$, we plot the values of $u'(0.2)$, and $u''(0.2)$ in Figure 1(a). It appears that $\hbar$ should at least lie within the interval $[-2,-1]$. For the best possible value within this region, the averaged square residual error at the 7th-order approximation was evaluated from Eq.(26) which gives rise to the optimal value $\hbar$ of $\hbar$ = -1.18613, resulting in a averaged square residual error $4.27 \times 10^{-4}$. For 10th-order approximation we found $\hbar = -1.12058$ and averaged square residual error $5.20 \times 10^{-5}$. The accuracy is improved by optimal choice of $\hbar$. In Table 1, we compare the absolute errors of the homotopy analysis method ($n = 7$ and $n = 10$) with those of the Runge-Kutta method (R-K) of [1,8], variational iteration method (VIM) [8] with $n_i = 7$ and the one-leg $\theta$ method [5,6] with $\theta = 0.8$, where $h = 0.01$ and homotopy perturbation method (HPM) [9] with $n = 7$.

**Table 1.** Comparison of absolute errors for Example 1.

| $t$ | R-K [8] | One-leg-$\theta$ [8] | VIM [8] | HPM [9] | HAM ($n = 7$) | HAM ($n = 10$) |
|---|---|---|---|---|---|---|
| 0.1 | 4.55E-4 | 2.57E-3 | 7.43E-4 | 6.73E-4 | 1.59E-4 | 2.32E-5 |
| 0.2 | 8.24E-4 | 8.86E-3 | 1.42E-3 | 1.16E-3 | 2.74E-4 | 4.00E-5 |
| 0.3 | 1.12E-3 | 1.72E-2 | 2.02E-3 | 1.50E-3 | 3.54E-4 | 5.18E-5 |
| 0.4 | 1.33E-3 | 2.66E-2 | 2.58E-3 | 1.73E-3 | 4.08E-4 | 5.97E-5 |
| 0.5 | 1.52E-3 | 3.63E-2 | 3.07E-3 | 1.86E-3 | 4.39E-4 | 6.44E-5 |
| 0.6 | 1.66E-3 | 4.58E-2 | 3.52E-3 | 1.94E-3 | 4.53E-4 | 6.69E-5 |
| 0.7 | 1.75E-3 | 5.47E-2 | 3.93E-3 | 1.95E-3 | 4.52E-4 | 6.75E-5 |
| 0.8 | 1.81E-3 | 6.29E-2 | 4.30E-3 | 1.93E-3 | 4.34E-4 | 6.68E-5 |
| 0.9 | 1.84E-3 | 7.02E-2 | 4.64E-3 | 1.89E-3 | 3.96E-4 | 6.52E-5 |
| 1.0 | 1.85E-3 | 7.66E-2 | 4.94E-3 | 1.82E-3 | 3.32E-4 | 6.30E-5 |

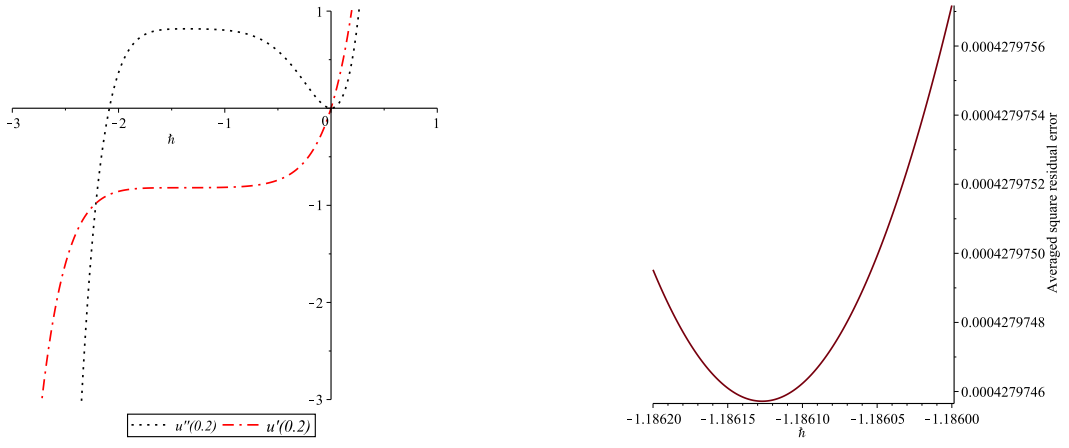


**(a)** Sub-figure 1 **(b)** Sub-figure 2

**Figure 1.** $\hbar$ curves for 7th-order of approximation of Example 1. (a) and 7th-order averaged square residual error for Example 1. (b).

**Example 2.** *Consider the second-order NFDE with proportional delay [8,9]:*

$$u''(t) = \frac{3}{4}u(t) + u(\frac{t}{2}) + u'(\frac{t}{2}) + \frac{1}{2}u''(\frac{t}{2}) - t^2 - t + 1, \quad 0 \le t \le 1, \tag{27}$$

*with initial conditions,*

$$u(0) = u'(0) = 0, \tag{28}$$

*which has the exact solution* $u(t) = t^2$ *[8].*

We select auxiliary linear operator,

$$L(\phi(t;p)) = \frac{d^2\phi(t;p)}{dt^2}, \tag{29}$$

with property

$$L(c_1 + c_2 t) = 0, \tag{30}$$

in which $c_1$ and $c_2$ are integral constants to be determined by initial condition Eq.(28).
Furthermore, Eq.(27) suggest that we define a nonlinear operator as

$$\begin{aligned} N[\phi(t;p)] &= \frac{d^2\phi(t;p)}{dt^2} - \frac{3}{4}\phi(t;p) - \phi(\frac{t}{2};p) \\ &- \frac{d\phi(\frac{t}{2};p)}{dt} - \frac{1}{2}\frac{d^2\phi(\frac{t}{2};p)}{dt^2} \\ &+ t^2 + t - 1. \end{aligned} \tag{31}$$

From $m$th-order deformation equation, we can obtain following components,

$$\begin{aligned} u_1(t) &= \frac{1}{12}\hbar t^4 + \frac{1}{6}\hbar t^3 - \frac{1}{2}\hbar t^2, \\ u_2(t) &= \frac{1}{12}\hbar t^4 + \frac{1}{6}\hbar t^3 - \frac{1}{2}\hbar t^2 - \frac{13}{5760}\hbar^2 t^6 \\ &- \frac{3}{320}\hbar^2 t^5 + \frac{5}{48}\hbar^2 t^4 + \frac{5}{24}\hbar^2 t^3 - \frac{1}{4}\hbar^2 t^2, \\ &\vdots \end{aligned}$$

We define the following residual function,

$$\begin{aligned} r_6(t,\hbar) &= \sum_{m=1}^{6} u''_m(t,\hbar) - \frac{3}{4}\sum_{m=1}^{6} u_m(t,\hbar) \\ &- \sum_{m=1}^{6} u_m(\frac{t}{2},\hbar) - \sum_{m=1}^{6} u'_m(\frac{t}{2},\hbar) \\ &- \frac{1}{2}\sum_{m=1}^{6} u''_m(\frac{t}{2},\hbar) + t^2 + t - 1, \end{aligned} \tag{32}$$

for obtaining optimal value of $\hbar$. Figure 2(b) shows averaged square residual error function for the 6th-order approximation, i.e.,

$$\sqrt{E_m} = \left( \frac{1}{501} \sum_{j=0}^{500} r_6\left(\frac{j}{500}, \hbar\right)^2 \right)^{1/2} \tag{33}$$

with respect to $\hbar$ for $t \in [0,1]$.
To determine the region of validity of the convergence-control parameter $\hbar$, we plot the values of $u'(0.1)$, and $u''(0.1)$, in Figure 2(a). It appears that $\hbar$ should at least lie within the interval $[-2,-1]$. For the best possible value within this region, the averaged square residual error at the 6th-order approximation was evaluated from Eq.(33) which gives rise to the optimal value $\hbar$ of $\hbar$ = -1.49346, resulting in a averaged square residual error $8.16 \times 10^{-4}$. For 10th-order approximation we found $\hbar = -1.45885$ and averaged square residual error $5.93 \times 10^{-6}$. In Table 2, we compare the absolute errors of the homotopy analysis method ($n = 6$ and $n = 10$) with those of the Runge-Kutta method of [1,8], variational iteration method [8] with $n_i = 6$ and the one-leg $\theta$ method [5,6] with $\theta = 0.8$, where $h = 0.01$ and homotopy perturbation method [9] with $n = 6$.

**Example 3.** *Consider the third-order neutral functional differential equation with proportional delay [8,9]:*

$$u'''(t) = u(t) + u'(\frac{t}{2}) + u''(\frac{t}{3}) + \frac{1}{2}u'''(\frac{t}{4}) - t^4 - \frac{t^3}{2} - \frac{4}{3}t^2 + 21t, \quad 0 \le t \le 1 \tag{34}$$

*with initial conditions,*

$$u(0) = u'(0) = u''(0) = 0, \tag{35}$$

*which has the exact solution* $u(t) = t^4$ *[8].*

We select auxiliary linear operator,

$$L(\phi(t;p)) = \frac{d^3\phi(t;p)}{dt^3}, \tag{36}$$

with property

$$L\left(c_1 + c_2 t + c_3 t^2\right) = 0, \tag{37}$$

in which $c_1$, $c_2$ and $c_3$ are integral constants to be determined by initial condition Eq.(35). Furthermore, Eq.(34) suggest that we define a nonlinear operator as

$$\begin{aligned} N[\phi(t;p)] &= \frac{d^3\phi(t;p)}{dt^3} - \frac{d\phi(\frac{t}{2};p)}{dt} - \frac{1}{2}\frac{d^3\phi(\frac{t}{4};p)}{dt^3} \\ &- \phi(t;p) + t^4 + \frac{t^3}{2} + \frac{4}{3}t^2 - 21t. \end{aligned} \tag{38}$$

From $m$th-order deformation equation we can obtain following components,

$$u_1(t) = \frac{1}{210}\hbar t^7 + \frac{1}{240}\hbar t^6 + \frac{1}{45}\hbar t^5 - \frac{7}{8}\hbar t^4,$$
$$\vdots$$

We define the following residual function,

$$\begin{aligned} r_4(t,\hbar) = &\sum_{m=1}^{4} u_m'''(t,\hbar) - \sum_{m=1}^{4} u_m(t,\hbar) \\ &- \sum_{m=1}^{4} u_m'(\frac{t}{2},\hbar) - \sum_{m=1}^{4} u_m''(\frac{t}{3},\hbar) \\ &- \frac{1}{2}\sum_{m=1}^{4} u_m'''(\frac{t}{4},\hbar) + t^4 + \frac{t^3}{2} \\ &+ \frac{4}{3}t^2 - 21t, \end{aligned} \tag{39}$$

for obtaining optimal value of $\hbar$. Figure 3(b) shows averaged square residual error function for the 4th-order approximation, i.e.,

$$\sqrt{E_m} = \left( \frac{1}{101} \sum_{j=0}^{100} r_4\left(\frac{j}{100},\hbar\right)^2 \right)^{1/2} \tag{40}$$

with respect to $\hbar$ for $t \in [0,1]$.

To determine the region of validity of the convergence-control parameter $\hbar$, we plot the values of $u'(0.2)$, and $u''(0.2)$ in Figure 3(a). It appears that $\hbar$ should at least lie within the interval $[-1.5, -0.5]$. For the best possible value within this region, the averaged square residual error at the 4th-order approximation was evaluated from Eq.(40) which gives rise to the optimal value $\hbar$ of $\hbar$ = -1.0932155, resulting in a averaged square residual error $1.77 \times 10^{-5}$. For 7th-order approximation we found $\hbar = -1.08382$ and averaged square residual error $2.05 \times 10^{-8}$. In Table 3, we compare the absolute errors of the homotopy analysis method ($n = 4$ and $n = 7$) with those of the Runge-Kutta method of [1,8], variational iteration method [8] with $n_i = 4$ and the one-leg $\theta$ method [5,6] with $\theta = 0.8$, where $h = 0.01$ and homotopy perturbation method [9] with $n = 5$.

**Table 2.** Comparison of absolute errors for Example 2.

| $t$ | R-K [8] | One-leg-$\theta$ [8] | VIM [8] | HPM [9] | HAM ($n = 6$) | HAM ($n = 10$) |
|---|---|---|---|---|---|---|
| 0.1 | 1.00E-3 | 6.10E-3 | 1.67E-4 | 1.67E-4 | 2.82E-6 | 2.25E-8 |
| 0.2 | 2.02E-3 | 2.58E-2 | 7.15E-4 | 7.15E-4 | 1.22E-5 | 9.81E-8 |
| 0.3 | 3.07E-3 | 6.47E-2 | 1.73E-3 | 1.72E-3 | 3.03E-5 | 2.44E-7 |
| 0.4 | 4.17E-3 | 1.37E-1 | 3.30E-3 | 3.30E-3 | 6.07E-5 | 4.90E-7 |
| 0.5 | 5.34E-3 | 2.81E-1 | 5.55E-3 | 5.55E-3 | 1.08E-4 | 8.69E-7 |

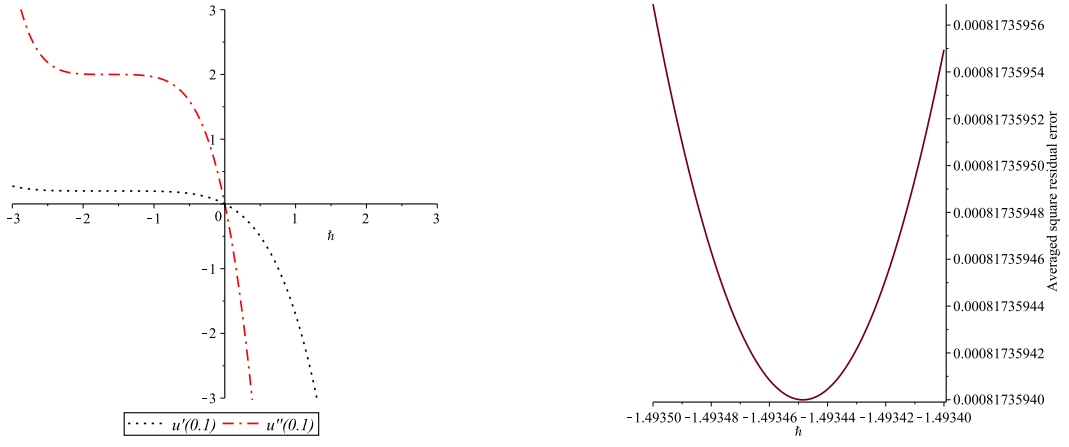


**(a)** Sub-figure 3 **(b)** Sub-figure 4

**Figure 2.** $\hbar$ curves for 6th-order of approximation of Example 2. (a) and 6th-order averaged square residual error for Example 2. (b).

**Table 3.** Comparison of absolute errors for Example 3.

| $t$ | R-K [8] | VIM [8] | HPM [9] | HAM ($n = 4$) | HAM ($n = 7$) |
|---|---|---|---|---|---|
| 0.1 | 4.97E-5 | 2.46E-8 | 2.50E-8 | 3.35E-10 | 1.20E-13 |
| 0.2 | 4.43E-4 | 4.03E-7 | 4.09E-7 | 5.03E-9 | 2.00E-12 |
| 0.3 | 1.57E-3 | 2.09E-6 | 2.12E-6 | 2.36E-8 | 1.10E-11 |
| 0.4 | 3.85E-3 | 6.80E-6 | 6.90E-6 | 6.84E-8 | 3.00E-11 |
| 0.5 | 7.78E-3 | 1.71E-5 | 1.73E-5 | 1.50E-7 | 1.00E-10 |
| 0.6 | 1.39E-2 | 3.64E-5 | 3.69E-5 | 2.76E-7 | 2.00E-10 |
| 0.7 | 2.28E-2 | 6.96E-5 | 7.06E-5 | 4.42E-7 | 5.00E-10 |
| 0.8 | 3.53E-2 | 1.23E-4 | 1.24E-4 | 6.37E-7 | 7.00E-10 |
| 0.9 | 5.19E-2 | 2.03E-4 | 2.06E-4 | 8.47E-7 | 1.10E-9 |
| 1.0 | 7.34E-2 | 3.21E-4 | 3.25E-4 | 1.07E-6 | 1.60E-9 |

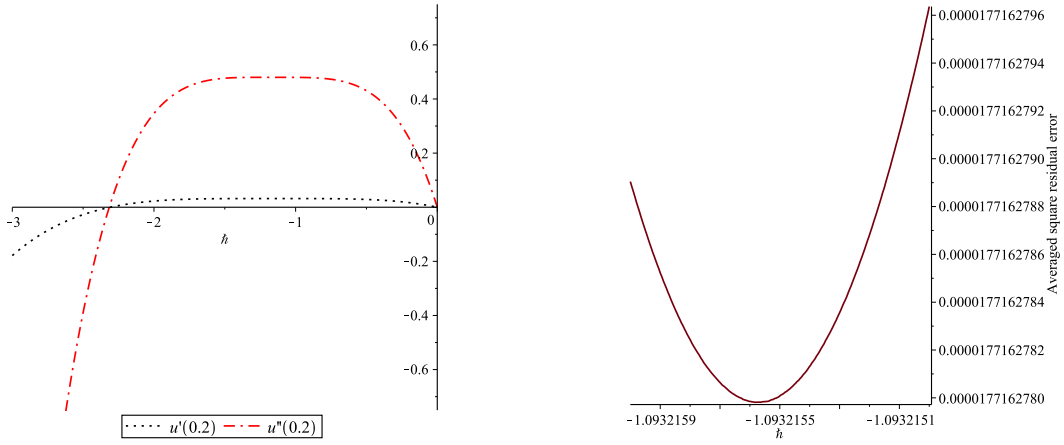


**(a)** Sub-figure 5 **(b)** Sub-figure 6

**Figure 3.** $\hbar$ curves for 4th-order of approximation of Example 3. (a) and 4th-order averaged square residual error for Example 3. (b).

## 5. Conclusion

In this paper, we have demonstrated the suitability of the homotopy analysis method with residual error function for solving neutral functional-differential equations with proportional delays. We obtain high-accuracy approximate solutions after only a few iterations. The numerical results also show that the HAM with residual error function is more effective than Runge-Kutta method, HPM, VIM and other methods for solving NFDEs with proportional delays.

## References

[1] Bellen, A., Zennaro, M., Numerical Methods for Delay Differential Equations, Numerical Mathematics and Scientific Computation, The Clarendon Press Oxford University Press, New York, NY, USA, (2003).

[2] Ishiwata, E., Muroya, Y., Rational approximation method for delay differential equations with proportional delay, Appl. Math. Comput. 187 (2) 741-747 (2007).

[3] Ishiwata, E., Muroya, Y., Brunner, H., A superattainable order in collocation methods for differential equations with proportional delay, Appl. Math. Comput. 198 (1) 227-236 (2008).

[4] Hu, P., Chengming, H., Shulin, W., Asymptotic stability of linear multistep methods for nonlinear delay differential equations, Appl. Math. Comput. 211 (1) 95-101 (2009).

[5] Wang, W., Zhang, Y., Li, S., Stability of continuous Runge-Kutta type methods for nonlinear neutral delay-differential equations, Appl. Math. Model. 33 (8) 3319-3329 (2009).

[6] Wang, W., Li, S., On the one-leg $\theta$ methods for solving nonlinear neutral functional-differential equations, Appl. Math. Comput. 193 (1) 285-301 (2007).

[7] Wang, W., Qin, T., Li, S., Stability of one-leg $\theta$ methods for nonlinear neutral differential equations with proportional delay, Appl. Math. Comput. 213 (1) 177-183 (2009).

[8] Chen, X., Wang, L., The variational iteration method for solving a neutral functional-differential equation with proportional delays, Comput. Math. Appl. 59 2696-2702 (2010).

[9] Biazar, J., Ghanbari, B., The homotopy perturbation method for solving a neutral functional-differential equation with proportional delays, J. King Saud University-Science 24 33-37 (2012).

[10] Lv, X., Gao, Y., The RKHSM for solving neutral functional-differential equations with proportional delays, Mathematical Methods in the Applied Sciences 36 (6) 642-649 (2009).

[11] Sakar, M. G., Uludag, F., Erdogan, F., Numerical solution of time-fractional nonlinear PDEs with proportional delays by homotopy perturbation method, Appl. Math. Model. 40 (13-14) 6639-6649 (2016).
[12] Liao, S. J., Beyond Perturbation: Introduction to the Homotopy Analysis Method, Chapman and Hall/CRC Press, Boca Raton, (2003).
[13] Liao, S. J., Notes on the homotopy analysis method: Some definitions and theorems, Commun. Nonlinear Sci. Numer. Simulat. 14 (4) 983-997 (2009).
[14] Alomari, A. K., Noorani, M. S. M., Nazar, R., Solution of delay differential equation by means of homotopy analysis method, Acta Appl. Math. 108 395-412 (2009).
[15] Kumar, S., Rashidi, M. M., New analytical method for gas dynamics equation arising in shock fronts, Computer Physics Communications 185 (7) 1947-1954 (2014).
[16] Abbasbandy, S., Homotopy analysis method for the Kawahara equation, Nonlin. Anal. Real. World Appl. 11 (1) 307-312 (2010) .
[17] Jafari, H. Seifi, S., Homotopy analysis method for solving linear and nonlinear fractional diffusion-wave equation, Commun. Nonlinear Sci. Numer. Simulat. 14 (5) 2006-2012 (2009).
[18] Sakar, M. G., Erdogan, F., The homotopy analysis method for solving time-fractional the Fornberg-Whitham equation and comparison with Adomian's decomposition method, Appl. Math. Model. 37 (20-21) 8876-8885 (2013).
[19] Liao, S. J., An optimal homotopy-analysis approach for strongly nonlinear differential equations, Commun. Nonlinear Sci. Numer. Simulat. 15 2003-2016 (2010).
[20] Ghanei, H., Hosseini, M. M., Mohyud-Din, S. Y., Modified variational iteration method for solving a neutral functional-differential equation with proportional delays, International Journal of Numerical Methods for Heat & Fluid Flow 22 (8) 1086-1095 (2012).

***Mehmet Giyas Sakar*** *is an Assistant Professor at the Department of Mathematics, Science Faculty, Yuzuncu Yil University. He received his B.Sc. (2000) degrees from Dicle University, M.Sc. (2007) and Ph.D (2012) degrees from Department of Mathematics, Yuzuncu Yil University, Turkey. His research areas include Fractional Differential Equations and Reproducing Kernel Spaces.*



An International Journal of Optimization and Control: Theories & Applications
ISSN:2146-0957 eISSN:2146-5703
Vol.7, No.2, pp.195-204 (2017)
http://doi.org/10.11121/ijocta.01.2017.00396

RESEARCH ARTICLE

# A Numerical Treatment Based on Haar Wavelets for Coupled KdV Equation

Ömer Oruç[a*], Fatih Bulut[b] and Alaattin Esen[c],

[a] *Aralık Anatolia High School, Iğdır, Turkey*
[b] *Department of Physics, İnönü University, Malatya, Turkey*
[c] *Department of Mathematics, İnönü University, Malatya, Turkey*
*omeroruc0@gmail.com, fatih.bulut@inonu.edu.tr, alaattin.esen@inonu.edu.tr*

ARTICLE INFO

Article History:
*Received 30 September 2016*
*Accepted 24 March 2017*
*Available 15 July 2017*

Keywords:
*Haar wavelet method*
*Coupled KdV equation*
*Linearization*
*Numerical solution*

AMS Classification 2010:
*35Q53, 65T60, 65N35*

ABSTRACT

In this paper, numerical solutions of one dimensional coupled KdV equation has been investigated by Haar Wavelet method. Time derivatives given in this equation are discretized by finite differences and nonlinear terms appearing in the equations are linearized by some linearization techniques and space derivatives are discretized by Haar wavelets. For examining performance of the proposed method, single soliton solution and conserved quantities of some test problems are used. Also error analysis of numerical scheme is investigated and numerical results are compared with some results already existing in the literature.



## 1. Introduction

Analytical or numerical solutions of nonlinear problems has a crucial importance in all areas of physical, mathematical and engineering sciences. Nonlinear equations have interesting characteristics for physical systems and they can be understood by the solution of these problems either analytically or numerically. In general, finding the analytical solution of nonlinear problems is very hard or even impossible for some cases, because of that, numerical solutions of these equations are particularly important.

In this paper, we will consider coupled KdV (cKdV) equation which is an important nonlinear evolution equation and given in the following form

$$\begin{aligned} u_t - 6auu_y - 2bvv_y - au_{yyy} = 0, \\ v_t + 3uv_y + v_{yyy} = 0, \quad y_1 \le y \le y_2 \end{aligned} \tag{1}$$

with the initial conditions

$$u(y,0) = f(y), \quad v(y,0) = g(y), \quad y \in [y_1, y_2] \tag{2}$$

and the boundary conditions

$$\begin{aligned} u(y_1,t) = u(y_2,t) = u_y(y_2,t) = 0 \quad t \in [0,T] \\ v(y_1,t) = v(y_2,t) = v_y(y_2,t) = 0 \quad t \in [0,T] \end{aligned} \tag{3}$$

where $a$ and $b$ are constants [1]. These equations describe interaction of two long waves with different dispersion relations, it is introduced by Hirota and Satsuma [1] in 1981. A lot of long waves with weak dispersion such as internal, acoustic, and planetary waves in geophysical hydrodynamics are related with (cKdV) equation [2, 3].

Because of the importance of cKdV system among evolution equations it is studied by many researchers both analytically and numerically: A

*Corresponding Author

difference scheme given in [4] by Zhu for the periodic initial-boundary value problem of the cKdV Equation. Adomian decomposition method is used to solve this system by Kaya and Inan [5]. Tanh method is used to find solution of the system by Fan [6]. By using the Jacobian elliptic function expansion approach and Hermite transformation Ma and Zhu [7] have obtained some new exact solutions of the cKdV equations. cKdV equation is solved by Assas [8] by using variational iteration method. Homotopy analysis method is used by Abbasbandy [9] for solving the generalized cKdV system. Analytic solutions of nonlinear cKdV equations are studied by Al-Khaled et al. [10] by using tanh and the He's variational iteration methods. Mokhtari and Mohammadi [11] solved a coupled system of nonlinear partial differential equations by using Exp-function method. Ismail solved cKdV system by using finite difference and finite element methods [12–14]. Halim et al. [2, 3] introduced a numerical scheme for general cKdV systems. For the periodic initial boundary value problem of the cKdV system a finite difference scheme produced by Wazwaz [15]. By using collocation method and quintic splines Ismail [16] solved cKdV system. A quadratic B-spline Galerkin approach applied by Kutluay and Ucar [17] for solving cKdV system. Ismail and Ashi [18] used a Petrov-Galerkin method and product approximation technique to solve numerically the Hirota-Satsuma cKdV equation.

In this paper, for obtaining numerical solutions of systems (1), we have employed Haar wavelet method. The paper is organized as follows; In Section 2, an introduction about Haar wavelets is given. In Section 3, time and space discretizations are described and error analysis is given. Numerical results are given in Section 4 and finally the paper is concluded in Section 5.

## 2. Haar wavelets

The wavelet methods have been attracting more attention lately in solving differential equations numerically since they were first applied to solve differential equations in early 1990s. Before explaining the method, we will give basic information about Haar wavelets. They are special kind of wavelets, introduced in 1910 by Alfred Haar and they are the simplest of all possible wavelets with compact support. They are box shaped functions, defined in the interval [0,1). Together they form an orthonormal system in the space of square interable functions. In order to use these wavelets in differential equations one must solve the discontinuity problem of Haar wavelets. This problem was overcome by Chen and Hsiao [19], they used integral method in which the highest derivative of the function in the dierential equation is expanded into Haar series. After this achievement researchers have been using Haar wavelets to obtain numerical solutions of differential equations because of their simplicity and computational features. Recently, many authors have used Haar wavelet method for solving ordinary and partial differential equations [20–31]. Especially high order pdes like KdV and fractional coupled KdV equations are considered in [32, 33].

Here we give an explanation of the method, starting with the definition of the $i$th Haar wavelet as follows for $x \in [0, 1]$

$$h_i(x) = \begin{cases} 1, & \text{for } x \in \left[\frac{k}{m}, \frac{k+0.5}{m}\right) \\ -1, & \text{for } x \in \left[\frac{k+0.5}{m}, \frac{k+1}{m}\right] \\ 0, & \text{elsewhere} \end{cases} \tag{4}$$

where $m = 2^j$, $j = 0, 1, ..., J$ and $k = 0, 1, ..., m-1$ is dilation parameter and translation parameter, respectively. The index of $h_i$ in Eq. (4) can be found by relation $i = m + k + 1$. For the lowest values of $m = 1$, $k = 0$, we have $i = 2$ and the greatest value of $i$ will be $i = 2M = 2^{J+1}$; where $J$ is the maximal resolution of the wavelet. For $i = 1$ we have Haar scaling function

$$h_1(x) = \begin{cases} 1, & \text{for } x \in [0, 1) \\ 0, & \text{elsewhere} \end{cases}$$

Any function $u(x) \in L^2[0, 1)$ can be expanded into Haar series as

$$u(x) = \sum_{i=1}^{\infty} c_i h_i(x),$$

where $c_i$ can be found by

$$c_i = 2^j \int_0^1 u(x) h_i(x) dx,$$
$$i = 2^j + k,\ j \geq 0,\ 0 \leq k < 2^j.$$

Practically, for approximating a square integrable function $u(x)$ on interval $[0, 1)$ finite terms of Haar series are needed, hence one may write

$$u(x) = \sum_{i=1}^{2M} c_i h_i(x) = c_{(2M)}^T h_{(2M)}(x),$$

In the above relation $M = 2^j$, $T$ denotes transpose and

$$c_{(2M)}^T = [c_1, c_2, ..., c_{(2M)}]$$
$$h_{(2M)}(x) = [h_1(x), h_2(x), ..., h_{(2M)}(x)]^T.$$

To employ Haar wavelet method for solving any order partial differential equation one needs the following integrals

$$p_{i,1}(x) = \int_0^x h_i(x)dx$$
$$p_{i,n+1}(x) = \int_0^x p_{i,n}(x)dx, \quad n = 1, 2, 3, ...$$

general form of the integral is given in [34]

$$p_{i,\alpha}(x) = \begin{cases} 0; \text{ for } x < \zeta_1 \\ \frac{1}{\alpha!}\left(x - \frac{k}{m}\right)^\alpha; \text{ for } x \in [\zeta_1, \zeta_2] \\ \frac{1}{\alpha!}\left[\left(x - \frac{k}{m}\right)^\alpha - 2\left(x - \zeta_2\right)^\alpha\right]; \\ \text{ for } x \in [\zeta_2, \zeta_3] \\ \frac{1}{\alpha!}\left[\left(x - \frac{k}{m}\right)^\alpha - 2\left(x - \zeta_2\right)^\alpha + \left(x - \zeta_3\right)^\alpha\right]; \\ \text{ for } x > \zeta_3 \end{cases}$$

For the first three integrals following expressions can be found from the above equation

$$p_{i,1}(x) = \begin{cases} x - \zeta_1, & \text{for } x \in [\zeta_1, \zeta_2] \\ \zeta_3 - x, & \text{for } x \in [\zeta_2, \zeta_3] \\ 0, & \text{elsewhere} \end{cases} \quad (5)$$

$$p_{i,2}(x) = \begin{cases} \frac{(x-\zeta_1)^2}{2}, & \text{for } x \in [\zeta_1, \zeta_2] \\ \frac{1}{4m^2} - \frac{(\zeta_3 - x)^2}{2}, & \text{for } x \in [\zeta_2, \zeta_3] \\ \frac{1}{4m^2}, & \text{for } x \in [\zeta_3, 1] \\ 0, & \text{elsewhere} \end{cases} \quad (6)$$

$$p_{i,3}(x) = \begin{cases} \frac{(x-\zeta_1)^3}{6}, & \text{for } x \in [\zeta_1, \zeta_2] \\ \frac{x-\zeta_2}{4m^2} - \frac{(\zeta_3 - x)^3}{6}, & \text{for } x \in [\zeta_2, \zeta_3] \\ \frac{x-\zeta_2}{4m^2}, & \text{for } x \in [\zeta_3, 1] \\ 0, & \text{elsewhere} \end{cases}. \quad (7)$$

where $\zeta_1$, $\zeta_2$ and $\zeta_3$ defined as follow.

$$\zeta_1 = \frac{k}{m}, \quad \zeta_2 = \frac{k + 0.5}{m}, \quad \zeta_3 = \frac{k+1}{m}.$$

Once the above integrals are computed we can store the results in memory and we can use them wherever they are needed.

## 3. Discretization scheme for cKdV

Since we defined Haar wavelets for $x \in [0, 1]$. We have to transform the domain of Eq. (1) into unit interval. By using transformation $x = \frac{y-y_1}{L}$, $L = y_2 - y_1$ the interval $y_1 \le y \le y_2$ can be transformed into the unit interval $0 \le x \le 1$. Hence Eqs. (1) become

$$u_t - \frac{6}{L}auu_x - \frac{2}{L}bvv_x - \frac{1}{L^3}au_{xxx} = 0,$$
$$v_t + \frac{3}{L}uv_x + \frac{1}{L^3}v_{xxx} = 0.$$

Now we can start to discretization process

### 3.1. Time discretization for cKdV

To discretize the Eq. (1), we use forward finite differences for time derivatives and time averages of the other terms, as follows

$$\frac{u_{n+1} - u_n}{\Delta t} - \frac{6a}{2L}\left[(uu_x)_{n+1} + (uu_x)_n\right] - \frac{2b}{2L}\left[(vv_x)_{n+1} + (vv_x)_n\right] - \frac{a}{2L^3}\left[(u_{xxx})_{n+1} + (u_{xxx})_n\right] = 0,$$
$$\frac{v_{n+1} - v_n}{\Delta t} + \frac{3}{2L}\left[(uv_x)_{n+1} + (uv_x)_n\right] + \frac{1}{2L^3}\left[(v_{xxx})_{n+1} + (v_{xxx})_n\right] = 0$$

For nonlinear term $(uu_x)_{n+1}$, we use $u_{n+1}(u_x)_n + u_n(u_x)_{n+1} - (uu_x)_n$ linearization [35] formula. We make similar linearization for $(vv_x)_{n+1}$ and $(uv_x)_{n+1}$. Hence we get

$$u_{n+1} - \frac{\Delta t}{L}3a\left[u_{n+1}(u_x)_n + u_n(u_x)_{n+1}\right] - \frac{\Delta t}{L}b\left[v_{n+1}(v_x)_n + v_n(v_x)_{n+1}\right] - \frac{a\Delta t}{2L^3}(u_{xxx})_{n+1} = u_n + \frac{a\Delta t}{2L^3}(u_{xxx})_n,$$
$$v_{n+1} + 3\frac{\Delta t}{2L}\left[u_{n+1}(v_x)_n + u_n(v_x)_{n+1}\right] + \frac{\Delta t}{2L}(v_{xxx})_{n+1} = v_n - \frac{\Delta t}{2L^3}(v_{xxx})_n \quad (8)$$

with the initial conditions

$$u_0 = f(x), \quad v_0 = g(x), \quad x \in [0, 1]$$

and boundary conditions

$$\begin{aligned} u_{n+1}(0) &= f_1(t_{n+1}), \quad u_{n+1}(1) = f_2(t_{n+1}), \\ (u_x)_{n+1}(1) &= f_3(t_{n+1}), \quad n = 0, 1, ..., N-1 \\ v_{n+1}(0) &= g_1(t_{n+1}), \quad v_{n+1}(1) = g_2(t_{n+1}), \\ (v_x)_{n+1}(1) &= g_3(t_{n+1}), \quad n = 0, 1, ..., N-1 \end{aligned} \tag{9}$$

where $u_{n+1}$ and $v_{n+1}$ are the solutions of the Eq. (8) at the $(n+1)$th time step.

### 3.2. Space discretization by Haar wavelets

In this subsection we show how to discretize space derivatives appeared in Eqs. (8), we start with the highest derivative by Haar wavelets. To do so we assume

$$(u_{xxx})_{n+1}(x) = \sum_{i=1}^{2M} c_i h_i(x) = c_{(2M)}^T h_{(2M)}(x) \tag{10}$$

where the row vector $c_{(2M)}^T$ is constant. Integrating Eq. (10) with respect to $x$ from 0 to $x$, we get the following equation

$$(u_{xx})_{n+1}(x) = (u_{xx})_{n+1}(0) + \sum_{i=1}^{2M} c_i p_{i,1}(x). \tag{11}$$

In Eq. (11), $(u_{xx})_{n+1}(0)$ is unknown so to find it, we need to integrate Eq. (11) from 0 to 1. After that, using boundary conditions (9) we get

$$\begin{aligned} (u_x)_{n+1}(1) - (u_x)_{n+1}(0) = &(u_{xx})_{n+1}(0) \\ &+ \sum_{i=1}^{2M} c_i p_{i,2}(1) \end{aligned}$$

$$\begin{aligned} (u_{xx})_{n+1}(0) = &f_3(t_{n+1}) - (u_x)_{n+1}(0) \\ &- \sum_{i=1}^{2M} c_i p_{i,2}(1). \end{aligned} \tag{12}$$

Substituting (12) into Eq. (11) results in the following equation

$$\begin{aligned} (u_{xx})_{n+1}(x) = &\sum_{i=1}^{2M} c_i p_{i,1}(x) + f_3(t_{n+1}) \\ &- (u_x)_{n+1}(0) - \sum_{i=1}^{2M} c_i p_{i,2}(1). \end{aligned} \tag{13}$$

Now, if we integrate Eq. (13) from 0 to $x$ we get

$$\begin{aligned} (u_x)_{n+1}(x) = &(u_x)_{n+1}(0) + \sum_{i=1}^{2M} c_i p_{i,2}(x) \\ &+ x\left(f_3(t_{n+1}) - (u_x)_{n+1}(0)\right) \\ &- x \sum_{i=1}^{2M} c_i p_{i,2}(1). \end{aligned} \tag{14}$$

In Eqs. (12), (13) and (14),$(u_x)_{n+1}(0)$ term is unknown. So to find $(u_x)_{n+1}(0)$ term we integrate Eq. (14) from 0 to 1 and use boundary conditions (9). Therefore we have

$$\begin{aligned} (u_x)_{n+1}(0) = 2\Bigg[&f_2(t_{n+1}) - f_1(t_{n+1}) - \frac{1}{2} f_3(t_{n+1}) \\ &- \sum_{i=1}^{2M} c_i p_{i,3}(1) + \frac{1}{2} \sum_{i=1}^{2M} c_i p_{i,2}(1)\Bigg] \end{aligned}$$

Now by plugging the calculated value of $(u_x)_{n+1}(0)$ into Eq. (14) we obtain

$$\begin{aligned} (u_x)_{n+1}(x) = 2\Bigg[&f_2(t_{n+1}) - f_1(t_{n+1}) - \frac{1}{2} f_3(t_{n+1}) \\ &- \sum_{i=1}^{2M} c_i p_{i,3}(1) + \frac{1}{2} \sum_{i=1}^{2M} c_i p_{i,2}(1)\Bigg](1-x) \\ &+ x\left(f_3(t_{n+1})\right) + \sum_{i=1}^{2M} c_i p_{i,2}(x) - x \sum_{i=1}^{2M} c_i p_{i,2}(1) \end{aligned} \tag{15}$$

Finally, integrating (15) from 0 to $x$, we obtain

$$\begin{aligned} u(x) = 2\Bigg[&f_2(t_{n+1}) - f_1(t_{n+1}) - \frac{1}{2} f_3(t_{n+1}) \\ &- \sum_{i=1}^{2M} c_i p_{i,3}(1) + \frac{1}{2} \sum_{i=1}^{2M} c_i p_{i,2}(1)\Bigg] \\ &\times \left(x - \frac{x^2}{2}\right) + \frac{x^2}{2}\left(f_3(t_{n+1})\right) \\ &+ \sum_{i=1}^{2M} c_i p_{i,3}(x) - \frac{x^2}{2} \sum_{i=1}^{2M} c_i p_{i,2}(1) + f_1(t_{n+1}) \end{aligned} \tag{16}$$

If we summarize, we have

$$
\left.\begin{aligned}
(u_{xxx})_{n+1}(x) &= \sum_{i=1}^{2M} c_i h_i(x) \\
(u_{xx})_{n+1}(x) &= \sum_{i=1}^{2M} c_i p_{i,1}(x) + f_3(t_{n+1}) \\
&\quad - 2\left[f_2(t_{n+1}) - f_1(t_{n+1})\right. \\
&\quad - \frac{1}{2} f_3(t_{n+1}) - \sum_{i=1}^{2M} c_i p_{i,3}(1) \\
&\quad \left. + \frac{1}{2}\sum_{i=1}^{2M} c_i p_{i,2}(1)\right] \\
&\quad - \sum_{i=1}^{2M} c_i p_{i,2}(1) \\
(u_x)_{n+1}(x) &= 2\left[f_2(t_{n+1}) - f_1(t_{n+1})\right. \\
&\quad - \frac{1}{2} f_3(t_{n+1}) - \sum_{i=1}^{2M} c_i p_{i,3}(1) \\
&\quad \left. + \frac{1}{2}\sum_{i=1}^{2M} c_i p_{i,2}(1)\right](1-x) \\
&\quad + x\left(f_3(t_{n+1})\right) + \sum_{i=1}^{2M} c_i p_{i,2}(x) \\
&\quad - x\sum_{i=1}^{2M} c_i p_{i,2}(1) \\
(u)_{n+1}(x) &= 2\left[f_2(t_{n+1}) - f_1(t_{n+1})\right. \\
&\quad - \frac{1}{2} f_3(t_{n+1}) - \sum_{i=1}^{2M} c_i p_{i,3}(1) \\
&\quad \left. + \frac{1}{2}\sum_{i=1}^{2M} c_i p_{i,2}(1)\right] \\
&\quad \times \left(x - \frac{x^2}{2}\right) + \frac{x^2}{2}\left(f_3(t_{n+1})\right) \\
&\quad + \sum_{i=1}^{2M} c_i p_{i,3}(x) - \frac{x^2}{2}\sum_{i=1}^{2M} c_i p_{i,2}(1) \\
&\quad + f_1(t_{n+1})
\end{aligned}\right\} \quad (17)
$$

$$
\left.\begin{aligned}
(v_{xxx})_{n+1}(x) &= \sum_{i=1}^{2M} d_i h_i(x) \\
(v_{xx})_{n+1}(x) &= \sum_{i=1}^{2M} d_i p_{i,1}(x) + g_3(t_{n+1}) \\
&\quad - 2\left[g_2(t_{n+1}) - g_1(t_{n+1})\right. \\
&\quad - \frac{1}{2} g_3(t_{n+1}) - \sum_{i=1}^{2M} d_i p_{i,3}(1) \\
&\quad \left. + \frac{1}{2}\sum_{i=1}^{2M} d_i p_{i,2}(1)\right] \\
&\quad - \sum_{i=1}^{2M} d_i p_{i,2}(1) \\
(v_x)_{n+1}(x) &= 2\left[g_2(t_{n+1}) - g_1(t_{n+1})\right. \\
&\quad - \frac{1}{2} g_3(t_{n+1}) - \sum_{i=1}^{2M} d_i p_{i,3}(1) \\
&\quad \left. + \frac{1}{2}\sum_{i=1}^{2M} d_i p_{i,2}(1)\right](1-x) \\
&\quad + x\left(g_3(t_{n+1})\right) + \sum_{i=1}^{2M} d_i p_{i,2}(x) \\
&\quad - x\sum_{i=1}^{2M} d_i p_{i,2}(1) \\
(v)_{n+1}(x) &= 2\left[g_2(t_{n+1}) - g_1(t_{n+1})\right. \\
&\quad - \frac{1}{2} g_3(t_{n+1}) - \sum_{i=1}^{2M} d_i p_{i,3}(1) \\
&\quad \left. + \frac{1}{2}\sum_{i=1}^{2M} d_i p_{i,2}(1)\right] \\
&\quad \times \left(x - \frac{x^2}{2}\right) + \frac{x^2}{2}\left(g_3(t_{n+1})\right) \\
&\quad + \sum_{i=1}^{2M} d_i p_{i,3}(x) - \frac{x^2}{2}\sum_{i=1}^{2M} d_i p_{i,2}(1) \\
&\quad + g_1(t_{n+1})
\end{aligned}\right\} \quad (18)
$$

Similarly, we have

Notice that for our problem

$$
\begin{aligned}
f_1(t_{n+1}) = 0, \quad g_1(t_{n+1}) = 0 \\
f_2(t_{n+1}) = 0, \quad g_2(t_{n+1}) = 0 \\
f_3(t_{n+1}) = 0, \quad g_3(t_{n+1}) = 0
\end{aligned}
$$

Substituting Eqs. (17), (18) into Eq. (8) and discretizing the results at the collocation points $x_l = \frac{l-0.5}{2M}$, $l = 1, 2, ..., 2M$ we found following system of equations for cKdV system

$$
\begin{aligned}
\mathbf{A}_{l,i}\mathbf{c}_i + \mathbf{B}_{l,i}\mathbf{d}_i &= u_n + \frac{a\Delta t}{2L^3}(u_{xxx})_n \\
\mathbf{D}_{l,i}\mathbf{c}_i + \mathbf{E}_{l,i}\mathbf{d}_i &= v_n - \frac{\Delta t}{2L^3}(v_{xxx})_n
\end{aligned} \quad (19)
$$

where

$$\begin{aligned}
\mathbf{A}_{l,i} =& \left(2\left[-p_{i,3}(1)+\frac{1}{2}p_{i,2}(1)\right]\left(x_l-\frac{x_l^2}{2}\right)+p_{i,3}(x_l)-\frac{x_l^2}{2}p_{i,2}(1)\right)\left(1-\frac{\Delta t}{L}.3a.(u_x)_n\right)\\
&-\frac{\Delta t}{L}.3a.u_n\left(2\left[-p_{i,3}(1)+\frac{1}{2}p_{i,2}(1)\right](1-x_l)+p_{i,2}(x_l)-x_lp_{i,2}(1)\right)-\frac{a\Delta t}{2L^3}h_i(x_l),\\
\mathbf{B}_{l,i} =& -\frac{\Delta t}{L}.b\left(\left[2\left[-p_{i,3}(1)+\frac{1}{2}p_{i,2}(1)\right]\left(x_l-\frac{x_l^2}{2}\right)+p_{i,3}(x_l)-\frac{x_l^2}{2}p_{i,2}(1)\right](v_x)_n\right)\\
&-\frac{\Delta t}{L}.b\left(v_n\left[2\left[-p_{i,3}(1)+\frac{1}{2}p_{i,2}(1)\right](1-x_l)+p_{i,2}(x_l)-x_lp_{i,2}(1)\right]\right),\\
\mathbf{D}_{l,i} =& \left[3\frac{\Delta t}{2L}(v_x)_n\left(2\left[-p_{i,3}(1)+\frac{1}{2}p_{i,2}(1)\right]\left(x_l-\frac{x_l^2}{2}\right)+p_{i,3}(x_l)-\frac{x_l^2}{2}p_{i,2}(1)\right)\right],\\
\mathbf{E}_{l,i} =& 2\left[-p_{i,3}(1)+\frac{1}{2}p_{i,2}(1)\right]\left(x_l-\frac{x_l^2}{2}\right)+p_{i,3}(x_l)-\frac{x_l^2}{2}p_{i,2}(1)\\
&+3\frac{\Delta t}{2L}u_n\left(2\left[-p_{i,3}(1)+\frac{1}{2}p_{i,2}(1)\right](1-x_l)+p_{i,2}(x_l)-x_lp_{i,2}(1)\right)+\frac{\Delta t}{2L^3}h_i(x_l).
\end{aligned}$$

$\mathbf{c}_i$ and $\mathbf{d}_i$ are column vectors of wavelet coefficients and right hand side of Eqs. (19) is column vectors calculated at $x_l$ collocation points for time steps $n$. By solving Eqs. (19) simultaneously, wavelet coefficients $\mathbf{c}_i$ and $\mathbf{d}_i$ can be calculated successively.

### 3.3. Error analysis

Convergence analysis of the Haar wavelets is taken from [28]. Using the asymptotic expansion of Eq. (16) as given in [28], one can write

$$\begin{aligned}
u(x) =& 2\left[f_2(t_{n+1})-f_1(t_{n+1})-\frac{1}{2}f_3(t_{n+1})\right.\\
&\left.-\sum_{i=1}^{\infty}c_ip_{i,3}(1)+\frac{1}{2}\sum_{i=1}^{\infty}c_ip_{i,2}(1)\right]\\
&\times\left(x-\frac{x^2}{2}\right)+\frac{x^2}{2}\left(f_3(t_{n+1})\right)\\
&+\sum_{i=1}^{\infty}c_ip_{i,3}(x)-\frac{x^2}{2}\sum_{i=1}^{\infty}c_ip_{i,2}(1)+f_1(t_{n+1})
\end{aligned}$$

**Lemma 1.** *Suppose that $u(x)\in L^2(R)$ with $\left|\frac{\partial u(x)}{\partial x}\right|\le K$, $\forall x\in(0,1)$; $K>0$ and $u(x)=\sum_{i=1}^{\infty}c_ih_i(x)$. Then $|c_i|\le K2^{(-3j-2)/2}$ [37].*

**Lemma 2.** *Let $u(x)\in L^2(R)$ be a continuous function defined in $(0,1)$. Then the error norm at $J$ th level satisfies the following inequality*

$$\|E_j\|^2\le\frac{K^2}{12}2^{-2J}$$

where $\left|\frac{\partial u(x)}{\partial x}\right|\le K$, $\forall x\in(0,1)$; $K>0$, $M$ is a positive number related to the $J$ th level resolution of the wavelet given by $M=2^J$ [37].

**Theorem 1.** *Suppose that $u(x)$ is exact and $u_{2M}(x)$ is approximate solution of the Eq. (16), then*

$$\|E_j\|=\|u(x)-u_{2M}(x)\|\le\frac{\sqrt{C}K2^{-3(2^J)-1}}{1-2^{-3/2}}$$

***Proof.*** See Kumar et al. [28] □

Similar procedure is valid for the convegence of $v_{2M}(x)$. It is clear from above equation that by increasing the level of resolution $J$ the error decreases.

## 4. Numerical Experiments

Numerical computations have been done with the free software package GNU Octave and graphical outputs were generated by Matplotlib package [36]. In order to measure the difference between the numerical and analytic solutions as the simulation proceeds we considered the error norms $L_2$ and $L_\infty$ defined by

$$L_2=\sqrt{\Delta x\sum_{i=1}^{2M}\left|u_i^{\text{exact}}-u_i^{\text{num}}\right|^2}$$
$$L_\infty=\max_i\left|u_i^{\text{exact}}-u_i^{\text{num}}\right|.$$

We also check the conservation laws of the cKdV equation given by

$$I_1=\int_{-\infty}^{\infty}u dy$$

$$I_2=\int_{-\infty}^{\infty}\left(u^2+\frac{2}{3}bv^2\right)dy$$

$$I_3 = \int_{-\infty}^{\infty} \left[ (1+a)\left(u^3 - \frac{1}{2}u_y^2\right) + b\left(uv^2 - v_y^2\right)\right] dy.$$

The invariants $I_1$,$I_2$ and $I_3$ [18] are monitored at the computations to check the conservation of the numerical scheme.

### 4.1. Single soliton

Firstly, we consider the following initial conditions for the single soliton problem for the Eq. (1)

$$u(y,0) = 2\lambda^2 \mathrm{sech}^2(\xi), \qquad v(y,0) = \frac{1}{2\sqrt{w}}\mathrm{sech}(\xi)$$

and the boundary conditions (3). This problem have the following exact solution [1].

$$u(y,t) = 2\lambda^2 \mathrm{sech}^2(\xi), \qquad v(y,t) = \frac{1}{2\sqrt{w}}\mathrm{sech}(\xi)$$

where

$$\xi = \lambda(y - \lambda^2 t) + \frac{1}{2\log(w)}, \qquad w = \frac{-b}{8(4a+1)\lambda^4}.$$

We solve the problem for $\Delta t = 0.01$, $\lambda = 0.5$, $a = -0.125$, $b = -3$ and different values of $2M$ at $t = 10$. Table 1 shows the $L_2$, $L_\infty$ error norms for both $u$ and $v$ for increasing collocation points. We can easily see from the table that the error norms decrease with the increasing collocation points as expected. In Table 2 we tabulated the error norms with the invariants, for various values of time. We see that the error norms are sufficiently small and also the invariants are conserved with increasing time. Relative changes of invariants $I_1$, $I_2$ and $I_3$ between $t = 0$ and $t = 10$ are found as $\%9.5362 \times 10^{-6}$, $\%8.0525 \times 10^{-9}$, $\%3.5459 \times 10^{-6}$ respectively according to the formula $\frac{|I_i^{t=0} - I_i^{t=10}|}{I_i^{t=0}} \times 100$, $(i = 1, 2, 3)$.

Finally, for the single soliton problem we depicted the evolution of numerical solutions of $u$ and $v$ in Fig. 1 for $a = -0.125$, $b = -3$ and $\lambda = 0.5$.

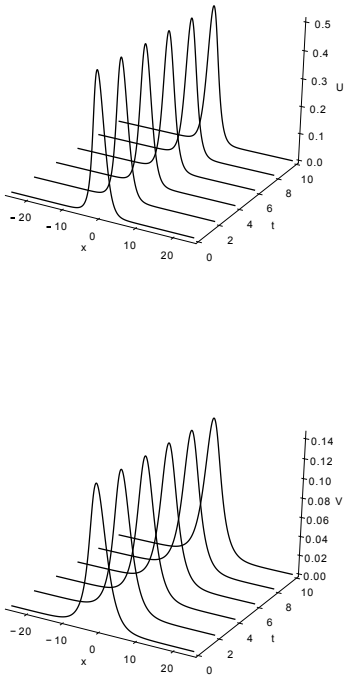


**Figure 1.** Numerical solutions for $\Delta t = 0.01$ and $2M = 1024$.

### 4.2. Birth of solitons

We consider Eq. (1) with the initial conditions

$$u(y,0) = e^{-0.01y^2}, \qquad v(x,0) = e^{-0.01y^2}$$

and the boundary conditions (3). Computer simulation of this problem are done for $a = 0.5$ and $b = -3$ in the interval $-50 \le y \le 150$. Numerical results of invariants and their comparison with Petrov-Galerkin method are tabulated in Table 4, as it can be seen from the table our results are agree with Ref. [18]. The positions and amplitudes of waves at $t = 25$ are given in Table 5. It is clearly seen from the table that for first three wave the positions are same for $u$ and $v$. Finally, evolution of numerical solutions between $t = 0$ and $t = 25$ for $\Delta t = 0.01$ and $2M = 2048$ is depicted in Fig. 2.

In Table 3, we give a comparison of our results with ref. [18] for $\Delta t = 0.01$, $\lambda = 0.5$, $a = -0.125$, $b = -3$ and $2M = 1024$. Numerical results of the present method are comparable with the other methods.

**Table 1.** Numerical results for $\Delta t = 0.01$, $\lambda = 0.5$, $a = -0.125$, $b = -3$ and different values of $2M$ at $t = 10$.

| $2M$ | $L_2(u)$ | $L_2(v)$ | $L_\infty(u)$ | $L_\infty(v)$ |
|---|---|---|---|---|
| 256 | 0.000951 | 0.000327 | 0.000583 | 0.000140 |
| 512 | 0.000240 | 0.000082 | 0.000147 | 0.000035 |
| 1024 | 0.000060 | 0.000021 | 0.000037 | 0.000009 |

**Table 2.** Numerical results for $\Delta t = 0.01$, $\lambda = 0.5$, $a = -0.125$, $b = -3$ and $2M = 1024$.

| $t$ | $I_1$ | $I_2$ | $I_3$ | $L_2(u)$ | $L_2(v)$ | $L_\infty(u)$ | $L_\infty(v)$ |
|---|---|---|---|---|---|---|---|
| 0 | 2.000000 | 0.500000 | 0.112500 | 0.000000 | 0.000000 | 0.000000 | 0.000000 |
| 2 | 2.000000 | 0.500000 | 0.112500 | 0.000025 | 0.000009 | 0.000019 | 0.000005 |
| 4 | 2.000000 | 0.500000 | 0.112500 | 0.000040 | 0.000014 | 0.000028 | 0.000007 |
| 6 | 2.000000 | 0.500000 | 0.112500 | 0.000050 | 0.000017 | 0.000033 | 0.000008 |
| 8 | 2.000000 | 0.500000 | 0.112500 | 0.000057 | 0.000019 | 0.000036 | 0.000008 |
| 10 | 2.000000 | 0.500000 | 0.112500 | 0.000060 | 0.000021 | 0.000037 | 0.000009 |

**Table 3.** A comparison for $\Delta t = 0.01$, $\lambda = 0.5$, $a = -0.125$, $b = -3$ and $2M = 1024$.

| $t$ | Present Method | | Petrov-Galerkin [18] | | Product Approx. Tech. [18] | |
|---|---|---|---|---|---|---|
| | $L_\infty(u)$ | $L_\infty(v)$ | $L_\infty(u)$ | $L_\infty(v)$ | $L_\infty(u)$ | $L_\infty(v)$ |
| 2 | 0.000019 | 0.000005 | 0.000015 | 0.000004 | 0.000004 | 0.000005 |
| 4 | 0.000028 | 0.000007 | 0.000021 | 0.000005 | 0.000008 | 0.000007 |
| 6 | 0.000033 | 0.000008 | 0.000023 | 0.000006 | 0.000010 | 0.000009 |
| 8 | 0.000036 | 0.000008 | 0.000024 | 0.000007 | 0.000013 | 0.000012 |
| 10 | 0.000036 | 0.000009 | 0.000025 | 0.000008 | 0.000014 | 0.000013 |

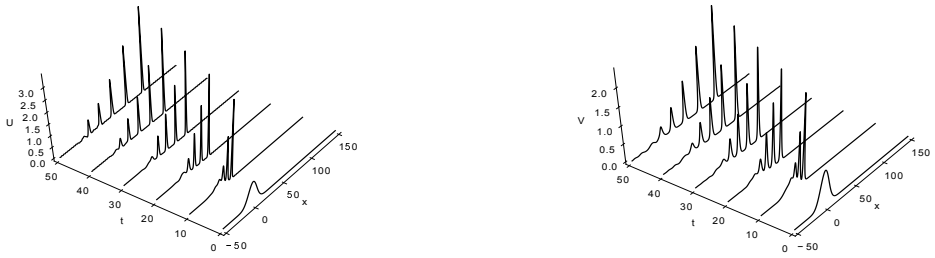


**Figure 2.** Numerical solutions for $\Delta t = 0.01$ and $2M = 1024$.

**Table 4.** Numerical results for $\Delta t = 0.01$ and $2M = 2048$ at various times.

| $t$ | $I_1$ | | $I_2$ | |
|---|---|---|---|---|
| | Haar | Petrov-Galerkin [18] | Haar | Petrov-Galerkin [18] |
| 0 | 17.7245385 | 17.724343 | -12.5331414 | -12.533142 |
| 5 | 17.7245385 | 17.723816 | -12.5331169 | -12.532956 |
| 10 | 17.7245385 | 17.723352 | -12.5325963 | -12.530116 |
| 15 | 17.7245385 | 17.722782 | -12.5324374 | -12.529239 |
| 20 | 17.7245020 | 17.722217 | -12.5323640 | -12.529013 |
| 25 | 17.7245998 | 17.721734 | -12.5306828 | -12.528983 |

**Table 5.** Amplitudes and positions of waves and their comparisons for $\Delta t = 0.01$ and $2M = 2048$ at $t = 25$.

| | Position ($y$) | Amplitude ($u$) | Position ($y$) | Amplitude ($v$) |
|---|---|---|---|---|
| First wave | 47.7 | 3.4508 | 47.7 | 2.4415 |
| Second wave | 32.4 | 2.4434 | 32.4 | 2.7298 |
| Third wave | 18.7 | 1.5601 | 18.7 | 1.1046 |
| Fourth wave | 7.0 | 0.6908 | 6.9 | 0.5236 |
| Fifth wave | -2.8 | 0.2214 | -3.6 | 0.1809 |

## 5. Conclusion

In conclusion, we have applied Haar wavelet method to coupled KdV equation in this study. Single soliton and birth of solitons have been used as test examples to see the efficiency of the Haar wavelet method. The error norms $L_2$ and $L_\infty$ obtained by Haar wavelet method are compared with the exact solutions and with those numerical ones available in the literature. The comparisons of error norms as well as conservation of invariants during simulations clearly indicate that the present method is both reliable and competitive with other methods. As a conclusion, the proposed method can safely and quickly be employed to solve similar coupled partial differential equations.

## References


[1] Hirota, R. and Satsuma, J., "Soliton solutions of a coupled Korteweg-de Vries equation," *Physics Letters A*, 85 (8-9), 407–408 (1981).

[2] Halim, A. A., Kshevetskii, S. P. and Leble, S. B., "Numerical integration of a coupled Korteweg-de Vries system," *Computers & Mathematics with Applications*, vol. 45 (4-5), 581–591 (2003).

[3] Halim, A. A. and Leble, S. B., "Analytical and numerical solution of a coupled KdV-MKdV System," *Chaos, Solitons and Fractals*, 19 (1), 99–108 (2004).

[4] Zhu, S., A difference scheme for the coupled KdV equation. *Communications in Nonlinear Science and Numerical Simulation*, 4 (1), 60-63 (1999).

[5] Kaya, D. and Inan, I. E., "Exact and numerical traveling wave solutions for nonlinear coupled equations using symbolic computation," *Applied Mathematics and Computation*, 151(3), 775–787 (2004).

[6] Fan, E. G., "Traveling wave solutions for nonlinear equations using symbolic computation," *Computers & Mathematics with Applications*, 43 (6-7), 671–680 (2002).

[7] Ma, Z. and Zhu, J., Jacobian elliptic function expansion solutions for the Wicktype stochastic coupled KdV equations. *Chaos Solitons Fractals*, 32, 1679-1685 (2007) .

[8] Assas, L. M. B., "Variational iteration method for solving coupled-KdV equations," *Chaos, Solitons and Fractals*, 38 (4), 1225–1228 (2008).

[9] Abbasbandy, S., "The application of homotopy analysis method to solve a generalized Hirota-Satsuma coupled KdV equation," Physics *Letters A: General, Atomic and Solid State Physics*, 361 (6), 478–483 (2007).

[10] Al-Khaled, K., Al-Refai, M. and Alawneh, A., Traveling wave solutions using the variational method and the tanh method for nonlinear coupled equations. *Applied Mathematics and Computation,* 202, 233-242 (2008).

[11] Mokhtari, R. and Mohammadi, M., New exact solutions to a class of coupled nonlinear PDEs. *The International Journal of Nonlinear Sciences and Numerical Simulation*, 10 (6) , 779-796 (2009).

[12] Ismail, M. S., "Numerical solution of coupled nonlinear Schrodinger equation by Galerkin method," *Mathematics and Computers in Simulation*, 78 (4), 532–547 (2008).

[13] Ismail, M. S. and Taha, T. R., "A linearly implicit conservative scheme for the coupled nonlinear Schrodinger equation," *Mathematics and Computers in Simulation*, 74 (4-5), 302– 311 (2007).

[14] Ismail, M. S. and Alamri, S. Z., "Highly accurate finite difference method for coupled nonlinear Schrdinger equation," *International Journal of Computer Mathematics*,81 (3), 333– 351 (2004).

[15] Wazwaz, A., "*The KdV equation*," *in Handbook of Differential Equations: Evolutionary Equations. VOL. IV, Handb. Differ. Equ.*, pp. 485–568, Elsevier/North-Holland, Amsterdam, The Netherlands, 2008.

[16] Ismail, M. S., "Numerical solution of a coupled Korteweg-de Vries equations by collocation method," *Numerical Methods for Partial Differential Equations*, 25 (2), 275–291 (2009).

[17] Kutluay, S. and Ucar,Y., "A quadratic B-splineGalerkin approach for solving a coupled KdV equation," *Mathematical Modelling and Analysis*, 18 (1), 103–121 (2013).

[18] Ismail, M. S. and Ashi, H. A., A Numerical Solution for Hirota-Satsuma Coupled KdV Equation, *Abstract and Applied Analysis*, Volume 2014, Article ID 819367, 9 pages http://dx.doi.org/10.1155/2014/819367

[19] Chen, C. and Hsiao, C.H., Haar wavelet method for solving lumped and distributed parameter systems, *IEE Proceedings - Control Theory and Applications*, 144, 87–94 (1997).

[20] Lepik, U., Numerical solution of differential equations using Haar wavelets, *Mathematics and Computers in Simulation*, 68, 127–143 (2005).

[21] Lepik, U., Numerical solution of evolution equations by the Haar wavelet method, *Applied Mathematics and Computation*, 185,695–704 (2007).

[22] Lepik, U., Solving PDEs with the aid of two-dimensional Haar wavelets, *Computers and Mathematics with Applications*, 61, 1873–1879 (2011) .

[23] Celik, I., Haar wavelet method for solving generalized Burgers–Huxley equation, *Arab Journal of Mathematical Sciences*, 18 (1), 25–37(2012) .
[24] Celik, I., Haar wavelet approximation for magnetohydrodynamic flow equations, *Applied Mathematical Modelling*, 37, 3894–3902(2013).
[25] Jiwari, R., A Haar wavelet quasilinearization approach for numerical simulation of Burgers' equation, *Computer Physics Communications*, 183, 2413–2423 (2012).
[26] Kaur, H., Mittal, R.C. and Mishra, V., Haar wavelet approximate solutions for the generalized Lane–Emden equations arising in astrophysics, *Computer Physics Communications*, 184, 2169–2177(2013).
[27] Shi, Z., Cao, Y., and Chen, Q.J., Solving 2D and 3D Poisson equations and biharmonic equations by the Haar wavelet method, *Applied Mathematical Modelling*, 36, 5143–5161 (2012).
[28] Kumar, M. and Pandit, S., A composite numerical scheme for the numerical simulation of coupled Burgers' equation, *Computer Physics Communications*, 185 (3), 809-817 (2014).
[29] Mittal, R.C., Kaur, H. and Mishra, V., Haar wavelet-based numerical investigation of coupled viscous Burgers' equation, *International Journal of Computer Mathematics*, 92 (8), 1643-1659 (2014).
[30] Oruç, Ö., Bulut, F. and Esen, A., Numerical Solutions of Regularized Long Wave Equation By Haar Wavelet Method, *Mediterranean Journal of Mathematics*, 13 (5), 32353253 (2016)
[31] Oruç, Ö., Bulut, F. and Esen, A., A Haar wavelet-finite difference hybrid method for the numerical solution of the modified Burgers' equation, *Journal of Mathematical Chemistry*, 53 (7) 1592-1607 (2015).
[32] Oruç, Ö., Bulut, F. and Esen, A., Numerical Solution of the KdV Equation by Haar Wavelet Method, *Pramana Journal of Physics*, doi:10.1007/s12043-016-1286-7, 87: 94 (2016)
[33] Bulut, F., Oruç, Ö. and Esen, A., Numerical Solutions of Fractional System of Partial Differential Equations By Haar Wavelets, *Computer Modeling in Engineering & Sciences*, 108 (4), 263-284 (2015).
[34] Hein, H.and Feklistova, L., Free vibrations of non-uniform and axially functionally graded beams using Haar wavelets, *Engineering Structures*, 33 (12), 3696-3701 (2011).
[35] Rubin, S. G. and Graves, R. A., Cubic spline approximation for problems in fluid mechanics, NASA TR R-436, Washington, DC, 1975.
[36] Hunter, J. D., Matplotlib: A 2D graphics environment, *Computing In Science & Engineering*, 9(3), 90-95 (2007).
[37] Ray, S.S., On Haar wavelet operational matrix of general order and its application for the numerical solution of fractional Bagley Torvik equation, *Applied Mathematics and Computation*, 218, 5239–5248 (2012).

***Ömer Oruç*** *obtained his M.Sc. degree in fuzzy differential equations from department of Mathematics, TOBB Economics and Technology University in 2011, and his Ph.D. in Haar wavelet based numerical methods from department of Mathematics, Inonu University in 2016. His current research areas include fuzzy theory, differential equations, numerical methods and scientific computing.*

***Fatih Bulut*** *currently works as an Assistant Professor at the Department of Physics at the Inonu University. He received his B.Sc. in Physics from Ankara University in 2000, his M.Sc. in 2005 from University of Iowa and his Ph.D. in 2008 form SUNY Buffalo. His main research field is Theoretical High Energy Physics, computational Physics and numerical analysis*

***Alaattin Esen*** *received his degree in mathematics from the Inonu University in 1994. He has completed his M.Sc. and Ph.D. degrees in applied mathematics. He is currently studying about the numerical solutions of a wide range of partial differential equations. He has many research papers published in various national and international journals. He has given many talks and conferences. His research interests include finite difference methods, finite element methods, computational methods and algorithms.*



An International Journal of Optimization and Control: Theories & Applications
ISSN:2146-0957 eISSN:2146-5703
Vol.7, No.2, pp.205-215 (2017)
http://doi.org/10.11121/ijocta.01.2017.00405

RESEARCH ARTICLE

# On the Hermite-Hadamard-Fejer-type inequalities for co-ordinated convex functions via fractional integrals

Hatice Yaldız[a*] , Mehmet Zeki Sarıkaya[a] and Zoubir Dahmani[b]

[a] *Department of Mathematics, Faculty of Science and Arts, Düzce University, Düzce, Turkey*
[b] *Laboratory of Pure and Applied Mathematics, UMAB, University of Mostaganem, Algeria*
*yaldizhatice@gmail.com, sarikayamz@gmail.com, zzdahmani@yahoo.fr*

ARTICLE INFO

Article History:
*Received 20 January 2017*
*Accepted 06 June 2017*
*Available 17 July 2017*

Keywords:
*Convex function*
*Co-ordinated convex mapping*
*Hermite-Hadamard-Fejer inequality*
*Riemann-Liouville fractional integrals*

AMS Classification 2010:
*26A33, 26A51, 26D15*

ABSTRACT

In this paper, using Riemann-Liouville integral operators, we establish new fractional integral inequalities of Hermite-Hadamard-Fejer type for co-ordinated convex functions on a rectangle of $\mathbb{R}^2$. The results presented here would provide extensions of those given in earlier works.



## 1. Introduction

Let $\Phi : I \subseteq \mathbb{R} \to \mathbb{R}$ be a convex mapping defined on the interval $I$ of real numbers and $a, b \in I$, with $a < b$. The following double inequality is well known in the literature as the Hermite-Hadamard inequality [13]:

$$\Phi\left(\frac{a+b}{2}\right) \tag{1}$$
$$\leq \frac{1}{b-a}\int_a^b \Phi(x)\,dx$$
$$\leq \frac{\Phi(a)+\Phi(b)}{2}.$$

The most well-known inequalities related to the integral mean of a convex function are the Hermite Hadamard inequalities or its weighted versions, the so-called Hermite-Hadamard-Fejér inequalities (see, [14], [19], [21]). In [11], Fejer gave a weighted generalizatinon of the inequalities (1) as the following:

**Theorem 1.** *Let $\Phi : [a, b] \to R$ be a convex function. Then the inequality hold:*

$$\Phi\left(\frac{a+b}{2}\right)\int_a^b \Psi(x)\,dx$$
$$\leq \int_a^b \Phi(x)\,\Psi(x)\,dx$$
$$\leq \frac{\Phi(a)+\Phi(b)}{2}\int_a^b \Psi(x)\,dx,$$

*where $\Psi : [a, b] \to R$ is nonnegative, integrable and symmetric to $\frac{(a+b)}{2}$.*

In the following, we will give some necessary definitions and mathematical preliminaries of fractional calculus theory which are used further in this paper. More details, one can consult [12, 18].

**Definition 1.** *( [4, 12, 18]) Let $\Phi \in L_1([a, b])$. The Riemann-Liouville integrals $J^{\alpha}_{a+}\Phi$ and $J^{\alpha}_{b-}\Phi$ of order $\alpha > 0$ with $a \geq 0$ are defined by*

*Corresponding Author

$$J_{a+}^{\alpha}\Phi(x)=\frac{1}{\Gamma(\alpha)}\int_{a}^{x}(x-t)^{\alpha-1}\Phi(t)dt,\quad x>a$$

*and*

$$J_{b-}^{\alpha}\Phi(x)=\frac{1}{\Gamma(\alpha)}\int_{x}^{b}(t-x)^{\alpha-1}\Phi(t)dt,\quad x<b$$

*respectively. Here,* $\Gamma(\alpha)$ *is the Gamma function and* $J_{a+}^{0}\Phi(x)=J_{b-}^{0}\Phi(x)=\Phi(x)$.

Meanwhile, in [24], Sarikaya et al. gave the following interesting Riemann-Liouville integral inequalities of Hermite-Hadamard-type:

**Theorem 2.** *Let* $K:[a,b]\to\mathbb{R}$ *be a positive function with* $0\leq a<b$ *and* $K\in L_1([a,b])$. *If* $K$ *is a convex function on* $[a,b]$, *then the following inequalities for fractional integrals hold:*

$$\begin{aligned}&K\left(\frac{a+b}{2}\right)\\&\leq\frac{\Gamma(\alpha+1)}{2(b-a)^{\alpha}}\left[J_{a+}^{\alpha}K(b)+J_{b-}^{\alpha}K(a)\right]\\&\leq\frac{K(a)+K(b)}{2}\end{aligned}\tag{2}$$

*with* $\alpha>0$.

Later, in [14], Iscan presented the following Hermite-Hadamard-Fejer type inequalities for convex functions via Riemann-Liouville fractional integrals:

**Theorem 3.** *Let* $K:[a,b]\to\mathbb{R}$ *be convex function with* $0\leq a<b$ *and* $K\in(L_1[a,b])$. *If* $L:[a,b]\to\mathbb{R}$ *is nonnegative, integrable and symmetric with respect to* $\frac{a+b}{2}$, *then the following inequalities for fractional integrals hold:*

$$\begin{aligned}&K\left(\frac{a+b}{2}\right)\left[J_{a+}^{\alpha}L(b)+J_{b-}^{\alpha}L(a)\right]\\&\leq\left[J_{a+}^{\alpha}K(b)+J_{b-}^{\alpha}K(a)\right]\\&\leq\frac{K(a)+K(b)}{2}\left[J_{a+}^{\alpha}L(b)+J_{b-}^{\alpha}L(a)\right]\end{aligned}\tag{3}$$

*with* $\alpha>0$.

Let us now consider a bi-demensional interval which will be used throughout this paper. So, we define $\Delta=:[a,b]\times[c,d]$ in $\mathbb{R}^2$ with $a<b$ and $c<d$. A mapping $\Phi:\Delta\to\mathbb{R}$ is said to be convex on the co-ordinates $\Delta$ if the following inequality:

$$\begin{aligned}&\Phi(tx+(1-t)z,ty+(1-t)r)\\&\leq t\Phi(x,y)+(1-t)\Phi(z,r)\end{aligned}$$

holds, for all $(x,y),(z,r)\in\Delta$ and $t\in[0,1]$.
A function $\Phi:\Delta\to\mathbb{R}$ is said to be convex on the co-ordinates on $\Delta$ if the partial mappings $\Phi_y:[a,b]\to\mathbb{R}$, $\Phi_y(u)=\Phi(u,y)$ and $\Phi_x:[c,d]\to\mathbb{R}$, $\Phi_x(v)=\Phi(x,v)$ are convex where defined for all $x\in[a,b]$ and $y\in[c,d]$ (see, [10]).

A formal definition for co-ordinated convex functions may be stated as follows:

**Definition 2.** *( [10]) A function* $\Phi:\Delta\to\mathbb{R}$ *will be called co-ordinated convex on* $\Delta$, *for all* $t,s\in[0,1]$ *and* $(x,y),(u,r)\in\Delta$, *if the following inequality holds:*

$$\begin{aligned}&\Phi(tx+(1-t)y,su+(1-s)r)\\\leq\;&ts\Phi(x,u)+s(1-t)\Phi(y,u)\\&+t(1-s)\Phi(x,r)+(1-t)(1-s)\Phi(y,r).\end{aligned}\tag{4}$$

Clearly, every convex function is a co-ordinated convex. Furthermore, there exists a co-ordinated convex function which is not convex, (see, [10]).

For several recent results concerning Hermite-Hadamard's inequality for some convex function on the co-ordinates on a rectangle of $\mathbb{R}^2$, we refer the reader to ( [1]- [3], [10], [15]- [17], [20], [22], [27]).

In [10], Dragomir established the following inequality of Hermite-Hadamard-type for co-ordinated convex mapping on a rectangle of $\mathbb{R}^2$ similar to (1).

**Theorem 4.** *Suppose that* $\Phi:\Delta\to\mathbb{R}$ *is co-ordinated convex on* $\Delta$. *Then one has the inequalities:*

$$
\begin{aligned}
&\Phi\left(\frac{a+b}{2},\frac{c+d}{2}\right)\\
\leq\ &\frac{1}{2}\left[\frac{1}{b-a}\int_a^b \Phi\left(x,\frac{c+d}{2}\right)dx\right.\\
&\left.+\frac{1}{d-c}\int_c^d \Phi\left(\frac{a+b}{2},y\right)dy\right]\\
\leq\ &\frac{1}{(b-a)(d-c)}\int_a^b\int_c^d \Phi(x,y)\,dydx \qquad (5)\\
\leq\ &\frac{1}{4}\left[\frac{1}{b-a}\int_a^b \Phi(x,c)\,dx+\frac{1}{b-a}\int_a^b \Phi(x,d)\,dx\right.\\
&\left.+\frac{1}{d-c}\int_c^d \Phi(a,y)\,dy+\frac{1}{d-c}\int_c^d \Phi(b,y)\,dy\right]\\
\leq\ &\frac{\Phi(a,c)+\Phi(a,d)+\Phi(b,c)+\Phi(b,d)}{4}.
\end{aligned}
$$

*The above inequalities are sharp.*

Later, in [27], Sarikaya and Yaldiz proved inequalities of the Hermite-Hadamard type by using the definition of co-ordinated convex functions for L-Lipschitzian mappings.

In [3], a Hermite-Hadamard-Fejer type inequality for co-ordinated convex mappings is established as follows:

**Theorem 5.** *Let $\Phi:\Delta\to R$ be a co-ordinated convex function. Then the following double inequality hold:*

$$
\begin{aligned}
&\Phi\left(\frac{a+b}{2},\frac{c+d}{2}\right)\\
&\leq\frac{\int_a^b\int_c^d \Phi(x,y)\,p(x,y)\,dydx}{\int_a^b\int_c^d p(x,y)\,dydx} \qquad (6)\\
&\leq\frac{\Phi(a,c)+\Phi(a,d)+\Phi(b,c)+\Phi(b,d)}{4},
\end{aligned}
$$

*where $p:\Delta\to R$ is positive, integrable and symmetric with respect to $x=\frac{a+b}{2}$ and $y=\frac{c+d}{2}$ on the co-ordinates on $\Delta$. The above inequalities are sharp.*

Because of the wide application of Hermite Hadamard type inequalities, Fejer type inequalities and Riemann-Liouville integrals for two-variable functions, many authors extend their studies to Hermite Hadamard type inequalities and Fejer type inequalities involving Riemann-Liouville integrals not limited to integer integrals.

**Definition 3.** *( [12, 18]) Let $\Phi\in L_1(\Delta)$. The Riemann-Liouville integrals $J^{\alpha,\beta}_{a+,c+}$, $J^{\alpha,\beta}_{a+,d-}$, $J^{\alpha,\beta}_{b-,c+}$ and$J^{\alpha,\beta}_{b-,d-}$ of order $\alpha,\beta>0$ with $a,c\geq 0$ are defined by*

$$J^{\alpha,\beta}_{a+,c+}\Phi(x,y)=$$

$$\frac{1}{\Gamma(\alpha)\Gamma(\beta)}\int_a^x\int_c^y (x-t)^{\alpha-1}(y-s)^{\beta-1}\Phi(t,s)dsdt,$$

$$x>a,y>c$$

$$J^{\alpha,\beta}_{a+,d-}\Phi(x,y)=$$

$$\frac{1}{\Gamma(\alpha)\Gamma(\beta)}\int_a^x\int_y^d (x-t)^{\alpha-1}(s-y)^{\beta-1}\Phi(t,s)dsdt,$$

$$x>a,y<d$$

$$J^{\alpha,\beta}_{b-,c+}\Phi(x,y)=$$

$$\frac{1}{\Gamma(\alpha)\Gamma(\beta)}\int_x^b\int_c^y (t-x)^{\alpha-1}(y-s)^{\beta-1}\Phi(t,s)dsdt,$$

$$x<b,y>c$$

*and*

$$J^{\alpha,\beta}_{b-,d-}\Phi(x,y)=$$

$$\frac{1}{\Gamma(\alpha)\Gamma(\beta)}\int_x^b\int_y^d (t-x)^{\alpha-1}(s-y)^{\beta-1}\Phi(t,s)dsdt,$$

$$x<b,y<d$$

*respectively. Here, $\Gamma$ is the Gamma function,*

$$J^{0,0}_{a+,c+}\Phi(x,y)=J^{0,0}_{a+,d-}\Phi(x,y)$$

$$=J^{0,0}_{b-,c+}\Phi(x,y)=J^{0,0}_{b-,d-}\Phi(x,y)=\Phi(x,y)$$

*and*

$$J^{1,1}_{a+,c+}\Phi(x,y)=\int_a^x\int_c^y \Phi(t,s)dsdt.$$

Similar to Definition 1 and Definition 3, we introduce the following fractional integrals:

$$
\begin{aligned}
&J^{\alpha}_{a+}\Phi\left(x,\frac{c+d}{2}\right)\\
&=\frac{1}{\Gamma(\alpha)}\int_a^x (x-t)^{\alpha-1}\Phi\left(t,\frac{c+d}{2}\right)dt,\quad x>a;
\end{aligned}
$$

$$J_{b-}^{\alpha}\Phi\left(x,\frac{c+d}{2}\right)$$
$$=\frac{1}{\Gamma(\alpha)}\int_{x}^{b}(t-x)^{\alpha-1}\Phi\left(t,\frac{c+d}{2}\right)dt, x<b;$$
$$J_{c+}^{\beta}\Phi\left(\frac{a+b}{2},y\right)$$
$$=\frac{1}{\Gamma(\beta)}\int_{c}^{y}(y-s)^{\beta-1}\Phi\left(\frac{a+b}{2},s\right)ds,\quad y>c;$$
$$J_{d-}^{\beta}\Phi\left(\frac{a+b}{2},y\right)$$
$$=\frac{1}{\Gamma(\beta)}\int_{y}^{d}(s-y)^{\beta-1}\Phi\left(\frac{a+b}{2},s\right)ds,\quad y<d.$$

It is remarkable that Sarikaya et al.( [26]) and ( [28]) gave the following interesting integral inequalities of Hermite-Hadamard-type involving Riemann-Liouville fractional integrals by using convex functions of 2-variables on the co-ordinates.

**Theorem 6.** *Let $\Phi:\Delta\to\mathbb{R}$ be co-ordinated convex on $\Delta$, with $0\le a<b$, $0\le c<d$ and $\Phi\in L_1(\Delta)$. Then one has the inequalities:*

$$\Phi\left(\frac{a+b}{2},\frac{c+d}{2}\right) \tag{7}$$
$$\le \frac{\Gamma(\alpha+1)\Gamma(\beta+1)}{4(b-a)^{\alpha}(d-c)^{\beta}}$$
$$\times\left[J_{a+,c+}^{\alpha,\beta}\Phi(b,d)+J_{a+,d-}^{\alpha,\beta}\Phi(b,c)\right.$$
$$\left.+J_{b-,c+}^{\alpha,\beta}\Phi(a,d)+J_{b-,d-}^{\alpha,\beta}\Phi(a,c)\right]$$
$$\le \frac{\Phi(a,c)+\Phi(a,d)+\Phi(b,c)+\Phi(b,d)}{4}.$$

For some recent results connected with fractional integral inequalities, see ( [5]- [9], [23]- [26]).

The main aim of this paper is to establish new results on Hermite-Hadamard-Fejer type inequalities for co-ordinated convex functions on the rectangle $\Delta$ introduced in the first section of this paper. We will use the Riemann-Liouville integral operators to prove our main results.

## 2. Hermite-Hadamard-Fejer type inequalities for fractional integrals

In this section, using Riemann-Liouville fractional integral operators, we establish new results on Hermite-Hadamard-Fejer type inequalities for co-ordinated convex functions. We present evidence by using two different methods. We begin by the following theorem:

**Theorem 7.** *Let $\Phi:\Delta\to\mathbb{R}$ be a co-ordinated convex function such that $\Phi\in L_1(\Delta)$. If $\Psi:\Delta\to\mathbb{R}$ is nonnegative, integrable and symmetric with respect to $\frac{a+b}{2},\frac{c+d}{2}$ on the co-ordinates, then for any $\alpha,\beta>0$ with $a,c\ge 0$, the following integral inequalities hold*

$$\Phi\left(\frac{a+b}{2},\frac{c+d}{2}\right) \tag{8}$$
$$\times\left[J_{a^+c^+}^{\alpha,\beta}\Psi(b,d)+J_{a^+d^-}^{\alpha,\beta}\Psi(b,c)\right.$$
$$\left.+J_{b^-c^+}^{\alpha,\beta}\Psi(a,d)+J_{b^-d^-}^{\alpha,\beta}\Psi(a,c)\right]$$
$$\le \frac{1}{4}\left[J_{a^+c^+}^{\alpha,\beta}(\Phi\Psi)(b,d)+J_{a^+d^-}^{\alpha,\beta}(\Phi\Psi)(b,c)\right.$$
$$\left.+J_{b^-c^+}^{\alpha,\beta}(\Phi\Psi)(a,d)+J_{b^-d^-}^{\alpha,\beta}(\Phi\Psi)(a,c)\right]$$
$$\le \frac{\Phi(a,c)+\Phi(a,d)+\Phi(b,c)+\Phi(b,d)}{4}$$
$$\times\left[J_{a^+c^+}^{\alpha,\beta}\Psi(b,d)+J_{a^+d^-}^{\alpha,\beta}\Psi(b,c)\right.$$
$$\left.+J_{b^-c^+}^{\alpha,\beta}\Psi(a,d)+J_{b^-d^-}^{\alpha,\beta}\Psi(a,c)\right].$$

***Proof.*** Since $\Phi$ is a convex function on $\Delta$, then, for all $(t,s)\in[0,1]\times[0,1]$, we can write:

$$\Phi\left(\frac{a+b}{2},\frac{c+d}{2}\right) \tag{9}$$
$$=\Phi\left(\frac{ta+(1-t)b+(1-t)a+tb}{2},\right.$$
$$\left.\frac{sc+(1-s)d+(1-s)c+sd}{2}\right)$$
$$\le \frac{1}{4}[\Phi(ta+(1-t)b,sc+(1-s)d)$$
$$+\Phi(ta+(1-t)b,(1-s)c+sd)$$
$$+\Phi((1-t)a+tb,sc+(1-s)d)$$
$$+\Phi((1-t)a+tb,(1-s)c+sd)].$$

Multiplying both sides of (9) by $t^{\alpha-1}s^{\beta-1}\Psi((1-t)a+tb,(1-s)c+sd)$, and integrating the resulting inequality with respect to $(t,s)$ on $[0,1]\times[0,1]$, we obtain

$$\Phi\left(\frac{a+b}{2},\frac{c+d}{2}\right)$$

$$\times \int_0^1\int_0^1 t^{\alpha-1}s^{\beta-1}\Psi\left((1-t)a+tb,(1-s)c+sd\right)dsdt$$

$$\leq \frac{1}{4}\int_0^1\int_0^1 t^{\alpha-1}s^{\beta-1}\left[\Phi\left(ta+(1-t)b,sc+(1-s)d\right)\right.$$

$$+\Phi\left(ta+(1-t)b,(1-s)c+sd\right)$$

$$+\Phi\left((1-t)a+tb,sc+(1-s)d\right)$$

$$\left.+\Phi\left((1-t)a+tb,(1-s)c+sd\right)\right]$$

$$\times\Psi\left((1-t)a+tb,(1-s)c+sd\right)dsdt$$

$$= \frac{1}{4}\int_0^1\int_0^1 t^{\alpha-1}s^{\beta-1}\Phi\left(ta+(1-t)b,sc+(1-s)d\right)$$

$$\times\Psi\left((1-t)a+tb,(1-s)c+sd\right)dsdt$$

$$+\int_0^1\int_0^1 t^{\alpha-1}s^{\beta-1}\Phi\left(ta+(1-t)b,(1-s)c+sd\right)$$

$$\times\Psi\left((1-t)a+tb,(1-s)c+sd\right)dsdt$$

$$+\int_0^1\int_0^1 t^{\alpha-1}s^{\beta-1}\Phi\left((1-t)a+tb,sc+(1-s)d\right)$$

$$\times\Psi\left((1-t)a+tb,(1-s)c+sd\right)dsdt$$

$$+\int_0^1\int_0^1 t^{\alpha-1}s^{\beta-1}\Phi\left((1-t)a+tb,(1-s)c+sd\right)$$

$$\times\Psi\left((1-t)a+tb,(1-s)c+sd\right)dsdt.$$

Setting $x=tb+(1-t)a$, $y=sd+(1-s)c$ and $dx=(b-a)dt$, $dy=(d-c)ds$, we obtain:

$$\frac{1}{(b-a)^{\alpha}(d-c)^{\beta}}\Phi\left(\frac{a+b}{2},\frac{c+d}{2}\right)$$

$$\times\int_a^b\int_c^d (x-a)^{\alpha-1}(y-c)^{\beta-1}\Psi(x,y)\,dydx$$

$$\leq \frac{1}{4(b-a)^{\alpha}(d-c)^{\beta}}$$

$$\times\left\{\int_a^b\int_c^d (x-a)^{\alpha-1}(y-c)^{\beta-1}\right.$$

$$\times\Phi(a+b-x,c+d-y)\Psi(x,y)\,dydx$$

$$+\int_a^b\int_c^d (x-a)^{\alpha-1}(d-y)^{\beta-1}$$

$$\times\Phi(a+b-x,y)\Psi(x,y)\,dydx$$

$$+\int_a^b\int_c^d (b-x)^{\alpha-1}(y-c)^{\beta-1}$$

$$\times\Phi(x,c+d-y)\Psi(x,y)\,dydx$$

$$\left.+\int_a^b\int_c^d (b-x)^{\alpha-1}(d-y)^{\beta-1}\Phi(x,y)\Psi(x,y)\,dydx\right\}$$

$$= \frac{1}{4(b-a)^{\alpha}(d-c)^{\beta}}$$

$$\times\left\{\int_a^b\int_c^d (b-x)^{\alpha-1}(y-c)^{\beta-1}\right.$$

$$\times\Phi(x,c+d-y)\Psi(a+b-x,y)\,dydx$$

$$+\int_a^b\int_c^d (b-x)^{\alpha-1}(d-y)^{\beta-1}$$

$$\times\Phi(x,y)\Psi(a+b-x,y)\,dydx$$

$$+\int_a^b\int_c^d (b-x)^{\alpha-1}(y-c)^{\beta-1}$$

$$\times\Phi(x,c+d-y)\Psi(x,y)\,dydx$$

$$\left.+\int_a^b\int_c^d (b-x)^{\alpha-1}(d-y)^{\beta-1}\Phi(x,y)\Psi(x,y)\,dydx\right\}$$

$$= \frac{1}{4(b-a)^{\alpha}(d-c)^{\beta}} \left\{ \int_a^b \int_c^d (b-x)^{\alpha-1}(y-c)^{\beta-1} \times \Phi(x, c+d-y)\,\Psi(x,y)\,dydx + \int_a^b \int_c^d (b-x)^{\alpha-1}(d-y)^{\beta-1}\Phi(x,y)\,\Psi(x,y)\,dydx + \int_a^b \int_c^d (b-x)^{\alpha-1}(y-c)^{\beta-1} \times \Phi(x, c+d-y)\,\Psi(x,y)\,dydx + \int_a^b \int_c^d (b-x)^{\alpha-1}(d-y)^{\beta-1}\Phi(x,y)\,\Psi(x,y)\,dydx \right\}.$$

Therefore,

$$\begin{aligned} & \frac{\Gamma(\alpha)\Gamma(\beta)}{(b-a)^{\alpha}(d-c)^{\beta}} \Phi\left(\frac{a+b}{2}, \frac{c+d}{2}\right) \\ & \times \left[ J^{\alpha,\beta}_{a^+c^+}\Psi(b,d) + J^{\alpha,\beta}_{a^+d^-}\Psi(b,c) \right. \\ & \left. + J^{\alpha,\beta}_{b^-c^+}\Psi(a,d) + J^{\alpha,\beta}_{b^-d^-}\Psi(a,c) \right] \\ \leq & \frac{\Gamma(\alpha)\Gamma(\beta)}{4(b-a)^{\alpha}(d-c)^{\beta}} \\ & \times \left[ J^{\alpha,\beta}_{a^+c^+}(\Phi\Psi)(b,d) + J^{\alpha,\beta}_{a^+d^-}(\Phi\Psi)(b,c) \right. \\ & \left. + J^{\alpha,\beta}_{b^-c^+}(\Phi\Psi)(a,d) + J^{\alpha,\beta}_{b^-d^-}(\Phi\Psi)(a,c) \right]. \end{aligned}$$

The first inequality of (8) is thus proved.
We shall prove the second inequality of (8): Since $f$ is a convex function on $\Delta$, then, for all $(t,s) \in [0,1]\times[0,1]$, it yields

$$\begin{aligned} & \Phi(ta+(1-t)b, sc+(1-s)d) \\ & + \Phi(ta+(1-t)b, (1-s)c+sd) \\ & + \Phi((1-t)a+tb, sc+(1-s)d) \\ & + \Phi((1-t)a+tb, (1-s)c+sd) \qquad (10) \\ \leq & \Phi(a,c)+\Phi(b,c)+\Phi(a,d)+\Phi(b,d). \end{aligned}$$

Then, multiplying both sides of (10) by $t^{\alpha-1}s^{\beta-1}\Psi(tb+(1-t)a, sd+(1-s)c)$ and integrating the resulting inequality with respect to $(t,s)$ over $[0,1]\times[0,1]$, we get

$$\begin{aligned} & \int_0^1\int_0^1 t^{\alpha-1}s^{\beta-1}[\Phi(ta+(1-t)b, sc+(1-s)d) \\ & + \Phi(ta+(1-t)b, (1-s)c+sd) \\ & + \Phi((1-t)a+tb, sc+(1-s)d) \\ & + \Phi((1-t)a+tb, (1-s)c+sd)] \\ & \times \Psi(tb+(1-t)a, sd+(1-s)c)\,dsdt \\ \leq & [\Phi(a,c)+\Phi(b,c)+\Phi(a,d)+\Phi(b,d)] \\ \times & \int_0^1\int_0^1 t^{\alpha-1}s^{\beta-1}\Psi(tb+(1-t)a, sd+(1-s)c)\,dsdt. \end{aligned}$$

That is,

$$\begin{aligned} & \frac{1}{4}\left[ J^{\alpha,\beta}_{a^+c^+}(\Phi\Psi)(b,d) + J^{\alpha,\beta}_{a^+d^-}(\Phi\Psi)(b,c) \right. \\ & \left. + J^{\alpha,\beta}_{b^-c^+}(\Phi\Psi)(a,d) + J^{\alpha,\beta}_{b^-d^-}(\Phi\Psi)(a,c) \right] \\ \leq & \frac{\Phi(a,c)+\Phi(a,d)+\Phi(b,c)+\Phi(b,d)}{4} \\ & \times \left[ J^{\alpha,\beta}_{a^+c^+}\Psi(b,d) + J^{\alpha,\beta}_{a^+d^-}\Psi(b,c) \right. \\ & \left. + J^{\alpha,\beta}_{b^-c^+}\Psi(a,d) + J^{\alpha,\beta}_{b^-d^-}\Psi(a,c) \right]. \end{aligned}$$

The proof of Theorem 7 is thus achieved. □

**Remark 1.** *In Theorem 7:*
*(i) If we take $\alpha=\beta=1$, then the inequality (8) becomes the inequality (6) of Theorem 5.*
*(ii) If we take $\Psi(x,y)=1$, then (8) becomes (7) of Theorem 6.*

We prove also the following result:

**Theorem 8.** *Let $\Phi : \Delta \subset \mathbb{R}^2 \to \mathbb{R}$ be a co-ordinated convex function on $\Delta$, with $a,c \geq 0$, $\alpha,\beta > 0$ and $\Phi \in L_1(\Delta)$. If $\Psi : \Delta \to \mathbb{R}$ is non-negative, integrable and symmetric with respect to $\frac{a+b}{2}$ and $\frac{c+d}{2}$ on the co-ordinates, then we have:*

$$\begin{aligned} & \Phi\left(\frac{a+b}{2}, \frac{c+d}{2}\right) \times \left[ J^{\alpha,\beta}_{a+,c+}\Psi(b,d) + J^{\alpha,\beta}_{a+,d-}\Psi(b,c) \right. \\ & \left. + J^{\alpha,\beta}_{b-,c+}\Psi(a,d) + J^{\alpha,\beta}_{b-,d-}\Psi(a,c) \right] \qquad (11) \end{aligned}$$

$$
\begin{aligned}
&\leq J_{a+}^{\alpha}\left[\Phi\left(b,\frac{c+d}{2}\right)J_{c+}^{\beta}\Psi(b,d)\right]\\
&+J_{a+}^{\alpha}\left[\Phi\left(b,\frac{c+d}{2}\right)J_{d-}^{\beta}\Psi(b,c)\right]\\
&+J_{b-}^{\alpha}\left[\Phi\left(a,\frac{c+d}{2}\right)J_{c+}^{\beta}\Psi(a,d)\right]\\
&+J_{b-}^{\alpha}\left[\Phi\left(a,\frac{c+d}{2}\right)J_{d-}^{\beta}\Psi(a,c)\right]\\
&+J_{c+}^{\beta}\left[\Phi\left(\frac{a+b}{2},d\right)J_{a+}^{\alpha}\Psi(b,d)\right]\\
&+J_{c+}^{\beta}\left[\Phi\left(\frac{a+b}{2},d\right)J_{b-}^{\alpha}\Psi(a,d)\right]\\
&+J_{d-}^{\beta}\left[\Phi\left(\frac{a+b}{2},c\right)J_{a+}^{\alpha}\Psi(b,c)\right]\\
&+J_{d-}^{\beta}\left[\Phi\left(\frac{a+b}{2},c\right)J_{b-}^{\alpha}\Psi(a,c)\right]\\
\leq\ & 2\left[J_{a+,c+}^{\alpha,\beta}\left(\Phi\Psi\right)(b,d)+J_{a+,d-}^{\alpha,\beta}\left(\Phi\Psi\right)(b,c)\right.\\
&\left.+J_{b-,c+}^{\alpha,\beta}\left(\Phi\Psi\right)(a,d)+J_{b-,d-}^{\alpha,\beta}\left(\Phi\Psi\right)(a,c)\right]
\end{aligned}
$$

$$
\begin{aligned}
&\leq J_{a+}^{\alpha}\left[\Phi\left(b,c\right)J_{c+}^{\beta}\Psi(b,d)\right]\\
&+J_{a+}^{\alpha}\left[\Phi\left(b,d\right)J_{d-}^{\beta}\Psi(b,c)\right]\\
&+J_{b-}^{\alpha}\left[\Phi\left(a,c\right)J_{c+}^{\beta}\Psi(a,d)\right]\\
&+J_{b-}^{\alpha}\left[\Phi\left(a,d\right)J_{d-}^{\beta}\Psi(a,c)\right]\\
&+J_{c+}^{\beta}\left[\Phi\left(a,d\right)J_{a+}^{\alpha}\Psi(b,d)\right]\\
&+J_{c+}^{\beta}\left[\Phi\left(b,d\right)J_{b-}^{\alpha}\Psi(a,d)\right]\\
&+J_{d-}^{\beta}\left[\Phi\left(a,c\right)J_{a+}^{\alpha}\Psi(b,c)\right]\\
&+J_{d-}^{\beta}\left[\Phi\left(b,c\right)J_{b-}^{\alpha}\Psi(a,c)\right]\\
\leq\ & \frac{\Phi\left(a,c\right)+\Phi\left(a,d\right)+\Phi\left(b,c\right)+\Phi\left(b,d\right)}{4}\\
&\times\left[J_{a+,c+}^{\alpha,\beta}\Psi(b,d)+J_{a+,d-}^{\alpha,\beta}\Psi(b,c)\right.\\
&\left.+J_{b-,c+}^{\alpha,\beta}\Psi(a,d)+J_{b-,d-}^{\alpha,\beta}\Psi(a,c)\right].
\end{aligned}
$$

***Proof.*** Since $\Phi:\Delta\to\mathbb{R}$ is convex on the co-ordinates, it follows that the mapping $F_x:[c,d]\to\mathbb{R}$, $F_x(y)=\Phi(x,y)$, is convex on $[c,d]$ and the mapping $G_x:[c,d]\to\mathbb{R}$, $G_x(y)=\Psi(x,y)$ is nonnegative, integrable and symmetric with respect to $\frac{c+d}{2}$, for all $x\in[a,b]$. Then, thanks to the inequalities (3), we can write

$$
\begin{aligned}
&F_x\left(\frac{c+d}{2}\right)\left[J_{c+}^{\beta}G_x(d)+J_{d-}^{\beta}G_x(c)\right]\\
\leq\ & J_{c+}^{\beta}\left(F_xG_x\right)(d)+J_{d-}^{\beta}\left(F_xG_x\right)(c)\\
\leq\ & \frac{F_x\left(c\right)+F_x\left(d\right)}{2}\left[J_{c+}^{\beta}G_x(d)+J_{d-}^{\beta}G_x(c)\right],\\
&x\in[a,b].
\end{aligned}
$$

That is,

$$
\begin{aligned}
&\Phi\left(x,\frac{c+d}{2}\right)\frac{1}{\Gamma(\beta)}\left[\int_c^d(d-y)^{\beta-1}\Psi\left(x,y\right)dy\right.\\
&\left.+\int_c^d(y-c)^{\beta-1}\Psi\left(x,y\right)dy\right]\\
\leq\ & \frac{1}{\Gamma(\beta)}\left[\int_c^d(d-y)^{\beta-1}\Psi\left(x,y\right)\Phi\left(x,y\right)dy\right.\\
&\left.+\int_c^d(y-c)^{\beta-1}\Psi\left(x,y\right)\Phi\left(x,y\right)dy\right]\\
\leq\ & \frac{\Phi\left(x,c\right)+\Phi\left(x,d\right)}{2}\frac{1}{\Gamma(\beta)}\left[\int_c^d(d-y)^{\beta-1}\Psi\left(x,y\right)dy\right.\\
&\left.+\int_c^d(y-c)^{\beta-1}\Psi\left(x,y\right)dy\right],
\end{aligned}
\tag{12}
$$

for all $x\in[a,b]$.

Multiplying both sides of (12) by $\frac{(b-x)^{\alpha-1}}{\Gamma(\alpha)}$ and $\frac{(x-a)^{\alpha-1}}{\Gamma(\alpha)}$, and integrating with respect to $x$ over $[a,b]$, respectively, we have

$$
\begin{aligned}
&\frac{1}{\Gamma\left(\alpha\right)\Gamma(\beta)}\int_a^b\int_c^d(b-x)^{\alpha-1}(d-y)^{\beta-1}\\
&\times\Phi\left(x,\frac{c+d}{2}\right)\Psi\left(x,y\right)dydx\\
&+\frac{1}{\Gamma\left(\alpha\right)\Gamma(\beta)}\int_a^b\int_c^d(b-x)^{\alpha-1}(y-c)^{\beta-1}\\
&\times\Phi\left(x,\frac{c+d}{2}\right)\Psi\left(x,y\right)dydx
\end{aligned}
\tag{13}
$$

$$\leq \frac{1}{\Gamma(\alpha)\Gamma(\beta)}\left[\int_a^b\int_c^d (b-x)^{\alpha-1}(d-y)^{\beta-1} \times\Phi(x,y)\,\Psi(x,y)\,dydx + \int_a^b\int_c^d (b-x)^{\alpha-1}(y-c)^{\beta-1}\Phi(x,y)\,\Psi(x,y)\,dydx\right] \tag{14}$$

$$\leq \frac{1}{2\Gamma(\alpha)\Gamma(\beta)}\left[\int_a^b\int_c^d (b-x)^{\alpha-1}(d-y)^{\beta-1} \times\Phi(x,c)\,\Psi(x,y)\,dydx + \int_a^b\int_c^d (b-x)^{\alpha-1}(y-c)^{\beta-1}\Phi(x,c)\,\Psi(x,y)\,dydx + \int_a^b\int_c^d (b-x)^{\alpha-1}(d-y)^{\beta-1}\Phi(x,d)\,\Psi(x,y)\,dydx + \int_a^b\int_c^d (b-x)^{\alpha-1}(y-c)^{\beta-1}\Phi(x,d)\,\Psi(x,y)\,dydx\right].$$

and

$$\frac{1}{\Gamma(\alpha)\Gamma(\beta)}\int_a^b\int_c^d (x-a)^{\alpha-1}(d-y)^{\beta-1} \times\Phi\left(x,\frac{c+d}{2}\right)\Psi(x,y)\,dydx \tag{15}$$

$$+\frac{1}{\Gamma(\alpha)\Gamma(\beta)}\int_a^b\int_c^d (x-a)^{\alpha-1}(y-c)^{\beta-1} \times\Phi\left(x,\frac{c+d}{2}\right)\Psi(x,y)\,dydx$$

$$\leq \frac{1}{\Gamma(\alpha)\Gamma(\beta)}\times\left[\int_a^b\int_c^d (x-a)^{\alpha-1}(d-y)^{\beta-1} \times\Phi(x,y)\,\Psi(x,y)\,dydx + \int_a^b\int_c^d (x-a)^{\alpha-1}(y-c)^{\beta-1} \times\Phi(x,y)\,\Psi(x,y)\,dydx\right]$$

$$\leq \frac{1}{2\Gamma(\alpha)\Gamma(\beta)}\left[\int_a^b\int_c^d (x-a)^{\alpha-1}(d-y)^{\beta-1} \times\Phi(x,c)\,\Psi(x,y)\,dydx + \int_a^b\int_c^d (x-a)^{\alpha-1}(y-c)^{\beta-1}\Phi(x,c)\,\Psi(x,y)\,dydx + \int_a^b\int_c^d (x-a)^{\alpha-1}(d-y)^{\beta-1}\Phi(x,d)\,\Psi(x,y)\,dydx + \int_a^b\int_c^d (x-a)^{\alpha-1}(y-c)^{\beta-1}\Phi(x,d)\,\Psi(x,y)\,dydx\right].$$

For the mappings $F_y:[a,b]\to\mathbb{R}$, $F_y(x)=\Phi(x,y)$ and $G_y:[a,b]\to\mathbb{R}$, $G_y(x)=\Psi(x,y)$, we use the same arguments as before. So, we can state that

$$\frac{1}{\Gamma(\alpha)\Gamma(\beta)}\int_a^b\int_c^d (b-x)^{\alpha-1}(d-y)^{\beta-1} \times\Phi\left(\frac{a+b}{2},y\right)\Psi(x,y)\,dydx \tag{16}$$

$$+ \frac{1}{\Gamma(\alpha)\Gamma(\beta)}\int_a^b\int_c^d (x-a)^{\alpha-1}(d-y)^{\beta-1} \times\Phi\left(\frac{a+b}{2},y\right)\Psi(x,y)\,dydx$$

$$\leq \frac{1}{\Gamma(\alpha)\Gamma(\beta)}\left[\int_a^b\int_c^d (b-x)^{\alpha-1}(d-y)^{\beta-1} \times\Phi(x,y)\,\Psi(x,y)\,dydx + \int_a^b\int_c^d (x-a)^{\alpha-1}(d-y)^{\beta-1}\Phi(x,y)\,\Psi(x,y)\,dydx\right]$$

$$\leq \frac{1}{2\Gamma(\alpha)\Gamma(\beta)}\left[\int_a^b\int_c^d (b-x)^{\alpha-1}(d-y)^{\beta-1} \times\Phi(a,y)\,\Psi(x,y)\,dydx + \int_a^b\int_c^d (x-a)^{\alpha-1}(d-y)^{\beta-1}\Phi(a,y)\,\Psi(x,y)\,dydx + \int_a^b\int_c^d (b-x)^{\alpha-1}(d-y)^{\beta-1}\Phi(b,y)\,\Psi(x,y)\,dydx + \int_a^b\int_c^d (x-a)^{\alpha-1}(d-y)^{\beta-1}\Phi(b,y)\,\Psi(x,y)\,dydx\right]$$

and

$$\frac{1}{\Gamma(\alpha)\Gamma(\beta)}\int_a^b\int_c^d (b-x)^{\alpha-1}(y-c)^{\beta-1} \times\Phi\left(\frac{a+b}{2},y\right)\Psi(x,y)\,dydx \tag{17}$$

$$+\frac{1}{\Gamma(\alpha)\Gamma(\beta)}\int_a^b\int_c^d (x-a)^{\alpha-1}(y-c)^{\beta-1} \times\Phi\left(\frac{a+b}{2},y\right)\Psi(x,y)\,dydx$$

$$\leq \frac{1}{\Gamma(\alpha)\Gamma(\beta)}\left[\int_a^b\int_c^d (b-x)^{\alpha-1}(y-c)^{\beta-1} \times\Phi(x,y)\,\Psi(x,y)\,dydx + \int_a^b\int_c^d (x-a)^{\alpha-1}(y-c)^{\beta-1}\Phi(x,y)\,\Psi(x,y)\,dydx\right]$$

$$\leq \frac{1}{2\Gamma(\alpha)\Gamma(\beta)}\left[\int_a^b\int_c^d (b-x)^{\alpha-1}(y-c)^{\beta-1} \times\Phi(a,y)\,\Psi(x,y)\,dydx + \int_a^b\int_c^d (x-a)^{\alpha-1}(y-c)^{\beta-1}\Phi(a,y)\,\Psi(x,y)\,dydx + \int_a^b\int_c^d (b-x)^{\alpha-1}(y-c)^{\beta-1}\Phi(b,y)\,\Psi(x,y)\,dydx + \int_a^b\int_c^d (x-a)^{\alpha-1}(y-c)^{\beta-1} \times\Phi(b,y)\,\Psi(x,y)\,dydx\right].$$

Adding the inequalities (13)-(17), we can write

$$\begin{aligned} & J^{\alpha}_{a+}\left[\Phi\left(b,\frac{c+d}{2}\right)J^{\beta}_{c+}\Psi(b,d)\right] \\ & +J^{\alpha}_{a+}\left[\Phi\left(b,\frac{c+d}{2}\right)J^{\beta}_{d-}\Psi(b,c)\right] \\ & +J^{\alpha}_{b-}\left[\Phi\left(a,\frac{c+d}{2}\right)J^{\beta}_{c+}\Psi(a,d)\right] \\ & +J^{\alpha}_{b-}\left[\Phi\left(a,\frac{c+d}{2}\right)J^{\beta}_{d-}\Psi(a,c)\right] \\ & +J^{\beta}_{c+}\left[\Phi\left(\frac{a+b}{2},d\right)J^{\alpha}_{a+}\Psi(b,d)\right] \\ & +J^{\beta}_{c+}\left[\Phi\left(\frac{a+b}{2},d\right)J^{\alpha}_{b-}\Psi(a,d)\right] \\ & +J^{\beta}_{d-}\left[\Phi\left(\frac{a+b}{2},c\right)J^{\alpha}_{a+}\Psi(b,c)\right] \\ & +J^{\beta}_{d-}\left[\Phi\left(\frac{a+b}{2},c\right)J^{\alpha}_{b-}\Psi(a,c)\right] \\ \leq\ & 2\left[J^{\alpha,\beta}_{a+,c+}(\Phi\Psi)(b,d)+J^{\alpha,\beta}_{a+,d-}(\Phi\Psi)(b,c)\right. \\ & \left.+J^{\alpha,\beta}_{b-,c+}(\Phi\Psi)(a,d)+J^{\alpha,\beta}_{b-,d-}(\Phi\Psi)(a,c)\right] \\ \leq\ & J^{\alpha}_{a+}\left[\Phi(b,c)\,J^{\beta}_{c+}\Psi(b,d)\right] \\ & +J^{\alpha}_{a+}\left[\Phi(b,d)\,J^{\beta}_{d-}\Psi(b,c)\right] \\ & +J^{\alpha}_{b-}\left[\Phi(a,c)\,J^{\beta}_{c+}\Psi(a,d)\right] \\ & +J^{\alpha}_{b-}\left[\Phi(a,d)\,J^{\beta}_{d-}\Psi(a,c)\right] \\ & +J^{\beta}_{c+}\left[\Phi(a,d)\,J^{\alpha}_{a+}\Psi(b,d)\right] \\ & +J^{\beta}_{c+}\left[\Phi(b,d)\,J^{\alpha}_{b-}\Psi(a,d)\right] \\ & +J^{\beta}_{d-}\left[\Phi(a,c)\,J^{\alpha}_{a+}\Psi(b,c)\right] \\ & +J^{\beta}_{d-}\left[\Phi(b,c)\,J^{\alpha}_{b-}\Psi(a,c)\right]. \end{aligned}$$

These give the second and the third inequalities in (11).

Now, by using the first inequality in (3), it yields that

$$\begin{aligned} & \Phi\left(\frac{a+b}{2},\frac{c+d}{2}\right) \\ \times\ & \left[\int_a^b\int_c^d (b-x)^{\alpha-1}(d-y)^{\beta-1}\Psi(x,y)\,dydx\right. \\ +\ & \left.\int_a^b\int_c^d (x-a)^{\alpha-1}(d-y)^{\beta-1}\Psi(x,y)\,dydx\right] \\ \leq\ & \int_a^b\int_c^d (b-x)^{\alpha-1}(d-y)^{\beta-1} \\ & \times\Phi\left(x,\frac{c+d}{2}\right)\Psi(x,y)\,dydx \\ +\ & \int_a^b\int_c^d (x-a)^{\alpha-1}(d-y)^{\beta-1}\Phi\left(x,\frac{c+d}{2}\right)\Psi(x,y)\,dydx \end{aligned}$$

and

$$\begin{aligned} & \Phi\left(\frac{a+b}{2},\frac{c+d}{2}\right) \\ \times\ & \left[\int_a^b\int_c^d (b-x)^{\alpha-1}(d-y)^{\beta-1}\Psi(x,y)\,dydx\right. \\ +\ & \left.\int_a^b\int_c^d (b-x)^{\alpha-1}(y-c)^{\beta-1}\Psi(x,y)\,dydx\right] \\ \leq\ & \int_a^b\int_c^d (b-x)^{\alpha-1}(d-y)^{\beta-1} \\ & \times\Phi\left(\frac{a+b}{2},y\right)\Psi(x,y)\,dydx \\ +\ & \int_a^b\int_c^d (b-x)^{\alpha-1}(y-c)^{\beta-1} \\ & \times\Phi\left(\frac{a+b}{2},y\right)\Psi(x,y)\,dydx. \end{aligned}$$

By addition, and using the fact that $\Psi$ is symmetric, we get

$$
\begin{aligned}
&\Phi\left(\frac{a+b}{2},\frac{c+d}{2}\right)\\
\times\ &\left[J^{\alpha,\beta}_{a+,c+}\Psi(b,d)+J^{\alpha,\beta}_{a+,d-}\Psi(b,c)\right.\\
&\left.+J^{\alpha,\beta}_{b-,c+}\Psi(a,d)+J^{\alpha,\beta}_{b-,d-}\Psi(a,c)\right]\\
\leq\ &J^{\alpha}_{a+}\left[\Phi\left(b,\frac{c+d}{2}\right)J^{\beta}_{c+}\Psi(b,d)\right]\\
&+J^{\alpha}_{a+}\left[\Phi\left(b,\frac{c+d}{2}\right)J^{\beta}_{d-}\Psi(b,c)\right]\\
&+J^{\alpha}_{b-}\left[\Phi\left(a,\frac{c+d}{2}\right)J^{\beta}_{c+}\Psi(a,d)\right]\\
&+J^{\alpha}_{b-}\left[\Phi\left(a,\frac{c+d}{2}\right)J^{\beta}_{d-}\Psi(a,c)\right]\\
&+J^{\beta}_{c+}\left[\Phi\left(\frac{a+b}{2},d\right)J^{\alpha}_{a+}\Psi(b,d)\right]\\
&+J^{\beta}_{c+}\left[\Phi\left(\frac{a+b}{2},d\right)J^{\alpha}_{b-}\Psi(a,d)\right]\\
&+J^{\beta}_{d-}\left[\Phi\left(\frac{a+b}{2},c\right)J^{\alpha}_{a+}\Psi(b,c)\right]\\
&+J^{\beta}_{d-}\left[\Phi\left(\frac{a+b}{2},c\right)J^{\alpha}_{b-}\Psi(a,c)\right]
\end{aligned}
$$

which gives the first inequality in (11).

Finally, by using the second inequality in (3), we can state that:

$$
\begin{aligned}
&\frac{\alpha}{2(b-a)^{\alpha}}\left[\int_a^b(b-x)^{\alpha-1}\Phi(x,c)\,dx\right.\\
&\left.+\int_a^b(x-a)^{\alpha-1}\Phi(x,c)\,dx\right]\\
\leq\ &\frac{\Phi(a,c)+\Phi(b,c)}{2},\\
&\frac{\alpha}{2(b-a)^{\alpha}}\left[\int_a^b(b-x)^{\alpha-1}\Phi(x,d)\,dx\right.\\
&\left.+\int_a^b(x-a)^{\alpha-1}\Phi(x,d)\,dx\right]\\
\leq\ &\frac{\Phi(a,d)+\Phi(b,d)}{2},\\
&\frac{\beta}{2(d-c)^{\beta}}\left[\int_c^d(d-y)^{\beta-1}\Phi(a,y)\,dy\right.\\
&\left.+\int_c^d(y-c)^{\beta-1}\Phi(a,y)\,dy\right]\\
\leq\ &\frac{\Phi(a,c)+\Phi(a,d)}{2},\\
&\frac{\beta}{2(d-c)^{\beta}}\left[\int_c^d(d-y)^{\beta-1}\Phi(b,y)\,dy\right.\\
&\left.+\int_c^d(y-c)^{\beta-1}\Phi(b,y)\,dy\right]\\
\leq\ &\frac{\Phi(b,c)+\Phi(b,d)}{2}.
\end{aligned}
$$

By addition, we get the last inequality in (11). □

**Remark 2.** *In Theorem 8, if we take $\alpha=\beta=1$, then the inequalities (11) become (5).*

## 3. Conclusion

In this paper, we established the Hermite-Hadamard-Fejer type inequalities for co-ordinated mappings related results to present new type of inequalities involving Riemann-Liouville integral operator. The results presented in this paper would provide generalizations of those given in earlier works. The findings of this study have several significant implications for future applications.

## References


[1] Alomari, M., Darus, M., Co-ordinated s-convex function in the first sense with some Hadamard-type inequalities, Int. J. Contemp. Math. Sciences, 3 (32),1557-1567 (2008).

[2] Alomari, M., Darus, M., On the Hadamard's inequality for log-convex functions on the coordinates, J. of Inequal. and Appl, Article ID 283147, 13 pages,(2009).

[3] Alomari, M., Darus, M., Fejer inequality for double integrals, Facta Universitatis (Nis) Ser. Math. Inform., 24 , 15-28(2009).

[4] Kilbas, A.A., Srivastava H.M., Trujillo, J.J., Theory and Applications of Fractional Differential Equations, North-Holland Mathematics Studies, 204, Elsevier Sci. B.V., Amsterdam, (2006).

[5] Belarbi, S., Dahmani, Z., On some new fractional integral inequalities, J. Ineq. Pure and Appl. Math., 10(3) , Art. 86, (2009).

[6] Dahmani, Z., New inequalities in fractional integrals, International Journal of Nonlinear Scinece, 9(4) , 493-497, (2010).

[7] Dahmani, Z., On Minkowski and Hermite-Hadamard integral inequalities via fractional integration, Ann. Funct. Anal. 1(1), 51-58, (2010).
[8] Dahmani, Z., Tabharit, L., Taf, S., Some fractional integral inequalities, Nonl. Sci. Lett. A, 1(2) , 155-160, (2010).
[9] Dahmani, Z., Tabharit, L., Taf, S., New generalizations of Grüss inequality usin Riemann-Liouville fractional integrals, Bull. Math. Anal. Appl., 2(3) , 93-99, (2010).
[10] Dragomir, S.S., On Hadamard's inequality for convex functions on the co-ordinates in arectangle from the plane, Taiwanese Journal of Mathematics, 4, 775-788, (2001).
[11] Fejér, L., Uberdie Fourierreihen, II, Math. Naturwise. Anz Ungar. Akad., Wiss, 24, 369-390(1906), (in Hungarian).
[12] Gorenflo, R., Mainardi, F., Fractional calculus: integral and differential equations of fractional order, Springer Verlag, Wien, 223-276, (1997).
[13] Hadamard, J., Etude sur les proprietes des fonctions entieres et en particulier d'une fonction considree par, Riemann, J. Math. Pures. et Appl. 58, 171–215,(1893).
[14] scan, I., Hermite-Hadamard-Fejer type inequalities for convex functions via fractional integrals, 2014, arXiv:1404.7722v1.
[15] Latif, M.A., Alomari, M., Hadamard-type inequalities for product two convex functions on the co-ordinetes, Int. Math. Forum, 4(47), 2327-2338,(2009).
[16] Latif, M.A., Alomari, M., On the Hadamard-type inequalities for h-convex functions on the co-ordinetes, Int. J. of Math. Analysis, 3(33), 1645-1656,(2009).
[17] Latif, M.A., Hussain, S., New inequalities of Ostrowski type for co-ordineted convex functions via fractional integrals, Journal of Fractional Calculus and Applications,Vol. 2, No. 9, pp. 1-15, (2012).
[18] Miller, S., Ross, B., An introduction to the fractional calculus and fractional differential equations, John Wiley & Sons, USA, p.2, (1993).
[19] Minculete, N., Mitroi, F-C.,Fejer-type inequalities, Aust. J. Math. Anal. Appl. 9, no. 1, Art. 12, 8pp,(2012).
[20] Özdemir, M.E., Set, E., Sarikaya, M.Z., New some Hadamard's type inequalities for co-ordinated m-convex and $(\alpha, m)$-convex functions, Hacettepe Journal of Mathematics and Statistics , 40(2), 219-229, (2011).
[21] Sarikaya, M.Z., On new Hermite Hadamard Fejér type integral inequalities, Stud. Univ. Babeş-Bolyai Math. 57 (3), 377–386, (2012).
[22] Sarikaya, M.Z., Set, E., Ozdemir M.E., Dragomir, S.S., New some Hadamard's type inequalities for co-ordinated convex functions, Tamsui Oxford Journal of Information and Mathematical Sciences, 28(2),137-152, (2012) .
[23] Sarikaya M.Z., Ogunmez, H., On new inequalities via Riemann-Liouville fractional integration, Abstract and Applied Analysis, Volume 2012, Article ID 428983, 10 pages, doi:10.1155/2012/428983.
[24] Sarikaya, M.Z., Set, E., Yaldiz, H., Basak, N., Hermite-Hadamard's inequalities for fractional integrals and related fractional inequalities, Mathematical and Computer Modelling, 57, 2403–2407,(2013).
[25] Sarikaya, M.Z., Ostrowski type inequalities involving the right Caputo fractional derivatives belong to $L_p$, Facta Universitatis, Series Mathematics and Informatics , Vol. 27 No 2, 191-197, (2012).
[26] Sarikaya, M.Z., Yaldiz, H., On weighted Montogomery identities for Riemann-Liouville fractional integrals, Konuralp Journal of Mathematics, Volume 1 No. 1 pp. 48-53, (2013).
[27] Sarikaya, M.Z., Yaldiz, H., On the Hadamard's type inequalities for $L$-Lipschitzian mapping, Konuralp Journal of Mathematics, Volume 1 No. 2 pp. 33–40 (2013).
[28] Sarikaya, M.Z., On the Hermite–Hadamard-type inequalities for co-ordinated convex function via fractional integrals, Integral Transforms and Special Functions, Vol. 25, No. 2, 134–147, (2014).

***Hatice YALDIZ*** *received her Ph.D. degree in Applied Mathematics in 2016 from Düzce University, Düzce, Turkey. She has been in Western Kentucky University as a visiting researcher in 2015. Her major research interests include inequalities, Fractional theory, Discrete analysis, Time scales.*

***Mehmet Zeki SARIKAYA*** *is a Professor at the Department of Mathematics in Düzce University, Düzce, Turkey. He received his Ph.D. degree in Applied Mathematics in 2007 from Afyon Kocatepe University, Afyon, Turkey. He is editor on the Konuralp Journal. He has a lot of awards. He has many research papers about the Theory of inequalities, Potential Theory, Integral equations and Transforms, Time-scales..*

***Zoubir DAHMANI*** *is Professor, Labo. Pure and Appl. Maths., Faculty of Exact Sciences and Informatics, UMAB, University of Mostaganem, Algeria. He received his Ph.D. of Mathematics, USTHB(Algeria ) and La ROCHELLEUniversity(France ), 2009. He has many research papers about the Evolution Equations, Inequality Theory, Fractional Differential Equations, Fixed Point Theory, Numerical Analysis, Probability Theory, Generalized Metric Spaces.*



An International Journal of Optimization and Control: Theories & Applications
ISSN:2146-0957 eISSN:2146-5703
Vol.7, No.2, pp.216-224 (2017)
http://doi.org/10.11121/ijocta.01.2017.00398

RESEARCH ARTICLE

# On some properties of generalized Fibonacci and Lucas polynomials

Sümeyra Uçar

*Department of Mathematics, Balıkesir University, Turkey*
*sumeyraucar@balikesir.edu.tr*

ARTICLE INFO

Article History:
*Received 05 October 2016*
*Accepted 16 June 2017*
*Available 17 July 2017*

Keywords:
*Generalized Fibonacci polynomials*
*Generalized Lucas polynomials*

AMS Classification 2010:
*11B39, 11C20*

ABSTRACT

In this paper we investigate some properties of generalized Fibonacci and Lucas polynomials. We give some new identities using matrices and Laplace expansion for the generalized Fibonacci and Lucas polynomials. Also, we introduce new families of tridiagonal matrices whose successive determinants generate any subsequence of these polynomials.



## 1. Introduction

In [16], $h(x)$-Fibonacci polynomials are defined by $F_{h,0}(x) = 0$, $F_{h,1}(x) = 1$ and $F_{h,n+1}(x) = h(x)F_{h,n}(x) + F_{h,n-1}(x)$ for $n \geq 1$. $h(x)$-Lucas polynomials are defined by $L_{h,0}(x) = 2$, $L_{h,1}(x) = h(x)$ and $L_{h,n+1}(x) = h(x)L_{h,n}(x)+L_{h,n-1}(x)$ for $n \geq 1$. Therefore some properties of these polynomials are presented in that paper.

Let $p(x)$ and $q(x)$ be polynomials with real coefficients, $p(x) \neq 0$, $q(x) \neq 0$ and $p^2(x)+4q(x) > 0$. In [9], it was defined generalized Fibonacci polynomials $F_{p,q,n}(x)$ as

$$F_{p,q,n+1}(x) = p(x)F_{p,q,n}(x) + q(x)F_{p,q,n-1}(x), \quad n \geq 1 \tag{1}$$

with initial values $F_{p,q,0}(x) = 0, F_{p,q,1}(x) = 1$ and generalized Lucas polynomials $L_{p,q,n}(x)$ as

$$L_{p,q,n+1}(x) = p(x)L_{p,q,n}(x) + q(x)L_{p,q,n-1}(x), \quad n \geq 1 \tag{2}$$

with the initial values $L_{p,q,0}(x) = 2, L_{p,q,1}(x) = p(x)$. In that paper, it was derived factorizations and representations of polynomial analogue of an arbitrary binary sequence by matrix methods. In [11], it was given factorizations of Pascal matrix involving $(p, q)-$Fibonacci polynomials. In [19], it was obtained some arithmetic and combinatorial identities for the $(p, q)-$Fibonacci and Lucas polynomials. In Section 2, we obtain some basic properties of generalized Fibonacci and Lucas polynomials. In Section 3, we give some properties of these polynomials using $2 \times 2$ matrices. In Section 4, we make the proof of two idenitites concerning generalized Fibonacci and Lucas polynomials using Laplace expansion of determinants. In Section 5, we give new families of tridiagonal matrices whose successive determinants generate any subsequence of the generalized Fibonacci and Lucas polynomials.

## 2. Generalized Fibonacci and Lucas polynomials

Let $p(x)$ and $q(x)$ be polynomials with real coefficients, $p(x) \neq 0$, $q(x) \neq 0$ and $p^2(x)+4q(x) > 0$. In this section, firstly we consider the generalized Fibonacci polynomials $F_{p,q,n}(x)$ defined in (1). The first six generalized Fibonacci polynomials are given in the following table :

$F_{p,q,1}(x) = 1$
$F_{p,q,2}(x) = p(x)$
$F_{p,q,3}(x) = p^2(x) + q(x)$
$F_{p,q,4}(x) = p^3(x) + 2p(x)q(x)$
$F_{p,q,5}(x) = p^4(x) + 3p^2(x)q(x) + q^2(x)$
$F_{p,q,6}(x) = p^5(x) + 4p^3(x)q(x) + 3p(x)q^2(x).$

For $p(x) = x$ and $q(x) = 1$ we have Catalan's Fibonacci polynomials $F_n(x)$; for $p(x) = 2x$ and $q(x) = 1$ we have Byrd's polynomials $\varphi_n(x)$; for $p(x) = k$ and $q(x) = t$ we have generalized Fibonacci numbers $U_n$ ; for $p(x) = k$ and $q(x) = 1$ we have $k$-Fibonacci numbers $F_{k,n}$; for $p(x) = q(x) = 1$ we have classical Fibonacci numbers $F_n$ (for more details see [2], [4], [8], [10], [18] and the references therein).

The generating function $g_{F,p,q}(t)$ of the generalized Fibonacci polynomials $F_{p,q,n}(x)$ is defined by

$$g_{F,p,q}(t) = \sum_{n=0}^{\infty} F_{p,q,n}(x)t^n. \tag{3}$$

From [11], we know that the generating function of the generalized Fibonacci polynomials $F_{p,q,n}(x)$ is

$$g_{F,p,q}(t) = \frac{t}{1 - tp(x) - t^2q(x)}. \tag{4}$$

**Theorem 1.** *Assume that $p(x)$ is an odd polynomial and $q(x)$ is an even polynomial. Then $F_{p,q,n}(-x) = (-1)^{n+1}F_{p,q,n}(x)$ for $n \geq 0$.*

***Proof.*** From (3), and (4), we have

$$\sum_{n=0}^{\infty} F_{p,q,n}(-x)(-t)^n = \frac{-t}{1 - tp(x) - t^2q(x)}$$

and

$$\begin{aligned}\sum_{n=0}^{\infty}(-1)^{n+1}F_{p,q,n}(-x)t^n &= \frac{t}{1 - tp(x) - t^2q(x)} \\ &= \sum_{n=0}^{\infty} F_{p,q,n}(x)t^n.\end{aligned}$$

Then the proof is follows.

□

Binet's formulas are well known among the Fibonacci numbers. Let $\alpha(x)$ and $\beta(x)$ be the roots of the characteristic equation

$$v^2 - vp(x) - q(x) = 0, \tag{5}$$

of the recurrence relation (1). From [9], we know that

$$F_{p,q,n}(x) = \frac{\alpha^n(x) - \beta^n(x)}{\alpha(x) - \beta(x)}, \text{ for } n \geq 0, \tag{6}$$

where

$$\left.\begin{aligned}\alpha(x) &= \tfrac{p(x)+\sqrt{p^2(x)+4q(x)}}{2}, \\ \beta(x) &= \tfrac{p(x)-\sqrt{p^2(x)+4q(x)}}{2}.\end{aligned}\right\} \tag{7}$$

Notice that $\alpha(x)+\beta(x) = p(x)$, $\alpha(x)\beta(x) = -q(x)$ and $\alpha(x) - \beta(x) = \sqrt{p^2(x) + 4q(x)}$.

**Theorem 2.** *For $n \geq 1$, we have*

$$\begin{aligned}&F_{p,q,n}(x) \\ &= 2^{1-n}\sum_{j=0}^{\lfloor \frac{n-1}{2} \rfloor} \binom{n}{2j+1} p^{n-2j-1}(x)(p^2(x) + 4q(x))^j.\end{aligned}$$

***Proof.*** From (7), we have

$$\begin{aligned}&\alpha^n(x) - \beta^n(x) = 2^{-n}[(p(x) + \sqrt{p^2(x) + 4q(x)})^n \\ &-(p(x) - \sqrt{p^2(x) + 4q(x)})^n] \\ &= 2^{-n}[\sum_{j=0}^{n} \binom{n}{j} p^{n-j}(x)(\sqrt{p^2(x) + 4q(x)})^j \\ &-\sum_{j=0}^{n} \binom{n}{j} p^{n-j}(x)(-\sqrt{p^2(x) + 4q(x)})^j] \\ &= 2^{-n+1}\sum_{j=0}^{\lfloor \frac{n-1}{2} \rfloor} \binom{n}{2j+1} p^{n-2j-1}(x)(\sqrt{p^2(x) + 4q(x)})^{2j+1}.\end{aligned}$$

From the equation (6), then we obtain

$$\begin{aligned}&F_{p,q,n}(x) = \tfrac{\alpha^n(x)-\beta^n(x)}{\alpha(x)-\beta(x)} = \tfrac{\alpha^n(x)-\beta^n(x)}{\sqrt{p^2(x)+4q(x)}} \\ &= 2^{-n+1}\sum_{j=0}^{\lfloor \frac{n-1}{2} \rfloor} \binom{n}{2j+1} p^{n-2j-1}(x)(p^2(x) + 4q(x))^j.\end{aligned}$$

□

In [12], definitions of Chebyshev polynomials of the first and second kinds are given by the followings (resp.)

$$T_n(x) = \cos n\theta \text{ and } H_n(x) = \frac{\sin[(n+1)\theta]}{\sin\theta},$$

where $x = \cos\theta$, $0 \leq \theta \leq \pi$.

We know that the generating functions of Chebyshev polynomials of the first and second kinds are

$$\sum_{n=0}^{\infty} T_n(t)\, z^n = \frac{1 - tz}{1 - 2tz + z^2}$$

and

$$\sum_{n=0}^{\infty} H_n(t)\, z^n = \frac{1}{1-2tz+z^2},$$

respectively. Also we can write Chebyshev polynomials of the first and second kinds as follows:

$$T_n(t) = \frac{n}{2}\sum_{j=0}^{\lfloor \frac{n}{2} \rfloor} \frac{(-1)^j}{n-j} \left( \begin{array}{c} n-j \\ j \end{array} \right) (2t)^{n-2j}$$

with $T_0(t) = 1$ and

$$H_n(t) = \sum_{j=0}^{\lfloor \frac{n}{2} \rfloor} (-1)^j \left( \begin{array}{c} n-j \\ j \end{array} \right) (2t)^{n-2j}$$

with $H_0(t) = 1$ (for more details one can see [3], [13] and [17]).

**Theorem 3.** *For $n \geq 1$, we have*

$$F_{p,q,n}(x) = i^{n-1} q(x)^{\frac{n-1}{2}} H_{n-1}\left( \frac{p(x)}{2i\sqrt{q(x)}} \right),$$

*where $i^2 = -1$ and*

$$H_n(t) = \sum_{j=0}^{\lfloor \frac{n}{2} \rfloor} (-1)^j \left( \begin{array}{c} n-j \\ j \end{array} \right) (2t)^{n-2j}$$

*with $H_0(t) = 1$ is the Chebyshev polynomial of the second kind.*

***Proof.*** We know that the generating function for the second kind Chebyshev polynomial $H_n(t)$ is

$$\sum_{n=0}^{\infty} H_n(t) z^n = \frac{1}{1-2tz+z^2}.$$

Let $z = iy\sqrt{q(x)}$ and $t = \frac{p(x)}{2i\sqrt{q(x)}}$. Then we get

$$\begin{array}{l} \sum\limits_{n=0}^{\infty} i^n y^n q(x)^{\frac{n}{2}} H_n\left( \frac{p(x)}{2i\sqrt{q(x)}} \right) \\ = \frac{1}{1-yp(x)-y^2q(x)} \end{array}$$

or

$$\begin{array}{l} \sum\limits_{n=0}^{\infty} i^n y^{n+1} q(x)^{\frac{n}{2}} H_n\left( \frac{p(x)}{2i\sqrt{q(x)}} \right) \\ = \frac{y}{1-yp(x)-y^2q(x)}. \end{array}$$

From the equation (4), we find

$$F_{p,q,n}(x) = i^{n-1} q(x)^{\frac{n-1}{2}} H_{n-1}\left( \frac{p(x)}{2i\sqrt{q(x)}} \right).$$

□

Now, we consider the generalized Lucas polynomials $L_{p,q,n}(x)$ defined in (2). The first six generalized Lucas polynomials are given in the following table :

$$\begin{array}{l} L_{p,q,1}(x) = p(x) \\ L_{p,q,2}(x) = p^2(x) + 2q(x) \\ L_{p,q,3}(x) = p^3(x) + 3p(x)q(x) \\ L_{p,q,4}(x) = p^4(x) + 4p^2(x)q(x) + 2q^2(x) \\ L_{p,q,5}(x) = p^5(x) + 5p^3(x)q(x) + 5p(x)q^2(x) \\ L_{p,q,6}(x) = p^6(x) + 6p^4(x)q(x) \\ \qquad\qquad + 9p^2(x)q^2(x) + 2q^3(x). \end{array}$$

For $p(x) = x$ and $q(x) = 1$ we have Lucas polynomials $L_n(x)$; for $p(x) = k$ and $q(x) = t$ we have generalized Lucas numbers $V_n$; for $p(x) = k$ and $q(x) = 1$ we have $k$-Lucas numbers $L_{k,n}$; for $p(x) = q(x) = 1$ we have classical Lucas numbers $L_n$ (for more details see [5], [7], [10], [18] and the references therein).

The generating function $g_{L,p,q}(t)$ of the Lucas polynomials $L_{p,q,n}(x)$ is defined by

$$g_{L,p,q}(t) = \sum_{n=0}^{\infty} L_{p,q,n}(x) t^n.$$

From [11], we know that the generating function of the generalized Lucas polynomials $L_{p,q,n}(x)$ is

$$g_{L,p,q}(t) = \frac{2 - tp(x)}{1 - tp(x) - t^2 q(x)}. \tag{8}$$

**Theorem 4.** *Assume that $p(x)$ is an odd polynomial and $q(x)$ is an even polynomial. Then we have*

$$L_{p,q,n}(-x) = (-1)^n L_{p,q,n}(x), \text{ for } n \geq 0.$$

***Proof.*** Using the equation (8), the proof is clear. □

From [9], we know that Binet's formula for $L_{p,q,n}(x)$ is

$$L_{p,q,n}(x) = \alpha^n(x) + \beta^n(x) \text{ for } n \geq 0,$$

where $\alpha(x)$ and $\beta(x)$ are the roots of the characteristic equation (5). Using Binet formulas for the generalized Fibonacci and Lucas polynomials, we obtain the following corollaries.

**Corollary 1.** *For $n \geq 0$, we have*

$$L_{p,q,n}(x) = p(x) F_{p,q,n}(x) + 2q(x) F_{p,q,n-1}(x). \tag{9}$$

**Corollary 2.** *For $n \geq 0$, we have*

$$\alpha^n(x) = \frac{L_{p,q,n}(x) + \sqrt{p^2(x)+4q(x)}F_{p,q,n}(x)}{2}$$

*and*

$$\beta^n(x) = \frac{L_{p,q,n}(x) - \sqrt{p^2(x)+4q(x)}F_{p,q,n}(x)}{2}.$$

**Corollary 3.** *For $n \geq 0$, we have*

$$L^2_{p,q,n}(x) - (p^2(x)+4q(x))F^2_{p,q,n}(x) = 4q(x)(-1)^n.$$

**Corollary 4.** *For $n \geq 0$, we have*

$$F_{p,q,2n}(x) = F_{p,q,n}(x)L_{p,q,n}(x).$$

As similar to Theorem 3, we can give the following theorem giving the relation between $L_{p,q,n}(x)$ and $T_n(x)$. Since its proof is similar to that of Theorem 3, we omit it.

**Theorem 5.** *For $n \geq 0$, we have*

$$L_{p,q,n}(x) = 2i^n q(x)^{\frac{n}{2}} T_n\left(\frac{p(x)}{2i\sqrt{q(x)}}\right),$$

*where $i^2 = -1$ and*

$$T_n(t) = \frac{n}{2}\sum_{j=0}^{\lfloor \frac{n}{2} \rfloor} \frac{(-1)^j}{n-j}\binom{n-j}{j}(2t)^{n-2j}$$

*with $T_0(t) = 1$ is the Chebyshev polynomial of the first kind.*

## 3. Some new identities for generalized Fibonacci and Lucas polynomials

In [19], it was defined generalized Fibonacci and Lucas polynomials with negative subscript of the following form:

$$\left.\begin{aligned} F_{p,q,-n}(x) &= \tfrac{-F_{p,q,n}(x)}{(-q(x))^n}, \\ L_{p,q,-n}(x) &= \tfrac{L_{p,q,n}(x)}{(-q(x))^n}. \end{aligned}\right\} \qquad (10)$$

In this section we find some identities using the following $2\times 2$ matrices

$$A = \begin{bmatrix} p(x) & q(x) \\ 1 & 0 \end{bmatrix} \text{ and } B = \begin{bmatrix} 0 & 1 \\ q(x) & p(x) \end{bmatrix}.$$

Indeed the above matrices satisfy $X^2 = p(x)X + q(x)I$. We obtain some new identities using $2\times 2$ matrices of the form

$$X^2 = p(x)X + q(x)I. \qquad (11)$$

In the following theorems we use the proof methods like as [18].

**Theorem 6.** *If $X$ is a square matrix of the form $X^2 = p(x)X + q(x)I$, then we have*

$$X^n = F_{p,q,n}(x)X + q(x)F_{p,q,n-1}(x)I,$$

*for any integer $n$.*

***Proof.*** It can be easily seen that $X^n = F_{p,q,n}(x)X + q(x)F_{p,q,n-1}(x)I$ for every $n \in N$ using mathematical induction. Now we show that $X^{-n} = F_{p,q,-n}(x)X + q(x)F_{p,q,-n-1}(x)I$ for every $n \in N$. Let $K = p(x)I - X$, then we have

$$\begin{aligned} K^2 &= (p(x)I - X)^2 \\ &= p^2(x)I - p(x)X + q(x)I \\ &= p(x)K + q(x)I. \end{aligned}$$

So we get $K^n = F_{p,q,n}(x)K + q(x)F_{p,q,n-1}(x)I$. Then

$$\begin{aligned} &(-q(x))^n X^{-n} = K^n \\ &= F_{p,q,n}(x)K + q(x)F_{p,q,n-1}(x)I \\ &= F_{p,q,n}(x)\,(p(x)I - X) \\ &+ q(x)F_{p,q,n-1}(x)I \\ &= F_{p,q,n+1}(x)I - F_{p,q,n}(x)X. \end{aligned}$$

Thus using the equation (10), we find

$$X^{-n} = \frac{-F_{p,q,n}(x)X}{(-q(x))^n} + \frac{F_{p,q,n+1}(x)I}{(-q(x))^n}$$

and

$$X^{-n} = F_{p,q,-n}(x)X + q(x)F_{p,q,-n-1}(x)I.$$

□

**Theorem 7.** *Let $X$ be an arbitrary $2\times 2$ matrix. Then $X^2 = p(x)X + q(x)I$ if and only if $X$ is of the form*

$$X = \begin{bmatrix} a & b \\ c & p(x)-a \end{bmatrix}, \text{ with } detX = -q(x)$$

*or $X = \delta I$ where $\delta \in \{\alpha(x), \beta(x)\}$, $\alpha(x) = \frac{p(x)+\sqrt{p^2(x)+4q(x)}}{2}$ and $\beta(x) = \frac{p(x)-\sqrt{p^2(x)+4q(x)}}{2}$.*

***Proof.*** Assume that $X^2 = p(x)X + q(x)I$. Then the minimal polynomial of $X$ must divide $\lambda^2 - \lambda p(x) - q(x)$. So it must be $\lambda - \alpha(x)$, $\lambda - \beta(x)$ or $\lambda^2 - \lambda p(x) - q(x)$. In the first case $X = \alpha(x)I$, in the second case $X = \beta(x)I$ and in the third case characteristic polynomial of $X$ should be $\lambda^2 - \lambda p(x) - q(x)$ because $X$ is a $2 \times 2$ matrix. Clearly, its trace is $p(x)$ and its determinant is $-q(x)$. The rest of the proof can be similarly completed. □

**Corollary 5.** *If* $X = \begin{bmatrix} a & b \\ c & p(x) - a \end{bmatrix}$ *is a matrix with* $detX = -q(x)$*, then we have* $X^n = \begin{bmatrix} aF_{p,q,n}(x) + q(x)F_{p,q,n-1}(x) & bF_{p,q,n}(x) \\ cF_{p,q,n}(x) & F_{p,q,n+1}(x) - aF_{p,q,n}(x) \end{bmatrix}$.

***Proof.*** From Theorem 7, we know that $X^2 = p(x)X + q(x)I$. Then, from Theorem 6 we get $X^n = F_{p,q,n}(x)X + q(x)F_{p,q,n-1}(x)I$ for any integer $n$. Then the proof follows. □

**Corollary 6.** *Let* $S = \begin{bmatrix} \frac{p(x)}{2} & \frac{p^2(x)+4q(x)}{2} \\ \frac{1}{2} & \frac{p(x)}{2} \end{bmatrix}$, *then we have*

$$S^n = \begin{bmatrix} \frac{L_{p,q,n}(x)}{2} & \frac{\left(p^2(x)+4q(x)\right)F_{p,q,n}(x)}{2} \\ \frac{F_{p,q,n}(x)}{2} & \frac{L_{p,q,n}(x)}{2} \end{bmatrix}.$$

***Proof.*** Since $S^2 = p(x)S + q(x)I$ , the proof is completed by using Corollary 5. □

## 4. Generalized Fibonacci and Lucas polynomials with Laplace expansion

In [6], it was given some identities about Fibonacci numbers using Laplace expansion. In this section we give two theorems about generalized Fibonacci and Lucas polynomials and prove them using Laplace expansion of determinants.

Let us consider the $n \times n$ tridiagonal matrix $C(n)$ defined by the following form:

$$C(n) = \begin{pmatrix} p(x) & i\sqrt{q(x)} & & & & \\ i\sqrt{q(x)} & p(x) & i\sqrt{q(x)} & & & \\ & i\sqrt{q(x)} & p(x) & . & & \\ & & & . & . & . \\ & & & . & . & i\sqrt{q(x)} \\ & & & & i\sqrt{q(x)} & p(x) \end{pmatrix}.$$

**Theorem 8.** *For any integer* $k$ $(2 \le k \le n-1)$*, we have*

$$F_{p,q,n}(x) = F_{p,q,k}(x)F_{p,q,n-k+1}(x) + q(x)F_{p,q,k-1}(x)F_{p,q,n-k}(x). \quad (12)$$

***Proof.*** From $k = 2$ to $k = n-1$, the equation (12) becomes the followings:

$$\begin{aligned} F_{p,q,n}(x) &= F_{p,q,2}(x)F_{p,q,n-1}(x) \\ &\quad + q(x)F_{p,q,1}(x)F_{p,q,n-2}(x), \\ F_{p,q,n}(x) &= F_{p,q,3}(x)F_{p,q,n-2}(x) \\ &\quad + q(x)F_{p,q,2}(x)F_{p,q,n-3}(x), \\ &\quad \cdots \\ F_{p,q,n}(x) &= F_{p,q,n-2}(x)F_{p,q,3}(x) \\ &\quad + q(x)F_{p,q,n-3}(x)F_{p,q,2}(x), \\ F_{p,q,n}(x) &= F_{p,q,n-1}(x)F_{p,q,2}(x) \\ &\quad + q(x)F_{p,q,n-2}(x)F_{p,q,1}(x). \end{aligned}$$

It can be easily seen that $F_{p,q,n}(x) = |C(n-1)|$ for $n \ge 2$. Using Lemma 1 in [1] we get

$$\begin{aligned} &|C(n-1)| \\ &= p(x)\,|C(n-2)| + q(x)\,|C(n-3)| \\ &= p(x)F_{p,q,n-1}(x) + q(x)F_{p,q,n-2}(x) \\ &= F_{p,q,2}(x)F_{p,q,n-1}(x) + q(x)F_{p,q,n-2}(x) \end{aligned}$$

Then we find

$$F_{p,q,n}(x) = F_{p,q,2}(x)F_{p,q,n-1}(x) + q(x)F_{p,q,n-2}(x)$$

Now we use the techniques in [14] to find the determinant of the matrix $C(n-1)$. If we choose the first two rows of $C(n-1)$, there are only three $2\times2$ submatrices of $C(n-1)$ whoose determinants are not equal to zero.

$$\begin{aligned} C([1,2],[1,2]) &= \begin{vmatrix} p(x) & i\sqrt{q(x)} \\ i\sqrt{q(x)} & p(x) \end{vmatrix} \\ &= |C(2)| = F_{p,q,3}(x), \\ C([1,2],[1,3]) &= \begin{vmatrix} p(x) & 0 \\ i\sqrt{q(x)} & i\sqrt{q(x)} \end{vmatrix} \\ &= ip(x)\sqrt{q(x)}, \\ C([1,2],[2,3]) &= \begin{vmatrix} i\sqrt{q(x)} & 0 \\ p(x) & i\sqrt{q(x)} \end{vmatrix} \\ &= -q(x). \end{aligned}$$

Their corresponding cofactors are

$$\begin{aligned} &\widetilde{C}([1,2],[1,2]) = (-1)^{1+2+1+2}\,|C(n-3)| \\ &= F_{p,q,n-2}(x), \\ &\widetilde{C}([1,2],[1,3]) = (-1)^{1+2+1+3}i\sqrt{q(x)}\,|C(n-4)| \\ &= -i\sqrt{q(x)}F_{p,q,n-3}(x), \\ &\widetilde{C}([1,2],[2,3]) = 0. \end{aligned}$$

By the Laplace expansion in [14], we have

$$\begin{aligned}
&F_{p,q,n}(x) = |C(n-1)| \\
&= C([1,2],[1,2])\widetilde{C}([1,2],[1,2]) \\
&+C([1,2],[1,3])\widetilde{C}([1,2],[1,3]) \\
&+C([1,2],[2,3])\widetilde{C}([1,2],[2,3]) \\
&= |C(2)|\, F_{p,q,n-2}(x) + p(x)i\sqrt{q(x)} \\
&(-i\sqrt{q(x)})F_{p,q,n-3}(x) + (-q(x)).0 \\
&= F_{p,q,3}(x)F_{p,q,n-2}(x) \\
&+p(x)q(x)F_{p,q,n-3}(x).
\end{aligned}$$

Then we get

$$\begin{aligned}
F_{p,q,n}(x) = F_{p,q,3}(x)F_{p,q,n-2}(x) \\
+ q(x)F_{p,q,2}(x)F_{p,q,n-3}(x).
\end{aligned}$$

If we choose the first three rows of $C(n-1)$, there are only four $3\times 3$ submatrices of $C(n-1)$ whoose determinants are not equal to zero.

$$\begin{aligned}
&C([1,2,3],[1,2,3]) = \begin{vmatrix} p(x) & i\sqrt{q(x)} & 0 \\ i\sqrt{q(x)} & p(x) & i\sqrt{q(x)} \\ 0 & i\sqrt{q(x)} & p(x) \end{vmatrix} \\
&= |C(3)| = F_{p,q,4}(x), \\
&C([1,2,3],[1,2,4]) = \begin{vmatrix} p(x) & i\sqrt{q(x)} & 0 \\ i\sqrt{q(x)} & p(x) & 0 \\ 0 & i\sqrt{q(x)} & i\sqrt{q(x)} \end{vmatrix} \\
&= i\sqrt{q(x)}\,|C(2)| = i\sqrt{q(x)}F_{p,q,3}(x), \\
&C([1,2,3],[1,3,4]) = \begin{vmatrix} p(x) & 0 & 0 \\ i\sqrt{q(x)} & i\sqrt{q(x)} & 0 \\ 0 & p(x) & i\sqrt{q(x)} \end{vmatrix} \\
&= -p(x)q(x), \\
&C([1,2,3],[2,3,4]) = \begin{vmatrix} i\sqrt{q(x)} & 0 & 0 \\ p(x) & i\sqrt{q(x)} & 0 \\ i\sqrt{q(x)} & p(x) & i\sqrt{q(x)} \end{vmatrix} \\
&= -i\sqrt{q(x)}q(x).
\end{aligned}$$

Their corresponding cofactors are

$$\begin{aligned}
&\widetilde{C}([1,2,3],[1,2,3]) = (-1)^{6+6}\,|C(n-4)| \\
&= F_{p,q,n-3}(x), \\
&\widetilde{C}([1,2,3],[1,2,4]) = (-1)^{6+7}i\sqrt{q(x)}\,|C(n-5)| \\
&= -i\sqrt{q(x)}F_{p,q,n-4}(x), \\
&\widetilde{C}([1,2,3],[1,3,4]) = 0, \\
&\widetilde{C}([1,2,3],[2,3,4]) = 0.
\end{aligned}$$

By the Laplace expansion in [14], we have

$$\begin{aligned}
&F_{p,q,n}(x) = |C(n-1)| \\
&= C([1,2,3],[1,2,3])\widetilde{C}([1,2,3],[1,2,3]) \\
&+C([1,2,3],[1,2,4])\widetilde{C}([1,2,3],[1,2,4]) \\
&+C([1,2,3],[1,3,4])\widetilde{C}([1,2,3],[1,3,4]) \\
&+C([1,2,3],[2,3,4])\widetilde{C}([1,2,3],[2,3,4]) \\
&= F_{p,q,4}(x)F_{p,q,n-3}(x) \\
&+i\sqrt{q(x)}F_{p,q,3}(x)(-i)\sqrt{q(x)}F_{p,q,n-4}(x).
\end{aligned}$$

Then we get

$$\begin{aligned}
F_{p,q,n}(x) = F_{p,q,4}(x)F_{p,q,n-3}(x) \\
+ q(x)F_{p,q,3}(x)F_{p,q,n-4}(x).
\end{aligned}$$

By the mathematical induction, we prove the other identities in the equation (12). □

Let $D(n)$ be the $n \times n$ tridioganal matrix given of the following form:

$$D(n) = \begin{pmatrix} \frac{p(x)}{2} & i\sqrt{q(x)} & & & & \\ i\sqrt{q(x)} & p(x) & i\sqrt{q(x)} & & & \\ & i\sqrt{q(x)} & p(x) & . & & \\ & & . & . & . & \\ & & & . & . & i\sqrt{q(x)} \\ & & & & i\sqrt{q(x)} & p(x) \end{pmatrix}$$

**Theorem 9.** *For any integer $k$ $(1 \le k \le n-1)$, we have*

$$\begin{aligned}
L_{p,q,n}(x) = L_{p,q,k}(x)F_{p,q,n-k+1}(x) \\
+ q(x)L_{p,q,k-1}(x)F_{p,q,n-k}(x). \qquad (13)
\end{aligned}$$

***Proof.*** From $k = 1$ to $k = n-1$, the equation (13) becomes the followings:

$$\begin{aligned}
L_{p,q,n}(x) &= L_{p,q,1}(x)F_{p,q,n}(x) \\
&\quad + q(x)L_{p,q,0}(x)F_{p,q,n-1}(x), \\
L_{p,q,n}(x) &= L_{p,q,2}(x)F_{p,q,n-1}(x) \\
&\quad + q(x)L_{p,q,1}(x)F_{p,q,n-2}(x), \\
&\quad \cdots \\
L_{p,q,n}(x) &= L_{p,q,n-2}(x)F_{p,q,3}(x) \\
&\quad + q(x)L_{p,q,n-3}(x)F_{p,q,2}(x), \\
L_{p,q,n}(x) &= L_{p,q,n-1}(x)F_{p,q,2}(x) \\
&\quad + q(x)L_{p,q,n-2}(x)F_{p,q,1}(x).
\end{aligned}$$

It is clear that $L_{p,q,n}(x) = 2\,|D(n)|$, for $n \ge 1$. From the Corollary 1, we have $L_{p,q,n}(x) = p(x)F_{p,q,n}(x) + 2q(x)F_{p,q,n-1}(x)$. Then we get

$$\begin{aligned}
L_{p,q,n}(x) = L_{p,q,1}(x)F_{p,q,n}(x) \\
+ q(x)L_{p,q,0}(x)F_{p,q,n-1}(x).
\end{aligned}$$

The rest of the proof can be completed similar to the proof of the Theorem 8. □

In [19], for $m = 0$ in the equation (3.9) coincides with our Theorem 9 for $k = n - 1$.

## 5. Generalized Fibonacci and generalized Lucas polynomials subsequences

In this section we obtain another applications of Lemma 1 in [1]. We generalize the family of tridiagonal matrices to a subsequence of generalized Fibonacci (resp. generalized Lucas) polynomials which is a family of tridiagonal matrices whose successive determinants are given by that polynomials. To do this, we use the following identities. For $n \geq 1$ we have

$$F_{p,q,m+n}(x) = L_{p,q,n}(x)F_{p,q,m}(x) + (-1)^{n+1}q^n(x)F_{p,q,m-n}(x) \tag{14}$$

and

$$L_{p,q,m+n}(x) = L_{p,q,n}(x)L_{p,q,m}(x) + (-1)^{n+1}q^n(x)L_{p,q,m-n}(x). \tag{15}$$

These identities was proved in [15] for $p(x) = k$ and $q(x) = 1$. We give the following theorems using the proof methods given in [1].

**Theorem 10.** *Let $M_{\alpha,\beta}(n), n = 1, 2, ...$ be the family of symmetric tridiagonal matrices whose elements satisfy following conditions* :

$$\begin{array}{l} m_{1,1} = F_{p,q,\alpha+\beta}(x), \\ m_{2,2} = \left\lceil \frac{F_{p,q,2\alpha+\beta}(x)}{F_{p,q,\alpha+\beta}(x)} \right\rceil, \\ m_{1,2} = m_{2,1} \\ = \sqrt{m_{2,2}F_{p,q,\alpha+\beta}(x) - F_{p,q,2\alpha+\beta}(x)}, \\ m_{j,j+1} = m_{j+1,j} = \\ \sqrt{(-1)^{\alpha}q^{\alpha}(x)},\ 2 \leq j \leq 3, \\ m_{j,j} = L_{p,q,\alpha}(x),\ 3 \leq j \leq k, \end{array}$$

*with $\alpha \in \mathbb{Z}^+$ and $\beta \in \mathbb{N}$. The successive determinants of this family of matrices is*

$$|M_{\alpha,\beta}(n)| = F_{p,q,\alpha n+\beta}(x).$$

***Proof.*** We use the principle of mathematical induction. We have

$$|M_{\alpha,\beta}(1)| = \det F_{p,q,\alpha+\beta}(x) = F_{p,q,\alpha+\beta}(x)$$

and

$$\begin{array}{l} |M_{\alpha,\beta}(2)| \\ = \begin{vmatrix} F_{p,q,\alpha+\beta}(x) & \sqrt{m_{2,2}F_{p,q,\alpha+\beta}(x) - F_{p,q,2\alpha+\beta}(x)} \\ \sqrt{m_{2,2}F_{p,q,\alpha+\beta}(x) - F_{p,q,2\alpha+\beta}(x)} & \left\lceil \frac{F_{p,q,2\alpha+\beta}(x)}{F_{,p,q,\alpha+\beta}(x)} \right\rceil \end{vmatrix} \\ = F_{p,q,2\alpha+\beta}(x). \end{array}$$

Now we assume that $|M_{\alpha,\beta}(n)| = F_{p,q,\alpha n+\beta}(x)$ for $1 \leq k \leq n$. Then by Lemma 1 in [1] and (14) we have

$$\begin{array}{l} M_{\alpha,\beta}(n+1) \\ = m_{n,n}\left|M_{\alpha,\beta}(n)\right| - m_{n,n-1}m_{n-1,n}\left|M_{\alpha,\beta}(n-1)\right| \\ = L_{p,q,\alpha}(x)\left|M_{\alpha,\beta}(n)\right| - (-1)^{\alpha}q^{\alpha}(x)\left|M_{\alpha,\beta}(n-1)\right| \\ = L_{p,q,\alpha}(x)F_{p,q,\alpha n+\beta}(x) + (-1)^{\alpha+1}q^{\alpha}(x)F_{p,q,\alpha n+\beta-\alpha}(x). \end{array}$$

Using the equation (14), we get

$$\begin{array}{rl} M_{\alpha,\beta}(n+1) &= F_{p,q,\alpha+\alpha n+\beta}(x) \\ &= F_{p,q,\alpha(n+1)+\beta}(x). \end{array}$$

□

**Theorem 11.** *Let $R_{\alpha,\beta}(n), n = 1, 2, ...$ be the family of symmetric tridiagonal matrices whose elements satisfy the following conditions* :

$$\begin{array}{l} r_{1,1} = L_{p,q,\alpha+\beta}(x), \\ r_{2,2} = \left\lceil \frac{L_{p,q,2\alpha+\beta}(x)}{L_{p,q,\alpha+\beta}(x)} \right\rceil, \\ r_{1,2} = r_{2,1} \\ = \sqrt{r_{2,2}L_{p,q,\alpha+\beta}(x) - L_{p,q,2\alpha+\beta}(x)}, \\ r_{j,j+1} = r_{j+1,j} \\ = \sqrt{(-1)^{\alpha}q^{\alpha}(x)},\ 2 \leq j \leq 3, \\ r_{j,j} = L_{p,q,\alpha}(x),\ 3 \leq j \leq k, \end{array}$$

*with $\alpha \in \mathbb{Z}^+$ and $\beta \in \mathbb{N}$. The successive determinants of this family of matrices is*

$$|R_{\alpha,\beta}(n)| = L_{p,q,\alpha n+\beta}(x).$$

***Proof.*** We use the principle of mathematical induction. We have

$$|R_{\alpha,\beta}(1)| = \det L_{p,q,\alpha+\beta}(x) = L_{p,q,\alpha+\beta}(x)$$

and

$$\begin{array}{l} |R_{\alpha,\beta}(2)| \\ = \begin{vmatrix} L_{p,q,\alpha+\beta}(x) & \sqrt{m_{2,2}L_{p,q,\alpha+\beta}(x) - L_{p,q,2\alpha+\beta}(x)} \\ \sqrt{m_{2,2}L_{p,q,\alpha+\beta}(x) - L_{p,q,2\alpha+\beta}(x)} & \left\lceil \frac{L_{p,q,2\alpha+\beta}(x)}{L_{,p,q,\alpha+\beta}(x)} \right\rceil \end{vmatrix} \\ = L_{p,q,2\alpha+\beta}(x). \end{array}$$

Now we assume that $|R_{\alpha,\beta}(n)| = L_{p,q,\alpha n+\beta}(x)$ for $1 \leq k \leq n$. Then by Lemma 1 in [1] and (15) we find

$$\begin{aligned}
&R_{\alpha,\beta}(n+1)\\
&= r_{n,n}\left|R_{\alpha,\beta}(n)\right| - r_{n,n-1}r_{n-1,n}\left|R_{\alpha,\beta}(n-1)\right|\\
&= L_{p,q,\alpha}(x)\left|R_{\alpha,\beta}(n)\right| - (-1)^{\alpha}q^{\alpha}(x)\left|R_{\alpha,\beta}(n-1)\right|\\
&= L_{p,q,\alpha}(x)L_{p,q,\alpha n+\beta}(x)\\
&+(-1)^{\alpha+1}q^{\alpha}(x)L_{p,q,\alpha(n-1)+\beta}(x).
\end{aligned}$$

Using the equation (15), we get

$$\begin{aligned}
R_{\alpha,\beta}(n+1) &= L_{p,q,\alpha+\alpha n+\beta}(x)\\
&= L_{p,q,\alpha(n+1)+\beta}(x).
\end{aligned}$$

□

As a consequence of Theorem 10 and Theorem 11, we establish new families of tridiagonal matrices whose successive determinants generate any subsequence of the generalized Fibonacci and generalized Lucas polynomials. For example, we have

$$F_{p,q,4n-2}(x) = \begin{pmatrix}
p(x) & 0 & 0 & & & & \\
0 & p^4(x)+4p^2(x)q(x)+3q^2(x) & q^2(x) & & & & \\
0 & q^2(x) & p^4(x)+4p^2(x)q(x)+2q^2(x) & . & & & \\
 & & . & . & . & & \\
 & & & . & . & q^2(x) & \\
 & & & & q^2(x) & p^4(x)+4p^2(x)q(x)+2q^2(x)
\end{pmatrix}$$

and

$$L_{p,q,4n-2}(x) = \begin{pmatrix}
p^2(x)+2q(x) & 0 & 0 & & & & \\
0 & p^4(x)+4p^2(x)q(x)+q^2(x) & q^2(x) & & & & \\
0 & q^2(x) & p^4(x)+4p^2(x)q(x)+2q^2(x) & . & & & \\
 & & . & . & . & & \\
 & & & . & . & q^2(x) & \\
 & & & & q^2(x) & p^4(x)+4p^2(x)q(x)+2q^2(x)
\end{pmatrix}.$$

## 6. Conclusion

In this study we give some new properties of generalized Fibonacci and Lucas polynomials using matrices, complex numbers and Chebyshev polynomials. Our results generalize some known results in the literature.

## References


[1] Cahill, N. D., D'Errico, J. R., Spence, J. S., Complex factorizations of the Fibonacci and Lucas numbers. Fibonacci Quart., 41, 1, 13-19, (2003).

[2] Catarino, P., On some idenitities for $k$-Fibonacci sequence. Int. J. Contemp. Math. Sciences, 9, 1, 37-42, (2014).

[3] Doman, B. G. S., Generating functions for Chebyshev polynomials. Int. J. Pure Appl. Math. 63, 2, 197-205, (2010).

[4] Falcon, S., Plaza, A., On the Fibonacci $k$-numbers. Chaos Solitons Fractals. 32, 5, 1615-1624, (2007).

[5] Falcon, S., On the $k$-Lucas numbers. Int. J. Contemp. Math. Sci. 6, 21-24, 1039-1050, (2011).

[6] Feng, J., Fibonacci identities via the determinant of tridiagonal matrix. Appl. Math. Comput. 217, 12, 5978-5981, (2011).

[7] Godase, A. D., Dhakne, M. B., On the properties of $k$-Fibonacci and $k$-Lucas numbers. Int. J. Adv. Appl. Math. Mech. 2, 1, 100-106, (2014).

[8] Kalman, D., Mena, R., The Fibonacci Numbers-Exposed. Math. Mag. 76, 3, 167-181, (2003).

[9] Kılıç, E., Stanica, P., Factorizations and representations of binary polynomial recurrences by matrix methods. Rocky Mountain J. Math. 41, 4, 1247-1264, (2011).

[10] Koshy, T., Fibonacci and Lucas numbers with applications. Pure and Applied Mathematics (New York). Wiley-Interscience, New York, (2001).

[11] Lee, G. Y., Asci, M. Some properties of the $(p,q)-$ Fibonacci and $(p,q)-$ Lucas polynomials. J. Appl. Math., (2012).

[12] Mason, J. C., Chebyshev polynomials of the second, third and fourth kinds in approximation, indefinite integration and integral transforms. Proceedings of the Seventh Spanish Symposium on Orthogonal Polynomials and Applications (VII SPOA) (Granada, 1991). J. Comput. Appl. Math. 49, 1-3, 169-178, (1993).

[13] Mason, J. C., Handscomb, D. C., Chebyshev polynomials. Chapman&Hall/CRC, Boca Raton, FL, 2003. xiv+341 pp.

[14] Meyer, C., Matrix analysis and applied linear algebra, With 1 CD-ROM (Windows, Macintosh and UNIX) and a solutions manual (iv+171 pp.). Society for Industrial and Applied Mathematics (SIAM), Philadelphia, PA, (2000). xii+718 pp.

[15] Özgür, N. Y., Uçar, S., Öztunç, Ö. Complex Factorizations of the $k$-Fibonacci and $k$-Lucas numbers. An. Ştiinţ. Univ. Al. I. Cuza Iaşi. Mat. (N.S.) 62, 1, 13-20, (2016).

[16] Nalli, A., Haukkanen, P., On generalized Fibonacci and Lucas polynomials. Chaos Solitons Fractals 42, 5, 3179-3186, (2009).

[17] Rivlin, J. T., The Chebyshev polynomials. Pure and Applied Mathematics, Wiley-Interscience [John Wiley&Sons], New York-London-Sdyney, (1974). vi+186 pp.

[18] Şiar, Z., Keskin, R., Some new identites concerning Generalized Fibonacci and Lucas Numbers. Hacet. J. Math. Stat. 42, 3, 211-222, (2013).

[19] Wang, J., Some new results for the $(p,q)-$ Fibonacci and Lucas polynomials. Adv Differ Equ. 64, (2014).

***Sümeyra Uçar*** *received the Ph.D degree in Mathematics from the Balıkesir University in Turkey, in 2015. She is currently Research Asisstant at the Department of Mathematics in Balıkesir University. Her research areas are Möbius Transformations, Finite Blaschke Products, Generalized Fibonacci and Lucas Polynomials, Fibonacci and Lucas numbers.*

An International Journal of Optimization and Control: Theories & Applications (http://ijocta.balikesir.edu.tr)

An International Journal of Optimization and Control: Theories & Applications
ISSN:2146-0957 eISSN:2146-5703
Vol.7, No.2, pp.225-233 (2017)
http://doi.org/10.11121/ijocta.01.2017.00363

RESEARCH ARTICLE

# A novel method for the solution of blasius equation in semi-infinite domains

Ali Akgül

*Department of Mathematics, Art and Science Faculty, Siirt University, 56100, Turkey*
*aliakgul00727@gmail.com*

ARTICLE INFO

Article History:
*Received 29 June 2016*
*Accepted 16 June 2017*
*Available 17 July 2017*

Keywords:
*Reproducing kernel method*
*Blasius equations*
*Reproducing kernel functions*

AMS Classification 2010:
*30E25, 34B15, 47B32*
*46E22, 74S30*

ABSTRACT

In this work, we apply the reproducing kernel method for investigating Blasius equations with two different boundary conditions in semi-infinite domains. Convergence analysis of the reproducing kernel method is given. The numerical approximations are presented and compared with some other techniques, Howarth's numerical solution and Runge-Kutta Fehlberg method.



## 1. Introduction

Nonlinear differential equations are extensive in science and technology. However, finding analytical solutions for this class of equations has always been a challenging work [3]. Many approximate methods were introduced for the analytical solution of nonlinear differential equations in the recent years. Among these, Homotopy Analysis Method (HAM) [49], Adomian Decomposition Method (ADM) [2], Variational Iteration Method (VIM) [21], Differential Transformation Method (DTM) [31], and Homotopy Perturbation Method (HPM) [41] can be referred. Some new techniques for approximate solution of nonlinear differential equations are shown up recently, such as Optimal Homotopy Asymptotic Method (OHAM) [45], Generalized Homotopy Method (GHM) [46], and reproducing kernel method (RKM) [13].

In the present paper, the RKM has been applied for the solution of two different forms of nonlinear Blasius equation in a semi-infinite domain. Much notice has been given to the work of the RKM to solve many works. The work [13] presents great applications of the RKM. For more details see [1, 4–7, 10–12, 17, 22, 23, 26, 27, 32, 42, 44, 48, 51].

We present two forms of the Blasius equation arising in fluid flow inside the velocity boundary layer as follows.

The first form of the Blasius equation is given as:

$$\begin{cases} u^{(3)}(x) + \frac{u(x)u''(x)}{2} = 0, \quad 0 \le x \le \infty, \\ u(0) = u'(0) = 0, \quad u'(x) = 1 \quad \text{as} \quad x \to \infty. \end{cases} \tag{1}$$

The second form is given as:

$$\begin{cases} u^{(3)}(x) + \frac{u(x)u''(x)}{2} = 0, \quad 0 \le x \le \infty, \\ u(0) = 0, \quad u'(0) = 1, \quad u'(x) = 0 \quad \text{as} \quad x \to \infty. \end{cases} \tag{2}$$

These equations are the same except for boundary conditions. The first form of the equation is the well-known classical Blasius first derived by Blasius and dates back about a century, which

defines the velocity profile of two-dimensional viscous laminar flow over a finite flat plate. This form of the Blasius equation is the simplest form and the origin of all boundary layer equations in fluid mechanics. The second form of the equation, presented more recently, arises in the steady free convection about a vertical flat plate embedded in a saturated porous medium, Laminar boundary layers at the interface of cocurrent parallel streams, or the flow near the leading edge of a very long, steadily operating conveyor belt [3].

Many analytical techniques were introduced to investigate Blasius equation. He [24] presented a perturbation method. Comparison with Howarth's numerical solution finds out that this technique gives the approximate value $\sigma = 0.3296$ with 0.73 accuracy. Asaithambi [9] obtained this number correct to nine decimal positions as $\sigma = 0.332057336$. The variational iteration method (VIM) is implemented for a reliable treatment of two forms of Blasius equation [47]. Fazio [18] searched the Blasius problem numerically. Sinc-collocation technique is implemented in [36] and the HAM is employed by Yao and Chen in [49] and Liao in [29]. For more details see [8, 14–16, 19, 28, 30, 33–35, 37–40, 43, 49, 50].

We organize the paper as follows. We give some new reproducing kernel functions in Section 2. We present the linear operator in Section 3. We show the main results in Section 4. We give the approximate solutions of (1)–(2) in this section. We illustrate examples in Section 5. We give the conclusion in Section 6.

## 2. Preliminaries

**Definition 1.** *We describe the space* $W_2^4[0,\infty)$ *by*

$$W_2^4[0,\infty) = \{v \in AC[0,1] :\ v', v'', v^{(3)} \in AC[0,\infty),\ v^{(4)} \in L^2[0,\infty),\ v(0) = v'(0) = v'(\infty) = 0\}.$$

*The inner product and the norm in* $W_2^4[0,\infty)$ *are given by*

$$\begin{aligned}\langle v,h\rangle_{W_2^4} &= v(0)h(0) + v'(0)h'(0) + v''(0)h''(0)\\ &+ v^{(3)}(0)h^{(3)}(0) + \int_0^\infty u^{(4)}(t)h^{(4)}(t)\mathrm{d}t,\\ &\qquad v,h \in W_2^4[0,\infty)\end{aligned}$$

*and*

$$\|v\|_{W_2^4} = \sqrt{\langle v,v\rangle_{W_2^4}}, \quad v \in W_2^4[0,\infty).$$

*The space* $W_2^4[0,\infty)$ *is called a reproducing kernel space. A function* $R_y$ *is obtained as:*

$$v(y) = \langle v, R_y\rangle_{W_2^4}.$$

**Definition 2.** *We describe the space* $W_2^1[0,1]$ *by*

$$W_2^1[0,1] = \{v \in AC[0,1] :\ v' \in L^2[0,1]\}.$$

*The inner product and the norm in* $W_2^1[0,1]$ *are defined by*

$$\langle v,h\rangle_{W_2^1} = \int_0^1 v(t)h(t) + v'(t)h'(t)\mathrm{d}t, \qquad v,h \in G_2^1[0,1] \tag{3}$$

*and*

$$\|v\|_{W_2^1} = \sqrt{\langle v,v\rangle_{W_2^1}}, \quad v \in W_2^1[0,1]. \tag{4}$$

$W_2^1[0,1]$ *is a reproducing kernel space. Kernel function* $T_t(y)$ *is obtained as [13]*

$$T_t(y) = \frac{1}{2\sinh(1)}\left[\cosh(t+y-1) + \cosh(|t-y|-1)\right] \tag{5}$$

**Theorem 1.** $W_2^4[0,\infty)$ *is a reproducing kernel space. Kernel function* $R_y$ *is obtained as:*

$$R_y(t) = \begin{cases} \sum_{i=1}^8 c_i(y)t^{i-1}, & t \le y,\\ \sum_{i=1}^8 d_i(y)t^{i-1}, & t > y, \end{cases} \tag{6}$$

*where*

$$\begin{aligned}
c_1(y) &= 0, \quad c_2(y) = 0, \quad c_3(y) = \frac{1}{4}y^2,\\
c_4(y) &= \frac{1}{36}y^3, \quad c_5(y) = \frac{1}{144}y^3,\\
c_6(y) &= -\frac{1}{240}y^2, \quad c_7(y) = \frac{1}{720}y,\\
c_8(y) &= -\frac{1}{5040}, d_1(y) = -\frac{1}{5040}y^7\\
d_2(y) &= \frac{1}{720}y^6, d_3(y) = -\frac{1}{240}y^2(y^3-60),\\
d_4(y) &= \frac{1}{144}y^3(y+4), d_5(y) = 0, d_6(y) = 0,\\
d_7(y) &= 0, \quad d_8(y) = 0.
\end{aligned}$$

***Proof.***

$$\begin{aligned}\langle v(t), R_y(t)\rangle_{W_2^4} &= v(0)R_y(0) + v'(0)R_y'(0)\\ &+ v''(0)R_y''(0) + v^{(3)}(0)R_y^{(3)}(0)\\ &+ \int_0^\infty v^{(4)}(t)R_y^{(4)}(t)\mathrm{d}t,\end{aligned}$$

We obtain

$$\begin{aligned}\langle v, R_y\rangle_{W_2^4} &= v(0)R_y(0) + v'(0)R_y'(0)\\ &+ v''(0)R_y''(0) + v^{(3)}(0)R_y^{(3)}(0)\\ &+ v^{(3)}(1)R_y^{(4)}(1) - v^{(3)}(0)R_y^{(4)}(0)\\ &- v''(1)R_y^{(5)}(1) + v''(0)R_y^{(5)}(1)\\ &+ v'(1)R_y^{(6)}(1) - v'(0)R_y^{(6)}(0)\\ &- v(1)R_y^{(7)}(1) + v(0)R_y^{(7)}(0)\\ &+ \int_0^\infty v(t)R_y^{(8)}(t)\mathrm{d}t,\end{aligned} \tag{7}$$

with integrations by parts. We obtain

$$\langle v(t), R_y(t)\rangle_{W_2^4} = v(y), \tag{8}$$

by reproducing property. If

$$\begin{cases} R_y(0) = 0,\\ R_y'(0) = 0,\\ R_y'(\infty) = 0,\\ R_y''(0) + R_y^{(5)}(0) = 0,\\ R_y^{(3)}(0) - R_y^{(4)}(0) = 0,\\ R_y^{(4)}(\infty) = 0,\\ R_y^{(5)}(\infty) = 0,\\ R_y^{(7)}(\infty) = 0, \end{cases} \tag{9}$$

then (7) implies that

$$R_y^{(8)}(t) = \delta(t-y).$$

When $t \neq y$,

$$R_y^{(8)}(t) = 0,$$

therefore

$$R_y(t) = \begin{cases} \sum_{i=1}^8 c_i(y)t^{i-1}, & t \le y,\\ \sum_{i=1}^8 d_i(y)t^{i-1}, & t > y, \end{cases} \tag{10}$$

Since

$$R_y^{(8)}(t) = \delta(t-y),$$

we have

$$\partial^k R_{y^+}(y) = \partial^k R_{y^-}(y), \quad k = 0,1,2,3,4,5,6 \tag{11}$$

and

$$\partial^7 R_{y^+}(y) - \partial^7 R_{y^-}(y) = 1. \tag{12}$$

Due to $R_y(t) \in W_2^4[0,\infty)$, it follows that

$$R_y(0) = R_y'(0) = R_y'(\infty) = 0, \tag{13}$$

from (9)–(13), the unknown coefficients $c_i(y)$ and $d_i(y)$ $(i = 1,2,\ldots,8)$ can be acquired. Therefore, $R_y(t)$ is obtained as:

$$R_y(x) = \begin{cases} -\frac{1}{5040}t^2(21y^2t^3 + t^5 - 1260y^2 - 7yt^4)\\ -\frac{1}{5040}t^2(-140y^3t - 35y^3t^2), \quad t \le y\\ \\ -\frac{1}{5040}y^2(21t^2y^3 + y^5 - 1260t^2 - 7ty^4)\\ -\frac{1}{5040}y^2(-140t^3y - 35t^3y^2), \quad t > y \end{cases}$$

□

## 3. Solution representation in $W_2^4[0,\infty)$

In this section, the solutions of (1)–(2) are presented in the $W_2^4[0,\infty)$. On defining the linear operator $L : W_2^4[0,\infty) \to W_2^1[0,1]$ as

$$\begin{aligned} Lv(t) &= v^{(3)}(t) + \frac{\exp(-t) + t - 1}{2}v''(t)\\ &+ \frac{\exp(-t)}{2}v(t) \end{aligned} \tag{14}$$

the problem (1) gets the form:

$$\begin{cases} Lv = f(t,u), \quad t \in [0,\infty),\\ v(0) = v'(0) = v'(\infty) = 0 \end{cases} \tag{15}$$

where $f(t,v) = \exp(-t) - \frac{1}{2}v(t)v''(t) - \frac{1}{2}\exp(-t)(\exp(-t) + t - 1)$.

**Theorem 2.** *The $L$ given by* (14) *is a bounded linear operator.*

***Proof.*** We need to show $\|Lv\|_{W_2^1}^2 \le M\|v\|_{W_2^4}^2$, where $M > 0$ is a positive constant. By (3) and (4), we have

$$\|Lv\|_{W_2^1}^2 = \langle Lv, Lv\rangle_{W_2^1} = \int_0^1 [Lv(t)]^2 + \left[Lv'(t)\right]^2 \mathrm{d}t.$$

By (8), we have

$$v(t) = \langle v(\cdot), R_t(\cdot)\rangle_{W_2^4},$$

and

$$Lv(t) = \langle v(\cdot), LR_t(\cdot)\rangle_{W_2^4},$$

so

$$|Lv(t)| \le \|v\|_{W_2^4}\|LR_t\|_{W_2^4} = M_1\|u\|_{W_2^4},$$

where $M_1 > 0$ is positive. Therefore,

$$\int_0^1 [(Lv)(t)]^2 \, \mathrm{d}t \leq M_1^2 \|v\|_{W_2^4}^2 .$$

We have

$$(Lv)'(t) = \left\langle v(\cdot), (LR_t)'(\cdot) \right\rangle_{W_2^4},$$

by reproducing property. Thus, we get

$$\left|(Lv)'(t)\right| \leq \|v\|_{W_2^4} \left\|(LR_t)'\right\|_{W_2^4} = M_2 \|u\|_{W_2^4},$$

where $M_2 > 0$ is positive. Therefore, we obtain

$$\left[(Lv)'(t)\right]^2 \leq M_2^2 \|u\|_{W_2^4}^2,$$

and

$$\int_0^1 \left[(Lv)'(t)\right]^2 \mathrm{d}t \leq M_2^2 \|v\|_{W_2^4}^2,$$

that is

$$\begin{aligned} \|Lv\|_{W_2^1}^2 &\leq \int_0^1 \left( [(Lv)(t)]^2 + \left[(Lv)'(t)\right]^2 \right) \mathrm{d}t \\ &\leq \left(M_1^2 + M_2^2\right) \|v\|_{W_2^4}^2 = M \|v\|_{W_2^4}^2, \end{aligned}$$

where $M = M_1^2 + M_2^2 > 0$ is a positive constant. □

## 4. The main results

Let $\varphi_i(t) = T_{t_i}(t)$ and $\psi_i(t) = L^*\varphi_i(t)$, where $L^*$ is conjugate operator of $L$. The orthonormal system $\left\{\widehat{\Psi}_i(t)\right\}_{i=1}^{\infty}$ of $W_2^4[0,\infty)$ can be obtained from Gram-Schmidt orthogonalization process of $\{\psi_i(t)\}_{i=1}^{\infty}$,

$$\widehat{\psi}_i(t) = \sum_{k=1}^{i} \beta_{ik}\psi_k(t), \quad (\beta_{ii} > 0, \quad i = 1, 2, \ldots) \tag{16}$$

**Theorem 3.** *Let $\{t_i\}_{i=1}^{\infty}$ be dense in $[0,\infty)$ and $\psi_i(t) = L_y R_t(y)|_{y=t_i}$. The sequence $\{\psi_i(t)\}_{i=1}^{\infty}$ is a complete system in $W_2^4[0,\infty)$.*

***Proof.*** We obtain

$$\begin{aligned} \psi_i(t) &= (L^*\varphi_i)(t) = \langle (L^*\varphi_i)(y), R_t(y) \rangle \\ &= \langle (\varphi_i)(y), LyR_t(y) \rangle = L_y R_t(y)|_{y=t_i}. \end{aligned}$$

The subscript $y$ by the operator $L$ indicates that the operator $L$ applies to the function of $y$. Clearly, $\psi_i(t) \in W_2^4[0,\infty)$. For each fixed $v(t) \in W_2^4[0,\infty)$, let $\langle v(t), \psi_i(t) \rangle = 0$, $(i = 1, 2, \ldots)$, which means that,

$$\langle v(t), (L^*\varphi_i)(t) \rangle = \langle Lv(\cdot), \varphi_i(\cdot) \rangle = (Lv)(t_i) = 0.$$

$\{t_i\}_{i=1}^{\infty}$ is dense in $[0,\infty)$. Therefore, $(Lv)(t) = 0$. $u \equiv 0$ by $L^{-1}$. □

**Theorem 4.** *If $v(t)$ is the exact solution of (15), then*

$$v(t) = \sum_{i=1}^{\infty} \sum_{k=1}^{i} \beta_{ik} f(t_k, v_k) \widehat{\Psi}_i(t). \tag{17}$$

*where $\{(t_i)\}_{i=1}^{\infty}$ is dense in $[0,\infty)$.*

***Proof.*** We get

$$\begin{aligned} v(t) &= \sum_{i=1}^{\infty} \left\langle v(t), \widehat{\Psi}_i(t) \right\rangle_{W_2^4} \widehat{\Psi}_i(t) \\ &= \sum_{i=1}^{\infty} \sum_{k=1}^{i} \beta_{ik} \langle v(t), \Psi_k(t) \rangle_{W_2^4} \widehat{\Psi}_i(t) \\ &= \sum_{i=1}^{\infty} \sum_{k=1}^{i} \beta_{ik} \langle v(t), L^*\varphi_k(t) \rangle_{W_2^4} \widehat{\Psi}_i(t) \\ &= \sum_{i=1}^{\infty} \sum_{k=1}^{i} \beta_{ik} \langle Lv(t), \varphi_k(t) \rangle_{W_2^1} \widehat{\Psi}_i(t) \\ &= \sum_{i=1}^{\infty} \sum_{k=1}^{i} \beta_{ik} \langle f(t,v), T_{t_k} \rangle_{W_2^1} \widehat{\Psi}_i(t) \\ &= \sum_{i=1}^{\infty} \sum_{k=1}^{i} \beta_{ik} f(t_k, v_k) \widehat{\Psi}_i(x), \end{aligned}$$

by (16) and uniqueness of solution of (15). This completes the proof. □

The approximate solution $u_n(x)$ can be acquired as:

$$v_n(t) = \sum_{i=1}^{n} \sum_{k=1}^{i} \beta_{ik} f(t_k, v_k) \widehat{\Psi}_i(t). \tag{18}$$

**Lemma 1.** *If $\|v_n - v\|_{W_2^4} \to 0$, $t_n \to t$, $(n \to \infty)$ and $f(t,v)$ is continuous for $x \in [0,\infty)$, then [20]*

$$f(t_n, v_{n-1}(t_n)) \to f(t, v(t)) \quad as \ n \to \infty.$$

**Theorem 5.** *For any fixed $v_0(t) \in W_2^4[0,\infty)$ assume that the following conditions are hold:*

(i)

$$v_n(t) = \sum_{i=1}^{n} A_i \widehat{\psi}_i(t), \tag{19}$$

$$A_i = \sum_{k=1}^{i} \beta_{ik} f(t_k, u_{k-1}(t_k)), \tag{20}$$

(ii) $\|v_n\|_{W_2^4}$ *is bounded;*
(iii) $\{t_i\}_{i=1}^{\infty}$ *is dense in* $[0,\infty)$*;*
(iv) $f(t,u) \in W_2^1[0,1]$ *for any* $v(t) \in W_2^4[0,\infty)$.

*Then* $v_n(t)$ *in iterative formula* (19) *converges to the exact solution of* (17) *in* $W_2^4[0,\infty)$ *and*

$$v(t) = \sum_{i=1}^{\infty} A_i \widehat{\psi}_i(t).$$

***Proof.*** By (19), we obtain

$$v_{n+1}(t) = u_n(t) + A_{n+1}\widehat{\Psi}_{n+1}(t), \qquad (21)$$

from the orthonormality of $\{\widehat{\Psi}_i\}_{i=1}^{\infty}$, we get

$$\|v_{n+1}\|^2 = \|v_n\|^2 + A_{n+1}^2 = \|v_{n-1}\|^2 + A_n^2 + A_{n+1}^2 = \ldots = \sum_{i=1}^{n+1} A_i^2,$$

from boundedness of $\|u_n\|_{W_2^4}$, we obtain

$$\sum_{i=1}^{\infty} A_i^2 < \infty,$$

i.e.,

$$\{A_i\} \in l^2 \quad (i = 1, 2, \ldots).$$

Let $m > n$, in view of $(v_m - v_{m-1}) \perp (v_{m-1} - v_{m-2}) \perp \ldots \perp (v_{n+1} - v_n)$, we get

$$\begin{aligned} \|v_m - v_n\|_{W_2^4}^2 &= \|v_m - v_{m-1} + \ldots + u_{n+1} - v_n\|_{W_2^4}^2 \\ &\leq \|v_m - v_{m-1}\|_{W_2^3}^2 + \ldots + \|v_{n+1} - v_n\|_{W_2^4}^2 \\ &= \sum_{i=n+1}^{m} A_i^2 \to 0, \quad m, n \to \infty. \end{aligned}$$

By the completeness of $W_2^4[0,\infty)$, there exists $v(t) \in W_2^4[0,\infty)$, such that

$$v_n(t) \to v(t) \quad as\ n \to \infty.$$

(ii) Taking limits in (19),

$$v(t) = \sum_{i=1}^{\infty} A_i \widehat{\psi}_i(t).$$

We have

$$\begin{aligned} (Lv)(t_j) &= \sum_{i=1}^{\infty} A_i \left\langle L\widehat{\psi}_i(t), \varphi_j(t) \right\rangle_{W_2^1} \\ &= \sum_{i=1}^{\infty} A_i \left\langle \widehat{\psi}_i(t), L^*\varphi_j(t) \right\rangle_{W_2^4} \\ &= \sum_{i=1}^{\infty} A_i \left\langle \widehat{\psi}_i(t), \psi_j(t) \right\rangle_{W_2^4}. \end{aligned}$$

Therefore, we get

$$\sum_{j=1}^{n} \beta_{nj}(Lv)(t_j) = \sum_{i=1}^{\infty} A_i \left\langle \widehat{\psi}_i(t), \sum_{j=1}^{n} \beta_{nj}\psi_j(t) \right\rangle_{W_2^4} = \sum_{i=1}^{\infty} A_i \left\langle \widehat{\psi}_i(t), \widehat{\psi}_n(t) \right\rangle_{W_2^4} = A_n.$$

If $n = 1$, then

$$Lv(t_1) = f(t_1, v_0(t_1)). \qquad (22)$$

If $n = 2$, then

$$\begin{aligned} &\beta_{21}(Lv)(t_1) + \beta_{22}(Lv)(t_2) \\ &= \beta_{21} f(t_1, v_0(t_1)) + \beta_{22} f(t_2, v_1(t_2)). \end{aligned}$$

We have

$$(Lv(t_2) = f(t_2, u_1(t_2)).$$

Then, we get

$$(Lv)(t_j) = f(t_j, u_{j-1}(t_j)), \qquad (23)$$

by induction. We have,

$$(Lv)(y) = f(y, v(y)).$$

Therefore, $v(t)$ is the solution of (15) and

$$v(t) = \sum_{i=1}^{\infty} A_i \widehat{\psi}_i,$$

where $A_i$ are given by (20).

□

## 5. Numerical results

In this section, two examples are given to demonstrate the efficiency of the RKM. We have shown comparison tables to prove the power of the RKM. All computations are applied by Maple software

program. The accuracy of the RKM for the Blasius equations are controllable. The numerical results we obtained justify the advantage of this technique. We consider first and second forms of the Blasius equation by RKM. In Tables 1–3, $v$, $v'$, and $v''$ obtained from the RKM are compared with Howarth's numerical solution [25]. Furthermore, as it can be seen from Tables 1–3, the RKM is more accurate than the variational iteration method [24]. In Tables 4–6, the result of the RKM is given against that of exact (numerical) method. There is a good agreement between the results of the RKM and numerical solution. The results are in very good agreement with numerical and previous data available in the literature.

**Table 1.** Comparison between $v(t)$ obtained from RKM with VIM, HPM and numerical method, first form of the Blasius equation.

| t | Howarth [25] | VIM [24] | HPM [3] | RKM |
|---|---|---|---|---|
| 0 | 0.00000 | 0.00000 | 0.00000 | 0.00000 |
| 1 | 0.16577 | 0.19319 | 0.16557 | 0.16570 |
| 2 | 0.65003 | 0.67940 | 0.65001 | 0.65310 |
| 3 | 1.39682 | 1.39106 | 1.39679 | 1.39782 |
| 4 | 2.30576 | 2.24573 | 2.30572 | 2.33481 |
| 5 | 3.28329 | 3.17748 | 3.28309 | 3.29502 |
| 6 | 4.27964 | 4.14688 | 4.27767 | 4.28542 |
| 7 | 5.27926 | 5.13359 | 5.26736 | 5.26896 |

**Table 2.** Comparison between $v'(t)$ obtained from RKM with VIM, HPM and numerical method, first form of the Blasius equation.

| t | Howarth [25] | VIM [24] | HPM [3] | RKM |
|---|---|---|---|---|
| 0 | 0.00000 | 0.00000 | 0.00000 | 0.00000 |
| 1 | 0.32979 | 0.35064 | 0.32977 | 0.33005 |
| 2 | 0.62977 | 0.61218 | 0.62976 | 0.63039 |
| 3 | 0.84605 | 0.79640 | 0.84603 | 0.84469 |
| 4 | 0.95552 | 0.90185 | 0.95551 | 0.95294 |
| 5 | 0.99150 | 0.95523 | 0.99152 | 0.98514 |
| 6 | 0.99868 | 0.98032 | 0.99883 | 0.99131 |
| 7 | 0.99992 | 0.99158 | 0.99943 | 0.99378 |

**Table 3.** Comparison between $v''(t)$ obtained from RKM with VIM, HPM and numerical method, first form of the Blasius equation.

| t | Howarth [25] | VIM [24] | HPM [3] | RKM |
|---|---|---|---|---|
| 0 | 0.33206 | 0.54360 | 0.33205 | 0.33236 |
| 1 | 0.32301 | 0.27141 | 0.32300 | 0.32336 |
| 2 | 0.26675 | 0.22748 | 0.26675 | 0.26631 |
| 3 | 0.16136 | 0.14117 | 0.16135 | 0.16127 |
| 4 | 0.06424 | 0.07469 | 0.06422 | 0.06522 |
| 5 | 0.01591 | 0.03600 | 0.01586 | 0.01918 |
| 6 | 0.00240 | 0.01645 | 0.00110 | 0.00313 |
| 7 | 0.00022 | 0.00723 | 0.00060 | 0.00029 |

**Table 4.** Comparison between $v(t)$ obtained from RKM with HPM and numerical method, second form of the Blasius equation.

| t | Numerical [3] (5th order Runge-Kutta Fehlberg) | HPM [3] | RKM |
|---|---|---|---|
| 0 | 0.000000 | 0.00000 | 0.00000 |
| 1 | 0.786198 | 0.78620 | 0.78657 |
| 2 | 1.218546 | 1.21855 | 1.21310 |
| 3 | 1.432728 | 1.43273 | 1.43823 |
| 4 | 1.533086 | 1.53308 | 1.53938 |
| 5 | 1.578851 | 1.57884 | 1.57502 |
| 6 | 1.599437 | 1.59945 | 1.59266 |
| 7 | 1.612470 | 1.61280 | 1.61966 |

**Table 5.** Comparison between $v'(t)$ obtained from RKM with HPM and numerical method, second form of the Blasius equation.

| t | Numerical [3] (5th order Runge-Kutta Fehlberg) | HPM [3] | RKM |
|---|---|---|---|
| 0 | 1.000000 | 1.000000 | 1.000000 |
| 1 | 0.587153 | 0.587153 | 0.589473 |
| 2 | 0.301784 | 0.301783 | 0.308234 |
| 3 | 0.144016 | 0.144016 | 0.141545 |
| 4 | 0.066244 | 0.066243 | 0.066661 |
| 5 | 0.029956 | 0.029949 | 0.026618 |
| 6 | 0.013469 | 0.013434 | 0.011824 |
| 7 | 0.006119 | 0.006005 | 0.006437 |

**Table 6.** Comparison between $v''(t)$ obtained from RKM with HPM and numerical method, second form of the Blasius equation.

| t | Numerical [3] (5th order Runge-Kutta Fehlberg) | HPM [3] | RKM |
|---|---|---|---|
| 0 | −0.443749 | −0.443748 | −0.442162 |
| 1 | −0.358313 | −0.358312 | −0.359575 |
| 2 | −0.214505 | −0.214505 | −0.213139 |
| 3 | −0.109834 | −0.109834 | −0.109184 |
| 4 | −0.052157 | −0.052159 | −0.052283 |
| 5 | −0.023906 | −0.023922 | −0.023166 |
| 6 | −0.010736 | −0.010800 | −0.010687 |
| 7 | −0.046658 | −0.048415 | −0.044522 |

## 6. Conclusion

In this work, we introduced an algorithm for solving the Blasius equation with two different boundary conditions in semi-infinite domains. For illustration purposes, examples were chosen to show the computational accuracy. This work has confirmed that the RKM offers important benefits in terms its computational effectiveness to solve the strongly nonlinear equations.

## Acknowledgments

The author thanks the anonymous referees whose work largely constitutes this sample file. This research was supported by 2017-SİÜFED-39 and 2017-SİÜFEB-40.

## References

[1] Arqub, O. A., Mohammed A. S., and Momani, S., Application of reproducing kernel method for solving nonlinear Fredholm-Volterra integrodifferential equations. Abstr. Appl. Anal., pages Art. ID 839836, 16, (2012).

[2] Adair, D., and Jaeger, M.,. Simulation of tapered rotating beams with centrifugal stiffening using the Adomian decomposition method. Appl. Math. Model., 40(4):3230–3241, (2016).

[3] Aghakhani, M., Suhatril, M., Mohammadhassani, M., Daie, M., and Toghroli, A., A simple modification of homotopy perturbation method for the solution of Blasius equation in semi-infinite domains. Math. Probl. Eng., pages Art. ID 671527, 7, (2015).

[4] Akgül, A., A new method for approximate solutions of fractional order boundary value problems. Neural Parallel Sci. Comput., 22(1-2):223–237, (2014).

[5] Akgül, A., New reproducing kernel functions. Math. Probl. Eng., pages Art. ID 158134, 10, (2015).

[6] Akgül, A., Inc, M., and Karatas, E., Reproducing kernel functions for difference equations. Discrete Contin. Dyn. Syst. Ser. S, 8(6):1055–1064, (2015).

[7] Akgül, A., Inc, M., Karatas, E., and Baleanu, D., Numerical solutions of fractional differential equations of Lane-Emden type by an accurate technique. Adv. Difference Equ., pages 2015:220, 12, (2015).

[8] Aminikhah, H., An analytical approximation for solving nonlinear Blasius equation by NHPM. Numer. Methods Partial Differential Equations, 26(6):1291–1299, (2010).

[9] Asaithambi, A., Solution of the Falkner-Skan equation by recursive evaluation of Taylor coefficients. J. Comput. Appl. Math., 176(1):203–214, (2005).

[10] Bushnaq, S., Maayah, B., Momani, S., and Alsaedi, A., A reproducing kernel Hilbert space method for solving systems of fractional integrodifferential equations. Abstr. Appl. Anal., pages Art. ID 103016, 6, (2014).

[11] Bushnaq, S., Momani, S., and Zhou, Y., A reproducing kernel Hilbert space method for solving integrodifferential equations of fractional order. J. Optim. Theory Appl., 156(1):96–105, (2013).

[12] Chang, C. W., Chang, J. R. and Liu, C. S., The Lie-group shooting method for solving classical Blasius at-plate problem. CMC Comput. Mater. Continua, 7(3):139–153, (2008).

[13] Cui, M., and Lin, Y., Nonlinear numerical analysis in the reproducing kernel space. Nova Science Publishers, Inc., New York, (2009).

[14] Datta, B. K., Analytic solution for the Blasius equation. Indian J. Pure Appl. Math., 34(2):237–240, (2003).

[15] Ertürk, V. S., and Momani, S., Numerical solutions of two forms of Blasius equation on a half-infinite domain. J. Algorithms Comput. Technol., 2(3):359–370, (2008).

[16] Fang, T., Liang, W., and Lee, C. F., A new solution branch for the Blasius equation—a shrinking sheet problem. Comput. Math. Appl., 56(12):3088–3095, (2008).

[17] Fardi, M., Ghaziani, R. K., and Ghasemi, M., The Reproducing Kernel Method for Some Variational Problems Depending on Indefinite Integrals. Math. Model. Anal., 21(3):412–429, (2016).

[18] Fazio, R., Numerical transformation methods: Blasius problem and its variants. Appl. Math. Comput., 215(4):1513–1521, (2009).

[19] Ganji, D. D., Babazadeh, H., Noori, F., Pirouz, M. M., and Janipour, M., An application of homotopy perturbation method for non-linear Blasius equation to boundary layer flow over a at plate. Int. J. Nonlinear Sci., 7(4):399–404, (2009).

[20] Geng, F., and Cui, M., Solving singular nonlinear second-order periodic boundary value problems in the reproducing kernel space. Appl. Math. Comput., 192(2):389–398, (2007).

[21] Ghaneai, H., and Hosseini, M. M., Solving differential-algebraic equations through variational iteration method with an auxiliary parameter. Appl. Math. Model., 40(5-6):3991–4001, (2016).

[22] Hashemi, M. S., Constructing a new geometric numerical integration method to the nonlinear heat transfer equations. Commun. Nonlinear Sci. Numer. Simul., 22(1-3):990-1001, (2015).

[23] Hashemi, M. S., and Abbasbandy, S., A geometric approach for solving Troesch's problem. Bull. Malays. Math. Sci. Soc., 40(1):97–116, (2017).

[24] He, J. H., A simple perturbation approach to Blasius equation. Appl. Math. Comput., 140(2-3):217–222, (2003).

[25] Howarth, L., Laminar boundary layers. In Handbuch der Physik (herausgegeben von S. Flügge), Bd. 8 1, Strmungsmechanik I (Mitherausgeber C. Truesdell), pages 264 350. Springer-Verlag, Berlin-Gottingen-Heidelberg, (1959).

[26] Inc, M., and Akgül, A., Approximate solutions for MHD squeezing fluid flow by a novel method. Bound. Value Probl., pages 2014:18, 17, (2014).

[27] Inc, M., Akgül, A., and Geng, F., Reproducing kernel Hilbert space method for solving Bratu's problem. Bull. Malays. Math. Sci. Soc., 38(1):271–287, (2015).

[28] Kennedy, E. D., Application of a new method of approximation in the solution of ordinary differential equations to the Blasius equation. Trans. ASME Ser. E. J. Appl. Mech., 31:112–114, (1964).

[29] Liao, S. J., An explicit, totally analytic approximate solution for Blasius' viscous flow problems. Internat. J. Non-Linear Mech., 34(4):759–778, (1999).

[30] Lin, J., A new approximate iteration solution of Blasius equation. Commun. Nonlinear Sci. Numer. Simul., 4(2):91–99, (1999).

[31] Liu, C. C., Numerical study of mixed convection MHD flow in vertical channels using differential transformation method. Appl. Math. Inf. Sci., 9(1L):105–110, (2015).

[32] Maayah, B., Bushnaq, S., Momani, S., and Arqub, O. A., Iterative multistep reproducing kernel Hilbert space method for solving strongly nonlinear oscillators. Adv. Math. Phys., pages Art. ID 758195, 7, ( 2014).

[33] Marinca, V., and Herianu, N., The optimal homotopy asymptotic method for solving Blasius equation. Appl. Math. Comput., 231:134–139, (2014).

[34] Miansari, M. O., Miansari, M. E., Barari, A., and Domairry, G., Analysis of Blasius equation for flat-plate flow with infinite boundary value. Int. J. Comput. Methods Eng. Sci. Mech., 11(2):79–84, (2010).

[35] Panayotounakos, D. E., Sotiropoulos, N. B., Sotiropoulou, A. B., and Panayotounakou., N. D., Exact analytic solutions of nonlinear boundary value problems in fluid mechanics (Blasius equations). J. Math. Phys., 46(3):033101, 26, (2005).

[36] Parand, K., Dehghan, M., and Pirkhedri, A., Sinc-collocation method for solving the Blasius equation. Phys. Lett. A, 373(44):4060–4065, (2009).

[37] Peker, H. A., Karaolu, O., and Oturan, G.,. The differential transformation method and Pade approximant for a form of Blasius equation. Math. Comput. Appl., 16(2):507–513, (2011).

[38] Ranasinghe, A. I., and Majid, F. B., Solution of Blasius equation by decomposition. Appl. Math. Sci. (Ruse), 3(13-16):605–611, (2009).

[39] Robin, W., Some remarks on the homotopy-analysis method and series solutions to the Blasius equation. Int. Math. Forum, 8(25-28):1205–1213, (2013).

[40] Sajid, M., Abbas, Z., Ali, N., and Javed, T., A hybrid variational iteration method for Blasius equation. Appl. Appl. Math., 10(1):223–229, (2015).

[41] Sakar, M. G., Uludag, F., and Erdogan, F., Numerical solution of time-fractional nonlinear PDEs with proportional delays by homotopy perturbation method. Appl. Math. Model., 40(13-14):6639–6649, (2016).

[42] Shawagfeh, N., Arqub, O. A., and Momani, S., Analytical solution of nonlinear second-order periodic boundary value problem using reproducing kernel method. J. Comput. Anal. Appl., 16(4):750–762, (2014).

[43] Shishkin, G. I., Grid approximation of the solution of the Blasius equation and of its derivatives. Zh. Vychisl. Mat. Mat. Fiz., 41(1):39–56, (2001).

[44] Tang, Z. Q., and Geng, F.Z., Fitted reproducing kernel method for singularly perturbed delay initial value problems. Appl. Math. Comput., 284:169–174, (2016).

[45] Ullah, I., Khan, H., and Rahim, M. T., Approximation of first grade MHD squeezing fluid flow with slip boundary condition using DTM and OHAM. Math. Probl. Eng., pages Art. ID 816262, 9, (2013).

[46] Leal, H. V., Generalized homotopy method for solving nonlinear differential equations. Comput. Appl. Math., 33(1):275–288, (2014).

[47] Wazwaz, A. M., The variational iteration method for solving two forms of Blasius equation on a half-infinite domain. Appl. Math. Comput., 188(1):485–491, (2007).

[48] Xu, M. Q., and Lin, Y. Z., Simplified reproducing kernel method for fractional differential equations with delay. Appl. Math. Lett., 52:156–161, (2016).

[49] Yao, B., and Chen, J., A new analytical solution branch for the Blasius equation with a shrinking sheet. Appl. Math. Comput., 215(3):1146–1153, (2009).

[50] Yu, L. T., and Chen, C. K., The solution of the Blasius equation by the differential transformation method. Math. Comput. Modelling, 28(1):101–111, (1998).

[51] Zhao, Z., Lin, Y. and Niu, J., Convergence Order of the Reproducing Kernel Method for Solving Boundary Value Problems. Math. Model. Anal., 21(4):466–477, (2016)

***Ali Akgül*** *is an Associate Professor at the Department of Mathematics, Art and Science Faculty, Siirt University. He received his B.Sc. (2005) and M.Sc. (2010) degrees from Department of Mathematics, Dicle University, Turkey and Ph.D. (2014) from Firat University, Turkey. His research areas includes Differential Equations and Functional Analysis*

An International Journal of Optimization and Control: Theories & Applications (http://ijocta.balikesir.edu.tr)

## INSTRUCTIONS FOR AUTHORS

### Aims and Scope

This journal shares the research carried out through different disciplines in regards to optimization, control and their applications.

The basic fields of this journal are linear, nonlinear, stochastic, parametric, discrete and dynamic programming; heuristic algorithms in optimization, control theory, game theory and their applications. Problems such as managerial decisions, time minimization, profit maximizations and other related topics are also shared in this journal.

Besides the research articles expository papers, which are hard to express or model, conference proceedings, book reviews and announcements are also welcome.

### Journal Topics

- Applied Mathematics,
- Financial Mathematics,
- Control Theory,
- Game Theory,
- Fractional Calculus,
- Fractional Control,
- Modeling of Bio-systems for Optimization and Control,
- Linear Programming,
- Nonlinear Programming,
- Stochastic Programming,
- Parametric Programming,
- Conic Programming,
- Discrete Programming,
- Dynamic Programming,
- Optimization with Artificial Intelligence,
- Operational Research in Life and Human Sciences,
- Heuristic Algorithms in Optimization,
- Applications Related to Optimization on Engineering.

### Submission of Manuscripts

New Submissions

Solicited and contributed manuscripts should be submitted to IJOCTA via the journal's online submission system. You need to make registration prior to submitting a new manuscript (please click here to register and do not forget to define yourself as an "Author" in doing so). You may then click on the "New Submission" link on your User Home.

IMPORTANT: If you already have an account, please click here to login. It is likely that you will have created an account if you have reviewed or authored for the journal in the past.

On the submission page, enter data and answer questions as prompted. Click on the “Next” button on each screen to save your work and advance to the next screen. The names and contact details of at least four internationally recognized experts who can review your manuscript should be entered in the "Comments for the Editor" box.

You will be prompted to upload your files: Click on the “Browse” button and locate the file on your computer. Select the description of the file in the drop down next to the Browse button. When you have selected all files you wish to upload, click the “Upload” button. Review your submission before sending to the Editors. Click the “Submit” button when you are done reviewing. Authors are responsible for verifying all files have uploaded correctly.

You may stop a submission at any phase and save it to submit later. Acknowledgment of receipt of the manuscript by IJOCTA Online Submission System will be sent to the corresponding author, including an assigned manuscript number that should be included in all subsequent correspondence. You can also log-

on to submission web page of IJOCTA any time to check the status of your manuscript. You will receive an e-mail once a decision has been made on your manuscript.

Each manuscript must be accompanied by a statement that it has not been published elsewhere and that it has not been submitted simultaneously for publication elsewhere.

Manuscripts can be prepared using LaTeX (.tex) or MSWord (.docx). However, manuscripts with heavy mathematical content will only be accepted as LaTeX files.

Preferred first submission format (for reviewing purpose only) is Portable Document File (.pdf). Please find below the templates for first submission.

Click here to download Word template for first submission (.docx)

Click here to download LaTeX template for first submission (.tex)

Revised Manuscripts

Revised manuscripts should be submitted via IJOCTA online system to ensure that they are linked to the original submission. It is also necessary to attach a separate file in which a point-by-point explanation is given to the specific points/questions raised by the referees and the corresponding changes made in the revised version.

To upload your revised manuscript, please go to your author page and click on the related manuscript title. Navigate to the "Review" link on the top left and scroll down the page. Click on the "Choose File" button under the "Editor Decision" title, choose the revised article (in pdf format) that you want to submit, and click on the "Upload" button to upload the author version. Repeat the same steps to upload the "Responses to Reviewers/Editor" file and make sure that you click the "Upload" button again.

To avoid any delay in making the article available freely online, the authors also need to upload the source files (Word or LaTex) when submitting revised manuscripts. Files can be compressed if necessary. The two-column final submission templates are as follows:

Click here to download Word template for final submission (.docx)

Click here to download LaTeX template for final submission (.tex)

Authors are responsible for obtaining permission to reproduce copyrighted material from other sources and are required to sign an agreement for the transfer of copyright to IJOCTA.

## Article Processing Charges

There are no charges for submission and/or publication.

## English Editing

Papers must be in English. Both British and American spelling is acceptable, provided usage is consistent within the manuscript. Manuscripts that are written in English that is ambiguous or incomprehensible, in the opinion of the Editor, will be returned to the authors with a request to resubmit once the language issues have been improved. This policy does not imply that all papers must be written in "perfect" English, whatever that may mean. Rather, the criteria require that the intended meaning of the authors must be clearly understandable, i.e., not obscured by language problems, by referees who have agreed to review the paper.

## Presentation of Papers

Manuscript style

Use a standard font of the **11-point type: Times New Roman** is preferred. It is necessary to single line space your manuscript. Normally manuscripts are expected not to exceed 25 single-spaced pages including text, tables, figures and bibliography. All illustrations, figures, and tables are placed within the text at the appropriate points, rather than at the end.

During the submission process you must enter: (1) the full title, (2) names and affiliations of all authors and (3) the full address, including email, telephone and fax of the author who is to check the proofs. Supply a brief **biography** of each author at the end of the manuscript after references.

- Include the name(s) of any **sponsor(s)** of the research contained in the paper, along with **grant number(s).**
- Enter an **abstract** of no more than 250 words for all articles.

Keywords

Authors should prepare no more than 5 keywords for their manuscript.

Maximum five **AMS Classification number** (http://www.ams.org/mathscinet/msc/msc2010.html) of the study should be specified after keywords.

Writing Abstract

An abstract is a concise summary of the whole paper, not just the conclusions. The abstract should be no more than 250 words and convey the following:

1. An introduction to the work. This should be accessible by scientists in any field and express the necessity of the experiments executed.
2. Some scientific detail regarding the background to the problem.
3. A summary of the main result.
4. The implications of the result.
5. A broader perspective of the results, once again understandable across scientific disciplines.

It is crucial that the abstract conveys the importance of the work and be understandable without reference to the rest of the manuscript to a multidisciplinary audience. Abstracts should not contain any citation to other published works.

Reference Style

Reference citations in the text should be identified by numbers in square brackets "[ ]". All references must be complete and accurate. Please ensure that every reference cited in the text is also present in the reference list (and vice versa). Online citations should include date of access. References should be listed in the following style:

*Journal article*

Author, A.A. and Author, B., Title of article. *Title of Journal*, Vol (issue), pages (Year).

Evans, W.A., Approaches to intelligent information retrieval. *Information Processing and Management*, 7 (2), 147–168 (1994).

*Book*

Author, A., *Title of book*. Publisher, Place of Publication (Year).

Mercer, P.A. and Smith, G., *Private Viewdata in the UK*. 2nd ed. Longman, London (1993).

*Chapter*

Author, A., Title of chapter. *In*: A. Editor and B. Editor, eds. *Title of book*. Publisher, Place

of publication, pages (Year).

Bantz, C.R., Social dimensions of software development. *In*: J.A. Anderson, ed. *Annual*

*review of software management and development*. CA: Sage, Newbury Park, 502–510 (1995).

*Internet document*

Author, A., Year. *Title of document* [online]. Source. Available from: URL [Accessed date

Month Year].

Holland, M., 2004. *Guide to citing Internet sources* [online]. Poole, Bournemouth University.

Available from:

http://www.bournemouth.ac.uk/library/using/guide_to_citing_internet_sourc.html [Accessed

4 November 2004].

*Newspaper article*

Author, A. (or Title of Newspaper), Title of article. *Title of Newspaper*, day Month, page, column (Year).

Independent, Picking up the bills. *Independent*, 4 June, p. 28a (1992).

*Thesis*

Author, A., *Title of thesis*. Type of thesis (degree). Name of University (Year).

Agutter, A.J., *The linguistic significance of current British slang*. Thesis (PhD). Edinburgh University (1995).

Illustrations

Illustrations submitted (line drawings, halftones, photos, photomicrographs, etc.) should be clean originals or digital files. Digital files are recommended for highest quality reproduction and should follow these guidelines:

- 300 dpi or higher
- Sized to fit on journal page
- TIFF or JPEG format only
- Embedded in text files and submitted as separate files (if required)

Tables and Figures

Tables and figures (illustrations) should be embedded in the text at the appropriate points, rather than at the end. A short descriptive title should appear above each table with a clear legend and any footnotes suitably identified below.

Proofs

Page proofs are sent to the designated author using IJOCTA EProof system. They must be carefully checked and returned within 48 hours of receipt.

Offprints/Reprints

Each corresponding author of an article will receive a PDF file of the article via email. This file is for personal use only and may not be copied and disseminated in any form without prior written permission from IJOCTA.

**Submission Preparation Checklist**

As part of the submission process, authors are required to check off their submission's compliance with all of the following items, and submissions may be returned to authors that do not adhere to these guidelines.

1. The submission has not been previously published, nor is it before another journal for consideration (or an explanation has been provided in Comments for the Editor).
2. The submission file is in Portable Document Format (.pdf).
3. Where available, URLs for the references have been provided.
4. The text is single line spaced; uses a 11-point font; employs italics, rather than underlining (except with URL addresses); and all illustrations, figures, and tables are placed within the text at the appropriate points, rather than at the end.
5. The text adheres to the stylistic and bibliographic requirements outlined in the Author Guidelines, which is found in "About the Journal".
6. Maximum five AMS Classification number (http://www.ams.org/mathscinet/msc/msc2010.html) of the study have been provided after keywords.
7. After the acceptance of manuscript (before copy editing), Word (.docx) or LaTeX (.tex) version of the paper will be presented.
8. The names and email addresses of at least four (4) possible reviewers have been indicated in "Comments for the Editor" box in Paper Submission Step 1. Please note that at least two of the recommendations should be from different countries. Avoid suggesting reviewers who are at arms-length from you or your co-authors. This includes graduate advisors, people in your current department, or any others with a conflict of interest.

**Peer Review Process**

All contributions, prepared according to the author guidelines and submitted via IJOCTA online submission system are evaluated according to the criteria of originality and quality of their scientific content. The corresponding author will receive a confirmation e-mail with a reference number assigned to the paper, which he/she is asked to quote in all subsequent correspondence.

All manuscripts are first checked by the Technical Editor using plagiarism detection software (iThenticate) to verify originality and ensure the quality of the written work. If the result is not satisfactory (i.e. exceeding the limit of 30% of overlapping), the submission is rejected and the author is notified.

After the plagiarism check, the manuscripts are evaluated by the Editor-in-Chief and can be rejected without reviewing if considered not of sufficient interest or novelty, too preliminary or out of the scope of the journal. If the manuscript is considered suitable for further evaluation, it is first sent to the Area Editor. Based on his/her opinion the paper is then sent to at least two independent reviewers. Each reviewer is allowed up to four weeks to return his/her feedback but this duration may be extended based on his/her availability. IJOCTA has instituted a blind peer review process where the reviewers' identities are not known to authors. When the reviews are received, the Area Editor gives a decision and lets the author know it together with the reviewer comments and any supplementary files.

Should the reviews be positive, the authors are expected to submit the revised version usually within two months the editor decision is sent (this period can be extended when the authors contact to the editor and let him/her know that they need extra time for resubmission). If a revised paper is not resubmitted within the deadline, it is considered as a new submission after all the changes requested by reviewers have been made. Authors are required to submit a new cover letter, a response to reviewers letter and the revised manuscript (which ideally shows the revisions made in a different color or highlighted). If a change in authorship (addition or removal of author) has occurred during the revision, authors are requested to clarify the reason for change, and all authors (including the removed/added ones) need to submit a written consent for the change. The revised version is evaluated by the Area editor and/or reviewers and the Editor-in-Chief brings a decision about final acceptance based on their suggestions. If necessary, further revision can be asked for to fulfil all the requirements of the reviewers.

When a manuscript is accepted for publication, an acceptance letter is sent to the corresponding author and the authors are asked to submit the source file of the manuscript conforming to the IJOCTA two-column final submission template. After that stage, changes of authors of the manuscript are not possible. The manuscript is sent to the Copyeditor and a linguistic, metrological and technical revision is made, at which stage the authors are asked to make the final corrections in no more than a week. The layout editor prepares the galleys and the authors receive the galley proof for final check before printing. The authors are expected to correct only typographical errors on the proofs and return the proofs within 48 hours. After the final check by the layout editor and the proofreader, the manuscript is assigned a DOI number, made publicly available and listed in the forthcoming journal issue. After printing the issue, the corresponding metadata and files published in this issue are sent to the databases for indexing.

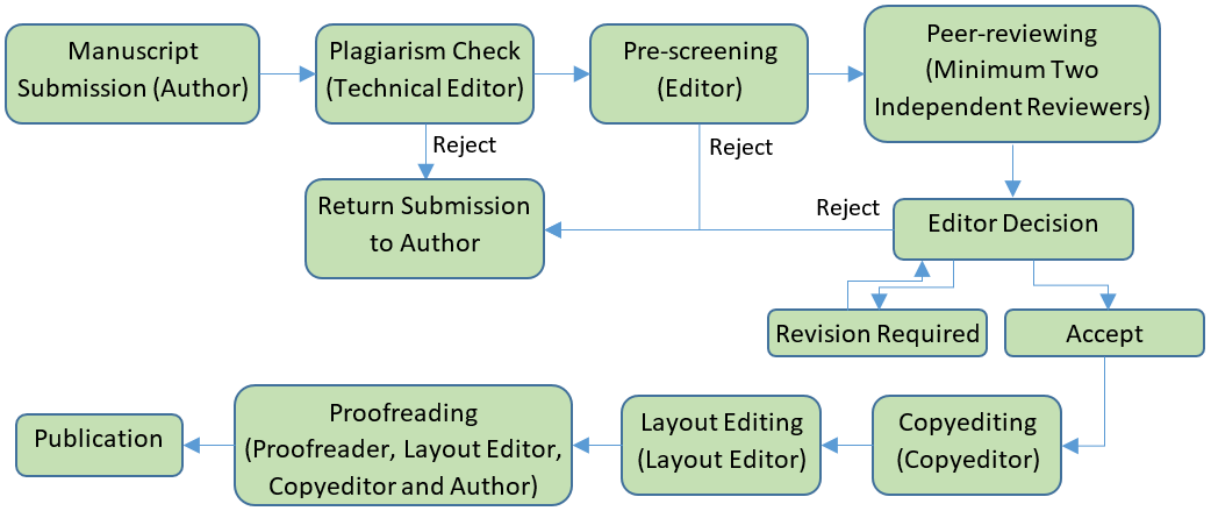

**Publication Ethics and Malpractice Statement**

IJOCTA is committed to ensuring ethics in publication and quality of articles. Conforming to standards of expected ethical behavior is therefore necessary for all parties (the author, the editor(s), the peer reviewer) involved in the act of publishing.

International Standards for Editors

The editors of the IJOCTA are responsible for deciding which of the articles submitted to the journal should be published considering their intellectual content without regard to race, gender, sexual orientation, religious belief, ethnic origin, citizenship, or political philosophy of the authors. The editors may be guided by the policies of the journal's editorial board and constrained by such legal requirements as shall then be in force regarding libel, copyright infringement and plagiarism. The editors may confer with other editors or reviewers in making this decision. As guardians and stewards of the research record, editors should encourage authors to strive for, and adhere themselves to, the highest standards of publication ethics. Furthermore, editors are in a unique position to indirectly foster responsible conduct of research through their policies and processes.

To achieve the maximum effect within the research community, ideally all editors should adhere to universal standards and good practices.

- Editors are accountable and should take responsibility for everything they publish.
- Editors should make fair and unbiased decisions independent from commercial consideration and ensure a fair and appropriate peer review process.
- Editors should adopt editorial policies that encourage maximum transparency and complete, honest reporting.
- Editors should guard the integrity of the published record by issuing corrections and retractions when needed and pursuing suspected or alleged research and publication misconduct.
- Editors should pursue reviewer and editorial misconduct.
- Editors should critically assess the ethical conduct of studies in humans and animals.
- Peer reviewers and authors should be told what is expected of them.
- Editors should have appropriate policies in place for handling editorial conflicts of interest.

*Reference:*

*Kleinert S & Wager E (2011). Responsible research publication: international standards for editors. A position statement developed at the 2nd World Conference on Research Integrity, Singapore, July 22-24, 2010. Chapter 51 in: Mayer T & Steneck N (eds) Promoting Research Integrity in a Global Environment. Imperial College Press / World Scientific Publishing, Singapore (pp 317-28). (ISBN 978-981-4340-97-7) [Link].*

International Standards for Authors

Publication is the final stage of research and therefore a responsibility for all researchers. Scholarly publications are expected to provide a detailed and permanent record of research. Because publications form the basis for both new research and the application of findings, they can affect not only the research community but also, indirectly, society at large. Researchers therefore have a responsibility to ensure that their publications are honest, clear, accurate, complete and balanced, and should avoid misleading, selective or ambiguous reporting. Journal editors also have responsibilities for ensuring the integrity of the research literature and these are set out in companion guidelines.

- The research being reported should have been conducted in an ethical and responsible manner and should comply with all relevant legislation.
- Researchers should present their results clearly, honestly, and without fabrication, falsification or inappropriate data manipulation.
- Researchers should strive to describe their methods clearly and unambiguously so that their findings can be confirmed by others.
- Researchers should adhere to publication requirements that submitted work is original, is not plagiarised, and has not been published elsewhere.
- Authors should take collective responsibility for submitted and published work.
- The authorship of research publications should accurately reflect individuals' contributions to the work and its reporting.

- Funding sources and relevant conflicts of interest should be disclosed.
- When an author discovers a significant error or inaccuracy in his/her own published work, it is the author's obligation to promptly notify the journal's Editor-in-Chief and cooperate with them to either retract the paper or to publish an appropriate erratum.

*Reference:*

*Wager E & Kleinert S (2011) Responsible research publication: international standards for authors. A position statement developed at the 2nd World Conference on Research Integrity, Singapore, July 22-24, 2010. Chapter 50 in: Mayer T & Steneck N (eds) Promoting Research Integrity in a Global Environment. Imperial College Press / World Scientific Publishing, Singapore (pp 309-16). (ISBN 978-981-4340-97-7) [Link].*

Basic principles to which peer reviewers should adhere

Peer review in all its forms plays an important role in ensuring the integrity of the scholarly record. The process depends to a large extent on trust and requires that everyone involved behaves responsibly and ethically. Peer reviewers play a central and critical part in the peer-review process as the peer review assists the Editors in making editorial decisions and, through the editorial communication with the author, may also assist the author in improving the manuscript.

Peer reviewers should:

- respect the confidentiality of peer review and not reveal any details of a manuscript or its review, during or after the peer-review process, beyond those that are released by the journal;
- not use information obtained during the peer-review process for their own or any other person's or organization's advantage, or to disadvantage or discredit others;
- only agree to review manuscripts for which they have the subject expertise required to carry out a proper assessment and which they can assess within a reasonable time-frame;
- declare all potential conflicting interests, seeking advice from the journal if they are unsure whether something constitutes a relevant conflict;
- not allow their reviews to be influenced by the origins of a manuscript, by the nationality, religion, political beliefs, gender or other characteristics of the authors, or by commercial considerations;
- be objective and constructive in their reviews, refraining from being hostile or inflammatory and from making libellous or derogatory personal comments;
- acknowledge that peer review is largely a reciprocal endeavour and undertake to carry out their fair share of reviewing, in a timely manner;
- provide personal and professional information that is accurate and a true representation of their expertise when creating or updating journal accounts.

*Reference:*

*Homes I (2013). COPE Ethical Guidelines for Peer Reviewers, March 2013, v1 [Link].*

**Copyright Notice**

An International Journal of Optimization and Control: Theories & Applications

Volume: 7 Number: 2
July 2017

## CONTENTS



www.ijocta.com
info@ijocta.com

ISSN 2146-0957